

Doctoral Dissertation

Ying Jiru

Mass Transfer Kinetics
of Carbon Dioxide into
Concentrated Aqueous
Solutions of Monoethanolamine



Telemark University College
Faculty of Technology

**Mass Transfer Kinetics of Carbon Dioxide into
Concentrated Aqueous Solutions of Monoethanolamine**

Ying Jiru

Ying Jiru

**Mass Transfer Kinetics of Carbon Dioxide into
Concentrated Aqueous Solutions of Monoethanolamine**

Thesis for the Degree of Doctor of Philosophy

Porsgrunn, Norway

February, 2013

Tel-Tek

Telemark University College

Tel-Tek

Telemark University College

Thesis for the degree of doctor of philosophy

©Ying Jiru

ISBN 978-82-7206-366-4

Doctoral Thesis at TUC, 2013

Acknowledge

I would like to give a great thank to my supervisor Prof. Dr. Dag A. Eimer who gave me this chance to carry out this PhD study in Norway and especially for the trust and expert guidance during my study. He always gave me a smile and motivated me when I met a problem in the research. He always supported me even he was ill! The numerous meetings and discussions were not only inspiring, but also relative to the Norwegian culture and have great fun. This thesis was realized with Dag's profound and abundance knowledge of chemical engineering and CO₂ capture processes.

My family is my life. I would like to give a special thank to my wife and my son who are a constant force in my life. You are my back supporter of my study and my hope! I also want to thank my extended family and friends.

I would like to express my sincere gratitude to Marit Larsen, the CEO of Tel–Tek, and Hans Aksel Haugen, our project manager, who gave me this opportunity of study and supported me to finish my PhD study.

I would like to thank my teachers of Telemark University College, Prof. Dr. Morten Ch. Melaen and Prof. Dr. Klaus. J. Jens, who taught me the background knowledge and gave me help during my study, especially gave me some good advice in the daily meeting. Also thank Trond Risberg, Per Morten Hansen, Talleiv Skredtveit and Eivind Fjelddalen, Joachim Lundberg, Chameera Jayarathna, who gave me very big favors in my experimental works!

I would also like to express my gratitude to Sigbjørn Wiersdalen, who is an old kind friend in my life and laboratory work. He has abundance practical experience of engineering. Many problems I met in the experiments he always helped to solve it one by one in time. Sigbjørn, thank you so much!

Dr. Espen Steinseth Hamborg from Statoil AS has been given me lots of help on the stirred cell research. He is an enthusiastic and erudite scholar. I really appreciate him for his friendly help.

I would also like to thank Wang Tielin, Li Bo, Yi Wenjuan and Han Jingyi. We entered the portal of TUC and Tel–Tek and studied together, we helped each other in our study and life.

Ying Jiru
2012–06

Abstract

Global warming arguments have gained more and more attention due to the new regulations of carbon dioxide (CO_2) emission in the world. Monoethanolamine (MEA) has been employed as an important industrial absorbent for CO_2 capture since the 1930s because of its high reaction rate, relatively low cost, and thermal stability. The concentration of MEA in aqueous solution is generally increased to 30 mass % in the CO_2 capture process. The energy consumption is high in the present MEA process because of the high reaction heat of MEA with CO_2 , and a large number of liquid transportation. To reduce the energy consumption and improve the efficiency of CO_2 capture in the present MEA process, further increase in solution concentration of MEA is a potential solution. Basic research on the properties and reaction kinetics with CO_2 of concentrated aqueous MEA solution is necessary to perform engineering calculations and important for the dimensioning of pipes, pumps and heat exchangers etc.

In this work, a novel solubility apparatus and technique was designed and built for the measurement of physical solubility of a gas in liquid. The technique employs a scaled spiral glass tube with a small drop of mercury inside as a eudiometer as an alternative to a three-branch U-tube setup to keep the system pressure constant, and measure the volume drop of absorbed gas at constant temperature. A “vacuum gas saturation” method is proposed for gas saturation operation in the measurement. The physical solubilities of N_2O in pure water over the temperature range from 298.15 to 323.15 K and in aqueous salt MEA solutions at 313.15 K were measured under a constant ambient pressure to validate the new technique. The new solubility apparatus and technique possesses some advantages including easy operation, lower mercury inventory, higher sensitivity and greater accurate. The physical mass transfer coefficients of N_2O in aqueous MEA solutions were performed using the new apparatus as well.

The physical solubilities of N_2O in aqueous MEA solutions over the full concentrations range were measured by the novel solubility apparatus over a temperature range from 298.15 to 323.15 K under a constant ambient pressure. The physical solubilities of CO_2 in aqueous MEA solutions were estimated using “ N_2O analogy” method. The results of the solubility measurements of N_2O and CO_2 in water and N_2O in aqueous MEA solutions agree with literature. A semiempirical model to solubility proposed by Wang et al. was used to correlate the solubilities of N_2O and CO_2 in aqueous MEA solutions, and the correlation results are in agreement with experiment data. The results show that the solubilities of both N_2O and CO_2

in aqueous MEA solutions showed negative deviation behaviors from the linear additive principle.

The viscosities of aqueous MEA solutions over the full concentration range were measured using a rheometer with a double-gap measuring system at a temperature range from 298.15 to 353.15 K. The measured viscosity data are in good agreement with the literature values. An exponent model proposed by DiGuilio et al. was used to correlate the data and the results are very satisfied for the regression of the viscosities of pure MEA from 298.15 to 353.15 K. The polynomial model proposed by Teng et al. with five parameters is satisfied the aqueous MEA solution. The relationship between the viscosity and mole fraction of MEA shows both positive and negative deviation behavior and the critical mole fraction of MEA was found is 0.2.

The molecular diffusivities of N₂O in aqueous MEA solutions up to 12 M were studied from 298.15 to 333.15 K using a laminar liquid jet absorber, and the diffusivities of CO₂ in aqueous MEA solutions were calculated by the N₂O analogy method. A modified construction of the temperature control for the laminar liquid jet was proposed. The relationship between the diffusivity and the viscosity of the solution is roughly in agreement with the modified Stokes–Einstein equations. On the other hand, an exponent mathematical model was used to correlate N₂O diffusivities in aqueous MEA solutions satisfactorily for calculation of the diffusivities of CO₂ in aqueous MEA solutions.

Based on the measured physical properties in this work, the chemical reaction kinetics of CO₂ with aqueous MEA solutions over a wide concentration range from 0.5 to 12 M were investigated using a stirred cell absorber with a plane gas–liquid interface over a temperature range from 298.15 to 323.15 K. To satisfy the criterion of pseudo-first-order reaction, low CO₂ partial pressure (3 – 4 kPa) was employed. The rates of CO₂ absorption in the solutions were determined from the fall in pressure, and the reaction rate constants were determined by two treatment methods on the same experimental data, viz. a “differential” and an “integral” method, which are derived from the mass balance principle and Henry’s law. The reaction between MEA and CO₂ is based on “zwitterion” mechanism in this work. The gas-phase resistance was investigated systematically in the stirred cell. To reduce the gas phase resistances in the measurements of CO₂ absorption in the solutions, speeding up the gas phase fans and employing very low inert gas pressures of N₂ and solution vapor were suggested. The chemical reaction kinetics of CO₂ in aqueous MEA solutions were measured over the concentration range from 0.5 to 12 M by a stirred cell absorber with batchwise operation for both gas and liquid. As same as the dilute solution, the reaction of concentrated aqueous

MEA solution with CO₂ is also first order with respect to MEA and the reaction is in the fast reaction regime. The reaction activation energy (E_a) of aqueous MEA + CO₂ is calculated based on the experimental data. The enhanced mass transfer coefficient in liquid phase, $k_L E$, increases with the concentration of MEA solutions but decreases when the molarity of MEA is higher than 8 M.

Last, some recommendations are given to the future work. CO₂-loaded MEA solution is suggested to focus on in the next-step work, the properties and gas absorption of the system can be measured and discussion by the same experimental method mentioned in this thesis. The gas absorption and desorption from the CO₂-loaded aqueous MEA solutions should be performed as well. The issue of heat transfer should be taken into account and investigated when the concentrated aqueous MEA solution is employed in the CO₂ capture process. The stirred cell or laminar liquid jet can be employed in these studies under a suitable pressure. However, to obtain more accurate experimental data, some modifications on the construction of both the laminar liquid jet and stirred cell should be made. For example, the absorption cell of the liquid laminar jet can be smaller, and the nozzle or receiver should be adjustable etc. Regarding the modification on the temperature control of these equipments, the main idea is to immerse all the gas and liquid pipes in to the same water bath or its hose. Some suggestions of these modifications are proposed in the appendix of this thesis.

Content

Acknowledge	I
Abstract	II
1. General Introduction	1
1.1. CO ₂ Capture.....	2
1.2. Chemical Absorption Absorbents.....	3
1.3. Monoethanolamine	6
1.4. Outline of This Thesis	7
References.....	9
2. Theory Background	12
Abstract.....	12
2.1. Mass Transfer without Chemical Reaction.....	13
2.2. Mass Transfer with Chemical Reaction.....	15
Nomenclature.....	19
References.....	20
3. Design and Validation of a New Apparatus for Physical Solubility Measurement.....	21
Abstract.....	21
3.1. Introduction.....	22
3.2. Description of the Equipment and Principle.....	24
3.2.1. Absorption Cell.....	25
3.2.2. Data Acquisition System.....	30
3.2.3. Liquid and Gas Feed System	33
3.2.4. Temperature Control and Vacuum System.....	33
3.3. The Determination of Gas Saturation Method.....	34
3.4. Operation of Equipment and the Procedure of the Measurement.....	36
3.5. Measurement Data	40
3.5.1. Measurement Data of Physical Solubility.....	40
3.5.2. Measurement Data of Physical Mass Transfer	40
3.6. Treatment and Mathematical Description for Data	41
3.6.1. Physical Solubility	41
3.6.2. Mass Transfer.....	43
3.7. Experimental Section.....	44
3.7.1. Reagent and Solution Preparation.....	44
3.8. Results and Discussion	44

3.8.1. Validation for the Novel Technique	44
3.8.2. Physical Solubility of N ₂ O in Aqueous Salt MEA Solutions	47
3.8.3. Mass Transfer Coefficient of N ₂ O in Aqueous MEA Solutions	52
3.9. Conclusions.....	54
Nomenclature.....	55
References.....	57
4. Measurements and Correlation of Physical Solubility of N ₂ O and CO ₂ in (Monoethanolamine + Water) by a Novel Technique	59
Abstract.....	59
4.1. Introduction.....	60
4.2. Experimental Section.....	64
4.2.1. Experimental Setup and Procedure of the Solubility Measurement	64
4.2.2. Reagent and Solution Preparation.....	67
4.3. Results and Discussion	67
4.3.1. Validation for the Novel Technique	67
4.3.2. N ₂ O Absorbed in Aqueous MEA Solution.....	68
4.3.3. Physical Solubility of CO ₂ in Aqueous MEA Solution	70
4.4. Uncertainty Analysis	76
4.5. Conclusions.....	78
Nomenclature.....	79
References.....	80
5. Viscosity Measurement of Aqueous Monoethanolamine Solution	82
Abstract.....	82
5.1. Introduction.....	83
5.2. Experimental Section.....	85
5.3. Results and Discussion	85
5.3.1. Viscosity of Pure MEA.....	85
5.3.2. Viscosity of the Aqueous MEA Solution.....	86
5.4. Conclusions.....	91
Nomenclature.....	91
References.....	91
6. Measurements and Correlations of Diffusivities of Nitrous Oxide and Carbon Dioxide in (Monoethanolamine + Water) by Laminar Liquid Jet.....	93
Abstract.....	93
6.1. Introduction.....	94

6.2.	Theory Background	98
6.3.	Experimental Section.....	100
6.3.1.	Experimental Equipment and Procedure	100
6.3.2.	Reagents and Solution Preparation	102
6.4.	Results and Discussion	102
6.4.1.	Diffusivity of N ₂ O in Pure Water	102
6.4.2.	Physical Solubility of N ₂ O in Aqueous MEA Solution	105
6.4.3.	Diffusivity of N ₂ O and CO ₂ in Aqueous MEA Solution	105
6.5.	Uncertainty Analysis	111
6.6.	Conclusions.....	113
	Nomenclature.....	114
	References.....	115
7.	Determination and Measurements of Mass Transfer Kinetics of CO ₂ in Concentrated Aqueous Monoethanolamine Solutions with a Stirred Cell.....	117
	Abstract.....	117
7.1.	Introduction.....	118
7.2.	Theory Background	122
7.2.1.	Zwitterion Mechanism	122
7.2.2.	Termolecular Mechanism	124
7.3.	Experimental Section.....	125
7.3.1.	Experimental Equipment and Procedures.....	125
7.3.2.	Reagent and Solution Preparation.....	129
7.4.	Results and Discussion	130
7.4.1.	Physical Solubility	130
7.4.2.	Diffusivity	130
7.4.3.	Determination of Gas–liquid Reaction Kinetics.....	131
7.4.4.	Estimation of Liquid Mass Transfer Coefficient without Chemical Reaction	134
7.4.5.	Investigation of Gas-phase resistance.....	138
7.4.6.	Kinetics of the Chemical Reaction of CO ₂ Absorbed in Aqueous MEA Solution	141
7.5.	Conclusions.....	145
	Nomenclature.....	146
	References.....	149
8.	Summary and Suggestion for Future Work	151

Appendix.....	155
A1.Raw Experimental Data of Solubility Measurement	155
A2.Raw Experimental Data of Diffusivity Measurement	157
A3.Raw Experimental Data of Chemical Reaction Kinetics Measurement	166
A4.Overshoot of Pressure and Temperature of Stirred Cell.....	172
A5.Deduction and Applications of Models and Equations.....	174
A5.1. Calculation of Dimensionless Solubility (m)	174
A5.2. Calculation of Mass Transfer Coefficient k_L (without Chemical Reaction).....	175
A5.3. Calculation for Mass Transfer Coefficient k_L by Volume-drop Method	176
A5.4. Calculation of Pseudo-first-order Chemical Reaction Rate by Pressure-drop Method (Stirred Cell) (1)	177
A5.5. Calculation of Pseudo-first-order Chemical Reaction Rate by Volume-drop Method (2)	178
A5.6. Calculation of Pseudo-first-order Chemical Reaction Rate (3)	179
A5.7. Deduction of the Reaction Kinetics for Amine+CO ₂	180
A6.The Modified Construction of Laminar Jet Absorber.....	181
A7.The Present Construction of Laminar Jet Absorber.....	184
A8.Flowsheet of Laminar Liquid Jet	189
A9.The Modified Construction of Stirred Cell Reactor	190
A10. Flow Sheet and Construction of Solubility Cell	191
A11. The Possible Method to Reduce the Influence of Pressure on Solubility Measurement	194
A12. The Issues of Viscosity Measurement	196
A13. Key Codes of Program for Solubility Measurement.....	199
A14. Lists of Publications.....	207

Chapter 1

1. General Introduction

Recently, global warming arguments have gained lots of attention due to the new regulations of carbon dioxide (CO₂) emission in the world. CO₂ is a typical greenhouse gas with huge amount on the earth, and is being emitted in the air continuously from the fossil carbon substances by human activities. The background is the yearly increase of CO₂ emission as shown in Figure 1.1: the increase of atmospheric CO₂ was 20% since 1958, 38% since pre-industrial time. The average annual increase was 37% of the year 2000 – 2011.¹ The emission rate of CO₂ by human activities is currently 135 times greater than by volcanoes, amounting to about 35 gigatons per year.²

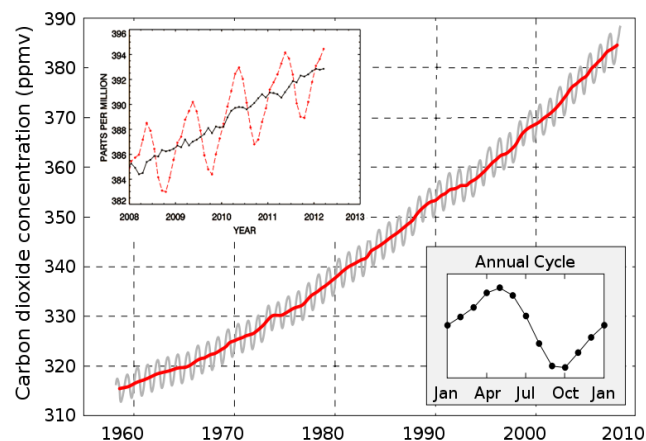


Figure 1.1 The keeling curve of atmospheric CO₂ concentrations from the years 1958 to 2012 measured at Mauna Loa Observatory³.

Global warming will cause sea levels to rise and a probable expansion of subtropical deserts. Other likely effects of the warming include more frequent occurrence of extreme-weather events including heat waves, droughts and heavy rainfall, species extinctions due to shifting temperature regimes, and changes in crop yields. In the 2007 Fourth Assessment Report (AR4), the Intergovernmental Panel on Climate Change (IPCC) revealed that during the 21st century the temperature of the global surface is likely to increase 1.1 – 2.9 °C for their lowest emissions scenario and 2.4 – 6.4 °C for their highest.⁴ The ranges of these estimates arise from the use of models with differing sensitivity to concentrations of greenhouse gas. The United Nations Framework Convention on Climate Change (UNFCCC) has adopted a range of policies designed to reduce greenhouse gas emissions and to assist in

adaptation to global warming. Parties to the UNFCCC have agreed that deep cuts in greenhouse gas emissions are required, and that future global warming should be limited to below 2 °C relative to the pre-industrial level. The United Nations Environment Programme and International Energy Agency in 2011 suggest that efforts as of the early 21st century to reduce emissions may be inadequately stringent to meet the UNFCCC's 2 °C target.

1.1. CO₂ Capture

The largest source (about 96.5%) of CO₂ emissions globally is the combustion of fossil fuels such as coal, oil and gas in power plants, automobiles, industrial facilities and other sources.⁵ The removal of CO₂ is essential for power plant, ammonia synthesis and LNG (liquefied natural gas) industry etc. To power plant, the main three technologies are post-combustion decarbonization, pre-combustion decarbonization and oxy-fuel combustion decarbonization.

Post-combustion decarbonization captures CO₂ from the flue gases, and just requires small modifications to the power cycle, but large quantity gases must be treated because CO₂ is diluted by the nitrogen of the combustion air. Chemical absorption for the CO₂ capture is considered to be the most suitable way for this case because of the low CO₂ partial pressure.

Pre-combustion decarbonization is performed by the conversion of the fossil fuel to CO- and H₂- enriched synthesis gas, and finally produces hydrogen fuel by a shift process, in which the CO is converted to CO₂, that is then captured. Depending on the operational conditions, mainly the pressure and CO₂ concentration, the CO₂ removal can be conducted by either physical or chemical absorption.

Oxy-fuel cycles are based on the close-to-stoichiometric combustion, where the fuel is burned with enriched oxygen and recycled flue gas. The combustion is accomplished in absence of the large amounts of nitrogen, and produces only CO₂ and H₂O. CO₂ separation is accomplished by condensing water from the flue gas.

Most common CO₂ capture technology in the present is the Post-combustion decarbonization by absorption. The main gas purification processes include 1) absorption into a liquid, 2) adsorption on a solid, 3) Permeation through a membrane barrier. 4) Chemical conversion to a product.⁸ In these processes, chemical absorption process is more suitable for CO₂ capture where the mixture gas is typically at atmospheric pressure and containing 3 – 12% CO₂ for LNG or power plant (Post-combustion) etc. Absorption into a liquid is a separation process based on selective absorption in a liquid. This process is followed by the process of desorption where the solution is regenerated. Figure 1.2 is the typical MEA CO₂

removal principle and process proposed by Bottoms.⁶ In the process, after cooling, the untreated acid gas stream is blown into the absorber from the bottom of the absorption column where it is contacted with the absorbent. The absorbent normally flows counter-currently down from the top of column, where it gradually absorbs more and more CO₂ until it leaves the absorber at the bottom. The CO₂ loading solution is then called rich solution. The purified gas leaves the absorber at the top. It can be emitted directly or enter further process. The rich solution is heated in a heat exchanger prior to entering the desorber column. In the desorber, the absorbed CO₂ in the solution is stripped due to a higher temperature and relatively lower pressure. Subsequently, the regenerated absorbent (so-called lean solution) goes through the heat exchanger to cool down and then is fed to the top of the absorber column again, while the stripped CO₂ from the desorber can be further processed for storage or application.

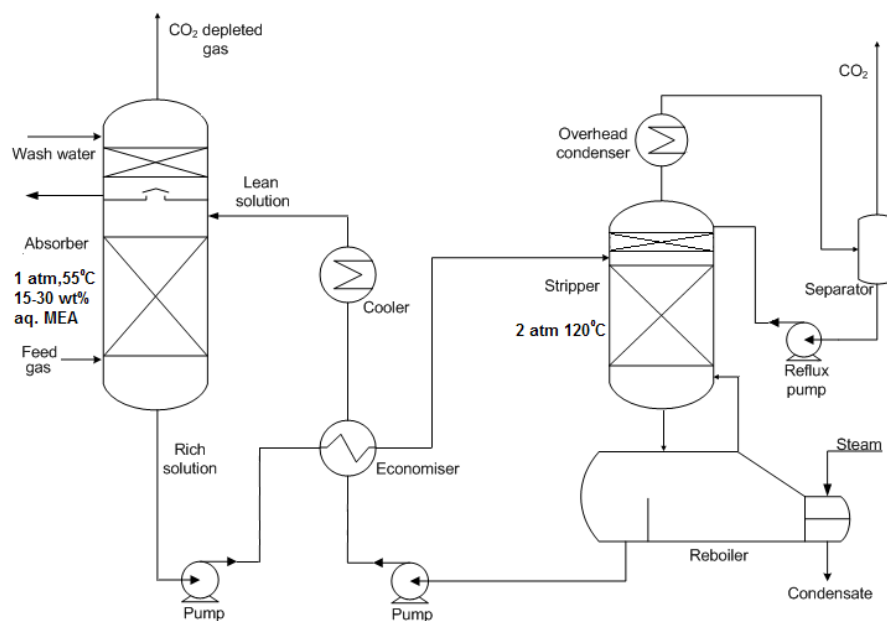


Figure 1.2 Typical process and principle of CO₂ capture with aqueous MEA solution⁶

1.2. Chemical Absorption Absorbents

In the absorption process, the selection of absorbent is very important. Different factors affect the efficiency of a solvent for CO₂ absorption; these include solvent solubility, reaction kinetics with CO₂, reaction heat and regeneration energy requirement, vapor pressure and molecular weight of the absorbent, foaming tendency, degradation and corrosion properties as well as the cyclic capacity. Environmental and cost factors are also to be considered. Since the 1930s, Triethanolamine (TEA) was employed as the first commercial absorbent in the gas

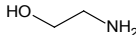
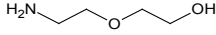
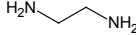
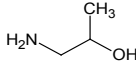
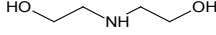
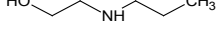
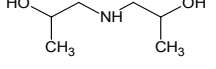
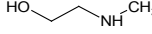
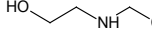
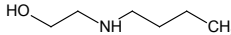
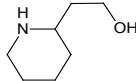
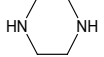
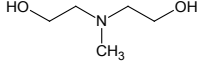
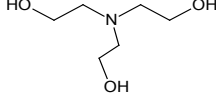
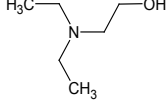
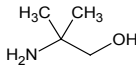
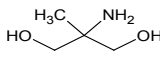
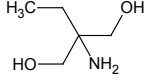
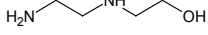
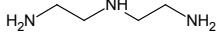
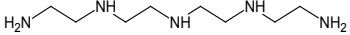
treating process.⁸ The other members of the alkanolamine family were introduced into the field gradually; they were also evaluated as possible acid–gas absorbents. The amines that have proved to be of principal commercial interest for gas treating are monoethanolamine (MEA),^{7–10} diethanolamine (DEA)¹¹ and methyldiethanolamine (MDEA). Triethanolamine¹² has been displaced largely because of its low capacity, its low reactivity, and its relatively poor stability.

As absorbents, each alkanolamine has at least one hydroxyl group and one amino group. In general, it can be considered that the hydroxyl group serves to reduce the vapor pressure and increase its solubility in water, while the amino group provides the necessary alkalinity in water solutions to cause the absorption of acidic gases. The alkanolamines are categorized as primary, secondary and tertiary alkanolamine by the number of hydrogen atoms on the amino group. A review of commercial and potential amines for industry is shown in Table 1.1.

Primary and secondary alkanolamines react rapidly with CO₂ to form carbamates, i.e. MEA and Diglycolamine (DGA). However, the heat of absorption is high, which results in high solvent regeneration costs. The CO₂ loading capacity of such alkanolamines is in practice limited to 0.5 mol of CO₂ per mole of amine. Tertiary alkanolamine has no hydrogen atom attached to the nitrogen atom; leads to the carbamate formation reaction cannot take place, and the reaction rate with CO₂ is low. Instead, tertiary amines facilitate the CO₂ hydrolysis reaction to form bicarbonates. The reaction heat of bicarbonate formation is lower than that of carbamate formation, thus reducing solvent regeneration costs. Moreover, tertiary amines have a high CO₂ loading capacity of 1 mol of CO₂ per mole of amine. These advantages attract more researchers to study and try to activate it. For instance, the reactions of MDEA, AMP and DEMEA with CO₂ are accelerated by promoters such as MEA, DEA and PZ.^{14–25}

Sterically hindered amines have recently received considerable attention due to its low regeneration costs^{26–38}. A sterically hindered amine is a primary amine in which the amino group is attached to a tertiary carbon atom, or a secondary amine in which the amino group is attached to a secondary or tertiary carbon atom. 2–Amino–2–methyl–1–propanol (AMP)^{27–32}, 2–amino–2–methyl–1,3–propanediol (AMPD),³³ and 2–amino–2–ethyl–1,3–propanediol (AEPD),³⁴ 2–piperidineethanol (PE)^{35–38} are examples of sterically hindered primary and secondary amines, respectively. These amines form carbamate of low stability due to a large group attached to the nitrogen atom, the CO₂ is thus bound as bicarbonate, resulting in a CO₂ capacity of 1 mol of CO₂ per mole of amine.

Table 1.1 A review of amine absorbents for CO₂ capture

Name of amine	Structure	k_s^b	pKa ^{7,39}	ΔH^{45} kJ mol ⁻¹
Primary amines				
MEA	monoethanolamine 	7000	9.50	-82
DGA	diglycolamine 	6663		
EDA	ethylenediamine 	12	9.9	
MIPA	Monoisopropanolamine 		9.4	
Secondary amines				
DEA	diethanolamine 	2375 ^a	8.88	-69
EEA	Ethyl ethanolamine 	8.0		
DIPA	diisopropanolamine 	2585 ^a	8.80	
MAE	2-methylaminoethanol 	4170 ^a	9.7	
EAE	2-ethylaminoethanol 	7940 ^a	9.8	
NBMEA	1-butylmonoethanolamine 	4760 ^a		
PE	2-piperidineethanol 			
PZ	piperazine 	53700		
Tertiary amines				
MDEA	methyldiethanolamine 	18.2 ^a	8.57	-49
TEA	triethanolamine 		7.76	
DEMEA	diethylmonoethanolamine 	34	9.882	
Hinder amines				
AMP	2-amino-2-methyl-1-propanol 	810.4 ^a	9.7	
AMPD	2-amino-2-methyl-1,3-propanediol 	382 ^a (at 303K)		
AEPD	2-amino-2-ethyl-1,3-propanediol 	378 ^a (at 303K)		
Polyamines				
AEEA	2-((2-aminoethyl)amino)ethanol 	12300		
DETA	diethylenetriamine 			
TEPA	Tetraethylenepentamine 			

a, from literature¹³; b, first order w.r.t. amine, 25°C, (m³kmol⁻¹s⁻¹); $pKa = -\lg K_p$, $K_p = \frac{[Am][H^+]}{[AmH^+]}$

Some researches are directed toward polyamines (alkanolamine) having more than one amino group. Examples are 2-((2-aminoethyl) amino) ethanol (AEEA),^{40,41} diethylenetriamine (DETA)⁴², and Tetraethylenepentamine (TEPA)⁴³ containing primary and secondary one or more amino groups. These amines show outstanding CO₂ absorption potentials, can have maintained very high absorption rates and removes high amounts of CO₂ per cycle. For example, 1.0M TEPA removes 3 times more CO₂ per cycle than 1.0M MEA; however, working with TEPA at higher concentrations has proved challenging due to viscosity and flashing problems experienced.⁴³

In the future, EAE (or EMEA),⁴⁴ DEMEA,⁴⁴ MAE (or MMEA),⁴⁶ TEPA and AEEA are candidate alkanolamines having good potential for the bulk removal of CO₂ from gaseous streams. EMEA and DEMEA have an additional advantage for an extensive use for CO₂ capture, as they can be prepared from renewable resources.⁴⁷

1.3. Monoethanolamine

MEA has been used for absorption of acid gases since the 1930s.⁷⁻¹⁰ Although other amines have become more popular, and the MEA process has some shortcomings such as high energy consumption, it is at present date considered the most mature technology of CO₂ capture in Post-combustion flue gases. The concentration of MEA solutions was generally increased to 30 mass % in the 1960s. This has been standard since then. Very large absorbent streams then need to be circulated, and a further increase in solution concentration would help reduce these flows to decrease the energy consumption and improve the CO₂ efficiency.

Peng⁴⁸ summarized the influence of the absorbent concentration on CO₂ absorption efficiency as shown in Figure 1.3. It is a trend that CO₂ absorption efficiency increases with the increase of absorbent concentration. When the absorbent concentration is low, CO₂ absorption efficiency increment is large when increasing absorbent concentration. However, when the absorbent concentration is high, CO₂ absorption efficiency increment is not so significant. This behavior is determined by reversible equilibrium conditions and gas-liquid two phase mass transfer conditions. In terms of chemical dynamics, increase of absorbent concentration is equivalent to increasing the reactant concentration, resulting in response moving to the positive direction, improving the reaction rate and CO₂ absorption efficiency. Thus, it is feasible to improve CO₂ absorption efficiency by increasing the concentration of absorbent.

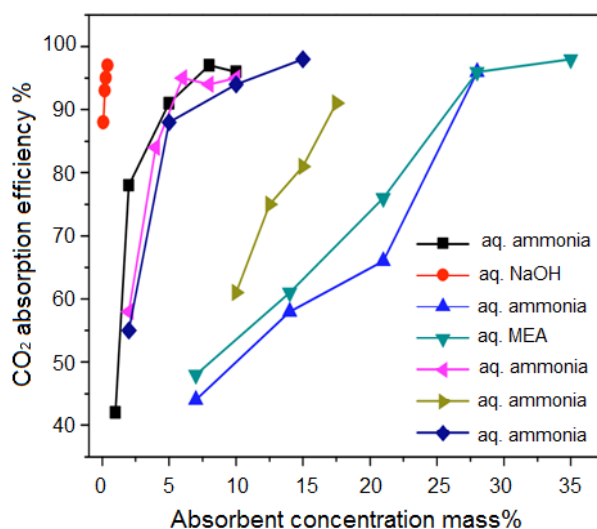


Figure 1.3 The concentration of absorbent effect on CO₂ absorption efficiency⁴⁸

1.4. Outline of This Thesis

To reduce the energy consumption and improve the efficiency of CO₂ absorption in the present MEA process, further increase in concentration of MEA is a potential solution. Basic research on the properties and reaction kinetics with CO₂ of concentrated aqueous MEA solution is necessary to perform engineering calculations and important for dimensioning of pipes, pumps and heat exchangers. The use of such data and mass transfer kinetics research are typically used for dimensioning column diameters and packing heights. In this work, the solubility, diffusivity and viscosity of concentrated aqueous MEA solution were measured and these properties as functions of MEA concentration and temperature were studied.

The mass transfer is the nature of the gas absorption behavior. The chapter 2 introduces the background theory and its derivation which will be applied in the calculation of the mass transfer and the measurement of the physical properties. The mass transfer of gas absorbed into liquid with/without chemical reaction is derived according to mass balance principle and Fick's law. The various conditions of the gas-liquid contact time (in a long/short time) are given as samples of stirred cell and laminar liquid jet.

Chapter 3 introduces the design of a new apparatus for measuring the physical solubility of a gas in a liquid, and a mathematical model was developed to treat the experimental data. It is different from the conventional apparatus, the new experimental technique employs a scaled spiral glass tube with a small drop of mercury inside as a eudiometer. This spiral tube replaces the conventional three-branch U-tube unit to keep the system pressure constant and measure the volume drop of the absorbed gas at a constant temperature. The gas saturation

method was investigated and a “vacuum gas saturation” method was proposed for the measurement. To validate the new technique, the physical solubilities of N_2O in pure water over a temperature range from 298.15 to 323.15 K and in aqueous salt MEA solutions at 313.15 K were measured. The experiments of mass transfer of N_2O in aqueous MEA solutions were performed, which exhibits a little wide applied scope of the new solubility cell.

Chapter 4 describes the measurement of the physical solubility of N_2O in aqueous MEA solution by using the new solubility apparatus and experimental technique. The physical solubility of CO_2 in aqueous MEA solutions over the full range of concentrations were estimated using the “ N_2O analogy” method over a temperature range from 298.15 to 323.15 K. Wang’s model was used to correlate the data and predict the (MEA + water) system.

Chapter 5 gives the measurements and correlations of the viscosities of the solutions over the full concentration range were measured at a temperature range from 298.15 to 353.15 K. An exponent model proposed by DiGuilio et al. and a polynomial model proposed by Teng et al. were used to correlate by regression analysis of the data of pure MEA and the aqueous MEA solution, respectively.

Chapter 6 provides the measurements and correlations of the molecular diffusivities of nitrous oxide (N_2O) with aqueous MEA solutions up to 12 M were studied over a temperature range from 298.15 to 333.15 K under atmospheric pressure using a laminar liquid jet absorber. The diffusivities of CO_2 in aqueous MEA solutions were calculated by “ N_2O analogy” method. A simple and effective thermal control technique was used to control the temperature of gas and liquid in the laminar liquid jet absorber. The relationship between the diffusivity and the viscosity of the solution was regressed by a modified Stokes–Einstein equation, and an exponent mathematical model was employed to simulate the diffusivity data.

In chapter 7, the absorption of a gas in a liquid was determined with a stirred cell from the fall in pressure and the liquid-side mass transfer coefficient and the reaction rate constant were determined by two data treatment methods, viz. a “differential” and an “integral” method. The gas-phase resistance was investigated to avoid the effect of the gas-phase resistance on the measurement of the reaction rate constant. The liquid-side mass transfer coefficient without chemical reaction in the stirred cell reactor was determined via the pressure drop method. The well-known equation with respect to the Sherwood number (Sh), the Reynolds (Re) and Schmidt (Sc) numbers were obtained. The kinetics of the reactions of CO_2 with aqueous MEA solutions over a wide concentration range from 0.5 to 12 M at a temperature range from 298.15 to 323.15 K were studied using the stirred cell absorber with a

plane gas–liquid interface. Low CO₂ partial pressure (4 kPa) was employed to satisfy the criterion of pseudo-first-order reaction. The enhanced mass transfer coefficient in liquid phase, $k_L E$, was obtained. Based on the measurements of $k_L E$, a suitable molarity of the concentrated aqueous MEA is suggested to the conventional CO₂ capture process for reducing energy consumption and improving the efficiency of the CO₂ absorption.

Chapter 8 summarizes the conclusions for all the above chapters and gives some suggestions for the future work, especially for the research object and the construction of laminar liquid jet and stirred cell.

References

1. Tans, P. Annual CO₂ mole fraction increase (ppm) for 1959–2007, National Oceanic and Atmospheric Administration Earth System Research Laboratory, Global Monitoring Division. 3 May **2008**.
2. Gerlach, T. M. Volcanic versus Anthropogenic Carbon Dioxide: *Eos Trans.* **2011**, *92*, 201–202.
3. <http://www.esrl.noaa.gov/gmd/obop/mlo/>
4. Meehl et al., Chap. 10: Global Climate Projections, Sec. 10. ES: Mean Temperature, IPCC AR4 WG1, **2007**.
5. Inventory of U.S. Greenhouse Gas Emissions and Sinks. *EPA*. **2008**.
6. Bottoms, R. R. Process for Separating Acidic Gases. Girdler Corp., **1930**. *US Patent* 1783901.
7. Versteeg, G. F.; van Swaaij, W. P. M. On the Kinetics between CO₂ and Alkanolamines Both in Aqueous and Non–Aqueous Solutions — I. Primary and Secondary Amines. *Chem. Eng. Sci.* **1988**, *43*, 573–585.
8. Kohl, A. L.; Nielsen, R. B. Gas Purification. Gulf Publishing Company, Houston, 5th edition, **1997**.
9. Hikita, H.; Asai, S.; Katsu, Y.; Ikuno, S. Absorption of Carbon Dioxide into Aqueous Monoethanolamine Solutions. *AIChE J.* **1979**, *25*, 793–800.
10. Sada, E.; Kumazawa, H.; Butt, M. A. Gas Absorption with Consecutive Chemical Reaction: Absorption of Carbon Dioxide into Aqueous Amine Solutions. *Can. J. Chem. Eng.* **1976**, *54*, 421–424.
11. Mohammed A. J.; Rochelle, G. T. Absorption of CO₂ in Aqueous Diglycolamine. *Ind. Eng. Chem. Res.* **2006**, *45*, 2473–2482.
12. Versteeg, G. F.; van Swaaij, W. P. M. On the Kinetics between CO₂ and Alkanolamines Both In Aqueous and Non–Aqueous Solutions — II. Tertiary Amines. *Chem. Eng. Sci.* **1988**, *43*, 587–591.
13. Vaidya, P. D.; Kenig, E. Y. CO₂–Alkanolamine Reaction Kinetics: A Review of Recent Studies. *Chem. Eng. Technol.* **2007**, *30*, 1467–1474.
14. Xu, W.; Zhang, C. F.; Qin, A. J.; Wang, Y. W. Kinetics Study on Absorption of Carbon Dioxide into Solutions of Activated Methyl-diethanolamine. *Ind. Eng. Chem. Res.*, **1992**, *31*, 921–927.
15. Zhang, X.; Zhang, C. F.; Qin, S. J.; Zheng, Z. S. A Kinetics Study on the Absorption of Carbon Dioxide into a Mixed Aqueous Solution of Methyl-diethanolamine and Piperazine. *Ind. Eng. Chem. Res.*, **2001**, *40*, 3785–3791.

16. Jenab, M. H.; Abdi, M. A.; Najibi, S. H.; Vahidi, W. V.; Matin, N. S. Solubility of Carbon Dioxide in Aqueous Mixtures of N-Methyldiethanolamine + Piperazine + Sulfolane. *J. Chem. Eng. Data* **2005**, *50*, 583–586.
17. Ramachandran, N.; Aboudheir, A.; Idem, R.; Tontiwachwuthikul P. Kinetics of the Absorption of CO₂ into Mixed Aqueous Loaded Solutions of Monoethanolamine and Methyldiethanolamine. *Ind. Eng. Chem. Res.* **2006**, *45*, 2608–2616.
18. Glasscock, D. A.; Critchfield, J. E.; Rochelle, G. T. Absorption of Carbon Dioxide in Mixtures of MDEA with MEA or DEA. *Chem. Eng. Sci.* **1991**, *46*, 2829–2845.
19. Rangwala, H. A.; Morrell, B. R.; Mather, A. E. Absorption of CO₂ into Aqueous Tertiary Amine/MEA Solutions. *Can. J. Chem. Eng.* **1992**, *70*, 482–490.
20. Hagewiesche, D. P.; Ashour, S. S.; Al-Ghawas, H. A.; Sandall, O. C. Absorption of Carbon Dioxide into Aqueous Blends of Monoethanolamine and N-Methyldiethanolamine. *Chem. Eng. Sci.* **1995**, *50*, 1071 – 1079.
21. Rinker, E. B.; Ashour, S. S.; Al-Ghawas, H. A.; Sandall, O. C. Absorption of Carbon Dioxide into Aqueous Blends of Diethanolamine and Methyldiethanolamine. *Ind. Eng. Chem. Res.* **2000**, *39*, 4346–4356.
22. Horng, S.; Li, M. H. Kinetics of Absorption of Carbon Dioxide into Aqueous Solutions of Monoethanolamine + Triethanolamine. *Ind. Eng. Chem. Res.* **2002**, *41*, 257–266.
23. Zhang, X.; Zhang, C. F.; Liu, Y. Kinetics of Absorption of Carbon Dioxide into Aqueous Solution of Methyldiethanolamine Blended with Diethanolamine. *Ind. Eng. Chem. Res.* **2002**, *41*, 1135–1141.
24. Bishnoi, S.; Rochelle, G. T. Absorption of Carbon Dioxide into Aqueous Piperazine: Reaction Kinetics, Mass Transfer and Solubility. *Chem. Eng. Sci.* **2000**, *55*, 5531–5543.
25. Liao, C. H.; Li, M. H. Kinetics of Absorption of Carbon Dioxide into Aqueous Solutions of Monoethanolamine + N-Methyldiethanolamine. *Chem. Eng. Sci.* **2002**, *57*, 4569–4582.
26. Sartori, G.; Savage, D. W. Sterically Hindered Amines for Carbon Dioxide Removal from Gases. *Ind. Eng. Chem. Fundam.* **1983**, *22*, 239–249.
27. Huang, Y. M.; Soriano, A. N.; Caparanga, A. R.; Li, M. H. Kinetics of Absorption of Carbon Dioxide in 2-Amino-2-Methyl-L-Propanol +N-Methyldiethanolamine + Water. *J. Taiwan Inst. of Chem. Eng.* **2011**, *42*, 76–85.
28. Alper, E., Reaction Mechanism and Kinetics of Aqueous Solutions of 2-Amino-2-Methyl-L-Propanol and Carbon Dioxide. *Ind. Eng. Chem. Res.* **1990**, *29*, 1725–1728.
29. Chakraborty, A. K.; Astarita, G.; Bischoff, K. B. CO₂ absorption In Aqueous Solutions in Hindered Amines. *Chem. Eng. Sci.* **1986**, *41*, 997–1003.
30. Saha, A. K.; Bandyopadhyay, S. S.; Biswas, A. K. Kinetics of Absorption of CO₂ into Aqueous Solutions of 2-Amino-2-Methyl-L-Propanol. *Chem. Eng. Sci.* **1995**, *50*, 3587–3598.
31. Yih, S. M.; Shen, K. P. Kinetics of Carbon Dioxide Reaction with Sterically Hindered 2-Amino-2-Methyl-L-Propanol Aqueous Solutions. *Ind. Eng. Chem. Res.* **1988**, *27*, 2237–2241.
32. Zioudas, A. P. and Z. Dadach, Absorption Rates of Carbon Dioxide and Hydrogen Sulphide in Sterically Hindered Amines. *Chem. Eng. Sci.* **1986**, *41*, 405–408.

33. Baek, J. I.; Yoon, J. H. Solubility of Carbon Dioxide in Aqueous Solutions of 2-Amino-2-Methyl-1, 3-Propanediol. *J. Chem. Eng. Data* **1998**, *43*, 635–637.
34. Yoon, S. J.; Lee, H.; Yoon, J. H.; Shim, J. G.; Lee, J. K.; Min, B. Y.; Eum, H. M. Kinetics of Absorption of Carbon Dioxide into Aqueous 2-Amino-2-Ethyl-1,3-Propanediol Solutions. *Ind. Eng. Chem. Res.* **2002**, *41*, 3651–3656.
35. Jou, F. Y.; Otto, F. D.; Mather, A. E. Solubility of H₂S, CO₂, and Their Mixtures in an Aqueous Solution of 2-Piperidineethanol and Sulfolane. *J. Chem. Eng. Data* **1998**, *43*, 409–412.
36. Shen, K. P.; Li, M. H.; Yih, S. M. Kinetics of Carbon Dioxide Reaction with Sterically Hindered 2-Piperidineethanol Aqueous Solutions. *Ind. Eng. Chem. Res.* **1991**, *30*, 1811–1813.
37. Paul, S.; Ghoshal, A. K.; Mandal, B. Absorption of Carbon Dioxide into Aqueous Solutions of 2-Piperidineethanol: Kinetics Analysis. *Ind. Eng. Chem. Res.* **2009**, *48*, 1414–1419.
38. Li, Y. G.; Mather, A. E. Correlation and Prediction of The Solubility of CO₂ and H₂S in an Aqueous Solution of 2-Piperidineethanol and Sulfolane. *Ind. Eng. Chem. Res.* **1998**, *37*, 3098–3104.
39. Perrin, D. D. Dissociation Constants of Organic Bases in Aqueous Solutions. Butterworths, London, **1965**.
40. Ma'mun, S.; Dindore, V. Y.; Svendsen, H. F. Kinetics of the Reaction of Carbon Dioxide With Aqueous Solutions of 2-((2-Aminoethyl) Amino) Ethanol. *Ind. Eng. Chem. Res.* **2007**, *46*, 385–394.
41. Kim, I.; Svendsen, H. F. Heat of Absorption of Carbon Dioxide (CO₂) in Monoethanolamine (MEA) 2-(Aminoethyl) Ethanolamine (AEEA) Solutions. *Ind. Eng. Chem. Res.* **2007**, *46*, 5803–5809.
42. Hartono, A.; da Silva, E. F.; Svendsen, H. F. Kinetics of Carbon Dioxide Absorption in Aqueous Solution of Diethylenetriamine (DETA). *Chem. Eng. Sci.* **2009**, *64*, 3205–3213.
43. Aronua, U. E.; Svendsen, H. F.; Hoffb, K. A.; Juliussen, O. Solvent selection For Carbon Dioxide Absorption. *Energy Procedia*, **2009**, *1*, 1051–1057.
44. Li, J. L.; Henni, A.; Tontiwachwuthikul, P. Reaction Kinetics of CO₂ in Aqueous Ethylenediamine, Ethyl Ethanolamine, and Diethyl Monoethanolamine Solutions in The Temperature Range of 298–313 K, Using The Stopped-Flow Technique. *Ind. Eng. Chem. Res.* **2007**, *46*, 4426–4434.
45. Carson, J. K.; Marsh, K.N.; Mather, A. E. Enthalpy of Solution of Carbon Dioxide in (Water + Monoethanolamine, Or Diethanolamine, Or N-Methyldiethanolamine) and (Water + Monoethanolamine + N-Methyldiethanolamine at 298.15 K. *J. Chem. Therm.* **2000**, *32*, 1285–1296.
46. Patil, G. N.; Vaidya, P. D.; Kenig, E. Y. Reaction Kinetics of CO₂ in Aqueous Methyl- and Dimethylmonoethanolamine Solutions. *Ind. Eng. Chem. Res.* **2012**, *51*, 1592–1600.
47. Vaidya, P. D.; Kenig, E. Y. Absorption of CO₂ into Aqueous Blends of Alkanolamines Prepared From Renewable Resources. *Chem. Eng. Sci.* **2007**, *62*, 7344–7350.
48. Peng, Y. C.; Zhao, B. T.; Li, L. L. Advance in Post-combustion CO₂ Capture with Alkaline Solution: A Brief Review. *Energy Procedia*, **2012**, *14*, 1515–1522.

Chapter 2

2. Theory Background

Abstract

The rate of mass transfer is the one substantial issue of the gas absorption in liquid. The background theory of mass transfer was introduced and derived according to Fick's law and mass balance with the boundary conditions. The various conditions of the gas-liquid contact time (in a long/short time) are given as samples of stirred cell and laminar liquid jet. The theory will be applied in the calculation of the measurement of the physical properties such as diffusivity and the mass transfer kinetics of the absorption of a gas in a liquid with/without chemical reaction.

2.1. Mass Transfer without Chemical Reaction

The classical mass transfer theories for absorption are two–film theory by Lewis and Whitman,¹ the penetration theory by Higbie² and surface renewal theory by Danckwert.³

According to the two–film theory, the concentration profiles of CO₂ in gas phase and liquid phase without chemical reaction are illustrated in Figure 2.1.

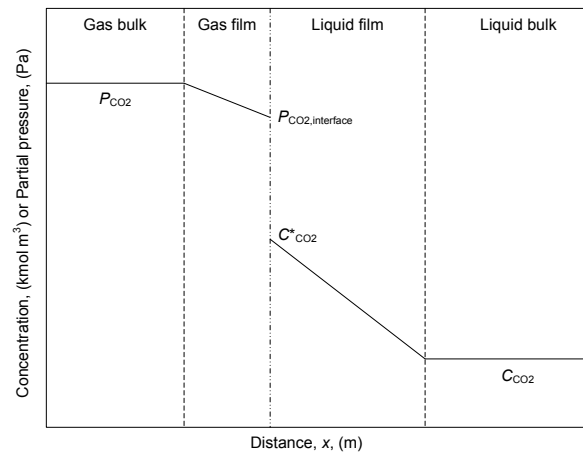


Figure 2.1 Illustration of the two–film model for the absorption of CO₂ in a liquid without chemical reaction

It is assumed that a gas is absorbed into a liquid with no chemical reaction takes place between the dissolved gas and the liquid. The liquid surface first contact with the gas at time $t = 0$, and it is assumed that from then on the concentration in the plane of the surface is uniformly equal to C^* . This concentration is assumed to be constant and corresponds to the physical solubility of the gas at the partial pressure on the liquid surface.

According to Fick's law,⁴ the absorption flux per unit area J_x or net rate of diffusion transfer across unit area of a plane perpendicular to the x –axis in the liquid film at a given moment is

$$J_x = -D_A \frac{\partial c}{\partial x} \quad (2.1)$$

Thus, the absorption flux per unit area J at the liquid surface and any time is

$$J = -D_A \left(\frac{\partial c}{\partial x} \right)_{x=0} \quad (2.2)$$

Assumed a differential element in the liquid film, combined the principle of mass balance, regarding the differential element, there is

$$[Diffusion\ in] - [Diffusion\ out] = [Accumulation]$$

which is described by

$$\left[-D_A \frac{\partial c}{\partial x} \right] + \left[D_A \left(\frac{\partial c}{\partial x} + dx \frac{\partial^2 c}{\partial x^2} \right) \right] = \left[dx \frac{\partial c}{\partial t} \right] \quad (2.3)$$

whence

$$D_A \frac{\partial^2 c}{\partial x^2} = \frac{\partial c}{\partial t} \quad (2.4)$$

For a smooth gas–liquid interface, the boundary conditions for the above absorption equation is

$$\left. \begin{aligned} c &= C^0, & x > 0, & t = 0 \\ c &= C^*, & x = 0, & t > 0 \\ c &= C^0, & x = \infty, & t > 0 \end{aligned} \right\} \quad (2.5)$$

Then, the numeric solution of equation (2.4) with the boundary condition equation (2.5) is ⁵

$$c - C^0 = (C^* - C^0) \operatorname{erfc} \left(\frac{x}{2\sqrt{D_A t}} \right) \quad (2.6)$$

It follows from equation (2.2) and equation (2.6) that

$$J = (C^* - C^0) \sqrt{\frac{D_A}{\pi t}} \quad (2.7)$$

Thus, the absorption flux per unit area is infinite when $t=0$, and decreases with time. The amount of gas absorbed per unit area of surface in time t is

$$Q = \int_0^t J dt = 2(C^* - C^0) \sqrt{\frac{D_A t}{\pi}} \quad (2.8)$$

It is assumed that $C^0=0$ when the liquid with very small gas loading, then

$$Q = 2C^* \sqrt{\frac{D_A t}{\pi}} \quad (2.9)$$

For a laminar jet, the area of a “rod–like” surface of the liquid is πdl , the total one–dementional flux R , $R=JA$, in a unit (mol s^{-1}), is given by

$$R = \frac{\pi dl Q}{t} \quad (2.10)$$

and the contact time by the laminar jet is given by

$$t = \frac{\pi d^2 l}{4q} \quad (2.11)$$

By combining equation (2.9), (2.10) and (2.11), the total rate of absorption is

$$R = 4C^* \sqrt{D_A q l} \quad (2.12)$$

Thus a plot of R vs. \sqrt{ql} at constant temperature and pressure should give a straight line through the origin, and has a slope $4C^* \sqrt{D_A}$. It is noted that the rate of absorption of a gas into a laminar liquid jet is independent of the diameter, so long as the velocity across any section is uniform, and the length of the free surface is not much different from the jet height.

Pohorecki⁶ employed a laminar jet absorber to investigate the mass transfer kinetics of CO_2 , H_2S and both of them simultaneous absorption in propylene carbonate modified with triethanolamine (TEA), respectively. He observed that the relationship of R vs. \sqrt{ql} shows distinct deviations from the values found for physical absorption and is most often nonlinear when the chemical reaction occurs between the absorbed gas and the solution components.

2.2. Mass Transfer with Chemical Reaction

The concentration profiles of CO_2 in gas phase and liquid phase and that of MEA the solution are shown in Figure 2.2 when the mass transfer is with chemical reaction. According to the principle of mass balance, when there is chemical reaction between the diffusant and liquid bulk, the difference between the rates of diffusion into and out of the element is equal to the sum of the accumulation and the rate of reaction.

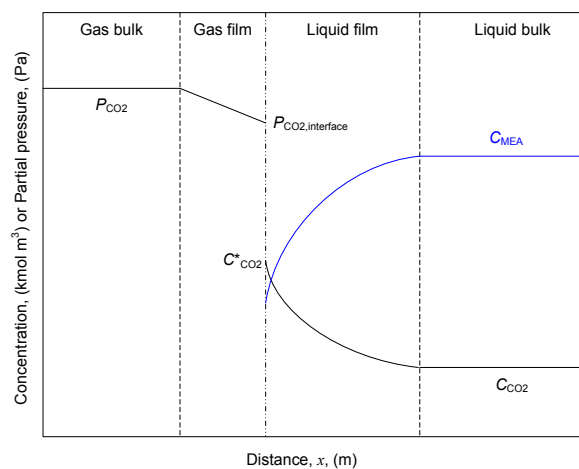


Figure 2.2 Typical concentration profiles of the absorption of the absorption of CO_2 in a MEA solution in fast chemical reaction regime

If the chemical reaction rate of a diffusant (per unit volume of liquid) in one–dimension at x is $r(x, t)$, according to the mass balance principle, regarding the differential element, there is

$$[\text{Diffusion in}] - [\text{Diffusion out}] = [\text{Accumulation}] + [\text{Reaction}]$$

In mathematical terms, the mass balance is

$$\left[-D_A \frac{\partial c}{\partial x}\right] + \left[D_A \left(\frac{\partial c}{\partial x} + dx \frac{\partial^2 c}{\partial x^2}\right)\right] = \left[dx \frac{\partial c}{\partial t}\right] + [r(x,t)dx] \quad (2.13)$$

then

$$D_A \frac{\partial^2 c}{\partial x^2} = \frac{\partial c}{\partial t} + r(x,t) \quad (2.14)$$

where $r(x, t)$ is the rate of a homogenous chemical reaction (per unit volume of liquid), which is consuming the solute gas in the liquid at time t and at a distance x below the surface. This rate generally depends on the local concentration of the gas, and of any other solute with which it reacts.

With respect to first–order reaction,

$$r = k_1 c \quad (2.15)$$

where k_1 is the reaction rate constant of first–order reaction, which the reaction rate is proportional to the concentration of the dissolved gas. Assuming $C^0 = 0$, with the boundary condition equation (2.5), the numerical solution of equation (2.14) is⁵

$$\frac{c}{C^*} = \frac{1}{2} e^{-x\sqrt{k_1/D_A}} \operatorname{erfc}\left(\frac{x}{2\sqrt{D_A t}} - \sqrt{k_1 t}\right) + \frac{1}{2} e^{x\sqrt{k_1/D_A}} \operatorname{erfc}\left(\frac{x}{2\sqrt{D_A t}} + \sqrt{k_1 t}\right) \quad (2.16)$$

Substituting equation (2.16) into equation (2.2), hence the result is⁵

$$J = C^* \sqrt{D_A k_1} \left[\operatorname{erf}(\sqrt{k_1 t}) + \frac{e^{-k_1 t}}{\sqrt{\pi k_1 t}} \right] \quad (2.17)$$

and

$$Q = C^* \sqrt{\frac{D_A}{k_1}} \left[(k_1 t + \frac{1}{2}) \operatorname{erf}(\sqrt{k_1 t}) + \sqrt{\frac{k_1 t}{\pi}} e^{-k_1 t} \right] \quad (2.18)$$

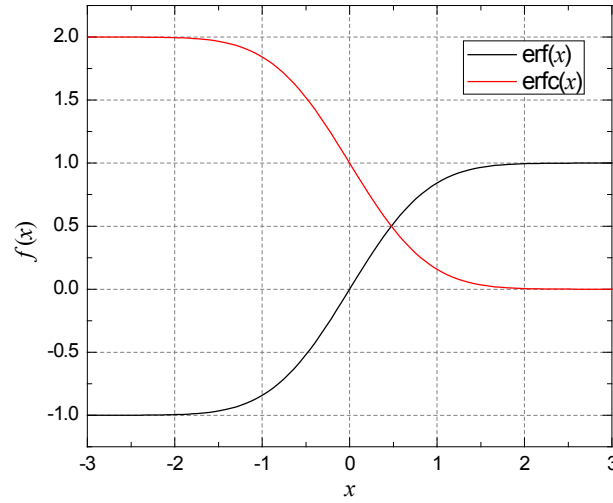


Figure 2.3 The plot of function $\text{erfc}(x)$ and $\text{erf}(x)$

As shown in Figure 2.3, the function $\text{erfc}(x)$ and $\text{erf}(x)$ approach 0 and 1 respectively when x is bigger than 2. Thus, when $k_1 t$ is large, the concentration distribution (c/C^*) will tend to a limiting value and no longer varies with time according to equation (2.16), and when $k_1 t \gg 1$,

$$\frac{c}{C^*} = e^{-x\sqrt{k_1/D_A}} \quad (2.19)$$

$$J = C^* \sqrt{D_A k_1} \quad (2.20)$$

$$Q = C^* \sqrt{\frac{D_A}{k_1}} \left(k_1 t + \frac{1}{2} \right) \quad (2.21)$$

This model can be used in the chemical kinetics measurement by stirred cell. Regarding total absorption amount per unit area (Q), when $k_1 t > 10$, the equation (2.21) can be simplified further as follows,

$$Q = (C^* \sqrt{D_A k_1}) t \quad (2.22)$$

If combining equations (2.22), (2.10) and (2.11), the total rate of absorption with chemical reaction using laminar jet is

$$R \approx dlC^* \sqrt{D_A k_1} \quad (2.23)$$

Plots of gas absorption rate against jet length in a figure will show a linear relationship consistent with the kinetic conditions underlying equation (2.23). Clarke⁷ carried out the kinetics measurement of the absorption of CO₂ with aqueous MEA solution with range from 1.6 to 4.9M, at short contact times of 3 to 20 msec, at gas pressures of 1 and 0.1 atm. with a fast chemical reaction taking place simultaneously. Absorption rates of gas at the lower pressure are in agreement with the penetration theory as equation (2.23) for pseudo-first-order reactions. Absorption at atmospheric pressure corresponds to a less amenable kinetic condition, since the concentration of un-reacted monoethanolamine at the interface becomes seriously depleted during even the shortest attainable contact time of gas and liquid, and heat of reaction appears to influence the observed rates of absorption. Thus, Clarke thought there is a limitation of application of equation (2.23) to the analysis given for the jet absorption data. He estimated the duration of gas-liquid contact required to effect a 10% depletion of chemical reagent at the interface, and proposed a relationship to correct it as follows:

$$0.1 = \frac{2C^*}{B_0} f(k_1 t) \quad (2.24)$$

where

$$f(k_1 t) = \begin{cases} \frac{k_1 t}{2}, & k_1 t < 1 \\ 2\sqrt{\frac{k_1 t}{\pi}} - 1, & k_1 t > 5 \end{cases} \quad (2.25)$$

For very short contact time or $k_1 t \ll 1$, for example, gas is absorbed in liquid measured by laminar jet or wetted-wall apparatus. Then, when $k_1 t \ll 1$,

$$J = C^* \sqrt{\frac{D_A}{\pi t}} (1 + k_1 t) \quad (2.26)$$

$$Q = 2C^* \sqrt{\frac{D_A t}{\pi}} \left(1 + \frac{k_1 t}{3}\right) \quad (2.27)$$

In practice, a truly first-order chemical reaction is very seldom encountered. Generally, a second-order reaction can be said to a pseudo-first order, which under certain situations the concentration of the reactant B may be almost uniform and the reaction rate of reactant A (i.e. dissolved gas) will then be approximately proportional to its local concentration. Then the above equations can be employed, and the reaction constant k_1 will be

$$k_1 = k_2 B_0 \quad (2.28)$$

A simple limiting kinetic condition exists if the diffusion rate of reagent to the reaction zone in the liquid is rapid relative to the consumption rate of reagent by chemical reaction with molecules of A. If the chemical reaction is fast, this condition may be observed only a very short contact times⁷, attainable by the laminar jet technique.

For any slow chemical reactions, there is only a small effect on the absorption rate. Haimour⁸ studied the gas absorption between CO₂ and MDEA by laminar jet apparatus, the gas–liquid contact time was short (< 0.012 s) and k_1 was not big yet, the reaction met the condition $k_1t \ll 1$, then, equation (2.27) can be applied. For this case, $k_1t/3$ is 0.03, and equation (2.27) can be simplified as follows,

$$Q \approx 2C^* \sqrt{\frac{D_A t}{\pi}} \quad (2.29)$$

The equation (2.29) is the same formula as equation (2.9), which describes the absorption with no chemical reaction, indicating that at these short contact times any reaction between CO₂ and MDEA does not influence the absorption rate.⁸

Nomenclature

A = area of the gas–liquid surface, (m²)

B_0 = concentration of amine in liquid phase, (mol L⁻¹)

c, C = molar concentration of a substance in a solution, (kmol m⁻³, mol L⁻¹)

C^* = concentration of solute gas in the liquid phase at gas–liquid interface, (mol L⁻¹)

C_0 = concentration of solute gas in the bulk of liquid phase, (mol L⁻¹)

d = diameter of the stirrer, (m)

D = diffusivity (m² s⁻¹)

D_A = diffusivity of gas A in a liquid, (m² s⁻¹)

J = the flux per unit area, (mol m⁻² s⁻¹)

k = chemical reaction rate constant.

k_1 = forward reaction rate constant with respect to C_{CO_2} , (s⁻¹)

k_2 = forward reaction rate constant with respect to C_{MEA} and C_{CO_2} , (m³ kmol⁻¹ s⁻¹)

l = jet length, (m)

q = flow rate of solution, (m³ s⁻¹)

Q = the amount of gas absorbed per unit area of the surface in time t , (mol m⁻²)

r = reaction rate (m³ kmol⁻¹ s⁻¹)

R = universal gas constant, =8.314, (Pa m³ K⁻¹ mol⁻¹)

R = the total one–dimensional flux, $R=JA$, (mol s⁻¹)

R_x = absorption rate at arbitrary position in the liquid, ($\text{mol m}^{-2} \text{s}^{-1}$)

t = contact time, (s)

T = temperature, (K)

x = the distance from the liquid surface, (m)

References

1. Lewis, W. K.; Whitman, W. G. Principles of Gas Absorption. *Ind. Eng. Chem. Res.* **1924**, *16*, 1215–1220.
2. Higbie, R. The rate of Absorption of a pure gas into a still liquid during short periods of exposure. *Trans. A. Inst. Chem. Eng.* **1935**, *31*, 365–383.
3. Danckwerts, P. V. Significance of liquid–film Coefficient in Gas Absorption. *Ind. Eng. Chem. Res.* **1951**, *43*, 1460–1467.
4. Cussler, E. L. Diffusion Mass Transfer in Fluid Systems, 3rd Edition, Cambridge University Press, **2009**.
5. Danckwerts, P. V. Gas–Liquid Reactions; McGraw–Hill: New York, **1970**.
6. Pohorecki, R.; Mozenski, C. A new absorbent for carbon dioxide and hydrogen sulphide absorption process. *Chem. Eng. Sci.* **1998**, *37*, 69–78.
7. Clarke, J. K. A. Kinetics of Absorption of CO_2 in Monoethanolamine Solution at Short Contact Time. *Ind. Eng. Chem. Fundam.* **1964**, *3*, 239–245.
8. Haimour, N.; Sandall, O. C. Absorption of carbon dioxide into aqueous methyldiethanolamine. *Chem. Eng. Sci.* **1984**, *39*, 1791–1796.

Chapter 3

3. Design and Validation of a New Apparatus for Physical Solubility Measurement

Abstract

A novel apparatus was designed and built for measuring the physical solubility of a gas in a liquid. A physical model was developed to treat the experimental data. This new experimental technique employs a scaled spiral glass tube with a small drop of mercury inside as a eudiometer instead of the classical three-branch U-tube setup to keep the system pressure constant and measure the volume drop of the gas at a constant temperature. The effect of insufficient saturation gas was investigated and the gas saturation method for the measurement was studied. To validate the new technique, the physical solubilities of N_2O in pure water over a temperature range from 298.15 to 323.15 K and in aqueous salt MEA solutions at 313.15 K were measured. Compared with the classical three-branch U-tube setup, the new setup and technique is easy to operate and more sensitive and accurate. The physical mass transfer coefficients of N_2O in aqueous MEA solutions were measured as well, which exhibits a little wide application scope of the new apparatus.

3.1. Introduction

Physical solubility is a key parameter requirement for interpreting diffusivity and reaction kinetics measurements, as well as for modeling and industrial design. Different principles and methods have been used to measure the physical solubility of gas in liquid^{1–16} based on two principle approaches. One is a “volumetric method”, namely, measuring the volume of the absorbed gas per unit volume of liquid at constant pressure and temperature. This method measures the absorbed volume of gas, so that the equilibrium molar concentration of gas in the solution can be obtained directly. The solubility can be represented by Henry’s law. In 1971, Weiland and Trass² set up a solubility measurement apparatus that employed a U–tube with a flexible tube and a glass buret filled with a lot of mercury to keep the absorption pressure constant by adjusting the mercury surface level. The apparatus was simple to set up. Volume of gas dissolved is read directly from the buret.

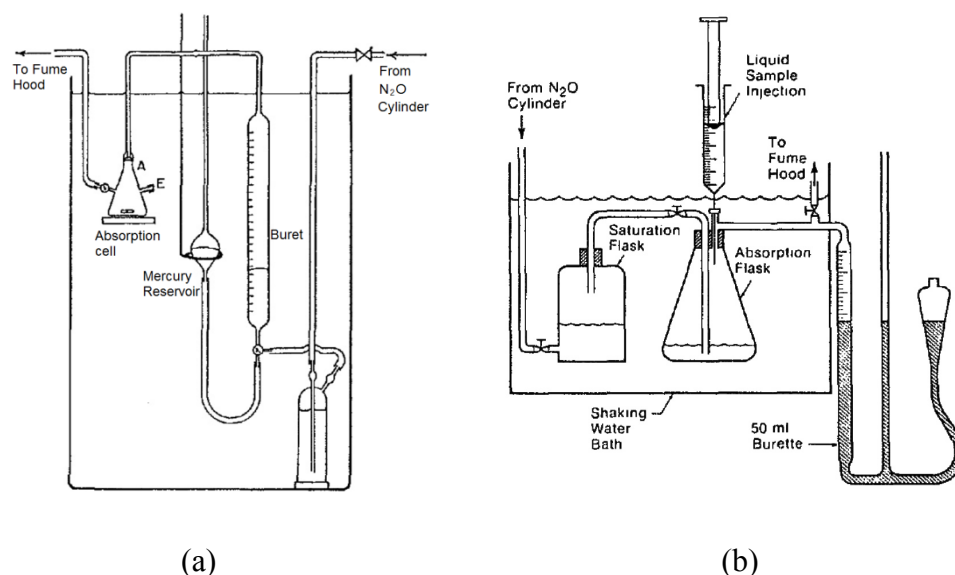


Figure 3.1 Solubility apparatus with two–branch U–tube by Weiland et al.² (a) and three branch U–tube by Haimour et al.³ (b)

Later researchers, Haimour and Sandall³, developed the apparatus from two–branch to three–branch to make the measurement accurate, as shown in Figure 3.1(b). However, in these cases, the eudiometer tube was kept outside of the thermostated water bath and the gas in the buret tube could affect the gas temperature in the absorption cell. In order to obtain a stable temperature, in 1989, Al–Ghawas⁵ put the whole setup including the mercury U–tube into the water bath, measured the solubility of CO₂ (or N₂O) in several aqueous amine solutions at different temperatures, as shown in Figure 3.2. Henceforward, this type setup is employed for the measurement of physical solubility of gas in liquid by later researchers^{7–14}.

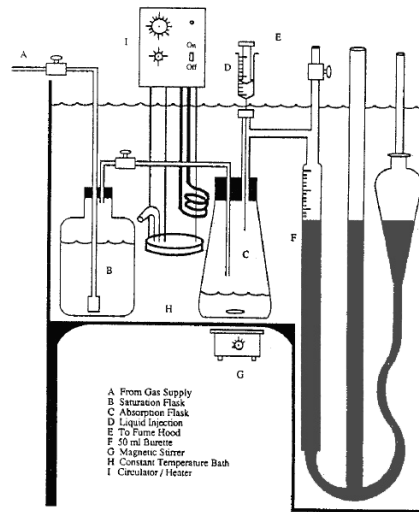


Figure 3.2 Solubility apparatus with three branches U-tube immersed in a water bath developed by Al-Ghawas et al.⁵

However, for this kind of absorption apparatus, it is cumbersome to keep the mercury surface at the same level in the three branches throughout the experiments. The operator must adjust the mercury reservoir to keep three mercury surfaces at the same level every 2 minutes during the measurement. It is noticed that the absorption rate is too high in the beginning of the measurement to operate the U-tube quickly enough for height adjustment to keep the pressure constant. On the other hand, the absorption rate is too low to accurately determine the end point in a three-branch U-tube. An undesirable feature of the mercury U-tube technique is the need to keep a substantial quantity of mercury in the apparatus.

The other principle technique for solubility measurements is a “pressure drop method”, which measures the pressure drop of the gas at constant volume and temperature. The solubility is then derived through the gas state equations and a model as follows,¹

$$H_A = \frac{P_A^{\text{end}} RT}{(P_A^{\text{ini}} - P_A^{\text{end}})} \cdot \frac{V_L}{V_G} \quad (3.1)$$

where H_A is Henry’s constant and P_A^{end} and P_A^{ini} are the partial pressures of the gas A at absorption equilibrium and before the absorption starts, respectively. V_L and V_G are the volumes of liquid and gas during the measurement, respectively. T is the temperature of the system, and R is the gas constant. Versteeg and van Swaaij¹ and Park and Sandall¹⁷ used the pressure drop method to measure the solubility by measuring the change in partial pressure of a gas before and after absorption in aqueous amine solutions. With this method, the pressure

is allowed to drop and asymptotically approach the end pressure, which is also the equilibrium pressure. This method demands very accurate pressure measurements to ensure a high accuracy. In the present work, a volumetric method was developed to reduce the mercury requirement of the apparatus to one small drop.

In this work, a novel absorption apparatus based on the principle of the volumetric method was designed and validated by measuring the physical solubilities of N₂O in water at temperatures from 298.15 to 323.15 K under a constant ambient pressure. In addition, the physical mass transfer coefficient of a gas in a liquid can be measured by this apparatus when the absorbed volume of gas as a function of time is recorded. The physical solubilities of N₂O in (salt + MEA + water) solutions were performed at 298.15 K as well.

3.2. Description of the Equipment and Principle

The novel absorption apparatus is based on the principle of volumetric method and a schematic diagram of the absorption apparatus is shown in Figure 3.3. The key parts of the absorption cell, including bottles, pipes, joints, and valves, were made of glass or metal. Rubber or plastic tubes were avoided to prevent gas leaks or diffusion from the cell during the absorption process, because it takes a long time to reach equilibrium for the absorption of a gas in a liquid (In particular, it will take about 24 hr for a high-viscosity liquid). The main differences of the solubility cell shown in Figure 3.3, compared with those of previous researchers,²⁻¹⁴ are as follows: A scaled spiral tube (with an inner diameter of 4 mm and a volume of 18 mL) was employed as a volumetric meter instead of the three-branch U-tube. A mercury droplet (approximately 2 g) was placed in this clean spiral tube, which was laid horizontally in a transparent water bath. The mercury droplet could move from the initial position B towards the end point A when the gas absorption in the liquid is taking place in the absorption cell.

The total volume of the closed gas system including the absorption cell and connecting pipe was 132 mL. The tube end beyond point B of the spiral tube was raised out of the water bath and open to the atmosphere to keep the pressure of the absorption cell constant and equal to room pressure. A small shaking motor was mounted on the end of the spiral tube to shake the tube and make the mercury droplet move more smoothly. The accuracy of temperature control by the water bath was ± 0.1 K.

Compared with the conventional U-tube method, this novel technique has some advantages, such as easy operation, lower mercury inventory, higher sensitivity and greater accuracy.

The equipment consists of major systems as follows:

- 1) Absorption cell
- 2) Data Acquisition system
- 3) Gas and liquid feed system
- 4) Temperature Control System
- 5) Vacuum system

The specifications of the main parts of the new solubility cell are listed in Figure 3.1. Each of the individual systems will be discussed in this section.

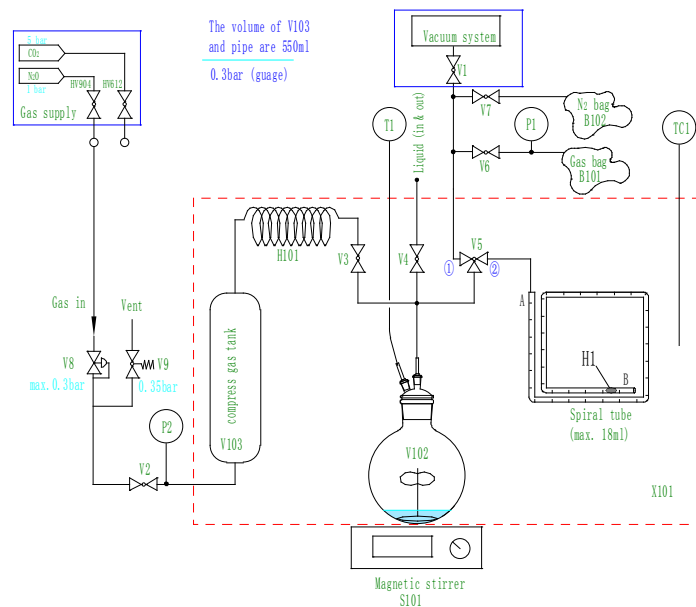


Figure 3.3 Schematic diagram of the physical absorption measurement apparatus:

X101, transparent water bath; V104, scaled spiral glass tube volumetric meter; H1, mercury droplet; V102, absorption cell with stirrer and gas stirring blades; S101– magnetic stirrer; TC1, thermal controller; T1, gas thermometer; P1/ P2, gas manometer; B101, gas bag (N₂O or CO₂); B102, N₂ bag; V103, compress gas tank; H101, copper pipe coil.

3.2.1. Absorption Cell

The absorption cell is the mass transfer place of the gas and liquid. The cell system is made up of following components:

- 1) Absorption bottle
- 2) The glass–metal joint of the cap of the absorption bottle
- 3) Liquid phase stirrer and gas phase stirrer
- 4) Magnetic stirrer system
- 5) Support system of the absorption bottle

The absorption bottle is a 100 mL glass round bottle made by Buchi, Switzerland. Because the cell is vacuumed to a very low pressure during measurement, a round bottle is chosen for safety. A magnetic stirrer as liquid phase stirrer is put on the bottom of the round bottle, and a Teflon sheet size 30mm x 15mm as the gas phase stirrer which is joined the magnetic stirrer with a steel wire, as shown in Figure 3.3. The gas stirrer is used for stirring the gas to approach quickly the temperature equilibrium and gas–liquid equilibrium.

Table 3.1 Specification of the novel solubility measurement equipment

No.	Equipment system	Component or specification	Manufacturer and model
1	Absorption bottle	100 mL	Buchi
2	Magnetic stirrers	100 –1000 rpm	IKA–WERKE, GMBH & CO.
3	Support of the absorption bottle	By aluminum	Made by our self
4	Water bath (Thermal controller)	20 –80 °C	Huber D77656 (Upgradeable CC–Pilot Controllers–112A)
5	Spiral tube	Scaled 18 mL max.	Made by Statoil glass workshop
6	Data Logger	Data collection card with 20 channel	Agilent, 34970
7	Thermo–couple	Type K	
8	Vacuum equipment (R–210/215)	Vacuum pump	Buchi V–710
		Vacuum controller	Buchi V–850
		Rota–vapor	Buchi R–210
		Heating bath	Buchi B–491
9	Pressure gauge (P1)	0 – 250 Pa (g)	Magnehelic
10	Pressure gauge (P2)	0 – 2.5 bar (g)	Swagelok
11	Weight indicator	Precision balance	Mettler Toledo XS403S
12	Gas storage tank	375 mL, 15 bar, steel	Swagelok
13	Valves and steel pipes	1/8', 1/16'	Swagelok
14	Glass–metal joint	1/8'	Made by Statoil glass workshop

To prevent gas leaks or diffusion from the valves and pipes during the absorption process, rubber or plastic tubes and joints were avoided and all the parts were made of glass or metal. The joints of the cell with steel pipes were made of glass–metal joint (see Figure 3.4) which was provided by the glass workshop of Statoil AS, Norway. A kind of hard hot–melt glue was used to fix the cap and the round bottle to avoid gas leaks. If we want to dismount the cap, we can put the bottle into an oven, and the hard glue can melt when temperature is higher than 120 °C.

Because the glass–metal joint is brittle, the absorption bottle with the cap and joints were all mounted on an aluminum frame. Figure 3.5 shows the design drawing of the frame. Valves 3 and 4 (shown in Figure 4.1) were mounted on the aluminum frame as well, this assembly can avoid the torque force acting on the glass–metal joints when operating the valves.

All the parts such as absorption chamber, pipes, valves and the aluminum frame support are immersed into the water bath to keep the all experimental temperature of the system identical.

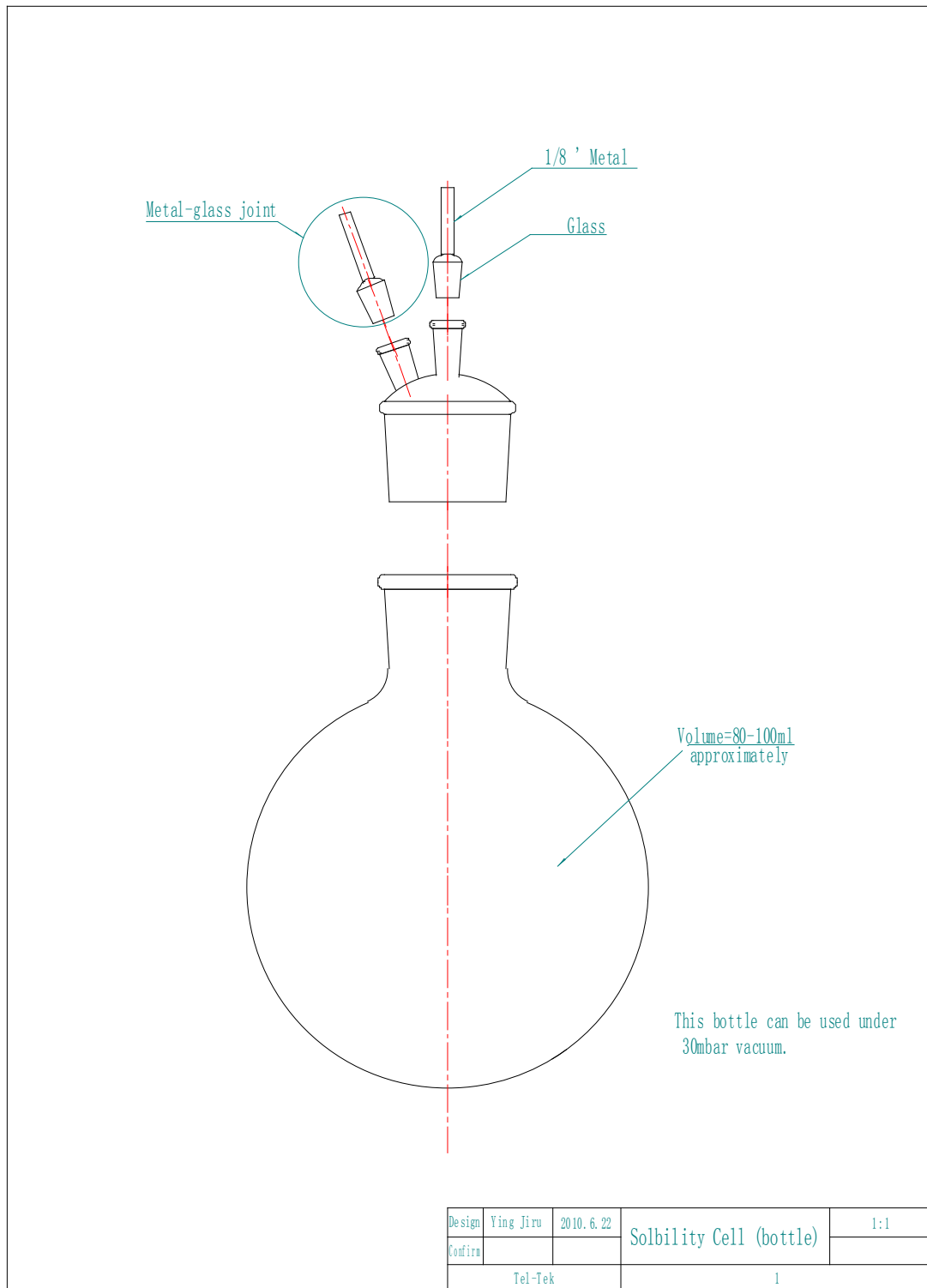


Figure 3.4 Design drawing of the absorption bottle

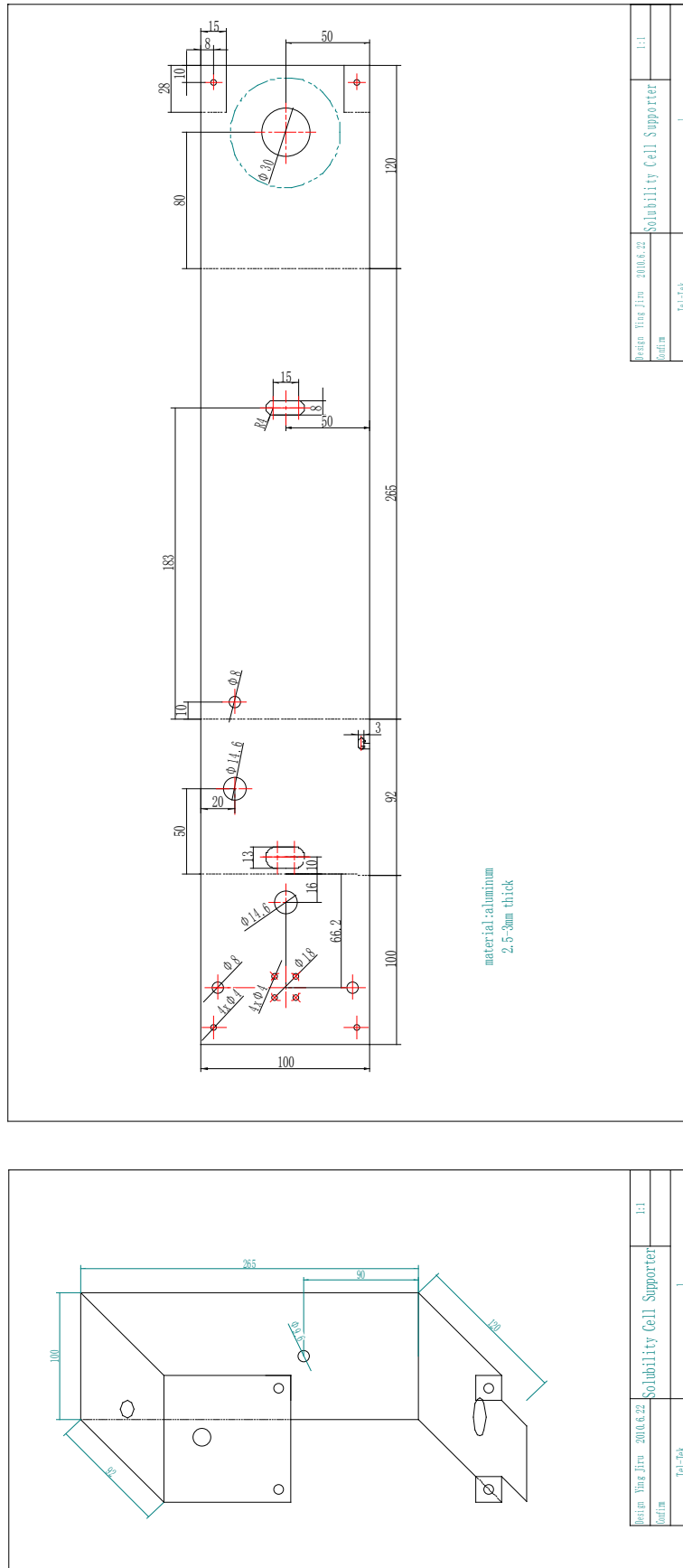


Figure 3.5 Design drawing of the absorption cell support

3.2.2. Data Acquisition System

The data acquisition system includes temperature monitor system and a gas absorbed volume record system. The temperature monitor system is a data logger with the two thermocouples (type K). One thermocouple is used to monitor the gas temperature in the absorption cell; the other is used for monitoring the temperature of the water bath, which can describe the liquid temperature in the absorption cell in practice. The logger frequency is adjustable from 0.1 s to several hours.

The gas absorbed volume record system includes a clean scaled spiral glass tube and a “volume record” software written by myself. The available volume scale of the spiral tube is 18 mL, which means the maximum measured gas volume of the spiral tube is limited to 18 mL. The design drawing of the spiral tube is shown in Figure 3.6. Both the ends of the spiral tube are spherical, (See Figure 3.6), this shape is a so called “mercury trap”, which prevents the mercury drop to blow (or suck) out of the tube. The bottom of the trap is just a little lower than the bottom of the tube, then the mercury can return into the tube easily and form a mercury drop. The spiral tube is mounted on the inner-wall of the water bath tank and placed absolutely horizontally. The tank of the water bath is made of polycarbonate and the wall is transparent, this ensures that the movement of the mercury drop can be observed easily.

Because the surface tension between mercury and glass is very low, the mercury drop can easily be formed in this 4 mm-id pipe and seal the gas, and the friction of mercury drop on the surface of glass is low. To make the movement of the mercury drop in the glass tube easily and smoothly during the measurement, a shaking motor is mounted on the tube end which is out of the water bath. The resistance caused by the friction can thus lessen further. The resistance was estimated experimentally in this work. When the shaking motor was turned on, the error caused by the resistance of the mercury drop movement was less than 0.1 kPa (the pressure difference between in the absorption cell and in the room). The method for measuring the resistance is as follows:

- 1) To dismount the gas bag B101 and close the port.
- 2) To open valve V6 and valve V5 to ensure the gauge P1 is opened to the cell V102 and the spiral tube V104.
- 3) To suck the cell V102 softly and read the pressure gauge P1 to measure how much pressure difference can make the mercury droplet move.

The maximum pressure difference is 0.1 kPa in the measurement, which can be used to characterize the resistance of the mercury droplet movement. Compared to the atmospheric

pressure (101.3 kPa), this resistance is very small and its uncertainty to the measurement is small (see the section 4.4 uncertainty analysis).

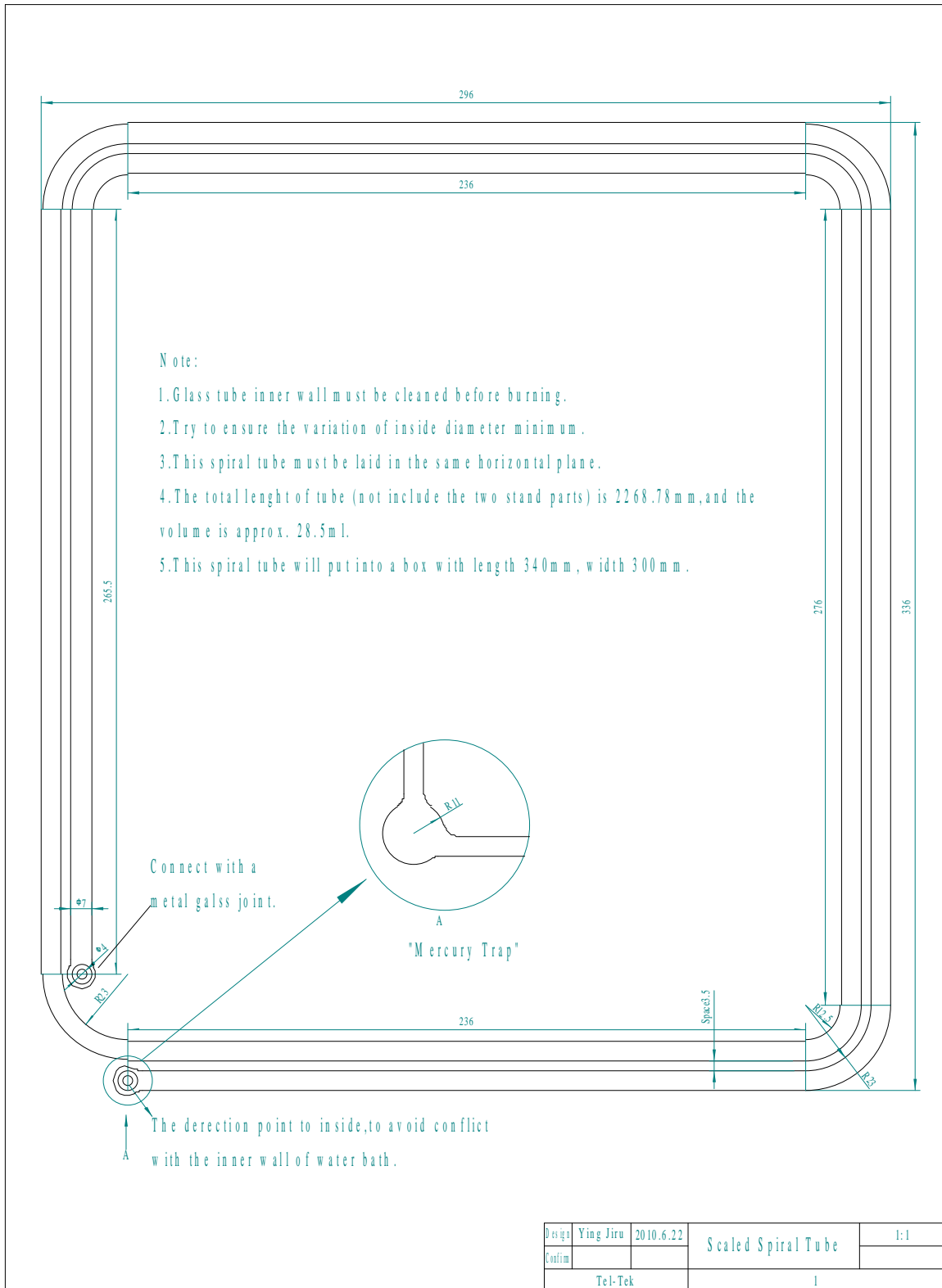


Figure 3.6 Design drawing of the scaled spiral glass tube

The position of the mercury in the spiral tube is monitored and recorded by a kind of software named “V–T Rec.,” which is written by me in Visual FoxPro language. The software can manage the whole procedure, record the relationship of the position of the mercury versus time during measurements, and calculate the Henry’s constant according to the experimental data and the conditions. The operation interface of the software is as follows,

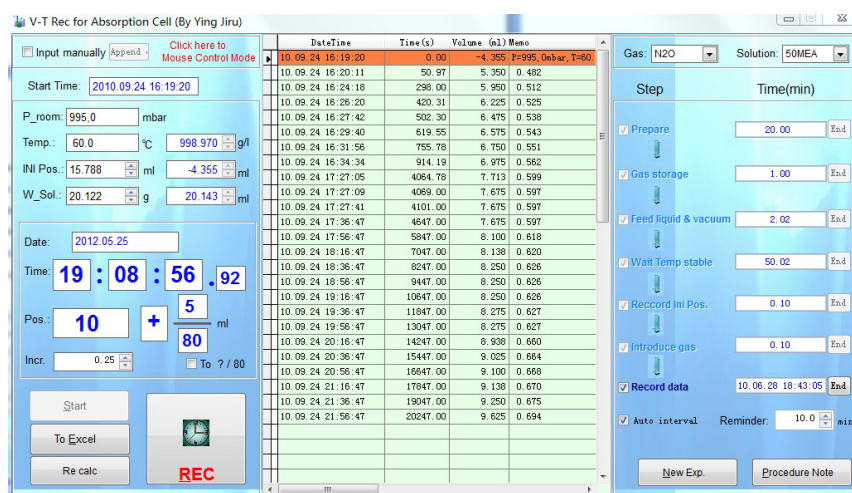


Figure 3.7 The operation interface of the software “V–T Rec.”

The software can call a sub-program named “Auto photo” to record the position information of the mercury. The sub-program is also written in Visual FoxPro. The main function of this sub-program is to control a camera to take pictures automatically in a given interval. The interface of the software is shown in Figure 3.8. The key code of both the software “V–T Rec.” and the sub-program “Auto photo” are presented in the Appendix A13.



Figure 3.8 The interface of the sub-program “Auto Photo” for capturing the position of the mercury drop of the novel solubility measurement setup

3.2.3. Liquid and Gas Feed System

The liquid feed system is very simple. The weighed solution to be investigated is injected (by a syringe) into the absorption cell where the cell is full with N_2 . The solution in the cell could be vacuumed to the vapor pressure of the solution of the desired temperature, and heated by the water in the bath till the temperature achieves the desired temperature.

The gas feed system is composed of

- 1) Compress gas storage tank (V103) and Coil copper coil (H101),
- 2) Pressure gauge (P2, range 0 – 2.5 bar)
- 3) Pressure gauge (P1, range 0 – 250 Pa)
- 4) Gas supply from the lab
- 5) Safety valve (V9), adjustable needle valve (V8) and other ball valves
- 6) The gas bags

The gas to be investigated is supplied by the gas supply system of the lab. The safety valve and adjustable needle valve provide stable low pressure gas. The compressed gas storage tank and coil copper pipe are mounted in the water bath and used to store the gas to be investigated under pressure about 0.3 bar (g) during measurement. The total volume of the tank and the coil is big enough to reduce pressure and temperature overshoot when introducing gas into the absorption cell. (A pressure overshoot investigation by a stirred cell is presented in the appendix A4). The pressure of the gas in the storage tank is monitored by the pressure gauge (P2), which pressure range is 0 to 2.5 bar (g).

After the gas is introduced into vacuumed absorption cell, the target pressure in the cell should be room pressure. At this time, the gas pressure in the cell is monitored by the pressure gauge (P1), which measuring range is small but accurate. The rest gas could flow to the soft gas bag B101 to help obtaining a room pressure in the cell during introducing gas into the cell.

3.2.4. Temperature Control and Vacuum System

The thermo controller (type D77656) of the water bath is provided by Huber, German. The temperature control accuracy of the water bath is ± 0.1 K. All parts relative to the gas and liquid are immersed in the water bath for keeping the experimental gas and liquid temperature identical. This kind of assembly ensures the uncertainty caused by temperature fluctuation is the lowest possible.

The vacuum system is made up of vacuum pump, condenser pipe, and buffer bottle. The vacuum pressure can be controlled precisely by a V–850 pressure control system produced by Buchi, Switzerland.

3.3. The Determination of Gas Saturation Method

How much the effect of the insufficiently saturated gas used on the solubility measurement is an important factor to be investigated first. Here, we assume that there is a closed bottle only with liquid inside and V_0 is the volume of the bottle except the liquid. After enough vaporization at a given temperature, n mole solution vapor is vaporized in the bottle, the vapor pressure is P_{vap} , and volume of this n mole vapor at room pressure is assumed V_{vap} . Then, according to the mass balance and gas–state equations, the follow equation is obtained.

$$P_{\text{room}} V_{\text{vap}} = P_{\text{vap}} V_0 \quad (3.2)$$

where P_{vap} , P_{room} are the saturated vapor pressure and room pressure at a given temperature, respectively. The vapor volume at room pressure V_{vap} is then

$$V_{\text{vap}} = \frac{P_{\text{vap}} V_0}{P_{\text{room}}} \quad (3.3)$$

In practice, the gas in the bottle includes the desired gas (N_2O or CO_2) and vapor under room pressure. Table 3.2 lists the vapor fraction (V_{vap}/V_0) in the gas of the bottle at various temperatures. It can be seen that the influence of the gas saturation on the measurement is low when the experimental temperature is low, for instance, at 25°C , $P_{\text{room}}=1$ bar, the value of V_{vap}/V_0 is small, just 3.17% and 2.98% for water and 3 M aqueous MEA solution, respectively. However, when the temperature is 70°C , the value of V_{vap}/V_0 is large, reach 31.18% and 29.32% for water and 3 M aqueous MEA solution, respectively.

Table 3.2 The influence of no saturated gas used on the solubility measurement

T/ °C	P_{vap} of water /bar	V_{vap}/V_0	P_{vap} of 3M aq. solution/bar	V_{vap}/V_0
25	0.0317	3.17%	0.0298	2.98%
40	0.0738	7.38%	0.0693	6.93%
50	0.1234	12.34%	0.1160	11.60%
60	0.1993	19.93%	0.1874	18.74%
70	0.3118	31.18%	0.2932	29.32%

The results show that the higher the temperature and the lower concentration are, the larger the influence of insufficient saturated gas used on the solubility measurement is. Therefore, gas saturation is important in the measurement of gas–liquid mass transfer.

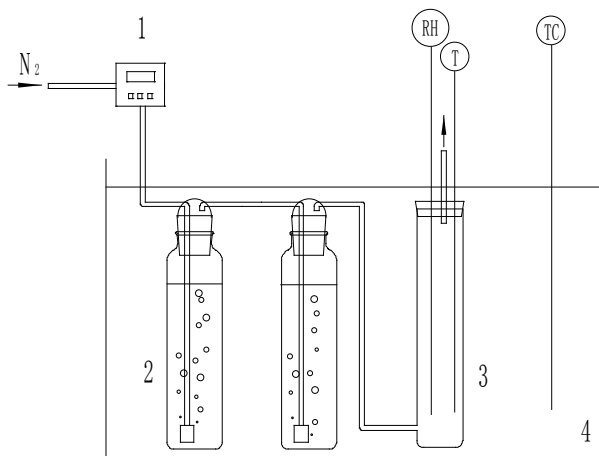


Figure 3.9 Gas saturation apparatus with two wash bottle filled with water:

1, mass flow meter; 2, wash gas bottle; 3, gas buffer bottle; 4, water bath; RH, relative humidity meter

The conventional method of gas saturation is that the gas goes through water (or solution) in a gas wash bottle at the given temperature for a while as shown in Figure 3.9. By this set-up, the known flow rate of dry N_2 goes through two wash gas bottle for 15 min to 15 hours, the relative humidity of the gas in the gas buffer bottles was measured. The experimental result shows that the relative humidity only achieved 80% for 15 hr, it is difficult to produce 100% RH in several hours by this way.

Table 3.3 The relative humidity of the gas saturated by vacuum method

No.	RH	$T_{liq}/^{\circ}C$	$T_{gas}/^{\circ}C$	Note*
1	90.6%	23.3	24.6	After 30 min, the Pressure rise to 21.5 kPa
2	91.2%	23.3	24.6	After 15 min, the Pressure rise to 16.5 kPa. Both T sensor and H sensor of the RH meter in gas phase
3	98.9%	23.3	24.6	T sensor was in liquid and H sensor was in gas phase.
4	94.5%	23.3	24.6	After 30 min, the Pressure rise to 26.9 kPa. Both T sensor and H sensor in gas phase
5	98.6%	24.2	24.6	T sensor was in liquid and H sensor was in gas phase.

*The RH meter includes a temperature sensor and a humidity sensor

Figure 3.10 is a setup that consists of gas storage tank, liquid vaporizing cell and gas bag. During an experiment, the liquid vaporizing cell is vacuumed at a given temperature (i.e. $23.3^{\circ}C$) to 3 kPa (the saturated vapor pressure is 2.99 kPa at this temperature), then close the

liquid vaporizing cell. After a certain time, the pressure of the gas in the cell increases and finally reaches a constant (equilibrium) value. Then the valves V2 and V4 are opened and dry N_2 is introduced from the gas storage tank into the cell to room pressure. The RH and temperature of the gas are recorded by the RH meter as the pressure is at room pressure. The result is shown in Table 3.3.

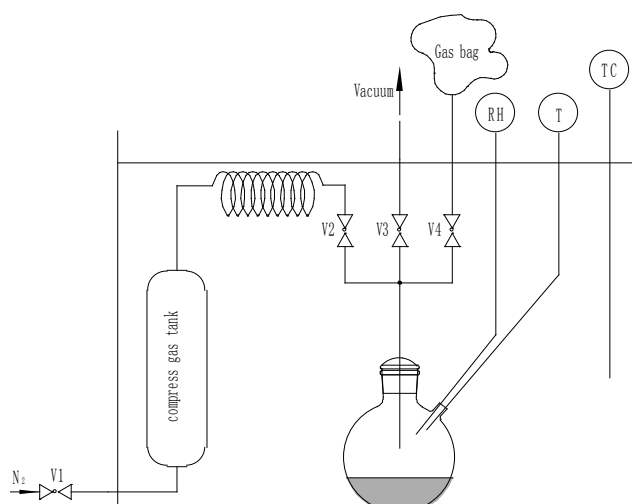


Figure 3.10 “Vacuum method” setup for gas saturation measurement

The gas phase can almost achieve 100% relative humidity using vacuum method in 30 min. This implies that the vacuum method can obtain saturated gas for solubility measurement. Then the vacuum saturation method will be employed in this work.

3.4. Operation of Equipment and the Procedure of the Measurement

Regarding the sequence of feeding the gas and liquid, the experimental procedure described in the literature²⁻¹⁴ is that the gas (N_2O or CO_2) is introduced into the cell first and then the liquid is injected. This could cause errors for the following reasons: First, it is difficult to make the gas fully saturated. As above mentioned, we attempted to produce 100% relative humidity (RH) saturated gas by blowing N_2 into a gas wash bottle with a 20-cm height of water for 15 hr, but only 80% RH was achieved. (See the section 3.2.2). Lack of saturation can cause an error, especially at higher experimental temperatures. Second, the method neglects the amount of absorption occurring while the liquid is being injected. This would introduce some errors, especially in the situation in which a small amount of solution is used. To avoid the gas saturation problem and the error of neglecting absorption while liquid is being injected, the liquid is added to the absorption cell first because it is faster to inject the gas. The cell is then vacuumed to the saturation vapor pressure of the liquid at the

experimental temperature. After the gas–liquid equilibrium and system thermal equilibrium have been reached, the gas to be investigated is introduced. In addition, this method of vacuuming to obtain saturated gas is faster than the traditional method in which the gas passes through a wash bottle.

For each run with the new technique, the gas tank (V103 with a volume including the connecting piping system of 550 mL) and the scaled spiral tube (V104) are filled the desired gas (N_2O or CO_2), and the dried and clean absorption cell V102 is filled with N_2 . The gas tank V103 is filled with gas to 30 kPa (gauge pressure) and keeps in the water bath to reach the desired temperature.

A precise weight (approximately 15 g) of freshly degassed aqueous MEA solution of the desired concentration is weighed on an analytical balance (Mettler Toledo XS403S) with an accuracy ± 1 mg and then feed into cell V102 in the N_2 gas atmosphere by a syringe. Cell V102 is vacuumed quickly down to the saturation vapor pressure of the solution. (To reduce the loss of vapor, the time to reach vacuum should be less than 1 min.). Then, the liquid is kept in the vacuum state for at least 20 min to wait for the system to reach its desired temperature and gas liquid equilibrium. The gas–phase stirrers are joined to the liquid–phase stirrer bar and are kept at 60 rpm to ensure a uniform liquid and gas phase temperature in the cell. The liquid stirrer is a 3–cm–long magnetic bar driven by an external magnet.

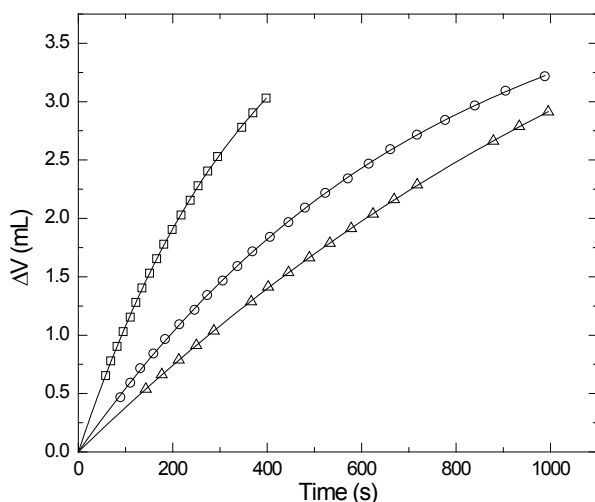


Figure 3.11 Absorbed volume of N_2O in aqueous MEA solution as a function of time at beginning of the absorption under ambient pressure at 323.15 K:

□, 3M; ○, 5M; △, 12M; the solid line was fitted by cubic regression equation

The initial position of the mercury droplet is recorded after the whole system had reached its thermal equilibrium. Then, the gas is introduced into V102 from gas tank V103. The pressure in V102 is ensured to be equal to the atmospheric pressure at the beginning by

connecting this vessel to the gas bag (B101); 15–20 s is allowed for this step to avoid pressure and temperature overshoot. A correction could be made for the quantity of gas absorbed during this 15–20 s by fitting the following several minutes of data on the absorbed gas volume as function of time to a cubic regression equation. (An example is shown in Figure 3.11).

Then, the absorbed volume of gas is recorded as function of time while the mercury droplet moves in the spiral tube during the absorption process. It takes about 5 to 24 hr to reach equilibrium for each absorption experiment. (How long the measurement takes depends on the temperature and concentration, with less time generally being needed at high temperature and low concentration).

The pressure difference between the two sides of the mercury droplet is less than 0.1 kPa during the absorption process as mentioned in section 3.2.2. The room pressure is recorded at the beginning ($P_{\text{room}}^{\text{ini}}$) and end ($P_{\text{room}}^{\text{end}}$) of the measurement.

The procedure of the physical solubility measurement is shown in the following block Figure 3.12.

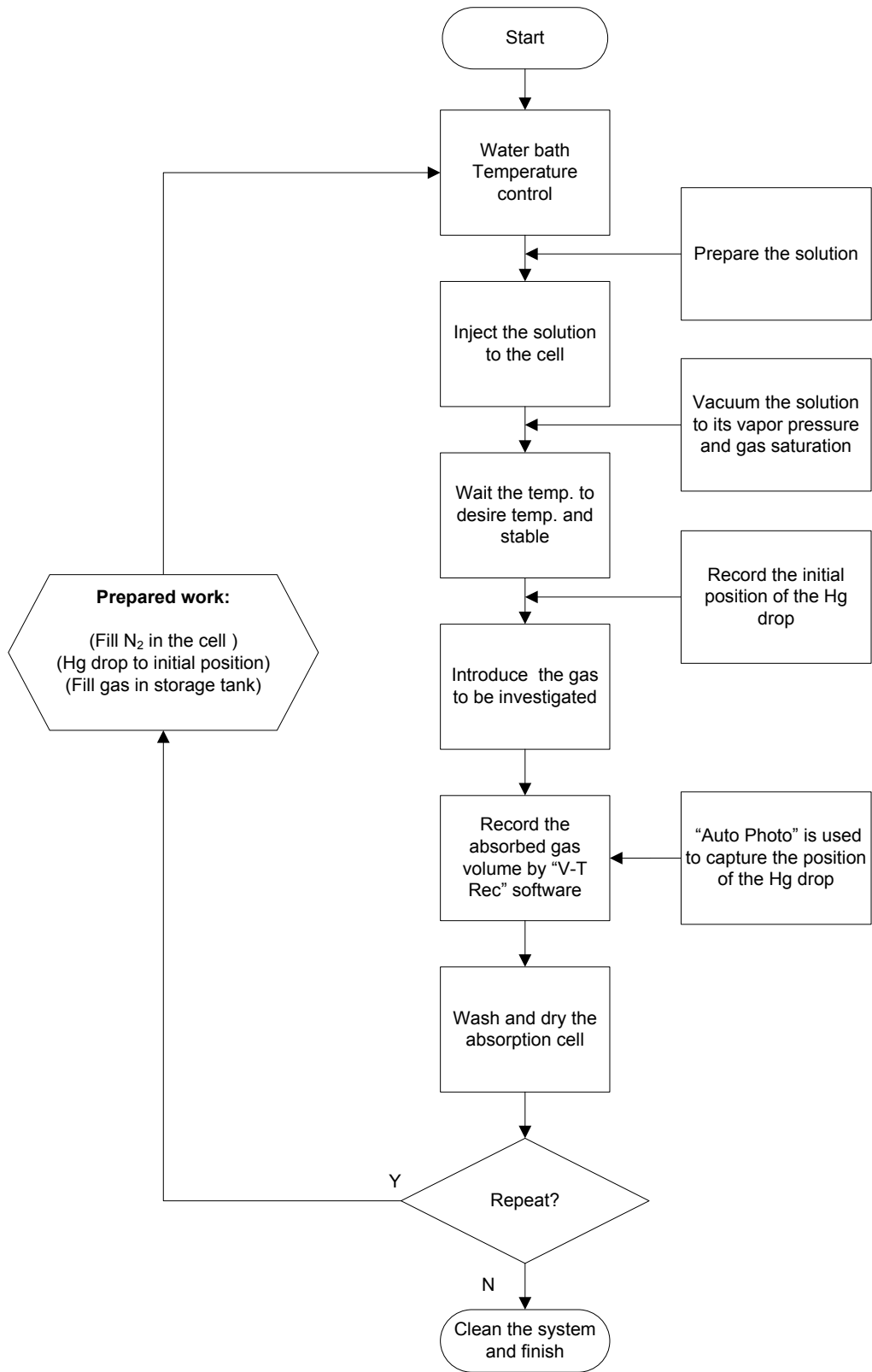


Figure 3.12 The procedure block diagram of the physical solubility measurement

3.5. Measurement Data

3.5.1. Measurement Data of Physical Solubility

The measurement data of physical solubility is the absorbed volume of the gas in the known volume solution under room pressure at the temperature range from 293.15 to 343.15 K. The temperature measuring range is limited by the water bath tank, which is made of polycarbonate. The detailed data need be recorded during the measurement include

- 1) The volume of the gas in the absorption cell and spiral tube (the position of the mercury drop) at the beginning of the absorption, V_G^{ini}
- 2) The volume of the gas in the absorption cell and spiral tube (the position of the mercury drop) at the end of the absorption, V_G^{end}
- 3) Room pressure at the beginning of the absorption, $P_{\text{room}}^{\text{ini}}$
- 4) Room pressure at the end of the absorption, $P_{\text{room}}^{\text{end}}$
- 5) The experimental temperature, T
- 6) The volume of the liquid, V_L
- 7) The relationship of gas absorbed volume and time at the beginning of the absorption for 10 min, V_A vs. t

3.5.2. Measurement Data of Physical Mass Transfer

Regarding the measurement of the mass transfer of a gas in a liquid, the measurement data is the relationship of gas absorbed volume and time at the beginning of the absorption. The detail of the experimental data need be recorded during the measurement are

- 1) The position of the mercury drop at the beginning of the absorption, V_G^{ini}
- 2) Room pressure at the beginning of the absorption, $P_{\text{room}}^{\text{ini}}$
- 3) The area of the interface of the gas and the liquid, A
- 4) The experimental temperature, T
- 5) The relationship of gas absorbed volume and time at the beginning of the absorption for 30 s, V_A vs. t

3.6. Treatment and Mathematical Description for Data

3.6.1. Physical Solubility

The physical solubility of gas A in a liquid can be expressed using Henry's law constant H_A as

$$H_A = P_A / C_A^* \quad (3.4)$$

where the partial pressure, P_A , of gas A at the experimental conditions is given by

$$P_A = P_{\text{room}}^{\text{end}} - (x_{\text{H}_2\text{O}} P_{\text{H}_2\text{O}}^{\text{v}} + x_{\text{MEA}} P_{\text{MEA}}^{\text{v}}) \quad (3.5)$$

where $P_{\text{H}_2\text{O}}^{\text{v}}$ is the vapor pressure of pure water, $P_{\text{MEA}}^{\text{v}}$ is the vapor pressure of pure MEA; and $x_{\text{H}_2\text{O}}$ and x_{MEA} are the mole fractions of water and MEA, respectively. Absorption data in the form of the volume of gas A per volume of liquid (V_A/V_L) were recorded in this experiment. If it is assumed that the room pressure is constant during the measurement and that the volume of liquid (V_L) is unchanged after absorption of the gas, then the concentration (C_A^*) at the absorption equilibrium is

$$C_A^* = n_A / V_L \quad (3.6)$$

According to the ideal gas state law, which describes the gas is in the spiral tube at room pressure.

$$P_{\text{room}}^{\text{end}} V_A = n_A RT \quad (3.7)$$

The solubility, which is described by Henry's constant H_A of gas A, can then be calculated for this measurement as

$$H_A = \frac{P_A}{C_A^*} = \frac{P_A RT}{P_{\text{room}}^{\text{end}} (V_A / V_L)} \quad (3.8)$$

If the room pressure is different between the beginning and end of the measurement, the absorbed volume of the gas should be corrected.

Figure 3.13 is the schematic drawing for calculating the correct volume of gas absorption. It is assumed that the temperature of the system is constant, and $P_{\text{room}}^{\text{ini}}$ is higher than $P_{\text{room}}^{\text{end}}$. Then the state of the gas in the cell is ($P_{\text{room}}^{\text{ini}}$, V_G^{ini} , T) at the beginning of the measurement, and ($P_{\text{room}}^{\text{end}}$, V_G^{end} , T) at the end of the measurement. The volume of the gas at

beginning is assumed V_G' under the pressure that equals to $P_{\text{room}}^{\text{end}}$, this gas state is $(P_{\text{room}}^{\text{end}}, V_G', T)$, and the increment of the gas volume because of the difference of the room pressure at the beginning and end of the measurement is ΔV , then

$$P_{\text{room}}^{\text{ini}} V_G^{\text{ini}} = P_{\text{room}}^{\text{end}} V_G' \quad (3.9)$$

and

$$\Delta V = V_G' - V_G^{\text{ini}} = \frac{P_{\text{room}}^{\text{ini}} V_G^{\text{ini}}}{P_{\text{room}}^{\text{end}}} - V_G^{\text{ini}} \quad (3.10)$$

Then, the corrected absorption volume of the gas, V_A , is

$$V_A = V_A^{\text{exp}} + \Delta V = V_A^{\text{exp}} + V_G^{\text{ini}} \left(\frac{P_{\text{room}}^{\text{ini}}}{P_{\text{room}}^{\text{end}}} - 1 \right) \quad (3.11)$$

where V_A^{exp} is the experimental volume of absorbed gas A, and V_G^{ini} is the gas volume in the absorption cell at the beginning of the measurement.

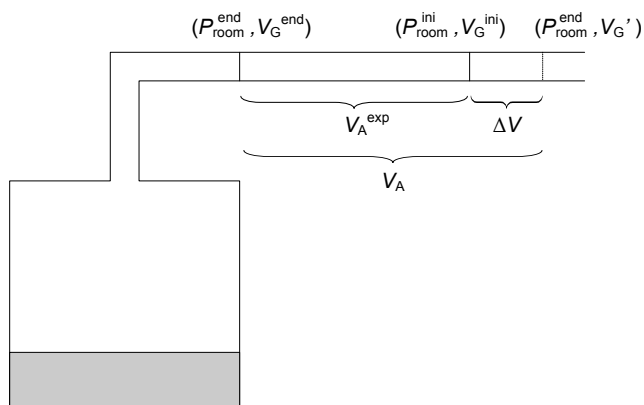


Figure 3.13 Model schematic diagram for calculating the correct volume of gas absorption for the situation of difference exists between initial and end room pressure

When the gas is introduced into V102 from gas tank V103, 10–20 s is allowed the cell opening to the atmosphere open to avoid pressure and temperature overshoot. Then the absorbed gas volume could not be recorded. This volume is corrected by fitting the following several minutes of data on the absorbed gas volume as function of time to a cubic regression equation. (Three examples are shown in Figure 3.11).

3.6.2. Mass Transfer

The mass transfer of a gas in a liquid can be measured by this absorption cell setup. The measurement is based on volumetric method, which measures the absorbed gas under a constant pressure. According to the mass transfer equation¹⁸

$$-\frac{dn_A}{dt} = k_L A (C_A^* - C_A^b) \quad (3.12)$$

where k_L is the physical mass transfer coefficient of the gas in the liquid. From the ideal gas state equation, the moles of the absorbed gas is

$$n_A = \frac{PV_A}{RT} \quad (3.13)$$

When the pressure of the gas to be investigated is constant, and it is assumed that $C_A^b \approx 0$, then

$$-\frac{dn_A}{dt} = -\frac{P}{RT} \frac{dV_A}{dt} = k_L A (C_A^* - 0) \quad (3.14)$$

C_A^* is calculated from Henry's law, $C_A^* = P/H_A$, then

$$V_A = \int_0^t \frac{RATk_L}{H_A} dt \quad (3.15)$$

After integration of equation (3.15),

$$V_A = \frac{RATk_L}{H_A} t + V_0 \quad (3.16)$$

or

$$(V_2 - V_1) = \frac{RATk_L}{H_A} (t_1 - t_2) \quad (3.17)$$

Plotting the relationship of the absorbed gas volume V_A vs. time or $(V_2 - V_1)$ vs. $(t_1 - t_2)$, the slope can be obtained, and then the physical mass transfer coefficient can be determined.

3.7. Experimental Section

3.7.1. Reagent and Solution Preparation

Deionized water (purified with a mini-Q system, conductivity of $18.2 \text{ M}\Omega\cdot\text{cm}$) was used for measuring the physical solubility N_2O in water. Reagent-grade MEA with a purity of $\geq 99.5 \text{ mass } \%$ was obtained from Merck and used without further purification. The sodium chloride (NaCl) with a purity of $\geq 99.5 \text{ mass } \%$ was purchased from Merck, Germany, and copper chloride (CuCl_2) is analytical pure, were obtained from BDH Prolabo, Belgium. The deionized water and MEA were degassed by application of a vacuum and then mixed to prepare various concentrations of (water + MEA) and (water + salt + MEA) solutions using an analytical balance and a 50 mL volumetric flask. The prepared solution was stored in three syringes and kept in a nitrogen atmosphere bag. The whole preparation process was carried out under a nitrogen atmosphere. The purity of N_2O is $\geq 99.7 \text{ mol } \%$, and was acquired from AGA Gas GmbH.

3.8. Results and Discussion

3.8.1. Validation for the Novel Technique

Figure 3.14 shows the typical profiles of absorbed volume per volume of liquid versus time for N_2O in pure MEA at different temperatures. It can be seen that the most parts of the absorption were achieved in 3 hours. But it could take a long time (i.e. 24 hr) to reach the absorption equilibrium, especially for high viscosity liquid at low temperature.

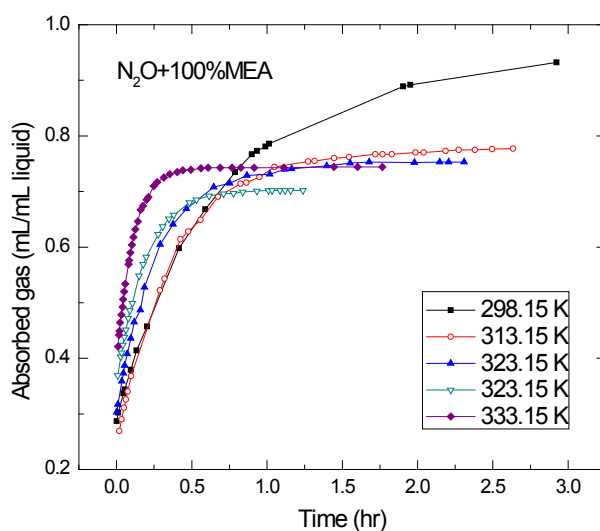


Figure 3.14 Typical curve of absorbed gas volume vs time of the measurement of physical solubility. (N_2O was absorbed in pure MEA from 298.15 to 333.15K)

To validate the novel solubility apparatus and procedure, the physical solubilities of N_2O and CO_2 in pure water were measured. The measured solubilities of N_2O in water at 298.15, 303.15, 313.15, and 323.15 K along with literature results are shown in Figure 3.15. The comparison between the literature values and the values obtained in this study for the solubilities of N_2O in water are presented in Figure 3.15 and Table 3.4. It can be seen that there is a good agreement between literature values and those of the present study, indicating that the novel technique is good and reliable for measuring the solubility of gases in liquids. The solubility data with respect to temperature can be represented by an exponential model, as shown in Figure 3.15. The solid lines are the regression models based on the experimental data of this work. The fitted equations are as follows

$$H_{N_2O,H_2O} = 8.449 \times 10^6 \exp(-2283/T) \quad (3.18)$$

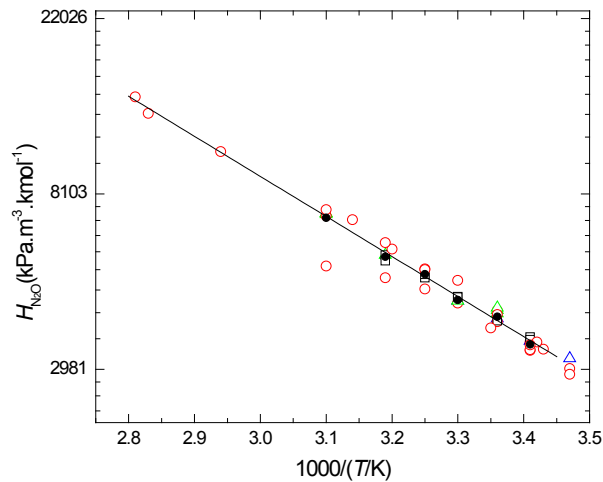


Figure 3.15 Physical solubility of N_2O in H_2O as a function of temperature compared with literature values by decade: \circ , 1980s^{1,3,5}; Δ , 1990s^{4,6,9,10,12}; \square , 2000s^{8,11}; \bullet , this work; The solid line was calculated using equation (3.18)

Table 3.4 Physical solubility of N₂O in H₂O measurement compared with literature values

<i>T</i> /K	<i>H</i> /kPa·m ³ ·kmol ⁻¹										
	ref.1	ref.3	ref.4	ref.5	ref.6	ref.8	ref.9	ref.10	ref.11	ref.12	This work
288.15		2992	3172	2897							
291.2	3344										
292.15	3484										
292.9	3333										
293.15	3425	3482	3506	3321		3581			3530		3433
298.15	4132	4169	3982	3910		4091	4101	4179	3932	4234	4022
298.6	3774										
302.9	4950										
303.15			4408	4350	4406	4512			4497		4422
308.15	5263	5284		4711		5023			5120		5124
312.9	5917										
313.15	6061			5021	5725	5715			5535		5660
318.15	6993										
322.6	7143										
322.9	7407										
323.15				5369	7264		7214	7260			7070
328.15											
333.15											
340.15	10309										
343.15											
353.15	12821										
355.4	14085										

3.8.2. Physical Solubility of N₂O in Aqueous Salt MEA Solutions

To validate the application of the new setup, physical solubility of N₂O in aqueous salt MEA solutions were conducted. Most research focused on the solubility of CO₂ in salt water solutions, aqueous amino acid salt solutions. Weisenberger and Schumpe¹⁹ reported the solubilities of twenty-two gases in dozens of aqueous salt solutions. Harned and Davis²⁰ investigated the physical solubility of CO₂ in aqueous salt solutions and Kumar et al.²¹ studied the solubility of N₂O in aqueous amino acid salt solutions. The physical solubility of CO₂ or N₂O in (water + salt + MEA) solution is not found in the present literature. However, it is common that some salts could be dissolved in the absorbent in the industrial process and causes more or less effect on the solubility of the gas in the absorbent. In this section, the solubilities of N₂O in various salt solutions (NaCl and CuCl₂) and (salt + aq. 5 M MEA) solutions were measured at 313.15 K under room pressure by the new solubility cell.

It is well known that with the increasing salt concentration, gas solubility is nearly always found to decrease, which is called the “salting-out” effect. The effect can be described in the form of the Sechenov relation, as shown in equation (3.19), when the salt concentration is equal to or lower than 5 M.¹⁹

$$\log\left(\frac{H_{A,m}}{H_{A,0}}\right) = KC_s \quad (3.19)$$

where $H_{A,0}$ is the solubility (Henry’s constant) of gas A in the solution without salt ions, $H_{A,m}$ is the solubility (Henry’s constant) of gas A in solution with salt ions, respectively. In this work, the definitions of $H_{A,0}$ and $H_{A,m}$ are extended to (salt + aq. MEA) solution. C_s is the molarity of the salt solution. K is the “Sechenov constant”,¹⁹ is specific to the gas and the salt, as shown in Figure 3.16.

Schumpe²² suggested a consistent model for mixed electrolyte solutions as follows

$$\log\left(\frac{H_{A,m}}{H_{A,0}}\right) = \sum (h_i + h_G)C_i \quad (3.20)$$

where h_i and h_G are the ion-specific and gas-specific parameter, C_i is the concentration of ion i respectively. For a single salt, the Sechenov constant K is then given by the following relation:

$$K = \sum (h_i + h_G)n_i \quad (3.21)$$

where n_i is the index of ion i in the formula of the salt. The gas-specific constant h_G is a linear function of the temperature:

$$h_G = h_{G,0} + h_T(T - 298.15 \text{ K}) \quad (3.22)$$

where the temperature of 298.15 K is employed as the reference $h_{G,0}$.

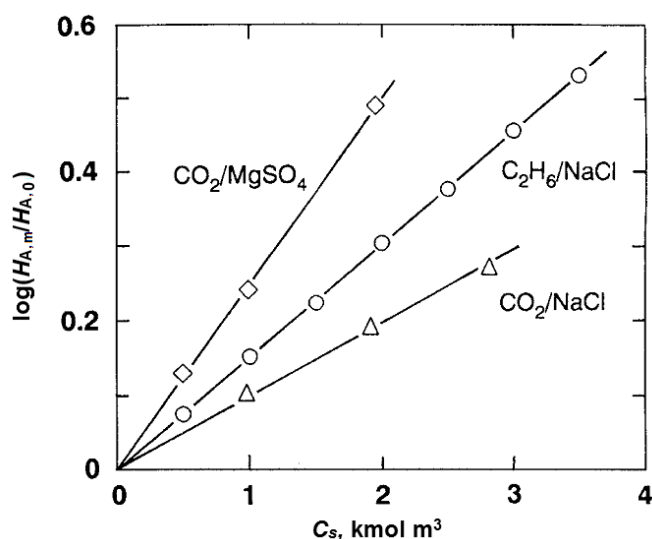


Figure 3.16 Sechenov plots for various gas/salt systems at 313.15 K (Markham and Kobe, 1941; Mishnina et al., 1961)¹⁹

The solubilities of N_2O in aqueous NaCl solutions and (NaCl + aq. 5 M MEA) solutions were measured at 313.15 K and the results are listed in Table 3.5 and plotted in Figure 3.17. It can be seen that the Henry's constants of N_2O in (NaCl + H_2O) and (NaCl + H_2O + MEA) solutions increase with the increasing concentration of NaCl; this implies that the solubilities of N_2O in aqueous NaCl solutions decrease with the increasing concentrations of NaCl. These results are in agreement with the so called "salting-out" effect. In addition, it can be found from Figure 3.17 that the "salting-out" effects of NaCl on the solubility of N_2O in H_2O and aqueous 5 M MEA solutions are almost same.

Table 3.5 The solubility of N_2O in aqueous NaCl and (NaCl + aq. 5 M MEA) solutions at 313.15 K

C_{NaCl} (mol L ⁻¹)	H_{N_2O} (kPa·m ³ kmol ⁻¹)	
	aq. NaCl	NaCl+ aq. 5M MEA
0.0	5660	5831
1.0	8007	7925
2.0	10220	10126
3.0	12789	12632

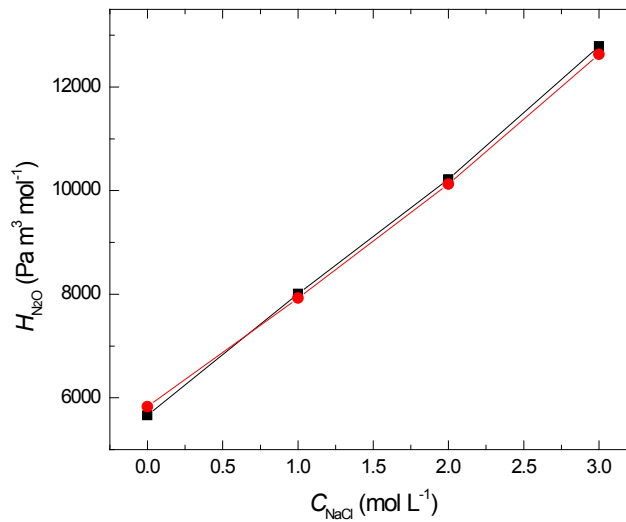


Figure 3.17 The solubilities of N_2O in aq. NaCl solutions and (NaCl + aq. 5 M MEA) solutions at 313.15 K
 ■, $\text{H}_2\text{O}+\text{NaCl}$; ●, NaCl+aq. 5 M MEA.

Figure 3.18 and Table 3.6 are shown the solubility of N_2O in (CuCl_2 + aq. 5 M MEA) solutions at 313.15 K. The “salting-out” effect plays a role on the solubility of N_2O in (CuCl_2 + aq. 5 M MEA) solutions and the trend of the solubility is as same as in aqueous NaCl solution and (NaCl + aq. 5 M MEA) solutions. But the “salting-out” effect caused by CuCl_2 is much stronger than NaCl, this comparison result can be explained by the Sechenov constant K of the two solution systems as shown in Figure 3.19 and Table 3.8.

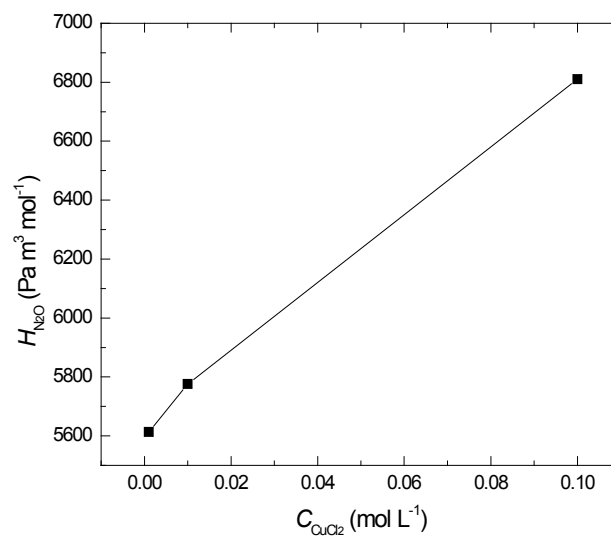


Figure 3.18 The solubilities of N_2O in aq. CuCl_2 +5 M MEA solutions at 313.15 K

Table 3.6 The solubility of N₂O in (CuCl₂ + aq. 5 M MEA) solutions at 313.15 K

C_{CuCl_2} mol L ⁻¹	$H_{\text{N}_2\text{O}}$ of CuCl ₂ +5M MEA kPa·m ³ kmol ⁻¹
0.001	5613
0.01	5776
0.1	6810

The relationship of $\log(H_{\text{N}_2\text{O},m}/H_{\text{N}_2\text{O},0})$ versus C_s are plotted in the Figure 3.19. The K values were fitted by linear regression with going through zero, and the results are shown in Table 3.8. The K values relative to NaCl in water and aqueous 5 M MEA solution are very close, but The K value relative to CuCl₂ in aqueous 5 M MEA solution is much higher than that of NaCl, this indicates that the “salting-out” effect caused by CuCl₂ (or Cu²⁺) is much stronger than that of caused by NaCl (or Na⁺).

Table 3.8 lists the K values experimentally determined and calculated by equation (3.21) of N₂O in aqueous salt and (salt+ aq. 5 M MEA) solutions at 313.15 K. The model parameters of Schumpe equation (3.20) – (3.22) for the ions, Na⁺, Cu²⁺, Cl⁻ and N₂O are obtained from the data reported by Weisenberger and Schumpe¹⁹ and tabulated in Table 3.7. It can be seen that the experimentally determined K values of NaCl agree with the K values calculated by equation (3.21). However, the experimental determined K value of CuCl₂ in the aqueous 5 M MEA solution, 0.662 m³ kmol⁻¹, is much higher than the calculated value, 0.184 m³ kmol⁻¹. The reason of this big difference maybe caused by the existence of chemical reaction between MEA + H₂O solution and Cu²⁺ as follows:



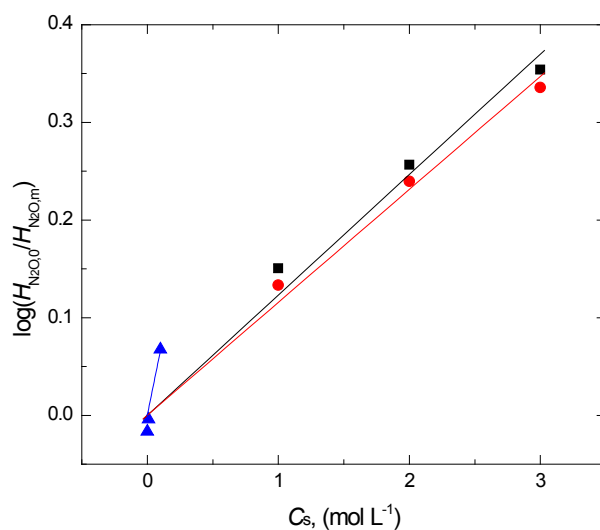


Figure 3.19 Sechenov plots for N_2O + salt (MEA) systems at 313.15 K
 ■, H_2O + NaCl; ●, NaCl + aq. 5 M MEA; ▲, CuCl_2 + aq. 5 M MEA;
 Solid lines are fitted by equation (3.20)

Table 3.7 The model parameters of Schumpe equation²²

Ion or gas	h_i ($\text{m}^3 \text{ kmol}^{-1}$)	$h_{G,0}$ ($\text{m}^3 \text{ kmol}^{-1}$)	h_T ($\text{m}^3 \text{ kmol}^{-1} \text{ K}^{-1}$)	$h_{G,313.15}^*$ ($\text{m}^3 \text{ kmol}^{-1}$)
Na^+	0.1143	—	—	—
Cl^-	0.0318	—	—	—
Cu^{2+}	0.1675	—	—	—
N_2O	—	-0.0085	-0.000479	-0.01569

* Calculated from equation (3.22)

Table 3.8 The K values of experimental determined and calculated by equation (3.21) of N_2O in aq. salt and (salt+ aq. 5 M MEA) solutions at 313.15 K

Solutions	$K_{\text{exp.}}$ ($\text{m}^3 \text{ kmol}^{-1}$)	$K_{\text{cal.}}$ ($\text{m}^3 \text{ kmol}^{-1}$)
NaCl+ H_2O	0.123	0.115
NaCl+aq.5 M MEA	0.116	0.115
CuCl_2 +aq.5 M MEA	0.662	0.184

3.8.3. Mass Transfer Coefficient of N₂O in Aqueous MEA Solutions

The new absorption cell can be used for measuring the mass transfer coefficient. The model has been developed in section 3.6.2. The dimensions of the absorption cell are presented in Table 3.9.

Table 3.9 Dimensions of the absorption cell

Parameters	Symbol	Value	Unit
Volume of the cell and pipes	V	0.132×10^{-6}	m^3
Volume liquid phase	V_L	0.015×10^{-6}	m^3
Interfacial area	A	9.4×10^{-4}	m^2
Stirrer revolutions per second (rps)	ω	1	s^{-1}
Diameter of liquid stirrer	d	3×10^{-2}	m

When the relationship of gas absorbed volume and time at the beginning of the absorption for 30 s is recorded, the mass transfer coefficient can be estimated by the equation (3.16) or (3.17). Plotting the relationship of the absorbed gas volume V_A vs. time or $(V_2 - V_1)$ vs. $(t_1 - t_2)$, the slope can be obtained, and then the physical mass transfer coefficient can be determined when the solubility is known.

The physical mass transfer of N₂O in aqueous MEA solutions over the full concentration range at temperatures from 298.15 to 323.15 K under the stirrer speed 1 rps were measured to estimate k_L . These data of the absorbed volume of N₂O versus time were obtained at the beginning 30 s during the physical solubility measurement, which will be presented in chapter 4. The relationships of V_A versus time were plotted and regressed to obtain the slope (in equation (3.16)). Then, the liquid-side mass transfer coefficients were calculated. The results are listed in Table 3.10.

A well-known correlation with respect to the Sherwood (Sh) number to the Reynolds (Re) and Schmidt (Sc) numbers can be applied to the absorption cell, the equation is

$$Sh = c_1 + c_2 Re^{c_3} Sc^{c_4} \quad (3.26)$$

The equation is discussed further in the section 7.4.4.

Table 3.10 Overview of results of the liquid-side mass transfer coefficient and Re , Sc and Sh numbers of the absorption cell

No.	C_{MEA} mol L ⁻¹	T K	Slope 10 ⁻⁹ m ³ s ⁻¹	$H_{\text{N}_2\text{O}}$ Pa m ⁻¹ mol ⁻¹	ρ kg m ⁻³	μ 10 ⁻⁴ pa s	D_A 10 ⁻⁹ m ² s ⁻¹	k_L 10 ⁻⁵ m s ⁻¹	Re	Sc	Sh
1	0	298.15	11.90	4022	997	0.909	1.78	2.05	9871	51	346
2	3	298.15	9.14	4221	1004	1.591	1.41	1.66	5679	112	352
3	5	298.15	7.85	4321	1010	2.673	1.16	1.46	3401	228	376
4	8	298.15	5.23	4428	1020	5.155	0.85	0.99	1781	595	351
5	12	298.15	2.34	4132	1026	13.972		0.41	661		
6	15	298.15	3.12	3515	1020	19.415		0.47	473		
7	16.4	298.15	4.28	2655	1012	18.903		0.49	482		
8	0	303.15	13.25	4422	996	0.814	2.01	2.47	11012	41	369
9	3	303.15	10.37	4692	1002	1.392	1.61	2.05	6478	86	383
10	5	303.15	9.11	4835	1008	2.28	1.38	1.86	3979	164	404
11	8	303.15	5.08	5060	1017	4.299	1.01	1.08	2129	419	322
12	12	303.15	3.03	4674	1023	11.005		0.60	837		
13	15	303.15	3.32	3797	1017	15.352		0.53	596		
14	16.4	303.15	4.58	2867	1008	15.099		0.55	601		
15	0	313.15	16.88	5660	992	0.668	2.51	3.90	13365	27	467
16	3	313.15	10.51	5831	998	1.093	2.17	2.50	8218	50	346
17	5	313.15	8.54	5991	1003	1.744	1.79	2.09	5176	97	350
18	8	313.15	5.46	6115	1011	3.11	1.26	1.36	2926	244	325
19	12	313.15	2.9	5814	1016	7.5	0.67	0.69	1219	1102	308
20	15	313.15	4.09	4413	1009	10.028		0.74	906		
21	16.4	313.15	6.22	3308	1000	10.026		0.84	898		
22	3	323.15	12.15	7155	995	0.884	2.61	3.44	10130	34	396
23	5	323.15	10.52	7311	1000	1.356	2.27	3.05	6637	60	402
24	8	323.15	5.77	7412	1008	2.328	1.65	1.69	3897	140	308
25	12	323.15	3.93	6853	1012	5.243	0.83	1.07	1737	624	385
26	15	323.15	5.88	5034	1005	6.863		1.17	1318		

To calculate the k_L , Sh , Sc and Re numbers, the data of solubility, diffusivity, viscosity and density are required. Solubility, diffusivity and viscosity data were measured in this work and presented in chapters 4, 5 and 6. The density refers to Han et al.'s report,²³ All the calculation results are tabulated in Table 3.10. The correlation of $Sh/Sc^{0.5}$ versus Re with respect to the absorption cell is plotted in Figure 3.20, and the regression result is

$$Sh = 0.0255Re^{0.84}Sc^{0.5} \quad (3.27)$$

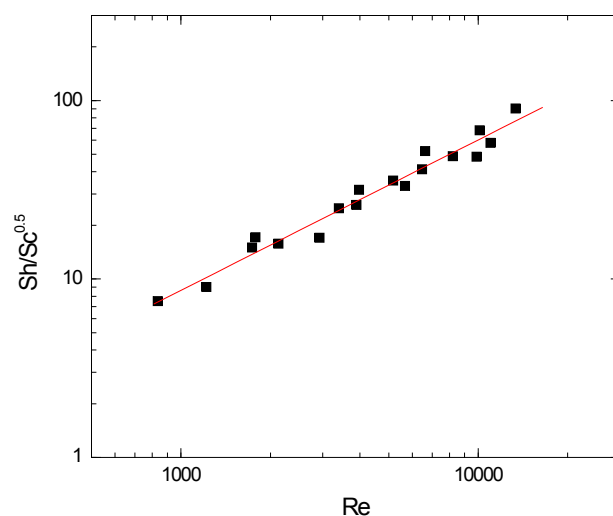


Figure 3.20 Correlation of $Sh/Sc^{0.5}$ versus Re of the absorption cell

The absolute average deviation (AAD, is defined in equation (4.14)) between the experimental and predicted data of Sh number is 0.086. It is interesting that the exponent on Re , 0.84, of the absorption cell is as same as that of stirred cell measured in section 7.4.4. (See equation (7.45)), and the pre-exponent factor, 0.0255, is much closed to the value, 0.0253, measured by stirred cell.

3.9. Conclusions

A novel apparatus was designed and built for measuring the physical solubility of a gas in a liquid, and a model was developed to treat the experimental data. This new experimental technique employs a scaled spiral glass tube with a small drop of mercury inside as a eudiometer to instead of the conventional three-branch U-tube setup to keep the system pressure constant and measure the volume drop of the absorbed gas at a constant temperature. The gas saturation method was investigated and found that the insufficient gas saturation

could cause big errors in the measurement at high temperature. A “vacuum gas saturation” method is proposed in the measurement.

To validate the new technique, the physical solubilities of N₂O in pure water were measured over the temperature range from 298.15 to 323.15 K under a constant ambient pressure. The results are in good agreement with literature values, suggesting that the technique is feasible and reliable. Compared with the three-branch U-tube setup, the new technique is easy to operate, more sensitive and accurate and low mercury inventory.

The solubilities of N₂O in aqueous NaCl solutions and (NaCl or CuCl₂ +aq. 5 M MEA) solutions were measured at 313.15 K and the results show that the solubilities of N₂O in the solution decrease with the increasing of salt concentration, namely “salting-out”. The Sechenov constant K was used to describe the “salting-out” effect. K values relative to NaCl in water and aqueous 5 M MEA solution are very close, but The K value relative to CuCl₂ in aqueous 5 M MEA solution is much higher than that of NaCl.

The physical mass transfer of N₂O in aqueous MEA solutions over the full concentration range at temperatures from 298.15 to 323.15 K were measured by this new apparatus with the volumetric method. The liquid-side mass transfer coefficients were estimated. The well-known equation with respect to the Sherwood (Sh) number to the Reynolds (Re) and Schmidt (Sc) numbers were obtained and the exponents on Re and Sc are 0.84 and 0.5, respectively.

Nomenclature

Parameters and Variables

A = the area of the interface of the gas and the liquid, (m²)

AAD = absolute average deviation between calculated values and experimental data, (%)

AMD = absolute maximum deviation between calculated values and experimental data, (%)

c_1, c_2, c_3, c_4 = parameters of equation (3.26).

C_A^* = equilibrium molar concentration of gas A in the solution, (kmol m⁻³)

C_A^b = molar concentration of gas A in the bulk solution, (kmol m⁻³)

C_i = concentration of ion i , (kmol m⁻³)

C_s = salt concentration, (kmol m⁻³)

d = diameter of liquid stirrer, (m)

h_G = gas-specific parameter, (m³ kmol⁻¹)

$h_{G,0}$ = gas-specific parameter at 298.15 K, (m³ kmol⁻¹)

h_i = ion-specific parameter, (m³ kmol⁻¹)

h_T = gas-specific parameter for the temperature effect, ($\text{m}^3 \text{ kmol}^{-1} \text{ K}^{-1}$)

k_L = physical mass transfer coefficient of the gas in liquid, (m s^{-1})

K = Sechenov constant, ($\text{m}^3 \text{ kmol}^{-1}$)

H_A = Henry's constant of gas A in a liquid, ($\text{kPa m}^3 \text{ kmol}^{-1}$)

$H_{A,i}$ = Henry's constant of absorbed gas A in a pure solvent i , ($\text{kPa m}^3 \text{ kmol}^{-1}$)

$H_{A,m}^{\text{cal}}$ = Henry's constant of calculated from Wang et al.'s model, ($\text{kPa m}^3 \text{ kmol}^{-1}$)

$H_{A,m}^{\text{exp}}$ = Henry's constant of experimental value, ($\text{kPa m}^3 \text{ kmol}^{-1}$)

$H_{A,m}$ = Henry's constant of absorbed gas A in the mixed solvent, ($\text{kPa m}^3 \text{ kmol}^{-1}$)

$H_{A,0}$ = Henry's constant of absorbed gas A in H_2O , ($\text{kPa m}^3 \text{ kmol}^{-1}$)

$H_{\text{N}_2\text{O},\text{H}_2\text{O}}$ = Henry's constant of absorbed N_2O in H_2O , ($\text{kPa m}^3 \text{ kmol}^{-1}$)

n_A = mole amount of gas A, (mol)

n_i = index of ion i in the formula of the salt, (-)

P_A = partial pressure of gas A, (kPa)

P_A^{end} = partial pressure of gas A at absorption equilibrium, (kPa)

P_A^{ini} = partial pressure of gas A before absorption starts, (kPa)

P_{room} = room pressure, (kPa)

V_G' = assumed gas volume at beginning under the pressure equals to $P_{\text{room}}^{\text{end}}$, (kPa)

$P_{\text{room}}^{\text{ini}}$ = room pressure at the beginning of the measurement, (kPa)

$P_{\text{room}}^{\text{end}}$ = room pressure at the end of the measurement, (kPa)

$P_{\text{H}_2\text{O}}^{\text{v}}$ = vapor pressure of pure water, (kPa)

$P_{\text{MEA}}^{\text{v}}$ = vapor pressure of pure MEA, (kPa)

P_{vap} = vapor pressure of solution, (kPa)

R = gas constant, ($\text{m}^3 \text{ kPa K}^{-1} \text{ kmol}^{-1}$)

R_A = excess Henry's coefficient from Wang et al.'s model, ($\text{kPa m}^3 \text{ kmol}^{-1}$)

Re = Reynolds number, (-)

RH = relative humidity (%)

Sc = Schmidt number, (-)

Sh = Sherwood number, (-)

t = time, (s)

T = temperature of the system, (K)

T_{gas} = temperature of gas, (K)

T_{liq} = temperature of liquid, (K)

V_0 = volume of the bottle except the liquid, (m^3)

V_A = corrected absorption volume of gas A at room pressure, (m^3)

V_A^{exp} = experimental gas A absorption volume at room pressure, (m^3)

V_G = volume of gas phase, (m³)

V_G^{end} = volume of gas phase in absorption cell at end of the measurement at room pressure, (m³)

V_G^{ini} = volume of gas phase in absorption cell at beginning of the measurement at room pressure, (m³)

V_L = volume of the liquid phase, (m³)

V_{vap} = volume of the vapor of the solution, (m³)

ΔV = the increment of the gas volume because of the difference of the room pressure at the beginning and end of the measurement, (m³)

$x_{\text{H}_2\text{O}}$ = mole fraction of water, (-)

x_{MEA} = mole fraction of MEA, (-)

Greek Symbols

ω = Stirrer revolutions per second, (rps)

References

1. Versteeg, G. F.; van Swaaij, W. P. M. Solubility and Diffusivity of Acid Gases (CO₂, N₂O) in Aqueous Alkanolamine Solutions. *J. Chem. Eng. Data* **1988**, *33*, 29–34.
2. Weiland, R. H.; Trass, O. Absorption of Carbon Dioxide in Ethylenediamine Solution. *Can. J. Chem. Eng.* **1971**, *49*, 767–772.
3. Haimour, N.; Sandall, O. C. Absorption of Carbon Dioxide into Aqueous Methyldiethanolamine. *Chem. Eng. Sci.* **1984**, *39*, 1791–1796.
4. Haimour, N. Solubility of N₂O in Aqueous Solutions of Diethanolamine at Different Temperatures. *J. Chem. Eng. Data* **1990**, *35*, 177–178.
5. Al-Ghawas, H. A.; Hagewiesche, D. P.; Ruiz-Ibanez, G.; Sandall, O. C. Physicochemical Properties Important for Carbon Dioxide Absorption in Aqueous Methyldiethanolamine. *J. Chem. Eng. Data* **1989**, *34*, 385–391.
6. Li, M. H.; Lai, M. D. Solubility and Diffusivity of N₂O and CO₂ in (Monoethanolamine + N-Methyldiethanolamine + Water) and in (Monoethanolamine + 2-Amino-2-methyl-1-propanol + Water). *J. Chem. Eng. Data* **1995**, *40*, 486–492.
7. Tai, T. -c., T.; Ko, J. -j; Li, M. H. Solubility of Nitrous Oxide in Alkanolamine Aqueous Solutions. *J. Chem. Eng. Data* **2000**, *45*, 341–347.
8. Mandal, B. P.; Kundu, M.; Padhiyar, N. U.; Bandyopadhyay, S. S. Physical Solubility and Diffusivity of N₂O and CO₂ into Aqueous Solutions of (2-Amino-2-methyl-1-propanol + Monoethanolamine) and (N-Methyldiethanolamine + Monoethanolamine). *J. Chem. Eng. Data* **2005**, *50*, 352–358.
9. Rinker, E. B.; Ashour, S. S.; Sandall, O. C. Kinetics and Modeling of Carbon Dioxide Absorption into Aqueous Solutions of N-Methyldiethanolamine. *Chem. Eng. Sci.* **1995**, *50*, 755–768.
10. Davis, R. A.; Pogalnis, B. J. Solubility of Nitrous Oxide in Aqueous Blends of N-Methyldiethanolamine and 2-Amino-2-methyl-1-propanol. *J. Chem. Eng. Data* **1995**, *40*, 1249–1251.

11. Samanta, A.; Roy, S.; Bandyopadhyay, S. S. Physical solubility and diffusivity of N₂O and CO₂ in aqueous solution of piperazine and (N-methyldiethanolamine + piperazine). *J. Chem. Eng. Data* **2007**, *52*, 1381–1385.
12. Browning, G. J.; Weiland, R. H. Physical Solubility of Carbon Dioxide in Aqueous Alkanolamines via Nitrous Oxide Analogy. *J. Chem. Eng. Data* **1994**, *39*, 817–822.
13. Wang, Y. W.; Xu, S.; Otto, F. D.; Mather, A. E. Solubility of N₂O in Alkanolamines and in Mixed Amines. *Chem. Eng. J.* **1992**, *48*, 31–40.
14. Mandal, B. P.; Kundu, M.; Padhiyar, N. U.; Bandyopadhyay, S. S. Physical Solubility and Diffusivity of N₂O and CO₂ into Aqueous Solutions of (2-Amino-2-methyl-1-propanol + Diethanolamine) and (N-Methyldiethanolamine + Diethanolamine). *J. Chem. Eng. Data* **2004**, *49*, 264–270.
15. Littel, R. J.; Versteeg, G. F.; van Swaaij, W. P. M., Solubility and Diffusivity Data for the Absorption of COS, CO₂, and N₂O in Amine Solutions. *J. Chem. Eng. Data* **1992**, *37*, 49–55.
16. Sada, E.; Kito, S., Solubilities of Gases in Aqueous Monoethanolamine Solutions. *Kagaku Kogaku* **1972**, *36*, 218–220.
17. Park, M. K.; Sandall O. C. Solubility of Carbon Dioxide and Nitrous Oxide in 50 mass % Methyldiethanolamine. *J. Chem. Eng. Data* **2001**, *46*, 166–168.
18. Cussler, E. L. Diffusion Mass Transfer in Fluid Systems, 3rd Edition, Cambridge University Press, 2009.
19. Weisenberger, S.; Schumpe, A. Estimation of gas Solubilities in Salt Solutions At Temperature from 273 K to 363 K. *AIChE Journal* **1996**, *42*, 298–300.
20. Harned, H. S. and Davis, R. The Ionization Constant of Carbonic Acid in Water and The Solubility of Carbon Dioxide in Water and Aqueous Salt Solutions from 0 to 50°C; *J. Am. Chem. Soc.* **1943**, *65*, 2030–2037.
21. Kumar, P. S.; Hogendoorn, J.A. and Versteeg, G. F. Density, Viscosity, Solubility, and Diffusivity of N₂O in Aqueous Amino Acid Salt Solutions; *J. Chem. Eng. Data* **2001**, *46*, 1357–1361.
22. Schumpe, A. The Estimation of Gas Solubilities in Salt Solutions. *Chem. Eng. Sci.* **1993**, *48*, 153–158.
23. Han, J. Y.; Jin, J.; Eimer, D. A.; Melaaen, C. C. Density of Water (1) + Monoethanolamine (2) + CO₂ (3) from (298.15 to 413.15) K and Surface Tension of Water (1) + Monoethanolamine (2) from (303.15 to 333.15) K. *J. Chem. Eng. Data* **2012**, *57*, 1095–1103.

Chapter 4

4. Measurements and Correlation of Physical Solubility of N₂O and CO₂ in (Monoethanolamine + Water) by a Novel Technique

Abstract

A novel experimental technique for measuring the physical solubility of CO₂ in aqueous monoethanolamine (MEA) solutions using the “N₂O analogy” method is proposed in this work. The novel technique employs a scaled spiral glass tube with a small drop of mercury as a eudiometer as an alternative to a three-branch U-tube setup to keep the system pressure constant and measure the volume of a drop of absorbed gas at constant temperature. The results were in good agreement with literature values, suggesting that the technique is feasible and reliable. Compared with the three-branch U-tube setup, the new technique is easy to operate and more sensitive and accurate. The physical solubilities of CO₂ in aqueous MEA solutions over the full range of concentrations were measured using this novel technique over the temperature range from 298.15 to 323.15 K under a constant ambient pressure. Wang et al.’s model was used to correlate the data, and the results show the model is good for predicting the behavior of the (monoethanolamine + water) system.

This chapter is based on a published paper (Ying et al. *Ind. Eng. Chem. Res.* **2012**, *51*, 6958–6966) and provides a short version of the documentation in chapter 3. It also extends the work by solubility measurements and data treatment.

4.1. Introduction

Monoethanolamine (MEA) has been employed as an important industrial absorbent since the 1930s because of its high reaction rate, relatively low cost, and thermal stability. In order to improve the absorption efficiency of MEA solutions, the MEA concentration in aqueous solution is generally increased to 30 mass %. A further increase has the potential for reducing the cost of CO₂ capture given that corrosion and degradation issues can be controlled.

Physical solubility is a key parameter needed for interpreting diffusivity and reaction kinetics measurements, as well as for modeling and industrial design. Different methods have been used to measure the physical solubility of gas in liquid¹⁻¹⁶ based on two principle approaches. One is the “volumetric method”, namely, measuring the volume of the absorbed gas per unit volume of liquid at constant pressure and temperature. The classical apparatus employed two- or three- U-tube to keep the absorption pressure constant by adjusting the mercury surface level. The apparatus was simple to set up. Volume of gas dissolved is read directly from the buret. However, for this kind of absorption apparatus, it is cumbersome to keep the mercury surface at the same level in the three branches throughout the experiments. The absorption rate is too high in the beginning of the experiment to operate the U-tube quickly enough for height adjustment to keep the pressure constant. On the other hand, the absorption rate is too low to accurately determine the end point in a three-branch U-tube. An undesirable feature of the mercury U-tube technique is the need to keep a substantial quantity of mercury in the apparatus.

The other principle technique for solubility measurements is the “pressure drop method”, which measures the pressure drop of the gas at constant volume and temperature. The solubility is then derived through the equations of state and the model as follows:¹

$$H_A = \frac{P_A^{\text{end}} RT}{(P_A^{\text{ini}} - P_A^{\text{end}})} \cdot \frac{V_L}{V_G} \quad (4.1)$$

where H_A is Henry’s constant and P_A^{end} and P_A^{ini} are the partial pressures of the gas A at absorption equilibrium and before the absorption starts, respectively. V_L and V_G are the volumes of liquid and gas, respectively. T is the temperature of the system, and R is the gas constant. Versteeg and van Swaaij¹ and Park and Sandall¹⁷ used the pressure drop method to measure the solubility by measuring the change in partial pressure of a gas before and after absorption in aqueous amine solutions. With this method, the pressure is allowed to drop and asymptotically approach the end pressure, which is also the equilibrium pressure. This method demands very accurate pressure measurements to ensure a high accuracy. In the

present work, a volumetric method was developed to reduce the mercury requirement of the apparatus to one small drop.

The physical solubility and diffusivity of CO₂ in the MEA solution cannot be measured directly because of the chemical reaction between CO₂ and MEA. Because of the similarity in mass and molecular structure between CO₂ and N₂O, Clarke¹⁸ first suggested the “N₂O analogy” method. Later researchers^{3–14} followed this approach to estimate the solubilities of CO₂ in different amine solutions of various concentrations. The N₂O analogy method for the CO₂–MEA system can be expressed as follows

$$H_{\text{CO}_2, \text{MEA}} = H_{\text{N}_2\text{O}, \text{MEA}} \left(\frac{H_{\text{CO}_2, \text{H}_2\text{O}}}{H_{\text{N}_2\text{O}, \text{H}_2\text{O}}} \right) \quad (4.2)$$

To obtain the ratio of the solubility of N₂O and CO₂ in water, most researchers measured the solubilities of N₂O and CO₂ in water at different temperature under constant ambient pressure. Reviews of N₂O and CO₂ in water are summarized in Table 3.4 and Table 4.1.

The solubilities of N₂O and CO₂ in aqueous MEA solutions lower than 6 M have been studied by many researchers, most of the studies focused on 1 – 5 M concentration range. The scattered data are presented in Table 4.2. For example, the solubility of N₂O in 5 M aqueous MEA solution at 1 atm and 303.15, 313.15 and 323.15 K, Tsai et al⁷ obtained 4361.9, 4696.4 and 5126.9 kPa·m³·kmol⁻¹, respectively, whereas Li and Lai⁶ reported 4924, 5262 and 5766 kPa·m³·kmol⁻¹, respectively. The relative deviation (RD) in the literature values is 6.0%. Regarding two parallel samples, X_1 and X_2 : the relative deviation is defined as:

$$RD(\%) = \frac{X_1 - (X_1 + X_2)/2}{(X_1 + X_2)/2} \times 100\% = \frac{(X_1 - X_2)}{(X_1 + X_2)} \times 100\% \quad (4.3)$$

Regarding a series of data, the average relative deviation (ARD) is defined as

$$ARD(\%) = \frac{1}{n} \sum_{i=1}^n \frac{|X_i - \bar{X}_{\text{exp}}|}{\bar{X}_{\text{exp}}} \times 100\% \quad (4.4)$$

The scatter in the results is probably caused by the different experimental methods used and various experimental details including gas saturation by solvent (mostly water), potential leakage, neglect of the influence of the room–pressure fluctuations, and imperfect purging of air from the equilibrium cell. For instance, Browning and Weiland’s results¹² for the Henry’s constant of N₂O in H₂O at 298.15 K (4234 kPa·m³·kmol⁻¹) is about 4.2% higher than the average of the values obtained by other researchers. The reason for this difference is probably

that Browning and Weiland neglected the absorption while the liquid was being injected into the cell. This would lead to an error even if the absorption were small during the injection. There is also a lack of data to describe the dependence of the Henry's coefficient on the MEA concentration, and no data was found for concentrations higher than 6 M. Therefore, it was necessary to develop a new test method and measure the solubility of CO₂ in aqueous MEA solutions over a wider concentration range.

Table 4.1 Physical solubility of CO₂ in H₂O measurement compared with literature values

<i>T</i> /K	<i>H</i> /kPa·m ³ ·kmol ⁻¹					This work
	ref.1	ref.5	ref.6	ref.8	ref.11	
288.15		2240				
291.15	2469.1					
292.15	2490.2					
293.15	2631.6	2590		2647	2619	2565
298.15	3003.5	2984		3096	2949	2951
303.15	3571.4	3394	3382	3314	3358	3360
308.15	3937.1	3810		3765	3850	
311.4	4098.4					
313.15	4219.4	4250	4227	4098	4264	4132
313.4	4201.7					
318.15	4854.4	4689				
323.15	5154.6	5167	5136			5069
328.15						5567
329.15						
333.15	6134.9					6021
343.5	7142.9					
350.2	7575.8					
355.2	8333.3					
360.1	9259.3					

In this work, a novel absorption apparatus based on the frequently used Haimour's^{3,4} setup was designed to measure the physical solubility of CO₂ in aqueous MEA solutions at constant ambient pressure and temperatures from 298.15 to 323.15 K. The detail of the apparatus is introduced in chapter 3. This apparatus was used to measure the N₂O (CO₂) solubility over a wide range of aqueous MEA concentrations. As has been done by other researchers, this study utilized the N₂O analogy method to estimate the physical solubility of CO₂ in MEA solutions.

Table 4.2 Literature values for the physical solubilities of N₂O in aqueous MEA solutions

T (K)	C_{MEA} (mol L ⁻¹)	$H_{\text{N}_2\text{O}}$ (kPa·m ³ ·kmol ⁻¹)	ref	T (K)	C_{MEA} (mol L ⁻¹)	$H_{\text{N}_2\text{O}}$ (kPa·m ³ ·kmol ⁻¹)	ref
293.15	2	3821	Mandal et al. ⁸	303	0.183	4564	Littel et al. ¹⁵
298.15	2	4205		303	0.391	4911	
303.15	2	4605		303	0.777	4780	
308.15	2	4972		303	1.550	4717	
313.15	2	5475		303	2.163	4863	
293.15	2.5	3840		303	3.226	4920	
298.15	2.5	4218		303	3.246	4901	
303.15	2.5	4643		318	0.197	7224	
308.15	2.5	5003		318	0.415	6976	
313.15	2.5	5493		318	0.875	6958	
293.15	3	3848		318	1.621	7013	
298.15	3	4244		318	2.465	7088	
303.15	3	4675		318	3.251	6921	
308.15	3	5042		318	3.533	7184	
313.15	3	5524		333	0.233	9107	
298.15	1.6	4299.5		333	0.584	9137	
298.15	3.3	4395.4	Browning and Weiland ¹²	333	0.871	9018	
298.15	5	4799.2		333	1.579	9077	
303.15	5	4361.9	Li and Lai ⁶	333	1.765	8817	
308.15	5	4696.4		333	2.593	8817	
313.15	5	5126.9		333	3.309	9167	
303.15	1	4685	Tai et al. ⁷	333	3.701	8264	
308.15	1	5163		348	0.211	11001	
313.15	1	5669		348	0.422	10445	
303.15	2	4722		348	0.886	10756	
308.15	2	5245		348	1.797	10676	
313.15	2	5750		348	2.669	10716	
303.15	3	4790		348	2.889	9775	
308.15	3	5233		348	3.644	9808	
313.15	3	5757		348	3.911	9333	
303.15	4	4820					
308.15	4	5216		298	0.50	4109	Sada et al. ¹⁶
313.15	4	5761		298	1.54	4135	
303.15	5	4924		298	2.46	4194	
308.15	5	5262		298	3.24	4238	
313.15	5	5766		298	4.38	4418	
303.15	6	5062		298	5.05	4530	
308.15	6	5422		298	6.01	4725	
313.15	6	5799					

4.2. Experimental Section

4.2.1. Experimental Setup and Procedure of the Solubility Measurement

This is a short version, used for a publication, of the extensive description in chapter 3.

A schematic diagram of the absorption apparatus is shown in Figure 4.1. The key parts of the absorption cell, including bottles, pipes, joints, and valves, were made of glass or metal. Rubber or plastic tubes were avoided to prevent gas leaks or diffusion from the cell during the absorption process, because it takes a long time to reach equilibrium for the absorption of a gas in a liquid (In particular, it will take about 24 hr for a high-viscosity liquid). The main modifications of the solubility cell shown in Figure 4.1, compared with those of previous researchers,²⁻¹⁴ are as follows: A scaled spiral tube (with an inner diameter of 4 mm and a volume of 18 mL) was employed as a volumetric meter instead of the three-branch U-tube. A mercury droplet (approximately 2 g) was placed in this clean spiral tube, which was laid horizontally in a transparent water bath. The accuracy of temperature control was ± 0.1 K. The mercury droplet moves from initial position B toward end point A when the gas is absorbed into the liquid in the absorption cell, (as shown in Figure 4.1). The total volume including the connecting pipe system was 132 mL. The tube end beyond point B of the spiral tube was raised out of the water bath and open to the atmosphere to keep the pressure of the absorption cell constant and equal to room pressure. A small shaking motor was mounted on the end of the spiral tube to shake the tube and make the mercury droplet move smoothly. The error caused by the resistance of the droplet to movement was less than 0.1 kPa when the shaking motor was turned on. The detail of the method for measuring the resistance is introduced in section 3.2.2. Compared with the traditional U-tube method, this novel technique has some advantages, such as easy operation, lower mercury inventory, higher sensitivity and greater accurate.

The experimental procedure described in the literature²⁻¹⁴ is that the gas (N_2O or CO_2) is introduced into the cell first and then the liquid is injected. This could cause errors for the following reasons: First, it is difficult to make the gas fully saturated. We attempted to produce 100% relative humidity (RH) saturated gas by blowing N_2 into a gas wash bottle with a 20-cm height of water for 15 hr, but only 80% RH was achieved. Lack of saturation could cause an error, especially at higher experimental temperatures. Second, the method neglects the amount of absorption occurring while the liquid was being injected. This would introduce some error, especially in situation in which a small amount of solution was used. To avoid the gas saturation problem and the error of neglecting absorption while liquid is

being injected, in this work, the liquid was added to the absorption cell first because it is faster to inject the gas. The cell was then vacuumed to the saturation vapor pressure of the liquid at the experimental temperature. After the gas–liquid equilibrium and system thermal equilibrium had been reached, the gas to be investigated was introduced. In addition, this method of vacuuming to obtain saturated gas is faster than the traditional method in which the gas passes through a wash bottle.

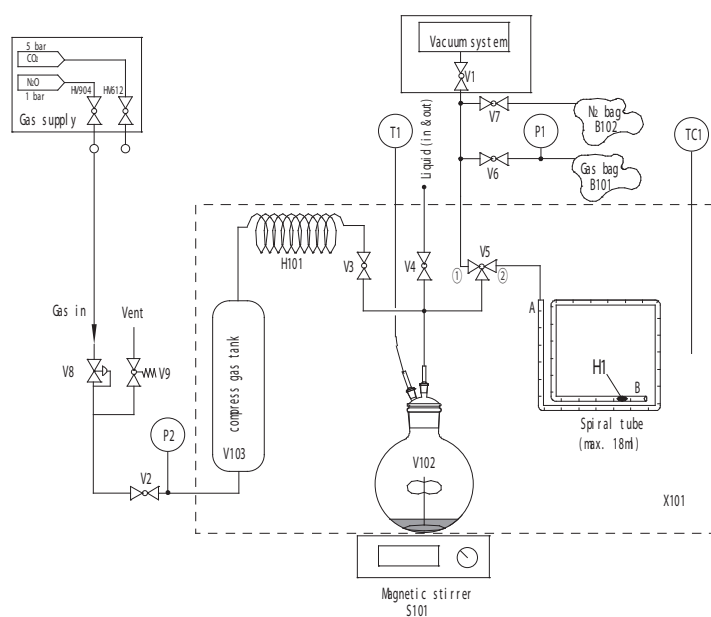


Figure 4.1 Schematic diagram of the physical absorption measurement apparatus:

X101, transparent water bath; V104, scaled spiral glass tube volumetric meter; H1, mercury droplet; V102, absorption cell with stirrer and gas stirring blades; S101– magnetic stirrer; TC1, thermal controller; T1, gas thermometer; P1/ P2, gas manometer; B101, gas bag (N₂O or CO₂); B102, N₂ bag; V103, compress gas tank; H101, copper pipe coil.

For each run with the novel technique, the gas tank (V103 with a volume including the connecting piping system of 550 mL) and the scaled spiral tube (V104) were filled the desired gas (N₂O or CO₂), and the dried and clean absorption cell V102 was filled with N₂. The gas tank V103 was filled with gas to 30 kPa (gauge pressure) and kept in the water bath to reach the desired temperature. A precise weight (approximately 15 g) of freshly degassed aqueous MEA solution of the desired concentration was weighed on an analytical balance (Mettler Toledo XS403S) with an accuracy ± 1 mg and fed into cell V102 in the N₂ gas atmosphere with a syringe. Cell V102 was vacuumed quickly down to the saturation vapor pressure of the solution. (To reduce the loss of vapor, the time to reach vacuum should be less than 1 min.) Then, the solution was kept in the vacuum state for at least 20 min to wait for the system to reach its desired temperature and gas liquid equilibrium. The gas–phase stirrers

were joined to the liquid–phase stirrer bar and were kept at 60 rpm to ensure a uniform liquid and gas phase temperature in the cell. The liquid stirrer was a 3–cm–long magnetic bar driven by an external magnet. The initial position of the mercury droplet was recorded after the whole system had reached its thermal equilibrium. Then, the gas was introduced into V102 from gas tank V103. The pressure in V102 was ensured to be equal to the atmospheric pressure at the beginning by connecting this vessel to the gas bag (B101); 15–20 s was allowed for this step to avoid pressure and temperature overshoot. Then, the absorbed volume of gas was recorded as function of time while the mercury droplet moved in the spiral tube during the absorption processing. It took about 5 to 24 hr to reach equilibrium for each absorption experiment. (How long the measurement takes depends on the temperature and concentration, with less time generally being needed at the high temperature and low concentration less time is needed). The pressure difference between the two sides of the mercury droplet was less than 0.1 kPa during the absorption process. The room pressure was recorded at the beginning ($P_{\text{room}}^{\text{ini}}$) and end ($P_{\text{room}}^{\text{end}}$) of the measurement. If the room pressure is different between the beginning and end of the measurement, the absorbed volume of the gas should be corrected. The corrected absorption volume of the gas, V_A , is

$$V_A = V_A^{\text{exp}} + \Delta V = V_A^{\text{exp}} + V_G^{\text{ini}} \left(\frac{P_{\text{room}}^{\text{ini}}}{P_{\text{room}}^{\text{end}}} - 1 \right) \quad (4.5)$$

where V_A^{exp} is the experimental volume of absorbed gas A, and V_G^{ini} is the gas volume in the absorption cell at the beginning of the measurement.

The uncertainty in the measurements was estimated to be $\pm 39 \text{ kPa} \cdot \text{m}^3 \cdot \text{kmol}^{-1}$. (See section 4.4 uncertainty analysis). The solubility of gas A can be expressed using Henry's law constant H_A as

$$H_A = P_A / C_A^* \quad (4.6)$$

where the partial pressure, P_A , of gas A at the experimental conditions is given by

$$P_A = P_{\text{room}}^{\text{end}} - (x_{\text{H}_2\text{O}} P_{\text{H}_2\text{O}}^{\text{v}} + x_{\text{MEA}} P_{\text{MEA}}^{\text{v}}) \quad (4.7)$$

where $P_{\text{H}_2\text{O}}^{\text{v}}$ is the vapor pressure of pure water, $P_{\text{MEA}}^{\text{v}}$ is the vapor pressure of pure MEA; and $x_{\text{H}_2\text{O}}$ and x_{MEA} are the mole fractions of water and MEA, respectively. Absorption data in the form of the volume of gas A volume per volume of liquid (V_A/V_L) were recorded in this experiment. If it is assumed that the room pressure is constant during the measurement and that the volume of liquid (V_L) is unchanged after absorption of the gas, then the concentration

(C_A^*) at the absorption equilibrium is $C_A^* = n_A / V_L$, according to the ideal gas state law $P_{\text{room}}^{\text{end}} V_A = n_A RT$, which describes the gas is in the spiral tube at room pressure. The solubility (Henry's constant H_A of gas A) can then be calculated for this measurement as

$$H_A = \frac{P_A}{C_A^*} = \frac{P_A RT}{P_{\text{room}}^{\text{end}} (V_A / V_L)} \quad (4.8)$$

4.2.2. Reagent and Solution Preparation

Reagent-grade MEA with a purity of ≥ 99.5 mass % was obtained from Merck and used without further purification. Deionized water (purified with a mini-Q system, conductivity of 18.2 M Ω cm) and MEA were degassed by application of a vacuum and then mixed to prepare various concentrations of aqueous MEA solutions using an analytical balance and a 50 mL volumetric flask. The concentrations of aqueous MEA solutions prepared were as follows: 0 M (0 mass %), 3 M (18.1 mass %), 5 M (30.2 mass %), 8 M (47.9 mass %), 12 M (71.4 mass %), 15 M (89.8 mass %), and 16.4 M (100 mass %). The whole preparation process was carried out under a nitrogen atmosphere. The purity of CO₂ was ≥ 99.995 mol % and that of N₂O ≥ 99.7 mol %, and both gases were obtained from AGA Gas GmbH.

4.3. Results and Discussion

4.3.1. Validation for the Novel Technique

To validate the novel solubility apparatus and procedure, the physical solubilities of N₂O and CO₂ in pure water were measured. The measured solubilities of N₂O in water at 298.15, 303.15, 313.15, and 323.15 K along with literature results are presented in Figure 3.15. The comparison between the literature values and values obtained in this study for the solubility of CO₂ in water are shown in Figure 4.2. (The solubilities of N₂O and CO₂ in water from the literature are reviewed in Table 3.4 and Table 4.1). It can be seen that there is a good agreement between literature values and those of the present study, indicating that the novel technique is good and reliable for measuring the solubility of gases in liquids. The solubility data with respect to temperature can be represented by an exponential model, as shown in Figure 3.15 and Figure 4.2. The solid lines are the regression models based on the experimental data of this work. The fitted equations are as follows,

$$H_{\text{N}_2\text{O},\text{H}_2\text{O}} = 8.449 \times 10^6 \exp(-2283 / T) \quad (4.9)$$

$$H_{\text{CO}_2,\text{H}_2\text{O}} = 3.520 \times 10^6 \exp(-2113 / T) \quad (4.10)$$

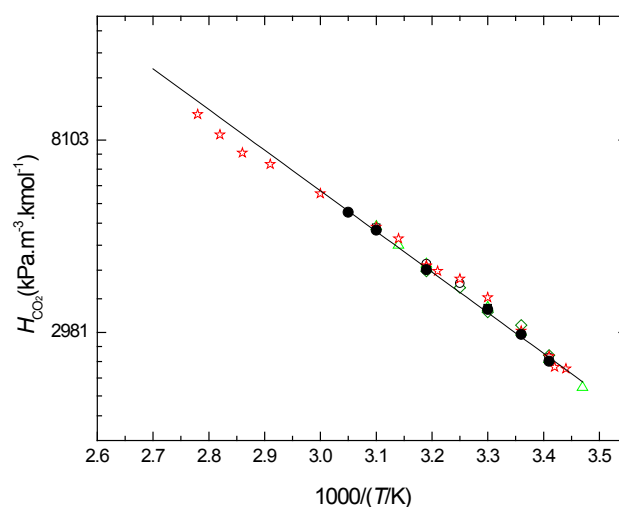


Figure 4.2 Physical solubility of CO₂ in H₂O as a function of temperature compared with literature values: Δ , Al-Ghawas⁵; \square , Li and Lai⁶; \diamond , Mandal⁸; \circ , Samanta¹¹; \star , Park¹⁷; \bullet , this work; The solid line was calculated using equation(4.10)

4.3.2. N₂O Absorbed in Aqueous MEA Solution

Many researchers have measured the solubility of N₂O in MEA solution, but only in the concentration range up to 6 M. There is still a lack of data for higher concentrations of MEA, and there is also scatter in the data available. The data for the solubility of N₂O in aqueous MEA solutions of various concentrations (0, 3, 5, 8, 12, 15, and 16.4 M) at 298.15, 303.15, 313.15 and 323.15 K are presented in Figure 4.3 and Table 4.3. As shown in Figure 4.3, the Henry's constants of N₂O in aqueous MEA solutions increase systematically with increasing temperature at a certain concentration. In addition, the plot of $\ln(H_{N_2O})$ versus $1/T$ shows a linear relationship, and the trend is similar to that of N₂O in pure water and MEA.

Table 4.3 Physical solubilities of N₂O in aqueous MEA solutions of various concentrations

T/K	$H_{N_2O} / \text{kPa} \cdot \text{m}^3 \cdot \text{kmol}^{-1}$						
	Pure H ₂ O	3M	5M	8M	12M	15M	Pure MEA
298.15	4022	4221	4321	4428	4132	3515	2655
303.15	4422	4692	4835	5060	4674	3797	2867
313.15	5660	5831	5991	6115	5814	4413	3308
323.15	7070	7155	7311	7412	6853	5034	3768

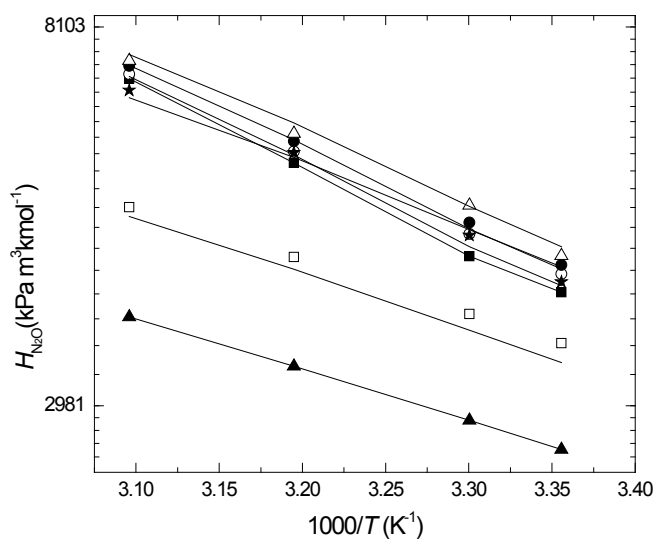


Figure 4.3 Comparison of experimental values and the regressed model for the physical solubility of N₂O in MEA+H₂O as a function of temperature: ■, H₂O; ○, 3M; ●, 5M; △, 8M; ★, 12M; □, 15M; ▲, MEA; The solid lines were calculated using equation(4.11)

Figure 4.4 shows the solubility of N₂O in various concentrations of MEA at temperature from 298.15 to 323.15 K, and the measurements compare well with literature values.^{7,8,12}

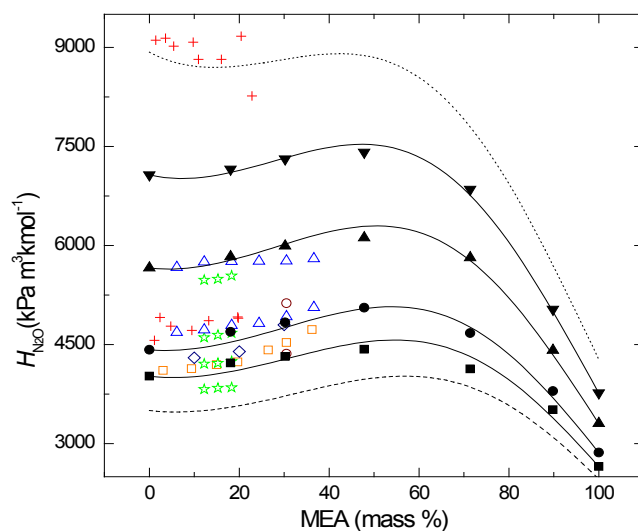


Figure 4.4 Comparison of experimental and literature values with the regressed model for the physical solubility of N₂O in MEA +H₂O as a function of MEA mass percentage for temperatures from 293.15 to 333.15 K: (■, 298.15 K; ●, 303.15 K; ▲, 313.15 K; ▼, 323.15 K), this work; ☆, Mandal et al.⁸; ◇, Browning and Weiland¹²; △, Tai et al.⁷; ○, Li and Lai⁶; □, Sada and Kito¹⁶; +, Littel et al.¹⁵; The solid (293.15–333.15) K; the dashed (293.15 K) and dotted (333.15 K) lines were calculated by equation (4.11)

The relative deviations of this work from the literature values are reported in Table 4.4. It can be seen that the Henry's constant of N₂O in MEA solution increases with increasing MEA concentration in the lower concentration range at a given temperature, but decreases with increasing MEA concentration in the higher concentration range. The inflection point is around 60 mass % MEA. It is interesting that the trend of solubility versus concentration is similar to that of density versus concentration for aqueous MEA solutions from density measurement work¹⁹⁻²¹. These works showed that the density of aqueous MEA solution was lower when the concentration was low or high, and the density was at its highest around 60 mass %. The explanation for these findings is that the excess (free) volume of solution becomes lowest at this concentration. Figure 4.4 also shows that the results in this work are close to the literature values in the range from 10 to 40 mass %, which is the concentration range on which the literature is focused.

Table 4.4 Relative deviations between the values obtained in this work and those reported in the literature for the solubility of N₂O in aqueous MEA solutions

C_{MEA} (mol/L)	T/K	RD%	reference
3	298.15–313.15	1.1	Mandal et al. ⁸
3	303.15–313.15	0.8	Tai et al. ⁷
5	303.15–313.15	1.4	Tai et al. ⁷
5	298.15	5.2	Browning and Weiland ¹²
5	303.15–313.15	6.5	Li and Lai ⁶

4.3.3. Physical Solubility of CO₂ in Aqueous MEA Solution

According to the N₂O analogy method, the Henry's constants of CO₂ in 3, 5, 8, 12, and 15 M aqueous MEA solutions and pure MEA can be estimated. The results are tabulated in Table 4.5, and the relationship between H_{CO_2} and MEA concentration is plotted in Figure 4.5. Compared with the solubility properties of N₂O shown in Figure 4.3 and Figure 4.4, the influence trends of both concentrations and temperature on the solubilities of CO₂ in MEA solution are very similar to those of N₂O.

Table 4.5 Solubilities of CO₂ derived for various concentrations aqueous MEA solutions

T/K	$H_{\text{CO}_2}/H_{\text{N}_2\text{O}}$ in water	$H_{\text{CO}_2}/\text{kPa}\cdot\text{m}^3\cdot\text{kmol}^{-1}$						
		pure H ₂ O	3 M	5 M	8 M	12 M	15 M	pure MEA
298.15	0.734	2951	3097	3170	3249	3032	2579	1948
303.15	0.760	3361	3566	3675	3846	3552	2886	2179
313.15	0.730	4133	4258	4375	4465	4245	3222	2416
323.15	0.717	5069	5130	5242	5314	4913	3609	2702

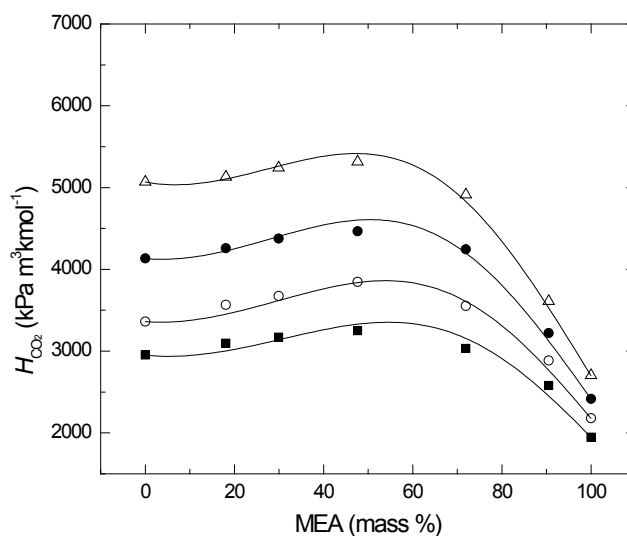


Figure 4.5 Comparison of experimental values with the regressed model for the physical solubility of CO₂ in MEA +H₂O as a function of MEA mass percentage for temperatures from 298.15 to 323.15 K:

■, 298.15 K; ○, 303.15 K; ●, 313.15 K; △, 323.15 K; The solid lines were calculated by equation (4.11)

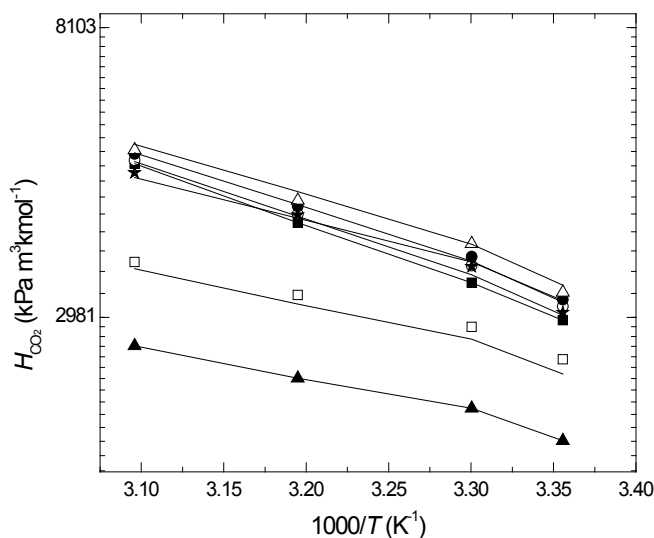


Figure 4.6 Comparison of experimental values and the regressed model for the physical solubility of CO₂ in MEA+H₂O as function of temperature:

■, H₂O; ○, 3 M; ●, 5 M; △, 8 M; ★, 12 M; □, 15 M; ▲, MEA; the solid lines were calculated by equation(4.11)

The data on the physical solubilities of absorbed gas (N₂O or CO₂) in various MEA solutions can be fitted by an exponential equation such as equation (4.9), but in this work, a semiempirical model proposed by Wang et al.¹³ was employed to fit the experimental data.

This model is more theoretically founded using parameters such as α_{12} to describe two-body interaction. As such the model seems more promising to use over a wider perspective including both industry and research. In this method, the “excess Henry’s coefficient” (R_A) for the MEA+H₂O binary–solvent system is defined as

$$R_A = \ln H_{A,m} - \sum_{i=1}^2 \varphi_i \ln H_{A,i} \quad (4.11)$$

where $H_{A,m}$ is the Henry’s constant of absorbed gas A in the mixed solvent (MEA+H₂O), $H_{A,i}$ is the Henry’s constant of absorbed gas A in a pure solvent i , and φ_i is the mass percentage of solvent i . R_A is zero when the gas–free solvent mixture forms an ideal solution, and positive values of R_A correspond to solubilities that are less than the ideal mixture value. Similarly, negative values of R_A correspond to higher solubilities than the ideal. From the equation, the excess Henry’s quantity R_A for the binary system is then correlated as a function of the mass percentage as follows

$$R_A = \varphi_1 \varphi_2 \alpha_{12} \quad (4.12)$$

where φ_1 and φ_2 are the mass percentage of MEA and water, respectively, in the system. The parameter α_{12} is the two–body interaction parameter between the two components of the solvent. For a binary absorption solvent, α_{12} can be estimated as a polynomial function of the temperature (T , K) and the mass percentage φ_2 of the second solvent as follows

$$\alpha_{12} = \sum_{i=1}^n a_i (T-273.15)^{i-1} + b\varphi_2 \quad (4.13)$$

We checked equation (4.13) from first to sixth–order polynomial for the (MEA+H₂O) system with experimental data by a nonlinear regression method and found that a second–order polynomial with respect to the temperature with the four parameters a_1 , a_2 , a_3 and b in equation (4.13) satisfies the experimental data; higher–order polynomials introduce more noise. The regression deviation between the calculated values and the experimental data can be described by the absolute average deviation (AAD) and the absolute maximum deviation (AMD), the AAD and AMD are calculated respectively from:

$$\text{AAD}(\%) = \frac{1}{n} \sum_1^n \frac{|A_{\text{cal}} - A_{\text{exp}}|}{A_{\text{exp}}} \times 100\% \quad (4.14)$$

$$\text{AMD}(\%) = \max \left(\frac{|A_{\text{cal}} - A_{\text{exp}}|}{A_{\text{exp}}} \right) \times 100\% \quad (4.15)$$

where A_{cal} and A_{exp} are the calculated and experimental values, respectively, of the property of the experimental object.

Table 4.6 Parameters in the Wang et al.'s model for CO₂ and N₂O in aqueous MEA solutions

	a_1	a_2	a_3	b	AAD	AMD
MEA+N ₂ O	1.71468	0.03955	-0.00043	-2.21209	1.49	4.97
MEA+CO ₂	1.70981	0.03972	-0.00043	-2.20377	1.48	4.92

Wang et al.'s model (equations (4.11) – (4.13)) was employed to fit the data at 298.15 and 323.15 K to obtain the parameters as tabulated in Table 4.6, and the predicted results are displayed in Figure 4.3, Figure 4.4, Figure 4.5 and Figure 4.6 (by the solid line). The AAD and AMD of H_A of N₂O in aqueous MEA solutions is 1.49% and 4.97%, respectively, the corresponding values for H_A of CO₂ is 1.48% and 4.92%. The comparisons between the experimental data and predicted values are delineated in Figure 4.7, which shows that the predicted values are in good agreement with the experimental data. There is no obvious systematic deviation between data and model. Only data from the present work were used to obtain fitted parameters.

The N₂O solubility in pure MEA was regressed from the experimental data using an equation of the form of equation (4.9) as follows

$$H_{\text{N}_2\text{O,MEA}} = 2.448 \times 10^5 \exp(-1348/T) \quad (4.16)$$

Then, combining the equations (4.9), (4.16) and Wang et al.'s model with its fitted parameters, more solubility values in different concentrations at various temperatures can be predicted. For instance, the solubilities of N₂O in aqueous MEA solutions at 293.15 K and 333.15 K are predicted and shown in Figure 4.4 by dashed and dotted lines, respectively. The average of the relative deviations of this work from the literature values are listed in Table 4.7.

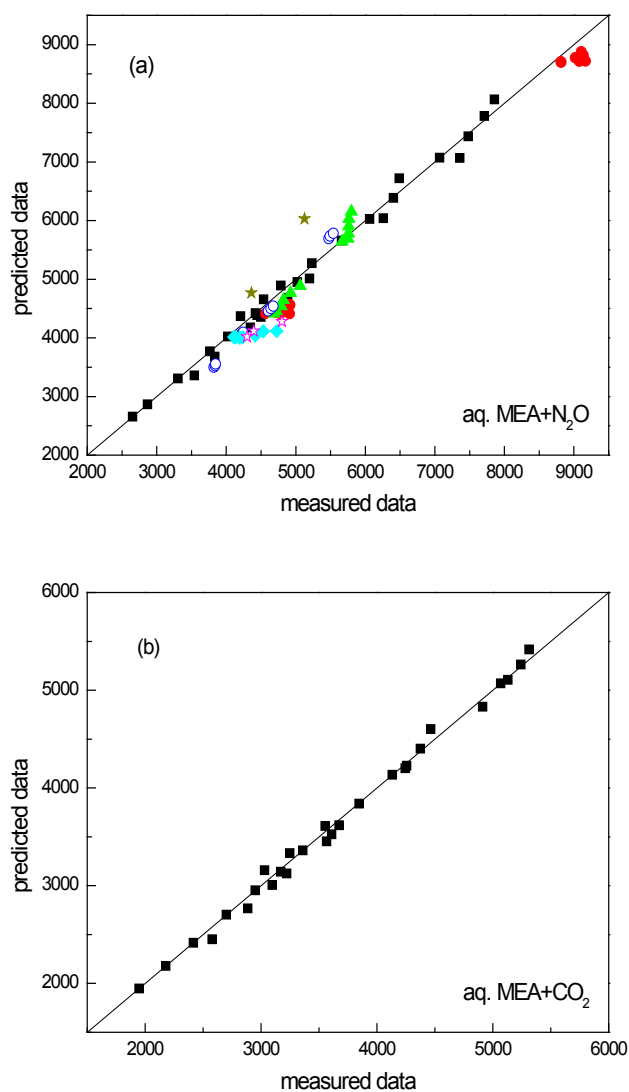


Figure 4.7 Comparisons between measured and predicted solubilities of N_2O (a) and CO_2 (b) in $\text{MEA}+\text{H}_2\text{O}$: ■, this work; ○, Mandal et al.⁸; ☆, Browning and Weiland¹²; ▲, Tai et al.⁷; ★, Li and Lai⁶; ◆, Sada and Kito¹⁶; ●, Littel et al.¹⁵

Table 4.7 Average relative deviation between the values predicted by Wang et al.'s model and those reported in literature for solubility of N_2O in aqueous MEA solutions

C_{MEA} (mol L ⁻¹)	T/K	ARD(%)	reference
2–3	298.15–313.15	1.9	Mandal et al. ⁸
1–6	303.15–313.15	1.8	Tai et al. ⁷
0.5–6	298.15	3.4	Sada et al. ¹⁶
1.6–5	298.15	4.1	Browning and Weiland ¹²
5	303.15–313.15	6.3	Li and Lai ⁶
0.183– 3.911	303.15, 333.15	2.6	Littel et al. ¹⁵

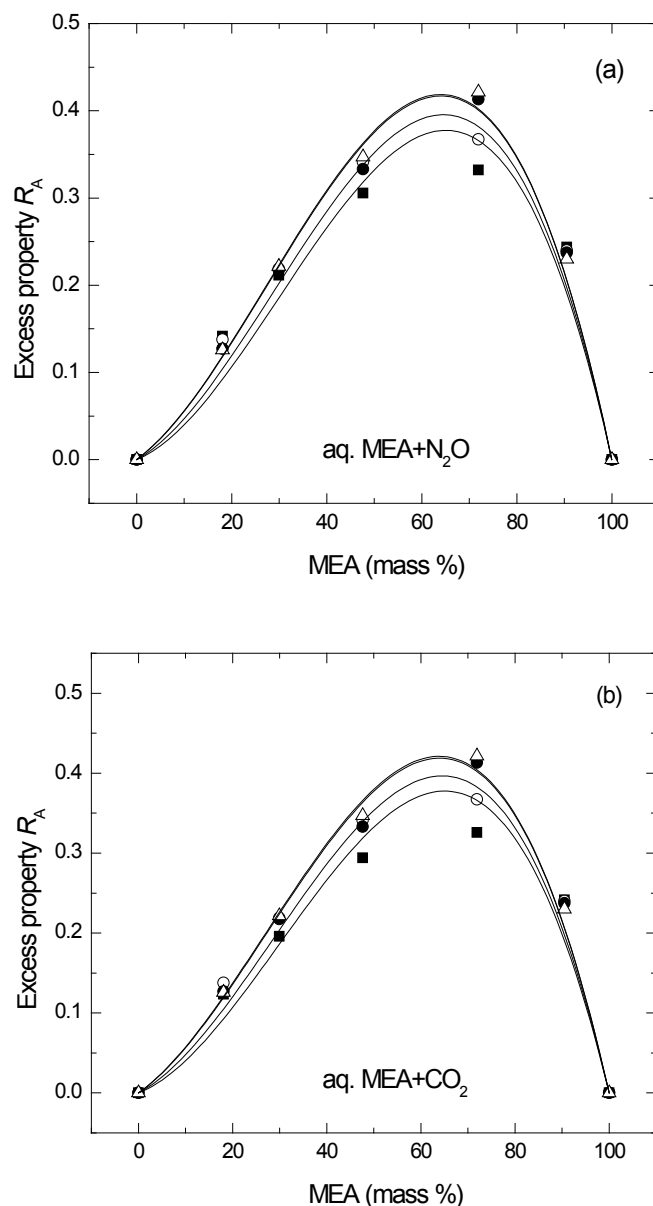


Figure 4.8 Dependence of the mass percentage for the solubility excess property R_A for N₂O (a) and CO₂ (b) in MEA+H₂O from (298.15 to 323.15) K:

■, 298.15 K; ○, 303.15 K; ●, 313.15 K; △, 323.15 K; The solid line was calculated by equation (4.11)

It is known that positive values of R_A corresponding to solubilities less than the ideal mixture value occur if the gas-free aqueous MEA solution reveals negative deviations from the linear additive principle.²² Conversely, negative values of R_A correspond to solubilities higher than that of the ideal mixture and manifest positive deviations of the gas-free aqueous MEA solution. The values of R_A for N₂O or CO₂ were calculated using equation (4.11) and the results are shown in Figure 4.8. It can be seen that the excess Henry's properties display positive deviations, which denote that the solubilities of N₂O and CO₂ in aqueous MEA solutions show negative deviations. This behavior can be explained as follows: The MEA

molecule involves the strong electronegative groups $-\text{NH}_2$ and $-\text{OH}$ which can form hydrogen bonds with H_2O resulting in strong interactions between MEA and H_2O . The strong interactions between MEA and H_2O weaken the interactions of both CO_2 and MEA and CO_2 and H_2O . This leads to a decrease of the solubility of the gas. The excess Henry's properties of MEA+ H_2O (N_2O or CO_2) system increased with increasing of MEA mass percentage as described in Figure 4.8 in the range from 0 to 60 mass %, but when the MEA mass percentage was about 60 mass %, the interactions between MEA and H_2O reached a maximum due to the proportions of MEA and H_2O in the solution and the quantities of hydrogen bonds were then at its peak. On the other hand, the lower the free volume in the solution is, the less the capacity for "holding" the molecules of a gas. The interactions (hydrogen bonds) between MEA and H_2O cause the free volumes in the solution to decrease, and these interactions are maximum and result in the lowest free volume in the solution as the MEA mass percentage is about 60 mass %. This is also the main explanation for the variation of the density with the concentration of aqueous MEA solutions as mentioned above.

4.4. Uncertainty Analysis

There are several sources of uncertainty that must be accounted for:

1. The uncertainties caused by weighing in the preparation of MEA solutions.
2. The uncertainties due to the fluctuation of the temperature.
3. The uncertainties due to the resistance caused by the friction between the inner glass and mercury as the mercury drop moves.
4. The uncertainties due to the visual reading from the scale on the spiral tube.
5. The other uncertainties such as due to estimating the 20 s gas absorption before the absorption cell connect to the spiral tube; the estimation of the fluctuation of room pressure between the beginning and end of the measurement, *etc.*

The combined standard uncertainty of this work has been evaluated by the method according to (NIST TN 1297; ISO guide "GUM"; also adopted by ANSI). The reported value, Henry's coefficient (H_A), should be broken down to analyze the effect of variables in our measurement program. This could be written as

$$H_A = f(w_{\text{MEA}}, T, r, H_{\text{instrument}}, \text{Other}) \quad (4.17)$$

where the variables are weight fraction MEA, temperature, friction, the instrument reading and other factors.

As recommended the focus is on the use of standard deviation. The size asked for is the combined standard uncertainty which is designated by $u_c(y)$. The mathematical formalism is using the variance, i.e. $u_c^2(y)$, and this is arrived at through

$$u_c^2(y) = \sum_{i=1}^N \left\{ \frac{\partial H}{\partial x_i} \right\}^2 u_i^2(x_i) \quad (4.18)$$

We now need to obtain / evaluate these relations one by one to quantify our “judgment” of uncertainties and eventually the combined standard uncertainty.

For the correction of the fluctuation of room pressure, the maximum variation of room pressure was from 99.8 kPa to 102.8 kPa, and then the difference was 3 kPa in this work. The corrected equation (4.5) is for ideal gas, the uncertainty is 1% for the real gas was measured. The change of gas volume with room pressure in this work is 1.18 mL/kPa. The pressure accuracy of the barometer in the lab is specified as ± 0.02 kPa. Then the error source causes 0.0236 mL error. The amount of equilibrium absorption is 5 mL when measure the 8 M solution at 323.15 K, the solubility value is 7412 kPa m³ kmol⁻¹, the maximum specific error is 1482 (kPa m³ kmol⁻¹)/mL. Then the uncertainty in H_A caused by the fluctuation of room pressure is 35.0 kPa·m³·kmol⁻¹.

The temperature controlled by the water bath, and the temperature accuracy is specified as ± 0.1 K. Based on the results, for $C_{\text{MEA}}=8$ M, the H_A changes from 4428 to 5060 kPa m⁻³ kmol⁻¹ from 298 to 303 K. This is the maximum change with temperature in this work. It implies that the maximum change of H_A is 141 kPa m³ kmol⁻¹ when the temperature changes 1K. This leads to an uncertainty in H_A of 14.1 kPa m³ kmol⁻¹ due to the temperature accuracy is specified as ± 0.1 K.

The resistance caused by the friction between the inner glass and the mercury as the mercury drop moves will lead to volume reading error. The maximum driving force (pressure difference between the two sides of the drop) for keeping the mercury moving is 100 Pa. under this pressure difference, it was measured that it generated maximum 0.005 mL error. Then it causes in 7.4 kPa m³ kmol⁻¹ uncertainty in H_A .

The maximum visual reading error is 0.0025 mL, and brings about 3.7 kPa·m³·kmol⁻¹ uncertainty in H_A .

The accuracy of weight fraction of MEA solution is estimated as ± 0.001 g. The work prepared 20 g, 3 M solution required about 3.7 g solution for each measurement. The maximum change of H_A in this work is 2716 kPa·m³·kmol⁻¹ when the change of weight fraction of is 1 g MEA. This corresponds to an uncertainty in H_A is 2.7 kPa·m³·kmol⁻¹.

The uncertainty in H_A is determined as $\pm 39 \text{ kPa} \cdot \text{m}^3 \cdot \text{kmol}^{-1}$ by combining the various sources of uncertainty calculating by the equation (4.18).

Table 4.8 Uncertainty analysis for the measurement of physical solubility

Source of Uncertainty	$\partial D_A / \partial x_i$	$u(x_i)$	$(\partial D_A / \partial x_i)u(x_i)$
1. The fluctuation of room pressure.	1482	0.0236 mL	35.0
2. The fluctuation of the temperature controlled.	141	0.1 K	14.1
3. The resistance caused by the moving friction of mercury drop.	1482	0.005 mL	7.4
4. Eye reading from the scale on the spiral tube.	1482	0.0025 mL	3.7
5. Weighing preparation of MEA solutions.	2716	0.001 g	2.7
Combined uncertainty			39 kPa · m³ · kmol⁻¹

4.5. Conclusions

The solubilities of N_2O in various aqueous MEA solutions ranging from 0 to 100 mass % were measured using a novel solubility apparatus, and the solubilities of CO_2 were obtained by the N_2O analogy method. The results of the solubility measurements of N_2O and CO_2 in water indicate that the novel technique is feasible and reliable. The advantages of the new method include easy operation, lower mercury inventory, higher sensitivity and greater accurate. A semiempirical model of the excess Henry's constant proposed by Wang et al. was used to correlate the solubilities of N_2O and CO_2 in MEA solutions, and the simulated results are found to be in agreement with experiment data. The parameters of the correlation were determined from the solubilities of N_2O and CO_2 obtained in this study. For the temperature range from 298.15 to 323.15 K, the obtained correlation was found to represent the data reasonably well, the errors of 1.49% and 1.48% respectively, in the solubilities of N_2O and CO_2 in MEA aqueous solutions. The Henry's constants of N_2O and CO_2 in MEA+ H_2O showed positive deviation behaviors from the linear additive principle. This implies that the solubilities of both N_2O and CO_2 in aqueous MEA solutions showed negative deviations, which can be explained by excess Henry's constants relative to the variation of the interactions of MEA and H_2O .

Nomenclature

Parameters and Variables

a_i = parameters in equation (4.13), $i=1,2,3,\dots$

a_{12} = two-body interaction parameter between the two components of the solvent.

A_{cal} = property value of calculated from a model.

A_{exp} = experimental value of the property.

AAD = absolute average deviation between calculated values and experimental data, (%)

AMD = absolute maximum deviation between calculated values and experimental data, (%)

ARD = the average relative deviation, (%)

b = parameter in equation (4.13)

C_A^* = equilibrium molar concentration of gas A in the solution, (kmol m^{-3})

H_A = Henry's constant of gas A in a liquid, ($\text{kPa m}^3 \text{ kmol}^{-1}$)

$H_{A,i}$ = Henry's constant of absorbed gas A in a pure solvent i , ($\text{kPa m}^3 \text{ kmol}^{-1}$)

$H_{A,m}^{\text{cal}}$ = Henry's constant of calculated from Wang et al.'s model, ($\text{kPa m}^3 \text{ kmol}^{-1}$)

$H_{A,m}^{\text{exp}}$ = Henry's constant of experimental value, ($\text{kPa m}^3 \text{ kmol}^{-1}$)

$H_{A,m}$ = Henry's constant of absorbed gas A in the mixed solvent, ($\text{kPa m}^3 \text{ kmol}^{-1}$)

n_A = mole amount of gas A, (mol)

P_A = partial pressure of gas A, (kPa)

P_A^{end} = partial pressure of gas A at absorption equilibrium, (kPa)

P_A^{ini} = partial pressure of gas A before absorption starts, (kPa)

$P_{\text{room}}^{\text{ini}}$ = room pressure at the beginning of the measurement, (kPa)

$P_{\text{room}}^{\text{end}}$ = room pressure at the end of the measurement, (kPa)

$P_{\text{H}_2\text{O}}^{\text{v}}$ = vapor pressure of pure water, (kPa)

$P_{\text{MEA}}^{\text{v}}$ = vapor pressure of pure MEA, (kPa)

R = gas constant, ($\text{m}^3 \text{ kPa K}^{-1} \text{ kmol}^{-1}$)

RD = relative deviation, (%)

R_A = excess Henry's coefficient from Wang et al.'s model, ($\text{kPa m}^3 \text{ kmol}^{-1}$)

T = temperature of the system, (K)

u_c = combined uncertainty

V_A = corrected absorption volume of gas A at room pressure, (m^3)

V_A^{exp} = experimental gas A absorption volume at room pressure, (m^3)

V_G = volume of gas phase, (m^3)

V_G^{end} = volume of gas phase in absorption cell at end of the measurement at room pressure, (m^3)

V_L = volume of the liquid phase, (m^3)

$x_{\text{H}_2\text{O}}$ = mole fraction of water

x_i = the influence factor result in the uncertainty

x_{MEA} = mole fraction of MEA

Greek Symbols

φ_i = the mass percentage of solvent i

φ_1 = the mass percentage of MEA

φ_2 = the mass percentage of water

α_{12} = the two-body interaction parameter between the two components of the solvent

References

1. Versteeg, G. F.; van Swaaij, W. P. M. Solubility and Diffusivity of Acid Gases (CO_2 , N_2O) in Aqueous Alkanolamine Solutions. *J. Chem. Eng. Data* **1988**, *33*, 29–34.
2. Weiland, R. H.; Trass, O. Absorption of Carbon Dioxide in Ethylenediamine Solution. *Can. J. Chem. Eng.* **1971**, *49*, 767–772.
3. Haimour, N.; Sandall, O. C. Absorption of Carbon Dioxide into Aqueous Methyldiethanolamine. *Chem. Eng. Sci.* **1984**, *39*, 1791–1796.
4. Haimour, N. Solubility of N_2O in Aqueous Solutions of Diethanolamine at Different Temperatures. *J. Chem. Eng. Data* **1990**, *35*, 177–178.
5. Al-Ghawas, H. A.; Hagewiesche, D. P.; Ruiz-Ibanez, G.; Sandall, O. C. Physicochemical Properties Important for Carbon Dioxide Absorption in Aqueous Methyldiethanolamine. *J. Chem. Eng. Data* **1989**, *34*, 385–391.
6. Li, M. H.; Lai, M. D. Solubility and Diffusivity of N_2O and CO_2 in (Monoethanolamine + N-Methyldiethanolamine + Water) and in (Monoethanolamine + 2-Amino-2-Methyl-1-Propanol + Water). *J. Chem. Eng. Data* **1995**, *40*, 486–492.
7. Tai, T. -c., T.; Ko, J. -j; Li, M. H. Solubility of Nitrous Oxide in Alkanolamine Aqueous Solutions. *J. Chem. Eng. Data* **2000**, *45*, 341–347.
8. Mandal, B. P.; Kundu, M.; Padhiyar, N. U.; Bandyopadhyay, S. S. Physical Solubility and Diffusivity of N_2O and CO_2 into Aqueous Solutions of (2-Amino-2-methyl-1-propanol + Monoethanolamine) and (N-Methyldiethanolamine + Monoethanolamine). *J. Chem. Eng. Data* **2005**, *50*, 352–358.
9. Rinker, E. B.; Ashour, S. S.; Sandall, O. C. Kinetics and Modeling of Carbon Dioxide Absorption into Aqueous Solutions of N-Methyldiethanolamine. *Chem. Eng. Sci.* **1995**, *50*, 755–768.
10. Davis, R. A.; Pogalnis, B. J. Solubility of Nitrous Oxide in Aqueous Blends of N-Methyldiethanolamine and 2-Amino-2-methyl-1-propanol. *J. Chem. Eng. Data* **1995**, *40*, 1249–1251.
11. Samanta, A.; Roy, S.; Bandyopadhyay, S. S. Physical Solubility and Diffusivity of N_2O and CO_2 in Aqueous Solution of Piperazine and (N-Methyldiethanolamine + Piperazine). *J. Chem. Eng. Data* **2007**, *52*, 1381–1385.
12. Browning, G. J.; Weiland, R. H. Physical Solubility of Carbon Dioxide in Aqueous Alkanolamines via Nitrous Oxide Analogy. *J. Chem. Eng. Data* **1994**, *39*, 817–822.

13. Wang, Y. W.; Xu, S.; Otto, F. D.; Mather, A. E. Solubility of N₂O in Alkanolamines and in Mixed Amines. *Chem. Eng. J.* **1992**, *48*, 31–40.
14. Mandal, B. P.; Kundu, M.; Padhiyar, N. U.; Bandyopadhyay, S. S. Physical Solubility and Diffusivity of N₂O and CO₂ into Aqueous Solutions of (2–Amino–2–Methyl–1–Propanol + Diethanolamine) and (N–Methyldiethanolamine + Diethanolamine). *J. Chem. Eng. Data* **2004**, *49*, 264–270.
15. Littel, R. J.; Versteeg, G. F.; van Swaaij, W. P. M. Solubility and Diffusivity Data for the Absorption of COS, CO₂, and N₂O in Amine Solutions. *J. Chem. Eng. Data* **1992**, *37*, 49–55.
16. Sada, E.; Kito, S. Solubilities of Gases in Aqueous Monoethanolamine Solutions. *Kagaku Kogaku* **1972**, *36*, 218–220.
17. Park, M. K.; Sandall O. C. Solubility of Carbon Dioxide and Nitrous Oxide in 50 mass % Methyldiethanolamine. *J. Chem. Eng. Data* **2001**, *46*, 166–168.
18. Clarke, J. K. A. Kinetics of Absorption of CO₂ in Monoethanolamine Solution at Short Contact Time. *Ind. Eng. Chem. Fundam.* **1964**, *3*, 239–245.
19. Amundsen, T. G.; Øi, L. E.; Eimer, D. Density and Viscosity of Monoethanolamine plus Water plus Carbon Dioxide from 25 to 80 degrees C. *J. Chem. Eng. Data* **2009**, *54*, 3096–3011.
20. Han, J. Y.; Jin, J.; Eimer, D. A.; Melaaen, C. C. Density of Water (1) + Monoethanolamine (2) + CO₂ (3) from (298.15 to 413.15) K and Surface Tension of Water (1) + Monoethanolamine (2) from (303.15 to 333.15) K. *J. Chem. Eng. Data* **2012**, *57*, 1095–1103.
21. Lee, M. J., Lin, T. K. Density and Viscosity for Monoethanolamine +Water, +Ethanol, and +2–Propanol, *J. Chem. Eng. Data* **1995**, *40*, 336–339.
22. Lakatos, T.; Johansson, L. G.; Simmingsköld, B. Viscosity Temperature Relations in the Glass System SiO₂–Al₂O₃–Na₂O–K₂O–CaO–MgO in the Composition Range of Technical Glasses. *Glass Technol.* **1972**, *13*, 88–95.

Chapter 5

5. Viscosity Measurement of Aqueous Monoethanolamine Solution

Abstract

Viscosities of aqueous MEA solutions over a full concentration range were examined at a temperature range from (298.15 to 343.15) K. The experimental values were compared with the available literature values. The experimental viscosities measured in this work are in good agreement with those reported in the literature. The equation proposed by DiGuilio et al. is used to correlate the pure amines' viscosities while the correlation from Teng et al. is selected for aqueous amine system. The average absolute deviations (AAD) between the correlated and measured data were calculated. Viscosities of the aqueous MEA solutions decrease as temperature increases. The relationship between the viscosity and mole fraction of MEA shows both positive deviation and negative deviation behaviors from Linear Additivity Principle.

5.1. Introduction

Alkanolamines have been used as absorbent for the acid gas absorption process since the 1930s. The physical properties of the absorbent are important to understand the mass transfer and the engineering calculations. The physical properties such as density, viscosity, surface tension, diffusivity and solubility data of chemical and physical solvents are important for the absorption and regeneration process of CO₂ capture. Different amines are available for the process, such as primary amines (MEA, DGA), secondary amines (DEA, DIPA), tertiary amines (MDEA, TEA), hindered amines (AMP, AMPD), cyclic amines (PZ, PE) and polyamines (AEEA). Important common alkanolamines for industrial performance are MEA, DEA, DIPA and MDEA.¹⁻⁹ Among these alkanolamines, aqueous MEA solution is widely used for CO₂ capture process due to high reactivity, low cost and ease of regeneration.

Table 5.1 Comparison of the viscosities of pure MEA measured in this work with literature values from temperature from 293.15 to 353.15 K

T/K	μ (mPa s)				
	This work	Li and Lie ¹	DiGuilio et al. ⁶	Mandal et al. ⁷	Song et al. ⁸
293.15				24.10	
298.15	18.903			18.98	
303.15	15.099	15.1088	14.86	15.11	15.1940
313.15	10.026	10.0209	9.89	10.02	10.0283
323.15	6.991	6.9715		6.972	6.9463
333.15	5.090	5.0473	4.99	5.047	5.0454
343.15	3.789	3.7793		3.779	3.8050
353.15	2.959	2.9120	2.90	2.912	

The viscosities of pure MEA from literature are summarized in Table 5.1 and the measured data in this work are also shown in this table. Some correlations were employed for prediction of viscosity of liquids from literature. Vogel¹¹ has proposed a simple form correlation with three constants for pure liquid viscosity and Viswanath¹² utilized a similar form for simulating both dynamic and kinematic viscosities. The equation reported by Vogel is modified by Goletz¹³ includes the boiling point of the liquid. Dutt¹⁴ presented a similar equation to Goletz and has derived a correlation with density and boiling point of the component. Pure liquid viscosity can be described by polynomial type equation suggested by Girifalco¹⁵ and Thorpe¹⁶ extended that. DiGuilio et al.⁶ reported the three constant equations

which is very close to Vogel's equation for pure amines' viscosity. Among those, DiGuilio's equation is selected for calculation of pure amines' viscosity due to less deviation.

The aqueous amine viscosities measured in this work are used to generate the polynomial for theoretical interpretation of amine viscosities using regression. Teng et al.¹⁷ and Chowdhury et al.¹⁸ have been reported the correlations for aqueous amine viscosity variation with molar concentration for specific temperature values. The correlation from Teng et al. is chosen for this study because of lower deviation.

Table 5.2 The viscosities of pure MEA from literature values at temperature from 298.15 to 353.15 K and the ARD from the eq.(5.2) by this work

mass %	μ (mPa s)						ARD(%)	reference
	298.15K	303.15K	313.15K	323.15K	333.15K	343.15K		
20%	1.70		1.18	0.95		0.67	0.58	
30%	2.48		1.67	1.33		0.92	0.77	
40%	3.58		2.28	1.75		1.14	0.95	
50%	5.51		3.39	2.54		1.57	1.28	1.6% Ref. 9
70%	12.46		6.96	4.94		2.79	2.18	
90%	19.40		10.20	7.06		3.81	2.93	
100%	17.90		9.61	6.72		3.69	2.85	
10%	1.77							
20%	1.72							
30%	2.52							5.5% Ref.10
40%	3.41							
20%		1.480	1.161	0.936	0.778	0.659	0.577	1.3% Ref.1
30%		2.109	1.616	1.277	1.035	0.868	0.732	

A limited source of viscosity data found for the system MEA with water are Li and Lie¹, Amundsen et al.⁹ and Weiland et al.¹⁰ as shown in Table 5.2. There are no available values for the concentration of MEA adopted by this work. To obtain more accurate viscosity data of the present concentration aqueous MEA solution, the present work measured the viscosity of (0.5, 3, 5, 8, 10, 12, 14) M aqueous MEA solution at the temperature range (298.15 to 353.15) K, and thus make investigation of more concentrated solutions easier. These data can be used in the Stokes–Einstein equation for the diffusivity measurement of aqueous MEA solution in chapter 5.

5.2. Experimental Section

The viscosity of aqueous MEA solution was measured using an Anton Paar rheometer (MCR 101) with a double-gap measuring system. The viscometer was calibrated against the petroleum distillate and mineral oil calibration fluid from Paragon Scientific Ltd. The calibration factors at various temperatures are determined by using the calibration liquid and the experimental viscosities are corrected by the calibration factors. Reagent grade MEA with mass fraction purity 99.5% was purchased from Merck and used without further purification. Deionized water (purified with a mini-Q system, purity defined by conductivity 18.2 MΩ·cm) and MEA were degassed by applying vacuum respectively, and then mixed to prepare various concentration of aqueous MEA solutions using an analytical balance (Mettler Toledo XS403S) with an accuracy ±1 mg and a 5000mL volumetric flask. This preparation procedure avoids the loss of the water vapor compared with the method of directly vacuuming the solution. Various concentrations aqueous MEA solutions were prepared: 0.5 M (3.1 mass %), 3 M (18.1 mass %), 5 M (30.2 mass %), 8 M (47.9 mass %), 10 M (59.6 mass %), 12 M (71.4 mass %), 14 M (83.6 mass %) and 16.4 M (100 mass %). The whole preparation process was protected by a nitrogen atmosphere. The purity of CO₂ was ≥ 99.995% and N₂O ≥ 99.7 mol %, both gases produced by AGA Gas GmbH.

5.3. Results and Discussion

5.3.1. Viscosity of Pure MEA

Viscosities of pure MEA were measured in the temperature range (298.15 to 353.15) K. The results are tabulated in Table 5.1 and shown in Figure 5.1. It can be seen that the viscosities of pure MEA are decreasing with the increase of temperature as expected. Agreement of the viscosities of pure MEA between the measurement data and literature values from Li and Lie¹, DiGuilio et al.³ Mandal et al.⁴ and Song et al.⁸ were found to be satisfactory.

The model proposed by DiGuilio et al.⁶ as equation (5.1) was used to calculate the pure MEA viscosities.

$$\ln \mu = b_1 + \frac{b_2}{T - b_3} \quad (5.1)$$

where T is temperature given in K and b_1 , b_2 and b_3 are constant values. The result fitted by equation (5.1) is shown in Figure 5.1 and the parameters are listed in Table 5.3 and the absolute average percentage deviation (AAD) between the experimental data and regression

value is also included. The AAD and absolute maximum deviation (AMD) are defined in equations (4.14) and (4.15), respectively.

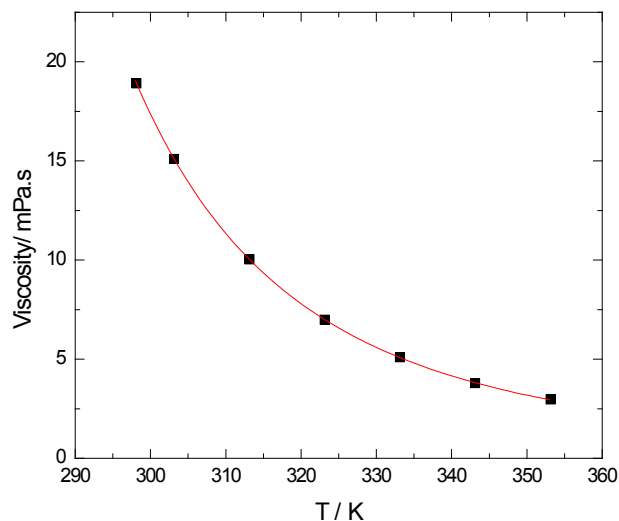


Figure 5.1 The viscosity of pure MEA as a function of temperature.
(The solid line was simulated by equation(5.1))

It is seen from the regression results that the AAD is only 0.21% and the AMD is 0.6%. It manifests the model proposed by DiGuilio et al.⁶ is very satisfactory for the correlation of the viscosity of pure MEA as function of temperature.

Table 5.3 Parameters in equation(5.1) for the Viscosities of pure MEA

amine	b_1	b_2	b_3	AAD	AMD
Pure MEA	-3.8214	980.18	153.17	0.21%	0.6%

5.3.2. Viscosity of the Aqueous MEA Solution

The viscosity measurements for aqueous MEA solutions over the full concentration range were performed at a temperature range from 298.15 to 353.15 K. The viscosity data for aqueous MEA solutions are listed in Table 5.4.

A polynomial mathematical model proposed by Teng et al.¹⁷ can be used for the data regression in this work.

$$\ln \mu = \ln \mu_0 + \sum_1^n a_i C^i \quad i = 1, 2, \dots, n \quad (5.2)$$

where μ and μ_0 represent the viscosity of the MEA solution and pure water respectively, and C is the mass fraction of the MEA solution. In this model, $\ln\mu_0$ is the constant item instead of a_0 . The equation was checked from 1st to 7th-order polynomial for (MEA+H₂O) system with the experimental data, and found 5th-order polynomial with respect to the mass fraction with five parameters a_1, a_2, a_3, a_4 and a_5 in equation (5.2) satisfied this work.

Table 5.4 Viscosities of Aqueous MEA Solutions from Temperature 298.15 to 353.15 K

C (mol L ⁻¹)	μ (mPa s)						
	298.15 K	303.15 K	313.15 K	323.15 K	333.15 K	343.15 K	353.15 K
0	0.909	0.814	0.668	0.559	0.477	0.412	0.363
0.5	0.980	0.871	0.715	0.598	0.508	0.438	0.386
3	1.591	1.392	1.093	0.884	0.733	0.616	0.532
5	2.673	2.280	1.744	1.356	1.091	0.888	0.733
8	5.155	4.299	3.110	2.328	1.800	1.411	1.137
10	9.342	7.577	5.226	3.777	2.836	2.196	1.744
12	13.972	11.005	7.500	5.243	3.817	2.867	2.186
14	18.502	14.623	9.577	6.569	4.732	3.494	2.718
16.4	18.903	15.099	10.026	6.991	5.090	3.789	2.959

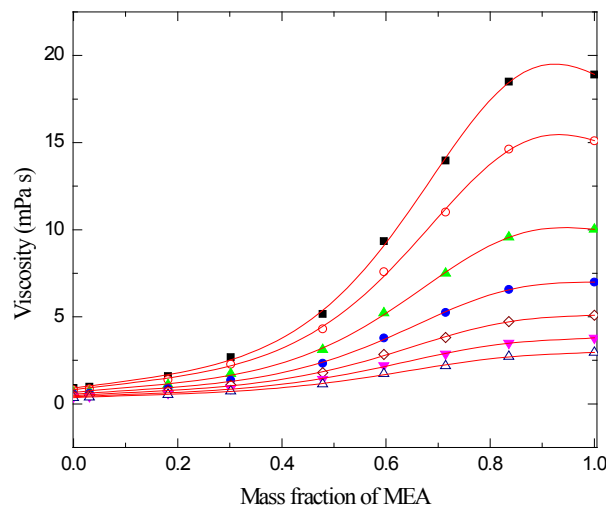


Figure 5.2 The viscosity of MEA +H₂O as function of MEA mass fraction from 298.15 to 353.15 K:

■, 298.15 K; ○, 303.15 K; ▲, 313.15 K; ●, 323.15 K; ◇, 333.15 K; ▼, 343.15 K; △, 353.15 K;

The solid line was simulated by equation (5.2)

Table 5.5 Parameters in equation (5.2) for the Viscosities of Aqueous MEA Solutions

T /K	a_1	a_2	a_3	a_4	a_5	AAD	AMD
298.15	4.4020	-11.0487	36.8093	-42.1525	15.0249	2.72%	5.58%
303.15	4.4935	-11.9212	37.4207	-41.8234	14.7514	2.88%	6.96%
313.15	4.0885	-11.3399	36.9195	-42.3684	15.4091	2.44%	5.51%
323.15	3.8933	-11.4494	37.1136	-42.9145	15.8835	2.26%	5.06%
333.15	3.7498	-11.4535	36.4918	-42.0863	15.6662	2.27%	5.02%
343.15	3.4346	-10.7758	35.3883	-41.6417	15.8139	2.18%	4.42%
353.15	3.2787	-10.1998	32.3783	-37.2871	13.9287	2.22%	4.03%

The regression coefficients from this work are tabulated in Table 5.5. The results of the AAD and AMD for the regression at various temperatures are also listed in Table 5.5. The simulated results and the experimental data are plotted in Figure 5.2. These low deviations (AAD and AMD) and the comparison between experimental and predicted data (is shown in Figure 5.3) show that this mathematical model can correlate the viscosity of the aqueous MEA solutions as function of mass fraction with good agreements.

The viscosity value, 1.77 mPa s, of 10 mass % at 298.15 K reported by Weiland et al.¹⁰ maybe is an outlier, the ARD is 15.1% compared with the value 1.306 mPa s calculated by this work, but we cannot find the value from other present literature to compare with it.

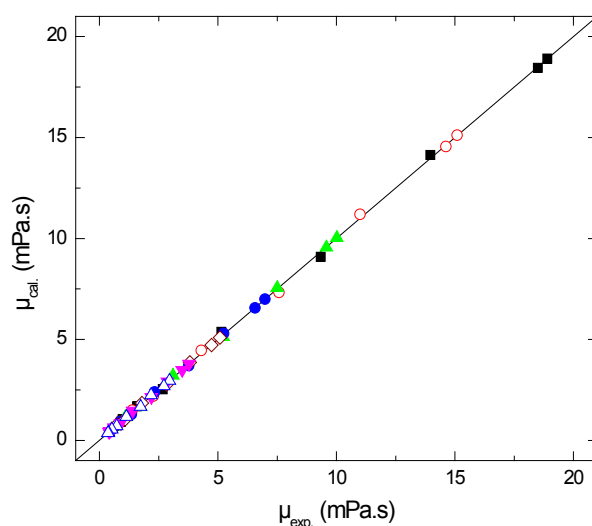


Figure 5.3 Comparisons the viscosities of aqueous MEA solutions between measured and predicted data by equation (5.2): ■, 298.15 K; ○, 303.15 K; ▲, 313.15 K; ●, 323.15 K; ◇, 333.15 K, ▼, 343.15 K; △, 353.15 K;

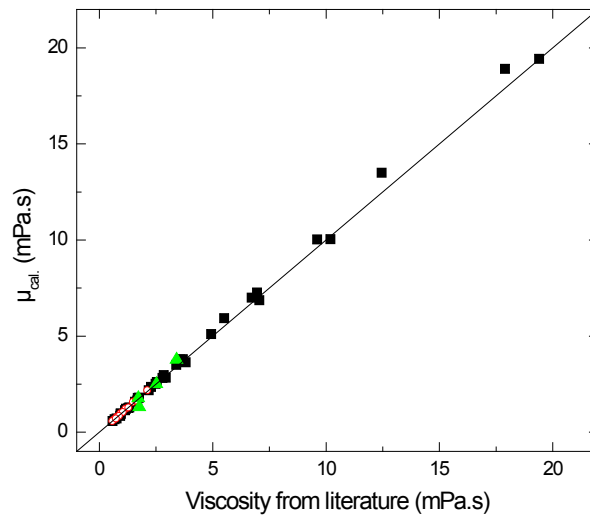


Figure 5.4 Comparisons the viscosities of aqueous MEA solutions between literature values and predicted data by equation (5.2): ■, Amundsen et al.⁹; ○, Li and Lie¹; ▲, Weiland et al.¹⁰

The viscosities of the aqueous MEA solutions as function of temperature are plotted in Figure 5.5. As similar trend as the relationship of pure MEA versus temperature, the viscosity of the aqueous MEA solution decreases with the increasing of temperature. This is because the higher the temperature is, the higher the energies of molecules are, and more easily the molecules of MEA and H₂O overcome the attraction forces among molecules, thus the movements of the molecules become easier, resulting in a lower viscosity of the solution.

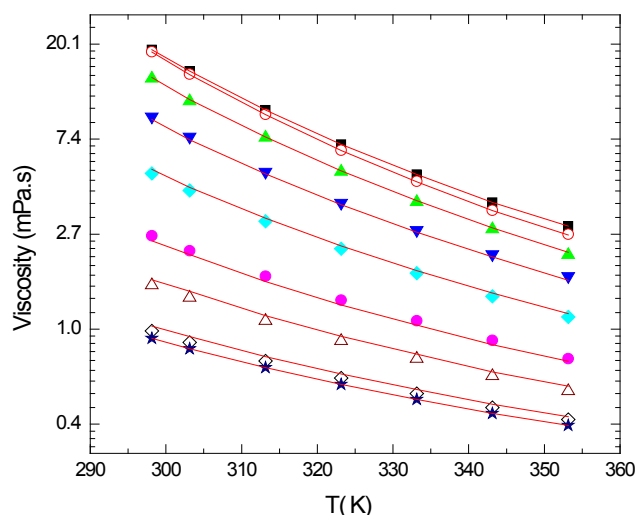


Figure 5.5 The viscosity of MEA +H₂O as a function of temperature:
 ■, pure MEA; ○, 14 M; ▲, 12 M; ▼, 10 M; ◆, 8 M; ●, 5 M; △, 3 M; ◇, 0.5 M; ★, H₂O;
 The solid line was simulated by equation (5.2)

Figure 5.6 shows the viscosity of the aqueous MEA solution as function of MEA mole fraction at 298.15 K. It is interesting that the relationship between the viscosity and mole fraction of MEA shows both negative deviation and positive deviation, and the same behavior is shown at the other temperatures. This is, the viscosities of the MEA solutions are lower than the ideal solution when the mole fraction of MEA is less than 0.2 and opposite as mole fraction is higher than 0.2. This behavior is determined by the interaction forces between the molecules in the solution according to the thermodynamic theory. with regard to the MEA+H₂O solution, the cohesive forces of MEA and MEA molecules are affected by a dilution effect of H₂O molecules and the attraction forces between MEA and H₂O molecules through the formation of hydrogen bonds. When the mole fraction of MEA is less than about 0.2, the dilution effect plays a lubrication and main role and lessens the cohesive forces of MEA molecules, resulting in the viscosities of the solutions being less than the expected viscosities from Linear Additivity Principle.¹⁹ and show a negative deviation behavior. Furthermore, the dilution effect is the strongest when the mole fraction reaches about 0.1. But when the mole fraction of MEA is higher than 0.2, the attraction forces by hydrogen bonds between MEA and H₂O molecules play a leading role compared to the dilution effect, causing the viscosities of the solutions to be higher than that of the ideal solution and show a positive deviation behavior. It is noted that the positive behavior is maximum when the mole fraction of MEA is about 0.6.

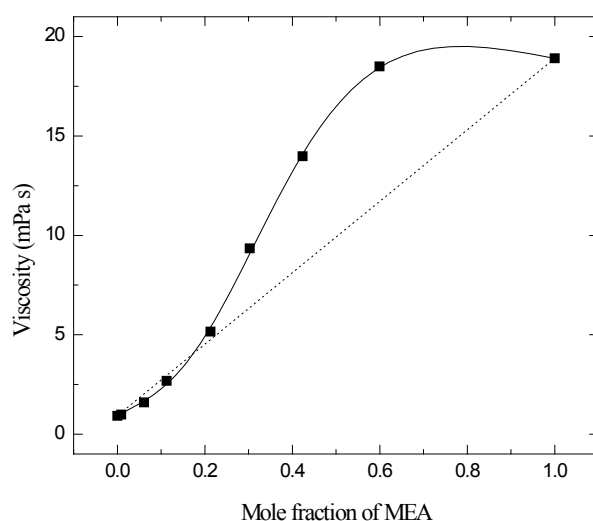


Figure 5.6 The viscosity of MEA +H₂O as a function of MEA mole fraction at 298.15 K. (The solid line was simulated by equation (5.2), the dotted line was calculated by Additivity principle)

5.4. Conclusions

The viscosities of aqueous MEA solutions over the full concentration range were measured at temperature range from (298.15 to 353.15) K. the results show that the viscosities of aqueous MEA solutions are decreasing with the increase of temperature. The measured viscosity data are in good agreement with the literature data. The exponent model of (viscosity versus temperature) with three parameters was proposed by DiGuilio et al.⁶ is very satisfied for the regression and simulation of pure MEA, and the polynomial model proposed by Teng et al.¹⁷ with respect to the mass fraction with five parameters a_1 , a_2 , a_3 , a_4 and a_5 satisfied the aqueous MEA solution. The relationship between the viscosity and mole fraction of MEA shows a positive deviation and negative deviation behaviors, and the critical mole fraction of MEA is 0.2.

Nomenclature

Parameters and Variables

a_i = parameters in equation (5.2), $i=1,2,3,\dots$

A_{cal} = property value of calculated from a model.

A_{exp} = experimental value of the property.

AAD = absolute average deviation between calculated values and experimental data, (%)

AMD = absolute maximum deviation between calculated values and experimental data, (%)

ARD = the average relative deviation, (%)

b_1, b_2, b_3 = parameters in equation (5.1)

C = mass fraction of the solution, (%)

RD = relative deviation, (%)

T = temperature of the system, (K)

Greek Symbols

μ = viscosity of the solution, (mPa s)

μ_0 = viscosity of pure water, (mPa s)

References

1. Li, M. H. and Lie, Y. C. Densities and Viscosities of Solutions of Monoethanolamine + N-methyldiethanolamine + Water and Monoethanolamine + 2-Amino-2-methyl-1-propanol + Water Chem. J. Eng. Data **1994**, 39, 444–447.

2. Kohl, A. L. and Nielsen, R. B. Gas Purification. Gulf Publishing Company, Houston, 5th edition, 1997.
3. Browning, G. J.; Weiland, R. H. Physical Solubility of Carbon Dioxide in Aqueous Alkanolamines via Nitrous Oxide Analogy. *J. Chem. Eng. Data* **1994**, *39*, 817–822.
4. Littel, R. J.; Versteeg, G. F.; van Swaaij, W. P. M., Solubility and Diffusivity Data for the Absorption of COS, CO₂, and N₂O in Amine Solutions. *J. Chem. Eng. Data* **1992**, *37*, 49–55.
5. Sada, E.; Kito, S., Solubilities of Gases in Aqueous Monoethanolamine Solutions. *Kagaku Kogaku* **1972**, *36*, 218–220.
6. DiGuilio, R. M.; Lee, R.-J.; Schaeffer, S. T.; Brasher, L. L.; Teja, A. S. Densities and Viscosities of the Ethanolamines. *J. Chem. Eng. Data* **1992**, *37*, 239–242.
7. Mandal, B. P.; Kundu, M.; Bandyopadhyay, S. S. Density and Viscosity of Aqueous Solutions of (N-Methyldiethanolamine + Monoethanolamine), (N-Methyldiethanolamine + Diethanolamine), (2-Amino-2-methyl-1-propanol + Monoethanolamine), and (2-Amino-2-methyl-1-propanol + Diethanolamine). *J. Chem. Eng. Data* **2003**, *48*, 703–707.
8. Song, J. H.; Park, S. B.; Yoon, J. H.; Lee, H.; Lee, K. H. Densities and Viscosities of Monoethanolamine + Ethylene Glycol + Water. *J. Chem. Eng. Data* **1996**, *41*, 1152–1154.
9. Amundsen, T. G.; Øi, L. E.; Eimer, D. A. Density and Viscosity of Monoethanolamine + Water + Carbon Dioxide from (25 to 80) °C. *J. Chem. Eng. Data* **2009**, *54*, 3096–3100.
10. Weiland, R. H.; Dingman, J. C.; Cronin, D. B.; Browning, G. J. Density and Viscosity of Some Partially Carbonated Aqueous Alkanolamine Solutions and Their Blends. *J. Chem. Eng. Data* **1998**, *43*, 378–382.
11. Vogel, H. Das Temperaturabhängigkeitsgesetz der Viskosität von Flüssigkeiten, *Physik Z.* **1921**, *22*, 645–646.
12. Viswanath, D. S.; Natarajan, G. Databook on Viscosity of Liquids, Hemisphere, New York, **1989**.
13. Goletz, Jr. E.; Tassios, D. An Antoine Type Equation for Liquid Viscosity Dependency to Temperature, *Ind. Eng. Chem. Proc.* **1977**, *16*, 75–79.
14. Dutt, N. V. K. A Simple Method of Estimating the Viscosity of Petroleum Crude Oil and Fractions. *Chem. Eng. J.* **1990**, *45*, 83–86.
15. Girifalco, L. A. Temperature Dependence of Viscosity and Its Relation to Vapor Pressure for Associated Liquids, *J. Chem. Phys.* **1955**, *23*, 2446–2447.
16. Thorpe, T. E.; Rodger, J. W. Bakerian Lecture: On the Relations between the Viscosity (Internal Friction) Of Liquids and Their Chemical Nature, *Phil. Trans.* **1895**, *185*, 397–710.
17. Teng, T. T.; Maham, Y.; Helper, L. G.; Mather, A. E. Viscosity of Aqueous Solutions of N-Methyldiethanolamine and of Diethanolamine. *J. Chem. Eng. Data* **1994**, *39*, 290–293.
18. Chowdhury, F. I.; Akhtar, S.; Saleh, M. A. Viscosities and Excess Viscosities of Aqueous Solutions of Some Diethanolamines. *J. Mole. Liq.* **2010**, *155*, 1–7.
19. Lakatos, T.; Johansson, L. G.; Simmingsköld, B. Viscosity Temperature Relations in the Glass System SiO₂-Al₂O₃-Na₂O-K₂O-CaO-MgO in the Composition Range of Technical Glasses. *Glass Technol.* **1972**, *13*, 88–95.

Chapter 6

6. Measurements and Correlations of Diffusivities of Nitrous Oxide and Carbon Dioxide in (Monoethanolamine + Water) by Laminar Liquid Jet

Abstract

The molecular diffusivities of nitrous oxide (N₂O) with aqueous monoethanolamine (MEA) solutions up to 12 M were studied over a temperature range from 298.15 to 333.15 K under atmospheric pressure using a laminar liquid jet absorber. The diffusivities of CO₂ in aqueous MEA solutions were calculated by the “N₂O analogy” method. A simple and effective thermal control technique was used to control the temperature of gas and liquid in the laminar liquid jet absorber. The rates of absorption were determined by measuring the flow of gas needed to replace the gas absorbed. The results showed that both the diffusivities of N₂O and CO₂ into aqueous MEA solution decrease with the increase of the concentration of MEA, and increase with an increase of the temperature of the solution. The relationship between the diffusivity and the viscosity of the solution roughly agrees with the modified Stokes–Einstein equation, but an exponent mathematical model was employed to simulate the diffusivity data and shows better agreement between data and model for the diffusivity of N₂O and CO₂ in the (monoethanolamine + water) system.

6.1. Introduction

Monoethanolamine has been commercially employed as an absorbent for capture of acid gases due to its high reaction rate, relatively low cost and thermal stability since the 1930s.¹⁻⁴ Although other amines have become more popular, and the MEA process has some shortcomings such as high energy consumption, it is presently considered the most mature technology for CO₂ capture in Post-combustion flue gases. The concentration of MEA solutions was generally increased to 30 mass % in the 1960s. This has been an industry standard since then. Very large absorbent streams then need to be circulated, and a further increase in solution concentration would help reduce these flows to decrease the energy consumption and improve the CO₂ capture efficiency. To improve the absorption efficiency and reduce the costs of acid gas capture of MEA solutions, increasing the concentration of the aqueous MEA solution may be a good choice when the potential corrosion and degradation issues can be controlled.^{5,6}

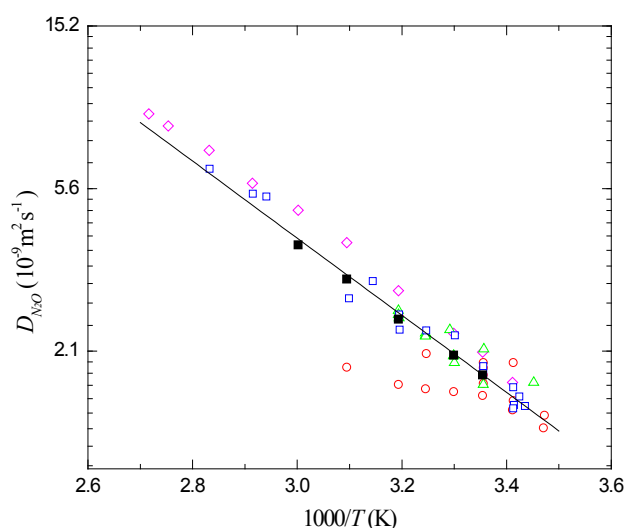


Figure 6.1 Diffusivity of N₂O in H₂O as a function of temperature compared with literature values apparatus category: ○, Liquid Laminar Jet⁷⁻¹³; ◇, Taylor Dispersion Cell¹⁹; △, Wetted Wall Absorber¹⁴⁻¹⁷; □, Diaphragm Cell¹⁸; ■, this work; The solid line was calculated by equation (6.2)

Data for diffusion coefficients are required for the design of absorbers and desorbers in the acid gas capture plant and to interpret reaction kinetics studies. For instance, the Sherwood and Schmidt numbers contain molecular diffusion coefficients to estimate mass transfer coefficients, which are used in the design of absorption, desorption and distillation processes. Diffusivity measurements of gas in liquids have been carried out with various experimental techniques like laminar liquid jet⁷⁻¹³, wetted wall absorber,¹⁴⁻¹⁷ diaphragm cell¹⁸ and Taylor dispersion technique¹⁹ and so on. Regarding the diffusivity of N₂O in H₂O,

a literature review classified by measurement method is given in Figure 6.1 and Table 6.1. It is observed that the average relative deviation (ARD) of literature values is higher than 20%. This scatter in results is probably caused by the use of different experimental methods with different instrument system errors and various experimental details which include gas saturation, accuracy of temperature control, and imperfect purging of air from the chamber and so on. The laminar liquid jet apparatus used in this work has its advantages compared to other laboratory apparatus. It is very versatile due to the gas–liquid contact time, and the surface area is well defined and can be easily varied via changing the jet length or liquid flow rate, and the gas absorption rate into a laminar liquid jet is usually well represented by the penetration theory.

The diffusivity of CO₂ in a MEA solution cannot be measured directly due to the chemical reaction between CO₂ and MEA. Due to the similarity in mass and molecular interaction parameters between CO₂ and N₂O, Clarke⁷ as the first, suggested the “N₂O analogy” method and argued its rationale. Later researchers^{11,16–18} followed this approach to estimate the diffusivity of CO₂ in different concentrations of amine solutions. This N₂O analogy method for the CO₂–MEA system can be expressed as follows

$$D_{\text{CO}_2,\text{MEA}} = D_{\text{N}_2\text{O},\text{MEA}} \left(\frac{D_{\text{CO}_2,\text{H}_2\text{O}}}{D_{\text{N}_2\text{O},\text{H}_2\text{O}}} \right) \quad (6.1)$$

where $D_{\text{CO}_2,\text{MEA}}$, $D_{\text{N}_2\text{O},\text{MEA}}$ are the diffusivities of CO₂ and N₂O in amine solution, and $D_{\text{CO}_2,\text{H}_2\text{O}}$, $D_{\text{N}_2\text{O},\text{H}_2\text{O}}$ are the diffusivities of CO₂ and N₂O in pure water, respectively. Versteeg and van Swaaij¹⁸ measured the diffusivity data of CO₂ and N₂O in water and developed the following correlations:

$$D_{\text{N}_2\text{O},\text{H}_2\text{O}} = 5.07 \times 10^{-6} \times \exp(-2371/T) \quad (6.2)$$

$$D_{\text{CO}_2,\text{H}_2\text{O}} = 2.35 \times 10^{-6} \times \exp(-2119/T) \quad (6.3)$$

where the units of the diffusivity are in m² s⁻¹ and the temperature is in K. Substitution from equations (6.2), (6.3) and $D_{\text{N}_2\text{O},\text{MEA}}$ at different temperatures and concentrations into equation (6.1) give the diffusivity of CO₂ in amine solutions.

Table 6.1 A review of the diffusivity of N₂O in H₂O and compared with this work

Temp(K)	$D_{N_2O}(10^{-9}m^2s^{-1})$	References	Method ^a
288	1.39	Haimour & Sandall, 1984	LLJ
288.15	1.285	Al-Ghawas et al, 1989	LLJ
289.7	1.70	Davidson & Cullen, 1957	WWA
291.1	1.47	Versteeg & van Swaaij, 1988	DC
292	1.56	Versteeg & van Swaaij, 1988	DC
292.9	1.48	Versteeg & van Swaaij, 1988	DC
293	1.45	Versteeg & van Swaaij, 1988	DC
293	1.65	Versteeg & van Swaaij, 1988	DC
293	1.52	Haimour & Sandall, 1984	LLJ
293	1.92	Thomas & Adams, 1965	LLJ
293.15	1.436	Al-Ghawas et al., 1989	LLJ
293.15	1.70	Hamborg & Versteeg, 2008	TDT
297.9	2.09	Davidson & Cullen, 1957	WWA
298	1.88	Versteeg & van Swaaij, 1988	DC
298	1.80	Versteeg & van Swaaij, 1988	DC
298	1.86	Haimour & Sandall, 1984	LLJ
298	1.69	Duda & Vrentas, 1968	LLJ
298	1.92	Joosten & Danckwerts, 1972	LLJ
298	1.78	Sada et al., 1978	LLJ
298	1.68	Samanta et al., 2007	WWA
298.15	1.569	Al-Ghawas et al., 1989	LLJ
298.15	2.05	Hamborg & Versteeg, 2008	TDT
298.15	1.78	This work	LLJ
302.9	2.27	Versteeg & van Swaaij, 1988	DC
303	1.92	Samanta et al., 2007	WWA
303.15	1.607	Al-Ghawas et al., 1989	LLJ
303.15	2.30	Hamborg & Versteeg, 2008	TDT
303.15	2.009	Li & Lai, 1995	WWA
303.15	2.00	Ko et al., 2001	WWA
303.15	2.01	This work	LLJ
303.8	2.35	Davidson & Cullen, 1957	WWA
308	2.34	Versteeg & van Swaaij, 1988	DC
308	2.03	Haimour & Sandall, 1984	LLJ
308.15	1.634	Al-Ghawas et al., 1989	LLJ
308.15	2.303	Li & Lai, 1995	WWA
308.15	2.27	Ko et al., 2001	WWA
308.15	2.26	Samanta et al., 2007	WWA
312.9	2.35	Versteeg & van Swaaij, 1988	DC
313	2.58	Versteeg & van Swaaij, 1988	DC
313	2.55	Duda & Vrentas, 1968	LLJ
313	2.53	Samanta et al., 2007	WWA
313.15	1.679	Al-Ghawas et al., 1989	LLJ
313.15	2.99	Hamborg & Versteeg, 2008	TDT
313.15	2.648	Li & Lai, 1995	WWA
313.15	2.58	Ko et al., 2001	WWA
313.15	2.51	This work	LLJ
318	3.17	Versteeg & van Swaaij, 1988	DC
322.7	2.85	Versteeg & van Swaaij, 1988	DC
323.15	1.868	Al-Ghawas et al., 1989	LLJ
323.15	4.02	Hamborg & Versteeg, 2008	TDT
323.15	3.21	This work	LLJ
333.15	4.90	Hamborg & Versteeg, 2008	TDT
333.15	3.96	This work	LLJ
340	5.33	Versteeg & van Swaaij, 1988	DC
343	5.43	Versteeg & van Swaaij, 1988	DC
343.15	5.79	Hamborg & Versteeg, 2008	TDT
353	6.32	Versteeg & van Swaaij, 1988	DC
353.15	7.09	Hamborg & Versteeg, 2008	TDT
363.15	8.23	Hamborg & Versteeg, 2008	TDT
368.15	8.87	Hamborg & Versteeg, 2008	TDT

^a LLJ = laminar liquid jet; DC = diaphragm cell; WWA = wetted wall absorber; TDT = Taylor dispersion technique.

The diffusivities of N₂O in aqueous MEA solutions have been measured by a number of researchers.^{7,11,16,17} A literature review of the diffusivities of N₂O in aqueous MEA solutions is shown in Table 6.2. There are some disagreements in the literature with respect to the diffusivity, and there is also a lack of data to describe systematically the dependence of the diffusivity in aqueous MEA solution over a wide range of concentrations and temperatures. No data were found for concentrations higher than 5 M and experimental temperatures higher than 313 K in the open literature. The present work extends the data range by measuring the diffusivities of N₂O and CO₂ in aqueous MEA solutions over a wider range of concentrations and temperatures.

Table 6.2 A review of diffusivity of N₂O in aqueous MEA solution

<i>C</i> (mol L ⁻¹)	<i>D</i> _{N₂O} (10 ⁻⁹ m ² s ⁻¹)				Ref.
	298 K	303 K	308 K	313 K	
0.5		1.98	2.16	2.46	
1		1.86	2.09	2.38	
1.5		1.75	2.01	2.30	
2		1.70	1.95	2.24	Ko et al. ¹⁷
2.5		1.67	1.89	2.22	
3		1.63	1.86	2.16	
5		1.41	1.61	1.91	
4.9		1.559	1.731	1.947	Davidson and Cullen ¹⁴
0	1.78				
0.731	1.74				
1.364	1.63				
2.203	1.46				Sada et al. ¹¹
2.766	1.24				
3.361	1.15				
1.637	1.52				
3.283	1.39				Clarke ⁷
4.877	1.20				

The uncertainty analysis (in the support information) manifests that the fluctuation of gas temperature in the absorption chamber is one of the main deviation sources for diffusivity measurement. In this work, a laminar liquid jet apparatus with an accurate temperature control method was employed to determine the diffusivity of N₂O in aqueous

monoethanolamine solutions over a wide concentration range from 0.5 to 12 M and temperature from 298.15 to 333.15 K under atmospheric pressure. These values can be used to estimate the diffusion of CO₂ in aqueous MEA solutions by means of the N₂O analogy method. The modified Stokes–Einstein equation was tested for modeling the relationship of the diffusivity and the viscosity of the solution. The viscosities of aqueous MEA solutions were measured for the diffusivity simulation of the modified Stokes–Einstein equation. To obtain a more precise simulation results, an exponent mathematical model was used to better represent the diffusivity data.

6.2. Theory Background

For the measurement of diffusivity of gas in liquid, the gas is absorbed into liquid with no chemical reaction taking place between the dissolved gas and the liquid. The liquid surface first contact with the gas is at time $t = 0$, and it is assumed that from then on the concentration in the plane of the surface is uniformly equal to C^* . This concentration is assumed to be constant and corresponds to the solubility of the gas at the partial pressure on the liquid surface. According to the well-known Fick's law, the flux per unit area, J , in a unit ($\text{mol m}^{-2} \text{s}^{-1}$), at the liquid surface and any time is in proportion to the concentration gradient of the gas molecule in the liquid as follows,

$$J = -D_A \left(\frac{\partial c}{\partial x} \right)_{x=0} \quad (6.4)$$

where D_A is the diffusivity of gas A in liquid. Regarding the diffusion of gas in liquid without chemical reaction, the mass conservation may be expressed:

$$[\text{Diffusion in}] - [\text{Diffusion out}] = [\text{Accumulation}]$$

this is described by

$$\left[-D_A \frac{\partial c}{\partial x} \right] + \left[D_A \left(\frac{\partial c}{\partial x} + dx \frac{\partial^2 c}{\partial x^2} \right) \right] = \left[dx \frac{\partial c}{\partial t} \right] \quad (6.5)$$

For smooth gas–liquid interface, the boundary conditions of the above absorption equation are

$$\left. \begin{aligned} c &= C^*, & x &= 0, & t &> 0 \\ c &= C^0, & x &> 0, & t &= 0 \\ c &= C^0, & x &= \infty, & t &> 0 \end{aligned} \right\} \quad (6.6)$$

where C^* is the dissolved gas concentration in equilibrium at the gas–liquid interface and C^0 is the concentration of the dissolved gas in the bulk of the solution, respectively. The analytical solution²¹ of equation (6.5) with the boundary conditions (6.6) is

$$c - C^0 = (C^* - C^0) \operatorname{erfc} \left(\frac{x}{2\sqrt{D_A t}} \right) \quad (6.7)$$

It follows from equation (6.4) and equation (6.7) that

$$J = (C^* - C^0) \sqrt{\frac{D_A}{\pi t}} \quad (6.8)$$

Thus, the absorption rate tends to infinity when t approaches zero, and decreases when t increases. It is safe to assume $C^0=0$ when the liquid has a very small gas loading. Then the amount of gas absorbed per unit area of the surface in time t , Q , in a unit (mol m^{-2}), is

$$Q = \int_0^t J dt = 2C^* \sqrt{\frac{D_A t}{\pi}} \quad (6.9)$$

For the laminar liquid jet, the total one–dementional flux R , in a unit (mol s^{-1}), is given by

$$R = \frac{\pi d l Q}{t} \quad (6.10)$$

where d and l are the diameter and length of the liquid jet in unit m, respectively. The contact time (t) for an element on the surface of the laminar jet is given by

$$t = \frac{\pi d^2 l}{4q} \quad (6.11)$$

where q is the flow rate of the liquid. By combining equations (6.9), (6.10) and (6.11), the total rate of absorption is

$$R = 4C^* \sqrt{D_A q l} \quad (6.12)$$

Thus, a plot of R vs. $(ql)^{1/2}$ at constant temperature and pressure should give a straight line across the origin, with a slope $(4C^* D_A^{1/2})$. This equation indicates that the rate of absorption for the jet is independent of the jet diameter, so long as the velocity across any section is uniform, and the length of the free surface does not differ much from the jet height.

The equilibrium concentration C^* can be calculated by Henry's law, and D_A can then be obtained.

6.3. Experimental Section

6.3.1. Experimental Equipment and Procedure

A schematic diagram of the laminar liquid jet absorber is shown Figure 6.2. The absorber comprises a total volume 405 cm^3 and inner diameter 5.13 cm of the chamber. The chamber is in a water jacket which is connected to a temperature controlled water bath. To obtain uniform temperatures of gas and liquid in the chamber, a simple and effective temperature control technique was employed. As shown in Figure 6.2, both the gas and liquid pipe rolls were immersed in the water bath and then pass through an insulating hose to then reach the jet chamber, where the hose is connected to the water bath and the jacket of the chamber. By using this method, the temperatures of the saturated gas, the solution and the chamber become uniform within the accuracy of control, and this was $\pm 0.1\text{ K}$. The entire assembly was demonstrated to have no leak. During experiments, the temperatures of the solution, gas and the chamber were recorded using a data acquisition system (data logger, Agilent BenchLink, 34972A).

After the water bath and water jacket reached the desired temperature, the chamber was purged by saturated gas (N_2O or CO_2) with a flow rate about 5 mL min^{-1} through the wash bottle which is in the water bath. The gas purge operation was stopped when the chamber and the gas pipes were filled with the saturated gas. The degassed solution was stored in the liquid feed tank and pumped to the constant pressure head system, then fed to the jet chamber to produce a "rod-like" laminar jet by gravity. The nozzle is a 0.07 mm thick stainless steel sheet with a 0.5 mm circular hole cut by laser, which was cut with laser process by Lanox Laser (Glen Arm, Mo, USA). The nozzle is mounted on the end of the liquid delivery pipe. The diameter of the receiver hole was 1 mm . The jet length is adjustable from $0 - 2.8\text{ cm}$. The constant pressure head tank (200 cm^3 cup inside) is mounted about 3 m above the absorption chamber to provide a sufficient and stable pressure head for the required rate of liquid flow. During the liquid feed operation, the inlet flow rate was kept higher than the outlet flow rate and the overflow from the cup in the constant pressure head device return to the liquid feed tank. The N_2 supply to replace the used liquid was stored in a N_2 bag connected to both the feed tank and the constant pressure head device. The flow rate of the liquid was controlled with a float flow meter, but the actual flow rate of the liquid was

determined by weighing the discharged liquid in a timed interval for each experiment. The liquid level in the receiver was adjusted to a suitable height with the constant-level device to avoid spillover of liquid or gas entrainment into the receiver. A two-dimensional travelling microscope with 0.01mm accuracy was used to measure the jet-length, and the diameter of the jet can be measured as well. However, according to the model (equation(6.12)), the measurement of the diffusivity is independent on the jet diameter, although the jet diameter will be influenced by solvent viscosity. The entrance and exit effects exist when the liquid jet is formed and when it exits. This causes the jet to deviate a perfect rod-shape. Cullen and Davidson²⁰ had analyzed this phenomenon. However, compared to 10 – 22 mm length of the jet, the influence of the entrance and exit effects can be neglected.^{21,22}

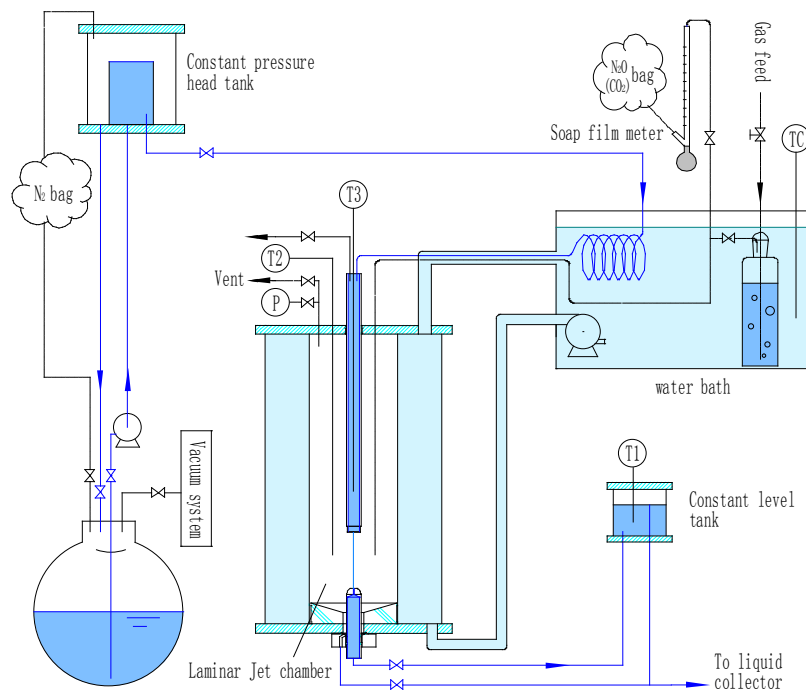


Figure 6.2 Schematic diagram of laminar liquid jet absorber.
(Solid line is the liquid line and dotted line is the gas line)

After obtaining an established jet-flow, the gas was absorbed by the liquid jet in the chamber and the absorbed volume was measured by reading the soap film meter (i.d. 3mm). At this point, the source of the gas for the absorption process was the gas bag. For a certain concentration of MEA solution at a desired temperature, various gas absorption rates (R) versus $(ql)^{1/2}$ can be measured by changing the jet length or the liquid flow rate. Experiments were repeated 5 – 7 times and R was plotted versus $(ql)^{1/2}$, and the data was regressed to get the slope $(4C^*D_A)^{1/2}$ by equation (6.12). D_A can be obtained when the solubility is known.

6.3.2. Reagents and Solution Preparation

Reagent grade MEA with mass fraction purity $\geq 99.5\%$ was purchased from Merck and used without further purification. Deionized water (purified with a mini-Q system, purity defined by conductivity $18.2 \text{ M}\Omega\cdot\text{cm}$) and MEA were degassed by applying vacuum on their own, and then mixed to prepare various concentrations of aqueous MEA solutions using an analytical balance (Mettler Toledo XS403S) with an accuracy $\pm 1 \text{ mg}$ and a 5000 mL volumetric flask. This preparation procedure avoids the loss of the water vapor compared with the method of directly vacuuming the mixed solution. Various concentrations aqueous of MEA solutions were prepared: 0.5 M (3.1 mass %), 3 M (18.1 mass %), 5 M (30.2 mass %), 8 M (47.9 mass %), 10 M (59.6 mass %), 12 M (71.4 mass %). The whole preparation process was protected by a nitrogen atmosphere. The purity of CO_2 was $\geq 99.995 \text{ mol } \%$ and $\text{N}_2\text{O} \geq 99.7 \text{ mol } \%$. Both gases are produced by AGA Gas GmbH.

6.4. Results and Discussion

6.4.1. Diffusivity of N_2O in Pure Water

To validate the application of the apparatus, the diffusivities of N_2O in pure water were conducted over a temperature range from 298.15 to 323.15 K under constant ambient pressure. Table 6.4 shows the raw experimental data with respect to the diffusivity. According to equation (6.12), plotting the absorption rate (R_A) vs. $4(qI)^{1/2}$, and regressing the slope ($C^*D^{1/2}$) through zero from the data, the diffusivity can be calculated. Figure 6.3 is an example for obtaining diffusivity by treating the data of N_2O in pure water at 303.15 K.

Table 6.3 shows the diffusivities of N_2O in pure water and the standard deviations (STD) of the raw experimental data at various temperatures, and the results compared with the literature values are shown in Figure 6.1 and Table 6.4. The comparison of results shows that the measured diffusivities of N_2O in water at various temperatures are in good agreement with literature values and the values simulated by equation (6.2). In Figure 6.1, it is found that the diffusivities of N_2O in water reported by Al-Ghawas et al.¹³ are lower than those of other literature values, especially at high temperatures. This may be caused by using an insufficiently saturated gas.

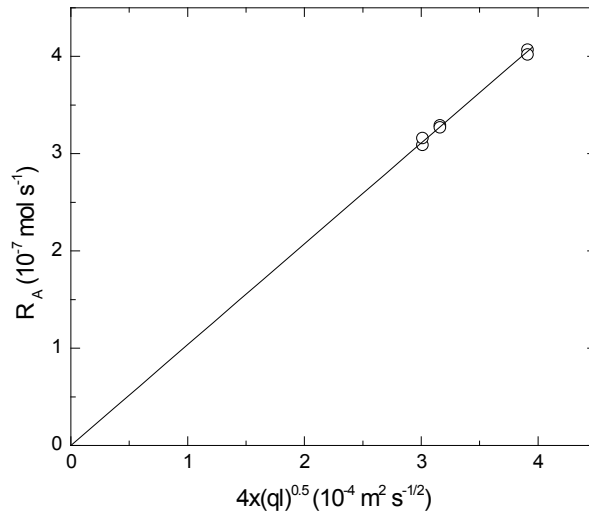


Figure 6.3 Plot R_A vs. $4\sqrt{ql}$ to calculate the diffusivity of N₂O in MEA +H₂O at 303.15 K

Additionally, it can be seen from Table 6.3 that the standard deviations of the experimental diffusivity values increase with the increasing of the experimental temperature. This manifests that the temperature is an important factor affecting the measurement. It is difficult to make a gas that is 100% saturated, furthermore, the higher the temperature is, the more the influence of the temperature on the gas saturation is, (see section 3.3). If the gas saturation is not enough, the liquid will vaporize and affect the change of the gas volume, and then lead to errors of the experimental results. On the other hand, the liquid transport pipe in the chamber is a potential factor that could affect the gas temperature. If the liquid temperature is different to the gas temperature, the gas volume could be affected by the liquid, and hence affect the reading of the soap film meter.

Table 6.3 The diffusivities of N₂O in pure water at various temperatures

	T /K				
	298.15	303.15	313.15	323.15	333.15
$D_{\text{N}_2\text{O}} (\text{m}^2 \text{s}^{-1})$	1.78E-09	2.01E-09	2.51E-09	3.21E-09	3.96E-09
STD	2.01E-11	3.53E-11	5.33E-11	6.38E-11	8.01E-11

Table 6.4 The experimental data of diffusivities of N₂O in pure water at various temperatures

No.	T_{room} °C	P_{room} mbar	T K	R_A 10^{-7}mol s^{-1}	flow rate (q) $10^{-7}\text{m}^3 \text{s}^{-1}$	length (l) 10^{-2}m	C^* mol m^{-3}	$D_{A-\text{exp.}}$ $10^{-9}\text{m}^2 \text{s}^{-1}$
W-25-01	23.1	1026	298.15	4.005	4.356	1.98	25.51	1.79
W-25-02	23.1	1026	298.15	3.967	4.356	1.976	25.51	1.76
W-25-03	23.1	1026	298.15	3.359	4.979	1.221	25.51	1.78
W-25-04	23.4	1024	298.15	3.323	4.979	1.221	25.46	1.75
W-25-05	23.4	1024	298.15	3.377	3.951	1.543	25.46	1.80
W-25-06	23.4	1024	298.15	3.349	3.951	1.543	25.46	1.77
W-30-01	22.8	1021	303.15	3.293	4.046	1.543	23.09	2.04
W-30-02	22.8	1021	303.15	3.267	4.046	1.543	23.09	2.00
W-30-03	22.8	1021	303.15	4.068	4.478	2.130	23.09	2.03
W-30-04	23.8	1023	303.15	4.023	4.478	2.130	23.13	1.98
W-30-05	23.8	1023	303.15	3.092	5.022	1.130	23.13	1.97
W-30-06	23.8	1023	303.15	3.163	5.022	1.130	23.13	2.06
W-40-01	23.1	1031	313.15	2.616	4.469	1.130	18.22	2.55
W-40-02	23.1	1031	313.15	2.600	4.469	1.130	18.22	2.52
W-40-03	23.3	1028	313.15	2.726	3.749	1.553	18.16	2.42
W-40-04	23.3	1028	313.15	2.781	3.749	1.553	18.16	2.52
W-40-05	23.3	1028	313.15	3.259	3.955	1.981	18.16	2.57
W-40-06	23.3	1028	313.15	3.208	3.955	1.981	18.16	2.49
W-50-01	22.8	1022	323.15	3.100	4.442	1.981	14.46	3.27
W-50-02	22.8	1022	323.15	3.032	4.442	1.981	14.46	3.12
W-50-03	22.5	1024	323.15	2.556	3.994	1.514	14.48	3.22
W-50-04	22.5	1024	323.15	2.525	3.994	1.514	14.48	3.14
W-50-05	22.5	1024	323.15	2.540	5.124	1.151	14.48	3.26
W-50-06	22.5	1024	323.15	2.540	5.124	1.151	14.48	3.26
W-60-01	23.2	1021	333.15	2.204	5.001	1.151	11.47	4.01
W-60-02	23.2	1021	333.15	2.216	5.001	1.151	11.47	4.05
W-60-03	23.1	1026.6	333.15	2.496	4.130	1.776	11.54	3.99
W-60-04	23.1	1026.6	333.15	2.459	4.130	1.776	11.54	3.87
W-60-05	23.1	1026.6	333.15	2.466	3.559	2.013	11.54	3.99
W-60-06	23.1	1026.6	333.15	2.423	3.559	2.013	11.54	3.85

6.4.2. Physical Solubility of N₂O in Aqueous MEA Solution

The physical solubilities of N₂O in aqueous MEA solutions are required for calculating its diffusivity according to equation (6.12). The physical solubilities of N₂O in aqueous MEA solutions were measured in a temperature range from 298.15 to 323.15 K under ambient pressure using a new technique in the previous work.²³ The Henry's constant of N₂O in 3 M, 5 M, 8 M, 12 M, 15 M aqueous MEA solutions and pure MEA were obtained and are summarized in Table 6.5, some of them were estimated by Wang's model in which the parameters were regressed in previous work.²³

Table 6.5 The physical solubility of N₂O in aqueous MEA solutions at various temperatures

<i>T</i> (K)	<i>H</i> _{N₂O} (kPa m ³ kmol ⁻¹)									
	Pure H ₂ O	0.5M	3M	5M	8M	10M	12M	14M	15M	Pure MEA
298.15	4022	4006	4221	4321	4428	4550	4132	3776	3515	2655
303.15	4422	4412	4692	4835	5060	5044	4674	4134	3797	2867
313.15	5660	5645	5831	5991	6115	6207	5814	4915	4413	3308
323.15	7070	7032	7155	7311	7412	7352	6853	5689	5034	3768
333.15	8899	8803	8676	8789	8846	8537	7774	6497	5691	4277

6.4.3. Diffusivity of N₂O and CO₂ in Aqueous MEA Solution

To validate the diffusivity measurement setup and the experimental procedure, the diffusivities of N₂O in pure water were measured first. The results are shown in Figure 6.1 and are summarized in Table 6.2. The comparison of results show that the measured diffusivities of N₂O in water are in good agreement with literature values and the values simulated by equation (6.2). In Figure 6.1, it is found that the diffusivities of N₂O in water reported by Al-Ghawas et al.¹³ are lower than those of other literature values, especially at high temperatures. This may be caused by using an insufficiently saturated gas and so on.

Table 6.6 The diffusivity of N₂O in aqueous MEA solutions at various temperatures under atmospheric pressure

<i>T</i> (K)	<i>D</i> _{N₂O} (10 ⁻⁹ m ² s ⁻¹)						
	0 M	0.5 M	3 M	5 M	8 M	10 M	12 M
298.15	1.78	1.68	1.41	1.16	0.85	—	—
303.15	2.01	1.94	1.61	1.38	1.01	0.74	—
313.15	2.51	2.41	2.17	1.79	1.26	0.95	0.67
323.15	3.21	3.08	2.61	2.27	1.65	1.22	0.83
333.15	3.96	3.78	3.32	2.72	2.00	1.55	1.03

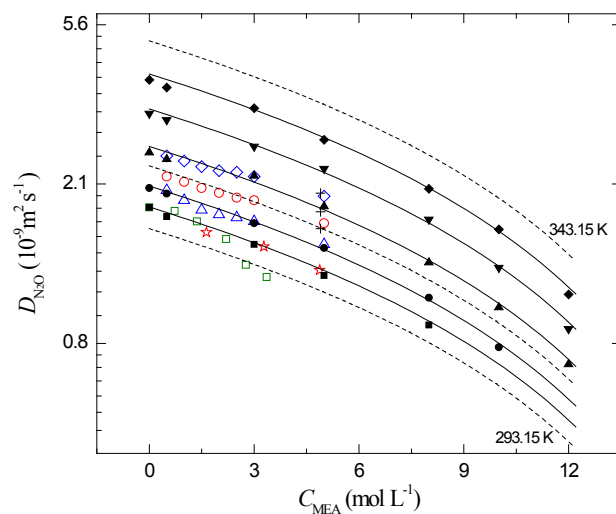


Figure 6.4 Diffusivities of N_2O in $MEA + H_2O$ as functions of MEA molarity in a temperatures range from 298.15 to 333.15 K and the comparison of this work and literature values with regressed model: (■, 298.15 K; ●, 303.15 K; ▲, 313.15 K; ▼, 323.15 K; ◆, 333.15 K) this work; (△, 303.15 K; ○, 308.15 K; ◇, 313.15 K), Ko et al.¹⁷; □, 298.15 K, Sada et al.¹¹; ☆, 298.15 K, Clarke¹; +, (303.15 to 313.15) K Davidson and Cullen¹⁴; The solid and dash lines are calculated by equation (6.15) from (293.15–343.15) K

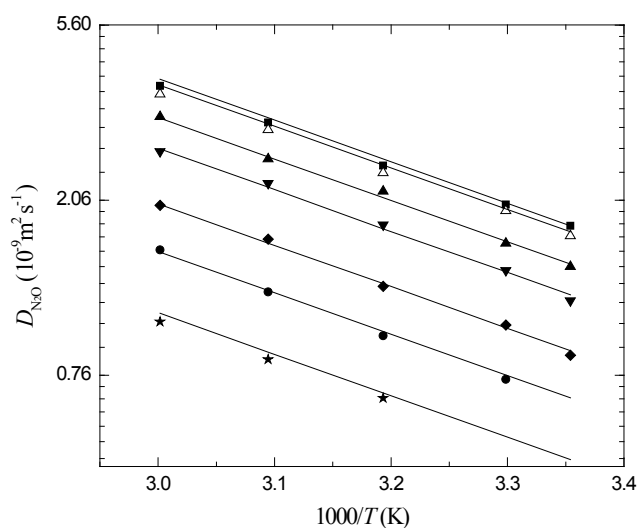


Figure 6.5 Diffusivities of N_2O in $MEA + H_2O$ as functions of temperature: ■, 0 M; △, 0.5 M; ▲, 3 M; ▼, 5 M; ◆, 8 M; ●, 10 M; ★, 12 M; The solid line was calculated by equation (6.15)

Table 6.7 The diffusivity of CO₂ in aqueous MEA solutions at various temperatures calculated by N₂O analogy method

<i>T</i> (K)	D_{CO_2}	$D_{CO_2} (10^{-9} m^2 s^{-1})$						
	D_{N_2O}	0 M	0.5 M	3 M	5 M	8 M	10 M	12 M
298.15	1.09	1.94	1.83	1.54	1.26	0.93	—	—
303.15	1.06	2.14	2.07	1.71	1.47	1.08	0.79	—
313.15	1.07	2.69	2.58	2.33	1.92	1.35	1.02	0.71
323.15	1.05	3.37	3.23	2.74	2.38	1.73	1.28	0.87
333.15	1.04	4.12	3.93	3.45	2.83	2.08	1.61	1.07

The diffusivities of N₂O in the aqueous MEA solutions were measured from (298.15 to 333.15) K and (0.5 to 12) M. It was difficult to operate this laminar liquid jet apparatus with high viscosity solutions (> 7.5 mPa s). For this reason there are some values vacant in this work reported in Table 6.7. The uncertainty of the measurements were estimated to be $\pm 9.4 \times 10^{-11} m^2 s^{-1}$, (estimation of the uncertainty is presented in the section 6.5). Figure 6.4 compares the present work with literature, and Figure 6.5 delineates the D_{N_2O} as a function of temperature. It can be seen from Figure 6.4 that the experimental data of this work agrees well with literature values. The diffusivities of N₂O in the aqueous MEA solutions increase when the temperature increases, and decrease with the increase of the MEA concentration. The diffusivities of CO₂ in various aqueous MEA solutions were estimated by the N₂O analogy method, and the results are tabulated in Table 6.7. Diffusivities of N₂O can be estimated with the modified Stokes–Einstein relation¹⁸, and this expression based on regression becomes

$$D_{N_2O} = 10^{-11.13} \mu^{-0.80} T \quad (6.13)$$

During the regression, the exponent -0.8 was fixed¹⁸ and the pre-exponential factor was regressed using the experimental data. The relationship between the diffusivity of N₂O and the viscosity of the aqueous MEA solution is plotted in Figure 6.6.

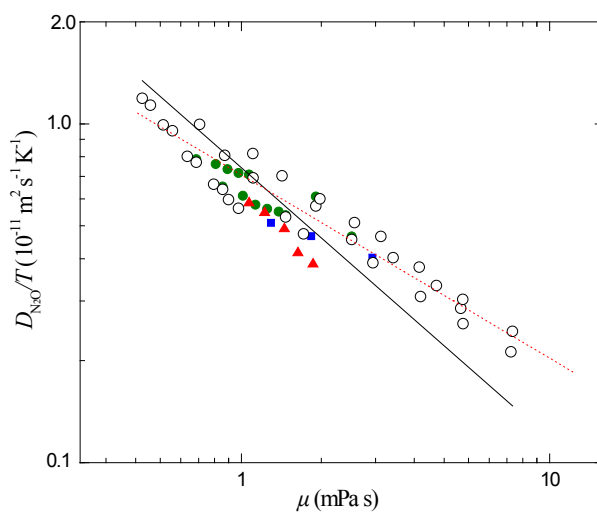


Figure 6.6 D_{N_2O}/T as a function of viscosity of the aqueous MEA solution by Stokes–Einstein equation: \blacksquare , Clarke¹; \bullet , Ko et al.¹⁷; \blacktriangle , Sada et al.¹¹; \circ , this work; Solid and dashed line were calculated by equation (6.13) and (6.14), respectively.

It is seen from Figure 6.6 that the Stokes–Einstein logarithmic plot, $\lg(D_{N_2O}/T)$ versus $\lg\mu$, shows a rough linear relationship. Equation (6.13) represents both the presently measured values and the values reported by Clarke¹, Sada et al.¹¹ and Ko et al.¹⁷. However, the AAD and AMD between the data gathered and equation (6.13) were 21.5% and 39.9%, respectively. A parity plot is shown in Figure 6.7.

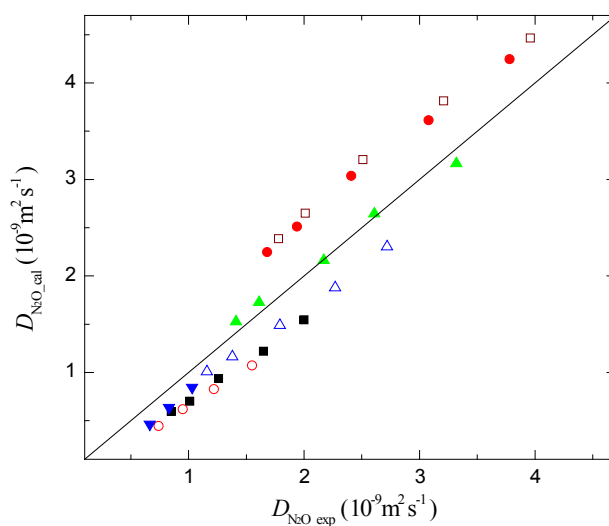


Figure 6.7 Comparisons the diffusivities of N_2O in MEA+ H_2O between measured and predicted by Stokes – Einstein equation: \square , 0 M; \bullet , 0.5 M; \blacktriangle , 3 M; \triangle , 5 M; \blacksquare , 8 M; \circ , 10 M; \blacktriangledown , 12 M

If both the exponent and pre-exponential factor of the modified Stokes–Einstein equation were regressed based on the experimental data, the modified Stokes–Einstein equation would be as given by equation (6.14). The linear regressed exponent, -0.54 , is in excellent agreement with the exponent (-0.54) proposed by Haimour et al.,²⁴ and the result is better than setting the fixed exponent as -0.8 , as shown by dashed line in Figure 6.6. The AAD and AMD between the experimental data and equation (6.14) are 10.6% and 20.7%, respectively.

$$D_{\text{N}_2\text{O}} = 10^{-11.15} \mu^{-0.54} T \quad (6.14)$$

The short-coming of the modified Stokes–Einstein equation is not surprising in view of the assumptions behind its development. These include assuming spherical particles and the solute being five or more times bigger than the solvent molecule. Neither is fulfilled with N₂O in an aqueous.²⁵

To improve the accuracy of the prediction further, an exponent mathematical model, as shown in the equation (6.15), was employed to model the data of the present work. This model includes the factors of both temperature (T/K) and molarity of MEA (C), which means the model is easy to apply for engineering purposes. Regarding the number of parameters to be used in the equation (6.15), we have checked the equation from 1st to 4th-order polynomial expression for (MEA+H₂O) system with experimental data by a non-linear regression method, and found second-order polynomial with respect to the molarity with five parameters a_0, a_1, a_2 and b_0, b_1 in equation (6.15) were enough to satisfy the experimental data in this work, higher order polynomials will introduce more noise. It is noted that when the concentration of the MEA solution is equal to zero, viz. the solution is pure water, the equation (6.15) should reduce to the diffusivity of N₂O in pure water, that is, equation (6.2). Therefore, we keep a_0 and b_0 of the equation (6.15) at the same values as that in the equation (6.2), and only the three parameters, a_1, a_2 and b_1 , are left to be fitted.

$$D_A = \left(\sum_0^n (a_i C^i) \right) \exp \left(\frac{\sum_0^n (b_i C^i)}{T} \right) \quad i = 0, 1, 2, \dots, n \quad (6.15)$$

The diffusivities of N₂O and CO₂ in aqueous MEA solutions in this work were regressed by this mathematical model. The diffusivities of CO₂ in aqueous MEA solutions were

calculated by the “N₂O analogy” method as mentioned above. Both the fitted parameters are tabulated in Table 6.8, and the predicted results of N₂O are displayed in Figure 6.4 and Figure 6.5 by the solid lines. The equation with the fitted parameters maybe can extend to 293.15 K and 343.15 K, which the simulated values are plotted by dash line in Figure 6.4. The AAD and the AMD for the simulation of the diffusivities of N₂O in aqueous MEA solutions are 2.33% and 5.03%, while that of CO₂ are 1.57% and 4.32%, respectively. A comparison of the experimental data and the predictions from equation (6.15) is displayed in Figure 6.8. The figure shows that the predicted values are in good agreement with experimental data.

Table 6.8 Parameters in the exponent model for diffusivity of gas in (MEA+H₂O)

	a_0	a_1	a_2	b_0	b_1	AAD	AMD
aq.MEA+N ₂ O	5.07×10^{-6}	-3.5443×10^{-7}	3.4294×10^{-9}	-2371	0.3749	2.33%	5.03%
aq.MEA+CO ₂	2.35×10^{-6}	2.9837×10^{-8}	-9.7078×10^{-9}	-2119	-20.1320	1.57%	4.32%

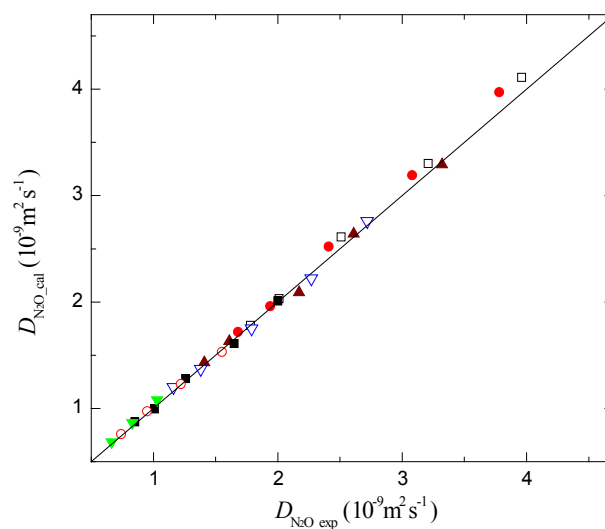


Figure 6.8 Comparisons the diffusivities of N₂O in MEA+H₂O between measured and predicted by equation (6.15):

□, 0 M; ●, 0.5 M; ▲, 3 M; △, 5 M; ■, 8 M; ○, 10 M; ▼, 12 M

6.5. Uncertainty Analysis

In these diffusivity measurements, there are several sources of uncertainty that must be accounted for:

1. The uncertainties due to the fluctuation of the gas temperature in the chamber.
2. The uncertainties introduced by the uncertainty of Henry's coefficient in the calculation of diffusivity.
3. The uncertainties caused by weighing in the preparation of MEA solutions.
4. The uncertainties due to the fluctuation of the liquid temperature in the chamber.
5. The uncertainties due to the measurement of the liquid jet length.
6. The uncertainties due to the visual reading from the scale on the soap film meter.
7. The uncertainties due to the liquid flow rate measurement.

The combined standard uncertainty of this work could be written as

$$D_A = f(T_{gas}, T_{liq}, H^2, w_{MEA}, R^2, q, l) \quad (6.16)$$

where the variables include all the influence factors such as weight fraction of MEA, experimental temperature of gas and liquid, the uncertainty of gas solubility, the instrument reading and so on.

As recommended focus is on the use of standard deviation. The size asked for is the combined standard uncertainty which is designated by $u_c(y)$. The mathematical formalism is using the variance, i.e. $u_c^2(y)$, and this is arrived at through

$$u_c^2(y) = \sum_{i=1}^N \left\{ \frac{\partial D}{\partial x_i} \right\}^2 u_i^2(x_i) \quad (6.17)$$

The temperature was controlled by the water bath, and almost all parts of the gas and liquid piping were immersed in the water bath. The temperature accuracy is specified as ± 0.1 K. The actual volume of the jet chamber is about 400 mL. The temperature fluctuation of the gas in the chamber will cause the gas volume absorbed to fluctuate and lead to error on the derived diffusivity. According to the gas state equation of $PV = nRT$, 1 K temperature fluctuation of the gas causes maximum 1.2 mL fluctuation at 333K in the work (Higher experimental temperature has a higher fluctuation). The minimum gas absorption rate is

about 1.5 mL per 5 min in this work, and the temperature fluctuation cycle is 0.1 K per at least 20 min. Then the absolute error on gas absorption rate (R) caused by gas temperature fluctuation is $3.82 \times 10^{-11} \text{ m}^2 \text{ s}^{-1}$. Because the final absorbed rate (R) is a function of this error source, according to the equation (2.12) or (6.16), the uncertainty on diffusivity is $7.65 \times 10^{-11} \text{ m}^2 \text{ s}^{-1}$.

The uncertainty of Henry's coefficient is $\pm 39 \text{ kPa m}^3 \text{ kmol}^{-1}$ as given in the chapter 4. The change in diffusivity is $4.40 \times 10^{-13} \text{ m}^2 \text{ s}^{-1}$ when Henry's coefficient varies $1 \text{ kPa m}^3 \text{ kmol}^{-1}$. According to the equation (2.12), the uncertainty on diffusivity caused by Henry's coefficient is $3.43 \times 10^{-11} \text{ m}^2 \text{ s}^{-1}$.

The accuracy of weight fraction of MEA solution is estimated as $\pm 0.001 \text{ g}$. According to the experimental data, 1 mass % of MEA solution causes maximum $5.89 \times 10^{-11} \text{ m}^2 \text{ s}^{-1}$ deviation on diffusivity. About 5000 g solution (1 mass %) requires about 50 g MEA. Then for 1g MEA weighing, the maximum error for diffusivity is $1.18 \times 10^{-12} \text{ m}^2 \text{ s}^{-1}$. Then the weight error corresponds to a relative uncertainty in D_A that is $1.18 \times 10^{-15} \text{ m}^2 \text{ s}^{-1}$.

The temperature of the liquid was controlled by the water bath with $\pm 0.1 \text{ K}$ accuracy. The maximum change of the diffusivity per 1 K is $7.50 \times 10^{-11} \text{ m}^2 \text{ s}^{-1}$ (as 5M, varies from 298.15 to 313.15K) in this work. Then the fluctuation of the liquid temperature corresponds to an uncertainty $7.50 \times 10^{-12} \text{ m}^2 \text{ s}^{-1}$.

The jet-length was measured using a two-dimensional travelling microscope with $\pm 0.01 \text{ mm}$ accuracy. The minimum jet-length was 8 mm in the present measurements. The maximum change of the diffusivity per 1 mm is $4.95 \times 10^{-10} \text{ m}^2 \text{ s}^{-1}$. Then the uncertainty caused by jet-length measurement is $4.95 \times 10^{-12} \text{ m}^2 \text{ s}^{-1}$.

The method of measuring the gas absorption rate is to fix the volume scale (i.e. 1 mL) and record the time. The recording time while reading the scale error is $\pm 0.5 \text{ s}$. The minimum recording time is 114 s. Because this error source affects the final absorbed rate (R), the uncertainty due to the visual reading error is $3.47 \times 10^{-11} \text{ m}^2 \text{ s}^{-1}$.

The method of liquid flow rate measurement is to weigh the discharged liquid per unit time. The balance accuracy is $\pm 0.001 \text{ g}$ and the accuracy of stop watch 0.01s, the minimum liquid is 220g for MEA in this work and the recording time is about 8 min. It causes a maximum $1.0 \times 10^{-8} \text{ m}^3 \text{ s}^{-1}$ error. The change is $2.11 \times 10^{-3} \text{ m}^2 \text{ s}^{-1}$ when liquid volume flow rate varies $1 \text{ m}^3 \text{ s}^{-1}$. Then measurement of the liquid flow rate causes an uncertainty of $2.11 \times 10^{-11} \text{ m}^2 \text{ s}^{-1}$.

The uncertainty in D_A is determined as $\pm 9.4 \times 10^{-11} \text{ m}^2 \text{ s}^{-1}$ by combining the various sources of uncertainty calculating by the equation (6.17). The details are summarized in Table 6.9. It can be seen that the main sources of the uncertainty are the fluctuation of the gas temperature in the chamber, the uncertainties of Henry's coefficient and the visual reading error from the scale on the soap film meter.

Table 6.9 Uncertainty analysis for the measurement of diffusivity

Source of Uncertainty	$\partial D_A / \partial x_i$	$u(x_i)$	$(\partial D_A / \partial x_i)u(x_i)$
1. The uncertainties due to the fluctuation of the gas temperature in the chamber.	3.82×10^{-10}	0.1 K	7.65×10^{-11}
2. The uncertainties introduced by the uncertainty of Henry's coefficient in the calculation of diffusivity.	4.40×10^{-13}	39 kPa m ³ kmol ⁻¹	3.43×10^{-11}
3. The uncertainties caused by weighing in the preparation of MEA solutions.	1.18×10^{-12}	0.001 g	1.18×10^{-15}
4. The uncertainties due to the fluctuation of the liquid temperature in the chamber.	7.50×10^{-11}	0.1 K	7.50×10^{-12}
5. The uncertainties due to the measurement of the liquid jet length.	4.95×10^{-10}	0.01 mm	4.95×10^{-12}
6. The uncertainties due to the visual reading error from the scale on the soap film meter.	3.47×10^{-11}	0.5 s	3.47×10^{-11}
7. The uncertainties due to the liquid flow rate measurement.	2.11×10^{-3}	$1.00 \times 10^{-8} \text{ m}^3 \text{ s}^{-1}$	2.11×10^{-11}
Combined Uncertainty, $u_c(y)$	$9.4 \times 10^{-11} \text{ m}^2 \text{ s}^{-1}$		

6.6. Conclusions

The molecular diffusivities of N₂O with aqueous monoethanolamine (MEA) solutions up to 12 M were studied from 298.15 to 333.15 K using a laminar liquid jet absorber. The uncertainty of the measurements was estimated to be $\pm 9.4 \times 10^{-11} \text{ m}^2 \text{ s}^{-1}$. The diffusivities of CO₂ in aqueous MEA solutions were calculated by the "N₂O analogy" method. The results showed that the diffusivities of N₂O and CO₂ into aqueous MEA solutions decrease with the increase of the concentration of MEA, and increase with the increase of temperature of the solution. The relationship between the diffusivity and the viscosity of the solution roughly agrees with the modified Stokes–Einstein equation, but a modification using an exponent mathematical model gives a better fit to data. It can be used to simulate N₂O diffusivities in

aqueous MEA solutions satisfactorily for calculation of the diffusivities of CO₂ in aqueous MEA solutions and for other engineering purposes.

Nomenclature

Parameters and Variables

A = the value of the property, viscosity or diffusivity in this work

AAD = absolute average deviation between calculated values and experimental data, (%)

AMD = absolute maximum deviation between calculated values and experimental data, (%)

a_i, b_i = parameters in equation (6.15), $i = 0, 1, 2, 3, \dots$

c, C = molar concentration of gas in the liquid, (kmol m^{-3} , mol L^{-1})

C^* = the dissolved gas molarity in equilibrium at the gas–liquid, $C^* = P_A/H_A$, (kmol m^{-3})

C^0 = the molarity of the dissolved gas in the bulk of the solution, (kmol m^{-3})

D_A = molecular diffusivity of gas A in a solution, ($\text{m}^2 \text{s}^{-1}$)

d = the diameter of the liquid jet, (m)

H_A = the Henry's constant of gas A in a solution, ($\text{kPa m}^3 \text{kmol}^{-1}$)

J = the flux per unit area, ($\text{mol m}^{-2} \text{s}^{-1}$),

l = the length of the liquid jet, (m)

P_A = the partial pressure of the gas A, (kPa)

q = the volume flow rate of the liquid, ($\text{m}^3 \text{s}^{-1}$)

Q = the amount of gas absorbed per unit area of the surface in time t , (mol m^{-2})

R = the total one–dimensional flux, (mol s^{-1})

STD = standard deviation.

t = contact time, (s)

T = temperature, (K)

x = the distance from the liquid surface, (m)

Subscript

A = gas A

exp = experimental value

cal = calculated value by a model

N₂O = nitrous oxide

CO₂ = carbon dioxide

Greek Symbols

μ = viscosity of the solution (mPa s)

References

1. Versteeg, G. F.; van Swaaij, W. P. M. On the Kinetics between CO₂ and Alkanolamines Both in Aqueous and Non-Aqueous Solutions — I. Primary and Secondary Amines. *Chem. Eng. Sci.* **1988**, *43*, 573–585.
2. Kohl, A. L.; Nielsen, R. B. Gas Purification. Gulf Publishing Company, Houston, 5th edition, **1997**.
3. Hikita, H.; Asai, S.; Katsu, Y.; Ikuno, S. Absorption of Carbon Dioxide into Aqueous Monoethanolamine Solutions. *AIChE J.* **1979**, *25*, 793–800.
4. Sada, E.; Kumuzawa, H.; Butt, M. A. Gas Absorption with Consecutive Chemical Reaction: Absorption of Carbon Dioxide into Aqueous Amine Solutions. *Can. J. Chem. Eng.* **1976**, *54*, 421–424.
5. Jassim, M. S.; Rochelle, G. Eimer, D.; Ramshaw, C. Carbon Dioxide Absorption and Desorption in Aqueous Monoethanolamine Solutions in a Rotating Packed Bed. *Ind. Eng. Chem. Res.* **2007**, *46*, 2823–2833.
6. Peng, Y. C.; Zhao, B. T.; Li, L. L. Advance in Post-combustion CO₂ Capture with Alkaline Solution: A Brief Review. *Energy Procedia*, **2012**, *14*, 1515–1522.
7. Clarke, J. K. A. Kinetics of absorption of Carbon Dioxide in Monoethanolamine Solutions at Short Contact Times. *Ind. Eng. Chem. Fundam.* **1964**, *3*, 239–245.
8. Thomas, W. J.; Adams, M. J. Measurement of Diffusion Coefficients of Carbon Dioxide and Nitrous Oxide in Water and Aqueous Solutions of Glycerol. *Trans. Faraday Soc.* **1965**, *61*, 668–673.
9. Duda, J. L.; Vrentas, J. S. Laminar Liquid Jet Diffusion Studies. *AIChE J.* **1968**, *14*, 286–294.
10. Joosten, G. E. H.; Danckwerts, P. V. Solubility and Diffusivity of Nitrous Oxide in Equimolar Potassium Carbonate–Potassium Bicarbonate Solutions at 25 °C and 1 Atm. *J. Chem. Eng. Data* **1972**, *17*, 452–454.
11. Sada, E.; Kumazawa, H.; Butt, M. A. Solubility and Diffusivity of Gases in Aqueous Solutions of Amines. *J. Chem. Eng. Data* **1978**, *23*, 161–163.
12. Haimour, N.; Sandall, O. C. Absorption of Carbon Dioxide into Aqueous Methyldiethanolamine. *Chem. Eng. Sci.* **1984**, *39*, 1791–1796.
13. Al-Ghawas, H. A.; Hagewiesche, D. P. and Sandall, O. C. et al. Physicochemical Properties Important for Carbon Dioxide Absorption in Aqueous Methyldiethanolamine. *J. Chem. Eng. Data* **1989**, *34*, 385–391.
14. Davidson, J. F.; Cullen, E. J. The Determination of Diffusion Coefficients of Sparingly Soluble Gases in Liquids. *Trans. Inst. Chem. Eng.* **1957**, *35*, 51–60.
15. Samanta, A.; Roy, S.; Bandyopadhyay, S. S. Physical Solubility and Diffusivity of N₂O and CO₂ in Aqueous Solutions of Piperazine and (N–Methyldiethanolamine + Piperazine). *J. Chem. Eng. Data* **2007**, *52*, 1381–1385.
16. Li, M. H.; Lai, M. D. Solubility and Diffusivity of N₂O and CO₂ in (Monoethanolamine+ N–Methyldiethanolamine + Water) and in (Monoethanolamine +2–Amino–2–Methyl–1 –Propanol + Water). *J. Chem. Eng. Data* **1995**, *40*, 486–492.
17. Ko, J. J.; Tsai, T. C.; Lin, C. Y. Diffusivity of Nitrous Oxide in Aqueous Alkanolamine Solutions. *J. Chem. Eng. Data* **2001**, *46*, 160–165.
18. Versteeg, G. F.; Swaaij, P. M. Solubility and Diffusivity of Acid Gases (CO₂, N₂O) in Aqueous Alkanolamine Solutions. *J. Chem. Eng. Data* **1988**, *33*, 29–34.

19. Hamborg, E. S.; Derks, P. W. J. and Versteeg, G. F. et al. Diffusion Coefficients of N₂O in Aqueous Piperazine Solutions Using the Taylor Dispersion Technique from (293 to 333) K and (0.3 to 1.4) mol dm⁻³. *J. Chem. Eng. Data* **2008**, *53*, 1462–1466.
20. Cullen, E. J.; Davidson, J. F. Absorption of Gas in Liquid Jet. *Trans. Faraday. Soc.* **1957**, *53*, 113–120.
21. Danckwerts, P. V. Gas–Liquid Reactions; McGraw–Hill: New York, **1970**.
22. Aboudheir, A.; Tontiwachwuthikul P.; Chakma, A.; Idem, R. Novel Design for the Nozzle of a Laminar Jet Absorber. *Ind. Eng. Chem. Res.* **2004**, *43*, 2568–2574.
23. Ying, J. R.; Eimer, D. A.; Yi, W. J. Measurements and Correlation of Physical Solubility of Carbon Dioxide in (Monoethanolamine + Water) by a Modified Technique. *Ind. Eng. Chem. Res.* **2012**, *51*, 6958–6966.
24. Haimour, N.; Bidarian, A.; Sandall, O. C. Kinetics of the Reaction between Carbon Dioxide and Methyldiethanolamine. *Chem. Eng. Sci.* **1987**, *42*, 1393–1398.
25. Cussler, E. L. Diffusion Mass Transfer in Fluid Systems, 3rd Edition, Cambridge University Press, **2009**

Chapter 7

7. Determination and Measurements of Mass Transfer Kinetics of CO₂ in Concentrated Aqueous Monoethanolamine Solutions with a Stirred Cell

Abstract

The gas–liquid reaction rate was determined with a stirred cell from the fall in pressure and the reaction rate constant was determined by two data treatment methods, viz. a “differential” and an “integral” method. The gas-phase resistance was investigated to avoid the effect of the gas-phase resistance on the measurement of the reaction rate constant. The liquid-side mass transfer coefficient without chemical reaction in the stirred cell reactor was determined via the pressure drop method. The kinetics of the reaction of carbon dioxide with aqueous monoethanolamine (MEA) solutions over a wide concentration range from 0.5 to 12 M at a temperature range from 298.15 to 323.15 K were studied using a stirred cell absorber with a plane gas–liquid interface. Low CO₂ partial pressure (3 – 4 kPa) was employed to satisfy the criterion for a pseudo-first-order reaction. Very low inert gas pressures of N₂ and solution vapor were kept, and the gas stirrer was sped up to reduce the gas phase resistance. The results showed that the investigated reactions took place in the pseudo-first-order fast reaction regime. The reaction rate constant obtained for MEA with CO₂ at 298.15 K agrees with literature. The reaction activation energy (E_a) of aqueous MEA + CO₂ is 44.89 kJ mol⁻¹, and the pre-exponential factor value is 4.14×10^{11} . The enhanced mass transfer coefficient in the liquid phase, $k_L E$, initially increases with the concentration of MEA solutions, but decreases when the molarity of MEA is higher than 8 M.

7.1. Introduction

Monoethanolamine (MEA) has been employed as an important industrial absorbent since the 1930s due to its high reaction rate, low cost and thermal stability. Although other amines have become more popular, and the MEA process has some shortcomings such as high energy consumption, it is at present date considered the most mature technology of CO₂ capture in Post-combustion flue gases.¹ In order to improve the absorption efficiency of MEA solutions and reduce the energy consumption, the mass fraction of aqueous solution was generally increased to 30 wt % in the 1960s. A further increase has potential for reducing the transport energy and cost of CO₂ capture given that corrosion and degradation issues can be controlled.

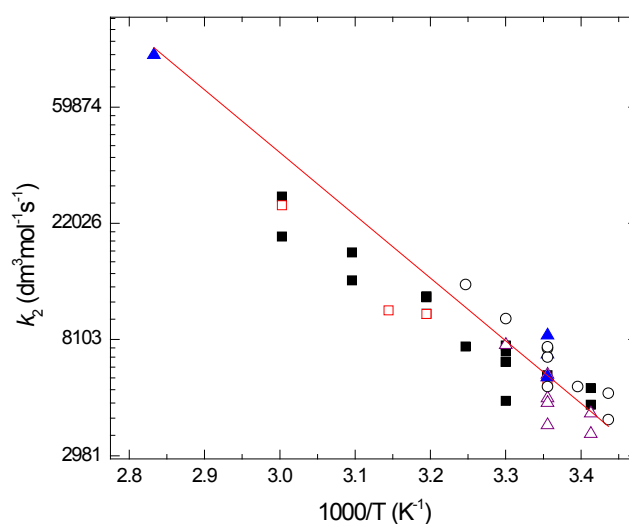


Figure 7.1 Reaction rate constant (k_2) of aq. MEA with CO₂ as a function of temperature compared with literature values by decade: ■, 2000s; □, 1990s; ▲, 1980s; ▲, 1970s; ○, 1950–1960s; Solid line, calculated from equation (7.1).

The chemical kinetics of MEA with CO₂ is very important for industrial designs and theoretical research. Even though that is a considerable number of studies, some disagreements exist between the published reaction rate data. Versteeg et al.² and Vaidya et al.³ made good reviews of the chemical kinetics of aqueous amines solutions including MEA solution. An overview of the reaction rate constant (k_2) of aqueous MEA with CO₂ from various sources is plotted in Figure 7.1. The Arrhenius equation for aqueous MEA with CO₂ was proposed by Versteeg et al.² as follows

$$k_2 = 4.4 \times 10^{11} \exp\left(\frac{-5400}{T}\right) \quad (7.1)$$

Table 7.1 A review of reaction rate constant (k₂) of aq. MEA with CO₂

Year	Author	C (mol dm ⁻³)	T (K)										k ₂ m ³ kmol ⁻¹ s ⁻¹	E _a /R	T range (K)		
			291	293	294.5	298	303	308	313	318	323	333				353	
1954	Jensen	0.1, 0.24065															
1961	Astarita	0.25–2.0			5400												
1962	Emmert	0.1–2			5400												
1964	Clarke	1.6–4.8			7500												
1965	Sharma	1			6970	9700											
1966	Dackwerts	15100			7600	13000											
1971	Leder												94000				
1976	Sada	0.245–1.905			7140												
1976	Sada	0.2–1.9			8400												
1979	Hikita	0.0152–0.177			5870 ^a								9.77E+10	-4955	279–309		
1980	Alvarez–Fuste	0.2–2.0	4300														
1980	Donaldson	0.03–0.08			6000												
1981	Laddha	0.49–1.71			5870												
1983	Penny	0–0.06			4891 ^a								1.23E+11	-5078	278–303		
1985	Sada	0.5–2.0			7740												
1986	Barth	0.02–0.05	3600		4700												
1989	Crooks	0.02–0.06			3880												
1990	Alper	0–0.45			5545 ^a								8.51E+11	-5617	278–298		
1992	Little	0–3.2							10400		25700						
1995	Hagewiesche							10090									
1996	Versteeg												4.40E+11	-5400 ^b			
2000	Xiao	0.1–0.4			4774	7618	11743										
2002	Hornig	0.1–0.5															
2003	Kucka	3.3			5959 ^a								4.49E+11	-5405	293–324		
2003	Aboudheir	3.0–9	4615		6674		10119			13479	19635						
2003	Aboudheir	3.0–9	5335		7691		11643			17141	27706						
2004	Aboudheir	0.22–2.02			6674												
2005	P.D. Vaidya	2.5			7311												

a – calculated values from Arrhenius equation

b — summarized by Versteeg from literature before 1996

where k_2 is the reaction rate coefficient of the reaction between aqueous MEA with CO_2 . However, it can be seen from Figure 7.1 that the reported values of k_2 at 298.15 K vary from 3880 to 8400 $\text{dm}^3 \text{mol}^{-1} \text{s}^{-1}$ measured by various absorbers, and the average relative deviation (ARD) is 26.5%, and the maximum relative deviation (MRD) reaches 67.3%. In summary, the disagreements of this wide range of k_2 values may be attributed to (1) uncertainties in the physical properties (solubility and diffusivity) used, (2) the assumption of negligible gas phase resistance, (3) inability to determine the exact gas–liquid interface area in some absorption processes, (4) possibility of existence of inner facial turbulence in some types of absorbers, and (5) the assumption of a pseudo–1st order reaction not being fulfilled.

The research in most of the literature was restricted to a narrow concentration of MEA solutions not exceeding 2 M, except for few studies conducted by Clarke⁴, Littel et al.⁵ and Aboudheir et al.⁶, where the upper concentrations there were 4.8, 3.2 and 9 M, respectively. In addition, almost all the literature made the assumption of negligible gas-phase resistance and no one investigated completely the influence of gas-phase resistance on the mass transfer process by stirred cell with batchwise operation.

So-called stirred cells are classical tools for studying reaction and mass transfer kinetics for gas-liquid systems with or without chemical reactions. Despite of such equipment having been in use for such purpose for several decades, there are still issues worth discussing. Stirred cells are less complicated than the classic tools including wetted walls, single spheres and laminar jets in the sense that less supporting equipment is needed. Hence the flowsheet and as a consequence the temperature control becomes much easier. Another convenient property is that less liquid is needed to do measurements, and normally, there is no chemical analysis needed for the liquid, but simple chemical analysis, such as titration, may be applied for determination of MEA concentration or CO_2 loading if needed. The structure of the stirred cell is simple and easy to operate. The only challenge with respect to construction is to arrange for the stirring, but this is in practice easily dealt with. If operated in batch fashion, the rate of reaction may be derived from pressure measurements. Semi-batch operation with gas flow-through will also involve flow measurements. In this work the focus is on batch operation. Danckwerts⁷, Versteeg⁸, Blauwhoff⁹, Sandall¹⁰, Vaidya¹¹ and other research groups have employed stirred cells to perform a large number of studies on mass transfer of gas-liquid. Recently, Kucka¹² discussed the analysis of rate data based on pressure measurements. Kucka analyzed and compared five analytical and numerical methods for the estimation of reaction rate constants from dynamic experiments in stirred cell reactors, and a reference method was developed and suggested. However, the methods II, III and IV summarized in his

review are actually the same method from the perspective of data numerical treatment. The reference method takes the load of the liquid bulk phase into account and thus offers the opportunity to perform several experiments in series, without time-consuming purification of the liquid phase. This is a good idea for the usage of a stirred cell when the load of the liquid bulk is a little high. However, it is found that the reference method is too complex in practice and not necessary if the liquid amount is large or the load of the liquid bulk is low.

The gas-phase resistance during the absorption of a gas into a liquid in the stirred cell was not investigated in the present literature, and it was always neglected in the measurements. Actually, as the gas phase in the stirred cell includes liquid vapors and inert gases such as N₂, it is impossible to completely remove non-reacting gas from the stirred cell. If the partial pressure of the reactant gas is very low and the gas absorption rate is high, the influence of the gas-phase resistance on the result is significant. For instance, with respect to the aqueous MEA+CO₂ system, the CO₂ partial pressure was set very low, to about 3 – 5 kPa, to meet the pseudo-first-order reaction regime requirements, but the partial pressure of the inert gas (MEA, H₂O vapor and N₂) is normally higher than this value for CO₂, about 3 – 12 kPa. The typical absorption curve and gas, liquid statuses are shown in Figure 7.2.

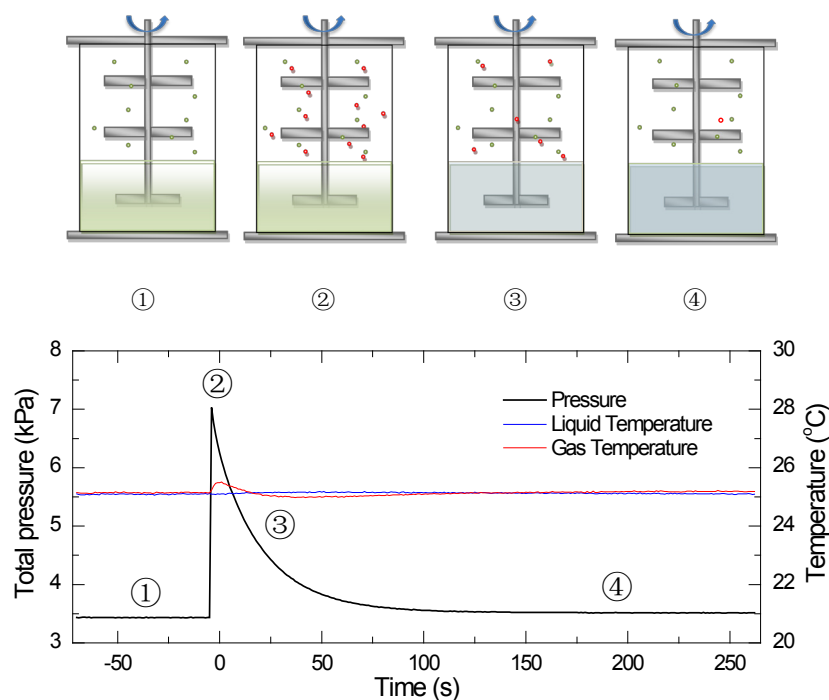
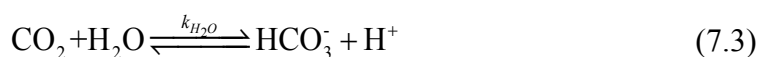


Figure 7.2 Schematic diagram of the gas and liquid status of the typical gas-liquid absorption in the stirred cell absorber: ①-solution and its vapors before the reactant gas introduction, ②- reactant gas is introduced and absorption starts, ③- gas is absorbing in liquid, ④- the absorption reaches an equilibrium.

In this work, the gas-phase resistance in the stirred cell was investigated in the absorption of CO₂ in MEA solutions with various solvents (water and ethylene glycol) at 303.15 K, respectively. The physical mass transfer coefficient of gas in water and aqueous MEA solutions were examined by a stirred cell. Two numerical methods for the calculation of the mass transfer coefficient were discussed, and the chemical reaction kinetics of CO₂ and aqueous MEA solutions were determined. The mass transfer kinetics of CO₂ in aqueous MEA solutions with chemical reaction were studied at the temperature range from 298.15 to 323.15K over a wide range of aqueous MEA concentrations (from 0.5 – 12 M) by using 3 – 4 kPa CO₂ partial pressure and low inert gas (N₂+ water vapor + MEA vapor) pressures.

7.2. Theory Background

In an aqueous MEA solution, CO₂ may simultaneously react with MEA, OH⁻, and H₂O. The CO₂ reactions with OH⁻ and H₂O can be represented as follows:



The rates of the reactions described by equations (7.2) and (7.3) are given by

$$r_1 = k_{\text{OH}^-} C_{\text{CO}_2} C_{\text{OH}^-} \quad (7.4)$$

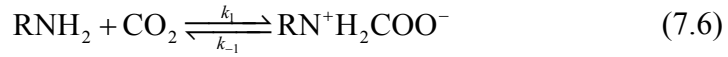
$$r_2 = k_{\text{H}_2\text{O}} C_{\text{CO}_2} C_{\text{H}_2\text{O}} \quad (7.5)$$

Thomas¹² made a review and suggested that the reactions (7.2) and (7.3) are very slow, only 0.8% CO₂ depletion at 298.15 K compared to other reactions. Therefore, the reactions (7.2) and (7.3) were neglected in this work.

Regarding the reaction between MEA and CO₂, generally, the kinetics can be described by either the two-step zwitterion mechanism, which was proposed by Caplow¹⁴ originally and later reintroduced by Danckwerts¹⁸, or by the single-step termolecular mechanism proposed by Crooks and Donellan¹⁶ originally and recently revisited by Da Silva and Svendsen.¹⁷

7.2.1. Zwitterion Mechanism

This mechanistic model assumes that the carbamate formation from MEA by reaction (7.6) and (7.7) takes place. The reaction steps involve the formation of a “zwitterion”



and the subsequent removal of the proton by a base B (base catalysis):



where B designates any species in the solution that can act as a base to attract the proton from the zwitterion. In this case, the dominating species for a MEA solution before reacts with CO₂ are [H₂O], [OH⁻], [CO₃²⁻], [HCO₃⁻] and [RNH₂]. For this mechanism, Danckwerts¹⁵ derived the forward reaction rate equation assuming that the zwitterion reaches a pseudo-equilibrium condition, according to above chemical reactions (7.6) and (7.7), the reaction rate of CO₂ in the reactions, $r_{\text{CO}_2} = k_1 C_{\text{CO}_2} C_{\text{RNH}_2} - k_{-1} C_Z = C_Z \sum k_B C_B$, thereby, the concentration of the intermediate “zwitterion”, $C_Z = k_1 C_{\text{CO}_2} C_{\text{RNH}_2} / (k_{-1} + \sum k_B C_B)$, then

$$r_{\text{CO}_2} = \frac{k_1 C_{\text{CO}_2} C_{\text{RNH}_2}}{1 + k_{-1} / \sum k_B C_B} \quad (7.8)$$

where $\sum k_B C_B$ indicates the contribution to the proton removal step (7.7) by all bases present in the solution. The reaction rate given by equation (7.8) exhibits a reaction order between 1 and 2 with respect to MEA.⁶ When deprotonation of the zwitterion is almost instantaneous compared to the reverse reaction in equation (7.6) (*viz.* $k_{-1} / \sum k_B C_B \ll 1$) and the zwitterion formation is rate-determining, the equation (7.8) takes the form as follows,

$$r_{\text{CO}_2} = k_1 C_{\text{CO}_2} C_{\text{RNH}_2} \quad (7.9)$$

Therefore, it is suggested that the reaction is first order with respect to both CO₂ and MEA, and the overall reaction is then second order. When the reaction of the zwitterion deprotonation is rate-determining (*viz.* $k_{-1} / \sum k_B C_B \gg 1$), the equation (7.8) takes the form

$$r_{\text{CO}_2} = \frac{k_1 \sum k_B C_B}{k_{-1}} C_{\text{CO}_2} C_{\text{RNH}_2} \quad (7.10)$$

This equation suggests a reaction order between 1 and 2 is similar as equation (7.8), with respect to the MEA concentration. When the contribution of the MEA as a base to zwitterion deprotonation reaction is much more significant than that of other bases, the overall reaction is second order for MEA.

7.2.2. Termolecular Mechanism

The termolecular mechanism assumes that the reaction is a single-step between MEA and CO₂ where the initial product is a loosely bound encounter complex instead of a zwitterion. Most of these complexes are intermediates, which break up to give reagent molecules again; a few react with a second molecule of amine, or a water molecule, to give ionic products. Bond-formation and charge-separation occur only in the second step. The forward reaction rate for this mechanism is represented by



For this case, where H₂O, OH⁻, and MEA are the dominating bases B, then the reaction rate is given by

$$r_{\text{CO}_2} = \left(\sum k_B C_B \right) C_{\text{RNH}_2} C_{\text{CO}_2} \quad (7.12)$$

The concentration can be regarded as a constant when the amount of MEA is much larger than that of CO₂. Then the reaction rate constant can be combined as k_{obs} , the equation (7.12) is given by

$$r_{\text{CO}_2} = k_{\text{obs}} C_{\text{CO}_2} \quad (7.13)$$

where $k_{\text{obs}} = \left(\sum k_B C_B \right) C_{\text{RNH}_2}$. Equation (7.12) suggests H₂O, OH⁻ and MEA can react in parallel. This case is similar to the case of the zwitterion mechanism represented by equation (7.10). When H₂O is the dominant base and the contributions of RNH₂ and OH⁻ to carbamate formation are neglected, the reaction is first order with respect to both MEA and CO₂, and the rate is given by

$$r_{\text{CO}_2} = k' C_{\text{RNH}_2} C_{\text{CO}_2} \quad (7.14)$$

where $k' = k_{\text{H}_2\text{O}} C_{\text{H}_2\text{O}}$. The reaction is second order with respect to MEA when MEA is the most dominant base, and the rate is then

$$r_{\text{CO}_2} = k_{\text{RNH}_2} (C_{\text{RNH}_2})^2 C_{\text{CO}_2} \quad (7.15)$$

It can be seen that the number of parameters to fit in equation (7.12) in the termolecular mechanism is fewer than that of equation (7.8) for the zwitterion mechanism.

Regarding the reaction rate dependence on the CO₂ concentration, a first order rate equation was by Blauwhoff.⁹ Therefore, only the reaction rate dependence on MEA concentration and temperature will be considered in this research work.

7.3. Experimental Section

7.3.1. Experimental Equipment and Procedures

A schematic diagram of the stirred cell absorber is shown in Figure 7.3. The stirred cell absorber comprises an inner diameter 12.5 cm chamber with a water jacket which is connected to a water bath. Deionized water is used in the double jacket to provide isothermal operating conditions. The entire assembly was proven to have no leaks. The gas phase stirrers were two fan turbines with six blades (length = 39 mm, width = 14 mm) each mounted in the gas phase while the liquid phase stirrer with two blades (length = 25 mm, width = 10 mm) placed halfway down the liquid's depth. The size and number of gas phase fans are bigger and two compared to one in the liquid phase. This structure can reduce the influence of gas-phase resistance in the measurements. Both gas- and liquid-phase stirrers were driven by the same shaft at speeds 0 – 2500 rpm that could be adjusted electronically within an accuracy of ± 1 rpm. Eight baffles were fitted inside the reactor to prevent vortex formation during the stirring of the liquid phase and also to ensure a flat horizontal interface. A pressure transducer (Druck, PTX1400, U.K., 0–100 kPa abs.) with an accuracy 0.15%, was mounted on the flange and coupled with a data acquisition system. This enabled measurement of the total pressure inside the reactor. A roll metal pipe with 10 cm³ volume was used for storage gas around the metal flange, whose temperature was controlled by an independent controller based on an electric heater, was used to provide the required temperature for the gas. Both the flanges and the roll metal pipe were insulated by thermal insulation materials to ensure a better temperature control. During experiments, the temperatures of the liquid and gas phases and the total pressure inside the reactor were recorded using the data acquisition system (data logger, Agilent BenchLink, 34972A).

For the kinetics of chemical absorption measurement runs, the stirred tank absorber was operated batchwise with respect to both the gas phase and liquid phase. For each experimental run, 500 – 600 cm³ of the freshly prepared solution was fed into the reaction chamber, and kept under vacuum (i.e., approx. 3.1 kPa at 298.15 K) for approximately 1 h to ensure that both the gas–liquid and the temperature reach equilibrium. Then, the liquid was kept under vacuum in preparation for the experimental run and data collection. The storage gas pipe was filled with the gas to be studied (CO₂) at 5 bar (gauge) and then heated to the

specified temperature. The temperature of the flange was a little higher (+0.3 K) than that of the liquid to avoid condensation on the surface of the metal flange. The dimensions of the equipment and operation condition are shown in Table 7.2.

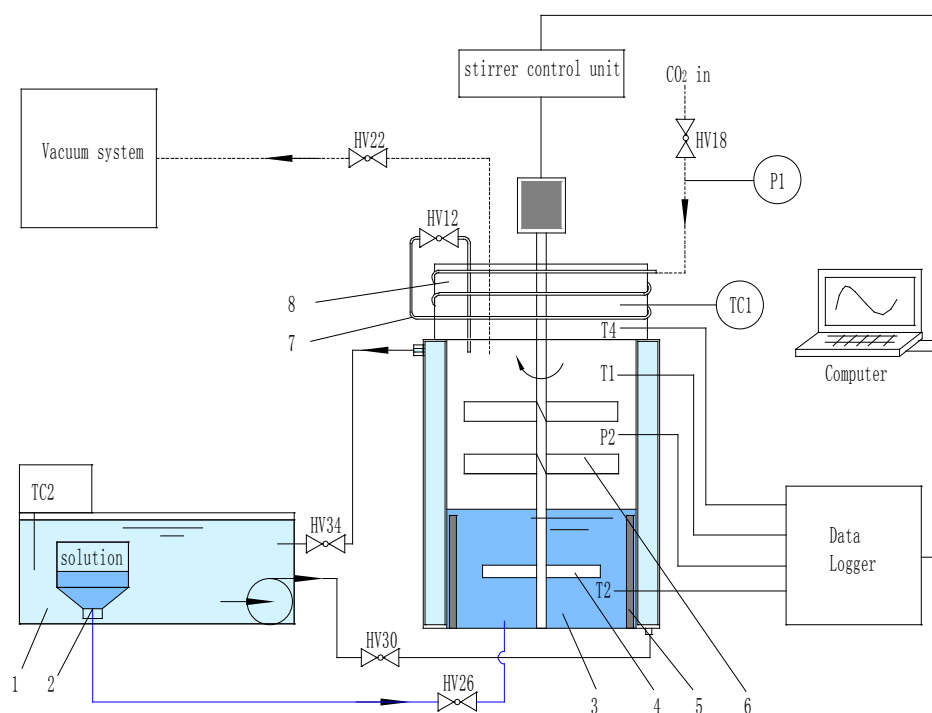


Figure 7.3 Schematic diagram of Stirred Cell absorber
 1– water bath, 2– solution tank, 3– stirred cell chamber, 4– stirrer of liquid, 5– baffles,
 6– stirrer of gas, 7– storage pipe of gas, 8– metal flange

Table 7.2 Dimensions of the stirred cell

Parameters	Symbol	Value	Unit
Volume of reactor	V	1.986×10^{-6}	m^3
Volume liquid phase	V_L	$0.5\text{--}0.6 \times 10^{-6}$	m^3
Interfacial area	A	1.227×10^{-2}	m^2
Stirrer revolutions per second (rps)	ω	1–1.33	s^{-1}
Diameter of liquid stirrer	d	8.85×10^{-2}	m

For each experiment of CO_2 absorption in MEA solution, CO_2 was introduced into the chamber and the initial partial pressure of CO_2 was very low, 3 – 5 kPa, to satisfy the criterion for a pseudo-first-order reaction, as given by Danckwerts¹⁸ as follows:

$$3 < Ha \ll E^\infty \quad (7.16)$$

where Ha is Hatta number defined as¹⁹

$$Ha = \frac{\sqrt{\frac{2}{m+1} k_{m,n} C_i^{m-1} C_j^n D_i}}{k_L} \quad (7.17)$$

where $k_{m,n}$ is the reaction rate constant of (m,n) th order, D_i is the diffusion coefficient of the reacting gas species in the liquid phase, and k_L is the mass transfer coefficient without chemical reaction in liquid. With respect to the MEA+CO₂ chemical reaction, if $m=1$ and $n=1$, then

$$Ha = \frac{\sqrt{k_2 C_{\text{MEA}} D_{\text{CO}_2}}}{k_L} \Leftrightarrow Ha^2 = \frac{k_2 C_{\text{MEA}} D_{\text{CO}_2}}{k_L^2} \quad (7.18)$$

where k_2 is the forward kinetic rate constant. By rewriting equation (7.18), the following relation was obtained:

$$Ha^2 = \frac{(k_2 C_{\text{MEA}} C_{\text{CO}_2}^i) \delta_L A}{k_L C_{\text{CO}_2}^i A} = \left(\frac{\text{max. chemical conversion rate}}{\text{max. diffusional mass transfer rate}} \right)_{\text{in liquid film}} \quad (7.19)$$

where

$$k_L = \frac{D_{\text{CO}_2}}{\delta_L} \quad (7.20)$$

and C_{CO_2} is the concentration of CO₂, A is the interfacial area available for mass transfer, δ_L is the film thickness, and the superscript i refers to the gas–liquid interface. From equation (7.19) the physical meaning of the Ha^2 number can easily be seen as the ratio of the maximum reactive conversion rate of CO₂ in the film per unit area interface to the maximum diffusional transport through the film in the case of absence of any reactions.²⁰

For the film theory of mass transfer:

$$E = \frac{Ha}{\tanh Ha} \quad (7.21)$$

and E^∞ is the limiting case of absorption, the infinite enhancement factor, with a single irreversible reaction, approximated by Higbie²¹ to be

$$E^\infty = \sqrt{\frac{D_{\text{CO}_2,\text{L}}}{D_{\text{MEA},\text{L}}}} \left(1 + \frac{D_{\text{MEA},\text{L}}}{D_{\text{CO}_2,\text{L}}} \frac{C_{\text{MEA}}}{\nu_{\text{MEA}} C_{\text{CO}_2}^i} \right) \quad (7.22)$$

or

$$E^\infty = \sqrt{\frac{D_{\text{CO}_2,\text{L}}}{D_{\text{MEA},\text{L}}}} + \sqrt{\frac{D_{\text{MEA},\text{L}}}{D_{\text{CO}_2,\text{L}}}} \frac{C_{\text{MEA}} H_{\text{CO}_2}}{\nu_{\text{MEA}} P_{\text{CO}_2}} \quad (7.23)$$

where ν_{MEA} is the stoichiometric coefficient of MEA, H_{CO_2} is the Henry's constant, $D_{\text{CO}_2,\text{L}}$ and $D_{\text{MEA},\text{L}}$ are the diffusivities of CO_2 and MEA in the liquid, respectively. E^∞ is defined as the enhancement factor with instantaneous conversion of reactants and the rate of absorption thus completely being limited by the diffusion of governing components. According to equation (7.23), if C_{MEA} is large enough or P_{CO_2} small enough, E^∞ will be large enough to satisfy the criterion equation (7.16). When the reaction is satisfied with the condition equation(7.16), $\tanh Ha \approx 1$, the reaction is then in the fast reaction regime, and

$$E \approx Ha = \frac{\sqrt{k_2 C_{\text{MEA}} D_{\text{CO}_2}}}{k_L} \quad (7.24)$$

Ha is low when the reaction rate is low according to the equation (7.24). In practice, to meet the pseudo-first-order reaction criterion, the requirement for the partial pressure of CO_2 is different for different reaction systems. For example, the CO_2 partial pressure is not required to be as low to meet one of the criterion conditions ($Ha \ll E^\infty$) for methyldiethanolamine (MDEA) + CO_2 reaction system due to the low reaction rate coefficient.^{2,3} However, for MEA + CO_2 , it is required that the CO_2 partial pressure is very low because of the high Ha value.

The influence of the CO_2 loading on the rate of the reverse reaction is only 1% at the maximum as was checked by Cornelisse et al.²² In this work, about 3 – 4 kPa CO_2 (volume=1.4 L) was used for the absorption measurement in 0.5 L MEA solution ranges from 0.5 to 12 M. After the absorption is finished, the CO_2 loading is $3 \times 10^{-6} - 7 \times 10^{-5}$ mol/mol each time, and the CO_2 back-pressure from this solution is very small according to the measurement of equilibrium solubility by Jou et al.²³ Therefore, it is safe to use the same solution for all the 298.15 – 323.15 K measurements with neglecting of CO_2 loading in the solution.

The influence of the agitation speed on the measurement of k_2 was investigated, and it was found that the measured k_2 was lower if the agitation speed was set too low (i.e., 50 rpm). This is because when the stirring speed is too low, the liquid surface does not renew itself

enough, and the gas-phase resistance is significant (note that the liquid fan and gas fans are mounted on the same shaft). However, if the stirring speed is too fast (i.e., 110 rpm) in this stirred cell reactor, turbulence in the liquid could be detected. Vaidya et al.¹¹ found that the effect of agitation speed on the measurement can be neglected when varying the stirring speed in the range of 60 – 120 rpm at 308 K, due to the fast reaction of the amine and CO₂. Our result is similar to theirs. The further experiments in this work were conducted at the speeds of 60 rpm and 80 rpm.

The entire amount of gas has to be injected in a very short time (typically < 5 s) because the absorption starts immediately once introducing the gas. The total pressure inside the reactor, the agitation speed (rps), and the gas and liquid temperatures are monitored and recorded continuously. The partial pressure of the gas A at the experimental condition was corrected for the vapor pressure of the solution as follows.

$$P_A = P_{\text{total}} - (P_{\text{N}_2} + x_{\text{H}_2\text{O}}P_{\text{H}_2\text{O}}^v + x_{\text{MEA}}P_{\text{MEA}}^v) \quad (7.25)$$

where P_{N_2} is the partial pressure of nitrogen, $P_{\text{H}_2\text{O}}^v$ is the water vapor pressure, P_{MEA}^v is the vapor pressure of MEA, $x_{\text{H}_2\text{O}}$ and x_{MEA} are the mole fraction of water and MEA, respectively.

To check the influence of gas-phase resistance on the measurement of chemical absorption, the reaction rate constants of MEA+CO₂ were measured in different inert gas (N₂+H₂O and MEA vapor) at a certain temperature. The experimental concentration of MEA was 3M, temperature was 303.15 K, stirred speed was 1 rps, and the partial pressure of CO₂ varied from 3 kPa to 40 kPa. The other procedure steps were same as for the kinetics measurement.

7.3.2. Reagent and Solution Preparation

Reagent grade MEA with mass fraction purity $\geq 99.5\%$ was obtained from Merck and used without further purification. Deionized water (was purified with a Mini-Q system (Millipore), 18.2 M Ω ·cm) and MEA were degassed by applying vacuum and then they were mixed to prepare various concentrations of aqueous MEA solutions using an analytical balance (Mettler Toledo XS403S) with an accuracy of ± 1 mg and a 500 mL volumetric flask. Various concentrations of aqueous MEA solutions were prepared: 0.5 M (3.1 mass %), 1 M (6.1 mass %), 2 M (12.1 mass %), 3.6 M (21.7 mass %), 5 M (30.2 mass %), 8 M (47.9 mass%), and 12 M (71.4 mass %). The whole preparation process was protected by a nitrogen atmosphere. The purity of CO₂ was ≥ 99.995 mol % and that of N₂O ≥ 99.7 mol %, both gases were produced by AGA Gas GmbH.

7.4. Results and Discussion

7.4.1. Physical Solubility

The physical solubility of CO₂ in aqueous MEA solution a over wide range of concentrations were measured using a novel solubility measurement technique²⁴ in temperature range from 298.15 to 323.15 K and a constant ambient pressure using N₂O analogy method. The Henry's constant of CO₂ in 3 M, 5 M, 8 M, 12 M, and 15 M aqueous MEA solutions and pure MEA are tabulated in Table 7.3. The solubilities of other concentrations were estimated by Wang et al.'s model and its parameters were regressed in previous work.²⁴

Table 7.3 Solubilities of CO₂ in various concentration aq. MEA solutions

T(K)	$H_{\text{CO}_2}(\text{kPa m}^3 \text{ kmol}^{-1})$								
	0.5 M	1 M	2 M	3 M	3.6 M	5 M	8 M	10 M	12 M
298.15	2940	2938	2959	3097	3042	3170	3249	3341	3032
303.15	3354	3358	3391	3566	3498	3675	3846	3838	3552
313.15	4123	4126	4161	4258	4276	4375	4465	4541	4245
323.15	5044	5035	5052	5130	5149	5242	5314	5285	4913

7.4.2. Diffusivity

The molecular diffusivities of N₂O with aqueous monoethanolamine (MEA) solutions up to 12 M were studied over a temperature range from 298.15 to 333.15 K under atmospheric pressure using a laminar liquid jet absorber in parallel work.²⁵ The diffusivities of CO₂ in aqueous MEA solutions were calculated by the N₂O analogy method. The measurements of high viscosity solutions ($> \sim 7.5$ mPa s) were difficult to measure by the laminar liquid jet apparatus, there are some values were calculated by the exponent mathematic model with the regressed parameters in the parallel work. The results are presented in Table 7.4.

Table 7.4 Diffusivities of CO₂ in various concentration aq. MEA solutions

T(K)	$D_{\text{CO}_2} (10^{-9} \text{ m}^2 \text{ s}^{-1})$								
	0.5 M	1 M	2 M	3 M	3.6 M	5 M	8 M	10 M	12 M
298.15	1.83	1.81	1.70	1.54	1.50	1.26	0.93	0.70	0.48
303.15	2.07	2.04	1.91	1.71	1.69	1.47	1.08	0.79	0.54
313.15	2.58	2.56	2.40	2.33	2.13	1.92	1.35	1.02	0.71
323.15	3.23	3.16	2.97	2.74	2.65	2.38	1.73	1.28	0.87

7.4.3. Determination of Gas-liquid Reaction Kinetics

The influence of chemical reactions on the gas absorption rate into the liquid, in which the reactions occur between dissolved CO₂ and reactants in the solution, is usually expressed by an enhancement factor, E , as defined in equation (7.21). The chemical reaction contributions and both gas- and liquid-phase mass transfer resistances to the overall mass transfer flux (N_A) can be estimated by the follow equation:

$$N_A = K_G A (P_A - P_A^e) = \frac{1}{1/k_G + H_A / Ek_L} A (P_A - P_A^e) \quad (7.26)$$

where P_A^e is the equilibrium pressure corresponding to the gas concentration in liquid bulk, K_G is the overall mass transfer coefficient, k_G is the gas phase mass transfer constant, and $(1/k_G + H_A/Ek_L)$ is the overall mass transfer resistance, respectively. The amount of CO₂ is small (partial pressure 3 – 4 kPa), and it is safe to assume that the CO₂ concentration in the liquid bulk is 0 throughout the measurements. Then, it follows that $P_A^e=0$, and, hence according to the principle of mass conservation,

$$N_A = -\frac{dn_A}{dt} = -\frac{dP_A}{dt} \frac{V_G}{RT} = \frac{1}{1/k_G + H_A / Ek_L} AP_A \quad (7.27)$$

which is arranged to yield

$$-\frac{dP_A}{dt} = \frac{RAT}{V_G(1/k_G + H_A / Ek_L)} P_A \quad (7.28)$$

Equation (7.24) is substituted in the equation(7.28), and then result in

$$-\frac{dP_A}{dt} = \left[\frac{RAT}{V_G(1/k_G + H_A / \sqrt{k_2 C_{MEA} D_{CO_2}})} \right] P_A \quad (7.29)$$

After the integration of equation (7.29),

$$\ln P_A = \left[\frac{RAT}{V_G(1/k_G + H_A / \sqrt{k_2 C_{MEA} D_{CO_2}})} \right] t + \ln P_{A,0} \quad (7.30)$$

If the partial pressure of inert gas is very low, the gas-phase resistance can be neglected. Equations (7.29) and (7.30) will then take the forms

$$-\frac{dP_A}{dt} = \frac{RAT\sqrt{k_2 C_{\text{MEA}} D_{\text{CO}_2}}}{H_A V_G} P_A \quad (7.31)$$

and

$$\ln P_A = \frac{RAT\sqrt{k_2 C_{\text{MEA}} D_{\text{CO}_2}}}{H_A V_G} t + \ln P_{A,0} \quad (7.32)$$

If plotting dP_A/dt vs. P_A or $\ln P_A$ vs. t from the equations (7.29) – (7.32), the slope b is given by

$$b = \frac{RAT}{V_G (1/k_G + H_A / \sqrt{k_2 C_{\text{MEA}} D_{\text{CO}_2}})} \quad (7.33)$$

or

$$b = \frac{RAT\sqrt{k_2 C_{\text{MEA}} D_{\text{CO}_2}}}{H_A V_G} \quad (7.34)$$

The slope b can be determined by linear regression of the plot dP_A/dt vs P_A or $\ln P_A$ vs t . Obviously, the slope b is proportional to $(k_2)^{0.5}$ and can reflect the absorption rate when diffusivity and solubility are unknown.

It is safe to ignore the influence of CO_2 loading on the bulk and assume that C_{MEA} is constant when the amount of MEA is much larger than that of CO_2 . The pseudo-first-order reaction rate constant is then given by

$$k_{\text{ps}} = k_2 C_{\text{MEA}} \quad (7.35)$$

There are two data treatment methods to estimate the k_{ps} and k_2 by using the same series of experimental data. One method is to plot the relationship $dP_A/dt - P_A$, according to equation (7.29) or (7.31), it is named the “differential method”; the other is to plot the relationship $\ln P - t$, according to equation (7.30) or (7.32), called the “integral method”. Both methods can give the slope b of the plot by regressing the data, and k_{ps} or k_2 can then be obtained when the diffusivity and the Henry’s constant are known. Figure 7.4 (a) is a typical curve of $\ln P_{\text{CO}_2}$ versus time of the reaction $\text{MEA} + \text{CO}_2$ at 298.15 K. In order to find the pressure region to meet the criterion of pseudo-first-order reaction, the partial pressure of CO_2 was set to start from 40 kPa. The decrease of the pressure during the experiment caused E^∞ to increase steadily according to equation(7.23), therefore, the criterion equation (7.16)

could always be met when the CO₂ pressure is lower than 3.5 kPa in this case (1 M aqueous MEA solution). However, the noise will be big if P_{CO_2} is too low compared to the inert gas pressure. In this case, the range of P_{CO_2} from 3 to 0.3 kPa meets the criterion of pseudo-first-order reaction and was used for the calculation of reaction rate constant, as shown in Figure 7.4.

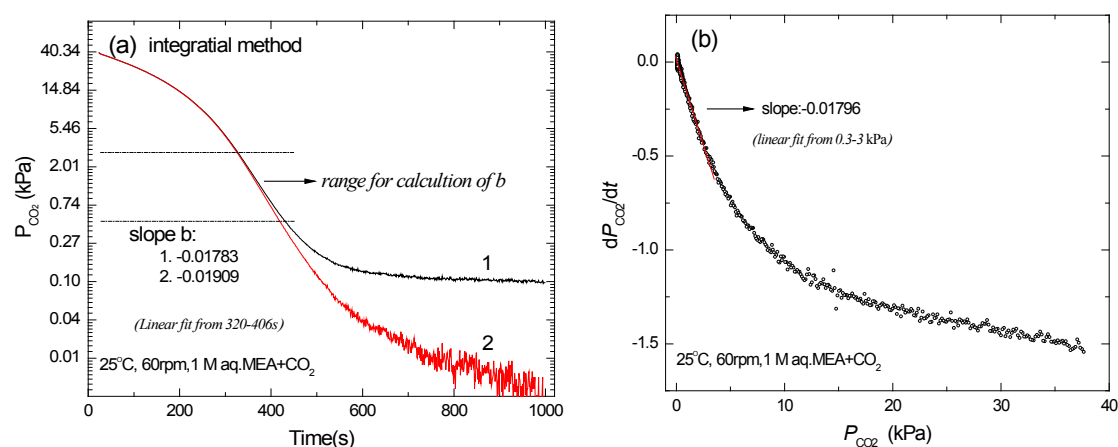


Figure 7.4 A typical P_{CO_2} – time curve measured by stirred cell absorber, $P_{\text{CO}_2}^{\text{ini}}=40$ kPa,
a– integrational method: black line, set $P_{\text{inert}}=3.505$ kPa; red line, set $P_{\text{inert}}=3.600$ kPa;
b– differential method: red line, fitted

Regarding the “integral method”, the trouble is that the initial inert gas pressure (N₂ and solution vapor) cannot be read accurately, but the calculation and $\ln P-t$ curve are very sensitive to P_{inert} . As shown in Figure 7.4 (a), the slope varies from -0.01783 to -0.01953 when P_{inert} shifts only from 3.505 to 3.600 kPa (Note, the error of pressure transducer is 0.15%, ± 0.054 kPa when the reading of pressure is 3.600 kPa), causes 3.4% relative deviation (RD). Compared to the integral method, the differential method is more stable because this treatment is independent of P_{inert} . As shown in Figure 7.4 (b), the reading shift of P_{inert} has no effect on the calculation for the slope, but the points are a little dispersed and the curve is not smooth. Therefore, the “differential method” was better for determining the gas–liquid reaction kinetic constant in this case due to the slope being large enough to reduce the deviation caused by the dispersion. With theoretical perfect pressure transducer and behavior of a stirred cell, the "differential method" and "integral method" would yield identical answers. The difference between the two methods, given in this work, provides a practical method for determination of reaction kinetics with high accuracies. More differences of experimental data treatments of these two methods are shown in Table 7.6.

7.4.4. Estimation of Liquid Mass Transfer Coefficient without Chemical Reaction

The mass transfer coefficient in the liquid phase without chemical reaction in the stirred cell reactor, k_L , can be determined via the pressure drop method. Different models have been used to measure the liquid-side mass transfer coefficient of a gas in a liquid, based on two different principles. One is derived by a mass balance for both the gas phase and the liquid phase and yields the following expression:^{26,27} (The deduction is in the Appendix A5.2)

$$\ln \frac{P(t) - P_g^\infty}{P_g^0 - P_g^\infty} = -\frac{(mV_L + V_g)k_L At}{V_L V_g} \quad (7.36)$$

This model requires the initial and equilibrium partial pressure of the investigated gas during the absorption and needs a long time to reach the equilibrium in practice. The relationship of $\ln[(P(t) - P_g^\infty)/(P_g^0 - P_g^\infty)]$ versus time t was plotted to estimate the value of k_L .

The other model to estimate k_L is deduced from the absorption equation (7.27) and may be expressed as:

$$-\frac{dP_A}{dt} = \left[\frac{RAT}{V_G(1/k_G + H_A/Ek_L)} \right] P_A \quad (7.37)$$

For the slow absorption without chemical reaction ($E=1$), $k_G \gg k_L$, $1/k_G$ is then much smaller than H_A/Ek_L , and

$$-\frac{dP_A}{dt} = \left[\frac{RATk_L}{H_A V_G} \right] P_A \quad (7.38)$$

after integration

$$\ln P_A = \frac{RATk_L}{H_A V_G} t + \ln P_{A,0} \quad (7.39)$$

Then, dP_A/dt versus P_A or $\ln P_A$ versus time t was plotted and regressed to obtain the slope that allows determination of the value of k_L . This method only needs to record the beginning (10 – 100 s) of the pressure drop measurement. Because the absorption without chemical reaction is slow and the slope is small, the deviation caused by the dispersion of the dP_A/dt versus P_A could be large, thus, the integral method is suggested as best for to estimating the value of k_L and equation (7.39) is employed to treat the experimental data in this work.

The dependency of the experimentally observed liquid-side mass transfer coefficient on the molecular diffusivity, density, viscosity, and hydrodynamics of the system (stirred speed etc.) is commonly described by a relationship of dimensionless numbers. The well-known equation with respect to the Sherwood (Sh) number to the Reynolds (Re) and Schmidt (Sc) numbers applied to a stirred cell is^{27,32}

$$Sh = c_1 + c_2 Re^{c_3} Sc^{c_4} \quad (7.40)$$

where

$$Re = \frac{\rho_L \omega d^2}{\mu_L} \quad (7.41)$$

$$Sc = \frac{\mu_L}{\rho_L D_A} \quad (7.42)$$

$$Sh = \frac{k_L d}{D_A} \quad (7.43)$$

and ρ_L is the density of the liquid, ω is the stirred speed, d is the diameter of the stirrer, μ_L is the dynamic viscosity of the liquid, D_A is the diffusivity of gas A in the liquid, k_L is the liquid phase mass transfer coefficient of gas A, respectively. The constants c_1 , c_2 , c_3 , and c_4 , in equation (7.40) depend on the type of equipment used such as geometry of the tank, stirrer type/speed, etc. At relatively high Sh numbers, the value of the constant c_1 is small and can be neglected. The equation (7.40) can then be written as

$$Sh = c_2 Re^{c_3} Sc^{c_4} \quad (7.44)$$

The power c_3 of the Re number can be determined by keeping Sc number constant and varying the hydrodynamic conditions, (i.e., stirrer speed and stirrer position). Then the exponent c_4 of the Sc number and the coefficient c_2 are determined by using different solutes/solvents or varying the experimental temperatures, and keeping the Re number constant simultaneously (i.e., keep the stirrer speed and stirrer position in the liquid constant). Versteeg et al.²⁷ and Haimour et al.³⁰ suggested based on the penetration theory, that the value c_4 is 0.5 for large Sc numbers. The coefficient c_2 and exponent c_4 can then be easily determined experimentally by changing solutes/solvents or varying the experimental

temperatures. Once the constants c_2 , c_3 , and c_4 in equation (7.44) for the stirred cell are obtained, the k_L of a gas in a liquid at a given temperature can be calculated from the equation (7.44) when the density, viscosity, and diffusivity are known.

The physical mass transfer of CO_2 and N_2O in water and N_2O in the 70 mass % aqueous MEA solution at various temperatures under the stirrer speeds 1 and 1.33 rps were measured to estimate k_L . The drop in pressure due to absorption was recorded and treated by the integral method. The viscosities of the liquid, solubilities, and diffusivities are taken from the above chapters and sections. The density of H_2O and the aqueous MEA solution are from Han et al.³³ The overview of the result is shown in Table 7.5.

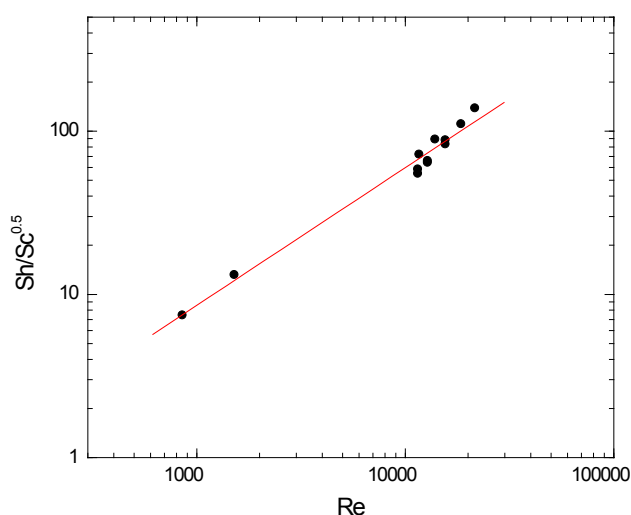


Figure 7.5 Correlation of $Sh/Sc^{0.5}$ versus Re of the stirred cell

A plot of $Sh/Sc^{0.5}$ versus Re is shown in Figure 7.5. The exponent on Re number is 0.84, is shown in the equation (7.45), which is close to the value 0.77 reported by Critchfield,²⁸ Hikita et al.²⁹ found c_3 to be 0.7, while Haimour et al.³⁰ found it to be 0.66. Hamborg and Versteeg³¹ reported that the value of c_3 is 0.694 and c_4 is 0.517 from the absorption measurement. The AAD between the experimental and predicted data of Sh number is 10%. This relationship was used to estimate k_L values and calculate the enhancement factors E in subsequent studies of the absorption of CO_2 in aqueous MEA solution.

$$Sh = 0.0253Re^{0.84}Sc^{0.5} \quad (7.45)$$

Table 7.5 Overview of results of the liquid-side mass transfer coefficient and Re , Sc and Sh numbers

No.	T K	slope $10^{-4}s^{-1}$	ω s^{-1}	H_A $Pa\ m^3\ mol^{-1}$	density $kg\ m^{-3}$	viscosity $10^{-4}pa\ s$	D_{A_2} $10^{-9}\ m^2\ s^{-1}$	k_L $10^{-5}\ m\ s^{-1}$	Re	Sc	Sh	$P_{CO_2,ini}$ Pa	P_{inert} Pa	note
1	298.15	1.953	1.33	2951	997	9.09	1.94	2.63	11451	470	1198	123933	3169	H ₂ O+CO ₂ , no N ₂
2	298.15	2.076	1.33	2951	997	9.09	1.94	2.79	11451	470	1273	95473	101966	H ₂ O+CO ₂ , fill N ₂
3	303.15	2.022	1.33	3361	995.6	8.14	2.14	3.05	12770	382	1260	96208	97416	H ₂ O+CO ₂ , fill N ₂
5	313.15	2.240	1.00	4133	992.2	6.68	2.69	4.02	15507	250	1322	126887	7381	H ₂ O+CO ₂ , no N ₂
5	313.15	1.939	1.00	4133	992.2	6.68	2.69	3.48	11633	250	1144	98719	87770	H ₂ O+CO ₂ , no N ₂
6	323.15	2.072	1.33	5069	988	5.59	3.37	4.42	13843	168	1160	126176	12300	H ₂ O+CO ₂ , no N ₂
7	303.15	1.526	1.33	4422	995.6	8.14	2.01	3.02	12770	407	1331	96534	82815	H ₂ O+N ₂ O, fill N ₂
8	313.15	1.674	1.33	5660	992.2	6.68	2.51	4.11	15507	268	1449	96775	81561	H ₂ O+N ₂ O, fill N ₂
9	323.15	1.802	1.33	7070	988	5.59	3.21	5.36	18453	176	1477	96065	83014	H ₂ O+N ₂ O, fill N ₂
10	333.15	1.898	1.33	8899	983.2	4.77	3.96	6.89	21520	123	1539	96073	82858	H ₂ O+N ₂ O, fill N ₂
11	298.15	0.358	1.33	4135	1026.3	126.02	0.52	0.67	850	23614	1148	96974	82228	70 %MEA+N ₂ O, fill N ₂
12	313.15	0.403	1.33	5820	1015.7	70.24	0.67	1.02	1510	10322	1344	97182	81025	70 %MEA+N ₂ O, fill N ₂

7.4.5. Investigation of Gas-phase resistance

It was investigated the gas-phase resistance should be taken into account or not in the research of kinetics of MEA with CO₂ reaction by stirred cell. It is well known that the overall mass transfer resistance is

$$\frac{1}{K_G} = \frac{1}{k_G} + \frac{H_A}{k_L E} \quad (7.46)$$

Obviously, if $H/k_L E \gg 1/k_G$, means that the Henry's constant H_A is big enough, $k_L E$ and $1/k_G$ are small enough, the gas-phase resistance can be neglected. Theoretically, according to the film theory, penetration theory and surface-renewal theory, the mass transfer coefficient is a function of diffusivity as follows³⁴

$$k = D^\alpha \quad (7.47)$$

where α is 0.5 – 1. The typical order of magnitude of diffusion of gas is $10^{-9} \text{ m}^2\text{s}^{-1}$ in liquid phase and $10^{-5} \text{ m}^2\text{s}^{-1}$ in gas phase, respectively. Theoretically, the typical value of the mass transfer coefficient k_G is 10^{-2} m s^{-1} and k_L is 10^{-5} m s^{-1} , respectively. Obviously, $k_G \gg k_L$, the mass transfer of a gas in the gas phase is much higher than in the liquid phase if the gas solubility in liquid is not high (viz. H_A is low). Since H_A is high in the present case, almost all researchers ignored the influence of the gas-phase resistance when they studied the reaction kinetics by stirred cell with batchwise operation on gas and liquid.

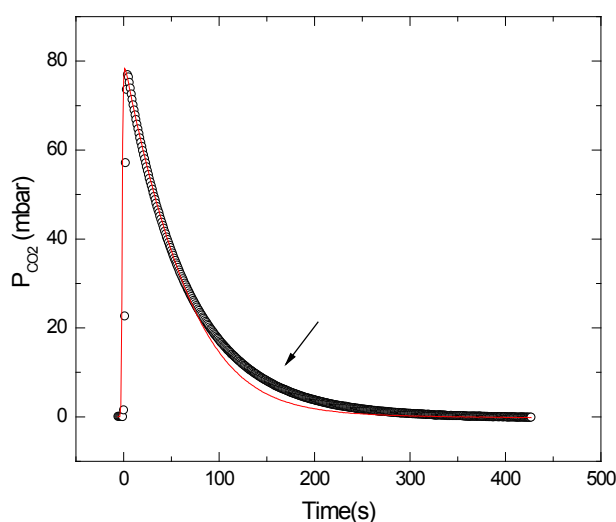


Figure 7.6 P_{CO_2} drop with time of CO₂ absorbed in 1 M MEA solution under different inert gas pressure at the CO₂ initial pressure 7.7 kPa and 303.15 K: \circ , $P_{\text{inert}}=12 \text{ kPa}$; red line is $P_{\text{inert}}=4.5 \text{ kPa}$

It is safe to neglect the gas-phase resistance if the mass transfer in liquid phase is slow, (i.e. without chemical reaction or with slow chemical reaction). However, for the mass transfer with fast chemical reaction, the absorption rate could be high due to the enhancement

by the chemical reaction, and the liquid side mass transfer resistance is $H_A/k_L E$. In the present work, the values of $k_L E$ were calculated, and the typical value is 10^{-2} m s^{-1} for 3.6 M aqueous MEA solution + CO₂ system (see Table. 7.7). Then the mass transfer coefficient in liquid phase is of the same order of magnitude as that in the gas phase, and if the concentrations of MEA solution increase, the values could be higher and even $k_G \leq k_L E$. Thus, the gas-phase resistance cannot be neglected for the fast chemical reaction system.

Experimentally, Figure 7.6 is shown the P_{CO_2} drop with time under different inert gas pressure (12 kPa and 4.5 kPa, absolute pressure) with a same CO₂ initial pressure in 1 M MEA solution at 303.15 K. It can be seen that the absorption rate of CO₂ under the inert gas pressure of 12 kPa is almost same as that of 4.5 kPa when P_{CO_2} is higher than 3 kPa, but lower than that of 4.5 kPa when P_{CO_2} is lower than 3 kPa. The same result is shown in Figure 7.7. It is noted that the pressure region of the CO₂ partial pressure, 0.1 – 3 kPa, is the region where the pseudo-first-order reaction criterion for calculating the reaction rate constant of MEA + CO₂ system is satisfied. Because the P_{CO_2} is low, about 3 – 4 kPa at beginning of the absorption, the pressure of inert gas (including N₂, the vapor of the solution) is about 3.2 kPa at 298.15 K and 12 kPa at 323.15 K, nearly equal to the P_{CO_2} and even higher if the temperature is high, therefore, the inert gas resistance should be taken into consideration.

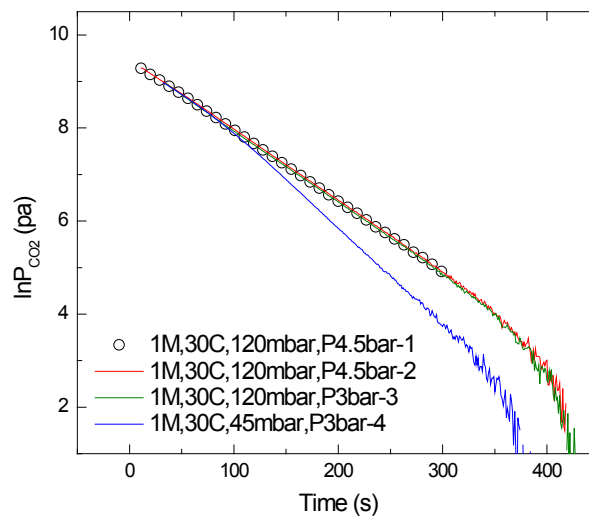


Figure 7.7 $\ln P_{\text{CO}_2} - t$ with different inert gas pressure (12 kPa and 4.5 kPa) and different initial CO₂ pressure at 303.15 K:

(○, solution used 1st time; red line, the same solution used 2nd time) with $P_{\text{inert}}=12 \text{ kPa}$ and $P_{\text{CO}_2, \text{ini}}=10.7 \text{ kPa}$;
 green line, the same solution used 3rd time with $P_{\text{inert}}=12 \text{ kPa}$ and $P_{\text{CO}_2, \text{ini}}=10.7 \text{ kPa}$;
 blue line, the same solution used 4th time with $P_{\text{ini}}=4.5 \text{ kPa}$ and $P_{\text{CO}_2, \text{ini}}=7.7 \text{ kPa}$.

Figure 7.8 shows the slope b as a function of the P_{inert} in 3 M MEA+CO₂ reaction system with the solvents H₂O and ethyleneglycol at 303 K, respectively. It is obvious that the

absorption rate of CO₂ in MEA solution increases with a decrease of the pressure of the inert gas. The absorption rate increases significantly when the inert gas pressure drops to less than 10 kPa. The minimum P_{inert} of the experiment with H₂O as solvent at 303 K is 4 kPa due to the vapor pressure of a 3 M solution being 4 kPa at this temperature. To reduce the P_{inert} further, ethyleneglycol was investigated as a solvent. Here the vapor pressure is lower, and the minimum P_{inert} can be decreased to 2 kPa at 303 K. The result of ethyleneglycol as a solvent shows that the absorption rate increases slightly when P_{inert} decreases from 4 kPa to 2 kPa. The slope and the estimated reaction rate constants are listed in Table 7.6. The results manifest that the influence of the gas-phase resistance cannot be ignored, because of the high chemical reaction speed in the mass transfer of the CO₂ in the solution.

Table 7.6 the slope b and k_2 of 3 M aq. MEA+CO₂ under various inert pressure at 303.15 K and the relative deviation (RD) between the differential and integral method*

P_{inert} (kPa)	Differential method		Integral method		RD(%) of these two method
	slope	k_2	slope	k_2	
4.09	0.03823	8420	0.03708	7921	3.1%
7.01	0.02856	4699	0.02472	3520	14.3%
10.11	0.02404	3329	0.02067	2461	15.0%
20.09	0.02047	2414	0.01700	1665	18.4%
30.01	0.01845	1961	0.01501	1298	20.3%
39.86	0.01794	1854	0.01412	1149	23.5%

* The initial Pressure of CO₂ is approx. 4 kPa for the measurements

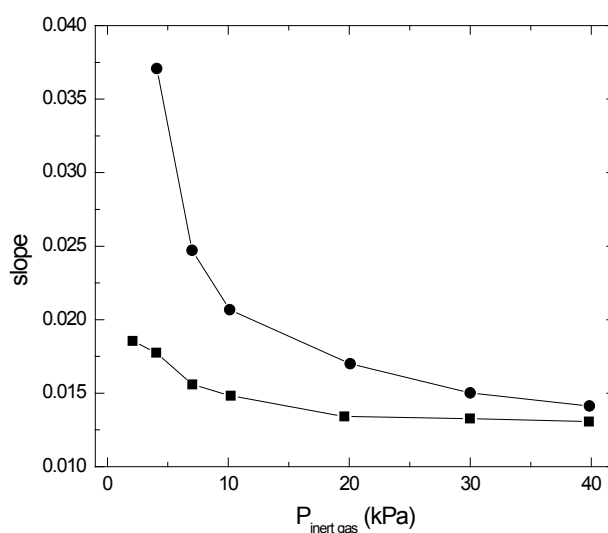


Figure 7.8 Slope versus the partial pressure of inert gas (N₂ and water vapor) of 3 M MEA+CO₂ at 303 K, 1 rps with different solvent: ■, ethyleneglycol; ●, H₂O

At present, there are three solutions to treat the gas-phase resistance as follows,

- 1) Measure the gas-phase resistance experimentally, then employ the equations (7.29) or (7.30) to calculate the mass transfer coefficient of liquid phase. This solution requires measuring the gas phase resistance, and it makes the experimental work more complex.
- 2) Employ the low volatile solvent such as ethyleneglycol to decrease the P_{inert} , and then the gas-phase resistance could be decreased such that P_{inert} could be neglected. But it is noted that different solvents lead to different chemical reaction rate constants due to different solvent effect.
- 3) Speed up the stirrer of gas phase to homogenize the gas and increase the mass transfer in gas phase. This method is easy to operate and do not change the solvent, but could increase the normal velocity of the gas to the gas-liquid interface and maybe affect slightly the mass transfer of liquid phase.

To simplify the measurement model with a stirred cell, the third method was employed in present study, viz. to speed up the stirrer to increase the mass transfer in gas phase. In this work, due to the gas stirrer and the liquid stirrer being mounted on the same shaft, the number of the fan turbine is increased to two and each turbine is mounted with six blades (39 mm × 14 mm × 2 mm) to increase the stirrer speed. Then, the gas-phase resistance can be reduced and neglected.

7.4.6. Kinetics of the Chemical Reaction of CO₂ Absorbed in Aqueous MEA Solution

To validate the experimental conditions of pseudo-first-order reaction for the aqueous MEA+CO₂ system, 3 and 5 kPa CO₂ partial pressure were used respectively for the absorption runs into 0.5 M and 3.6 M aqueous MEA solutions under low inert gas (the vapor of the solution). The results of Hatta number and infinite enhancement factor are listed in Table. 7.7. The solubility and diffusivity data of CO₂ in solutions were obtained from above work.

It can be seen that the experimental conditions of both 3 and 5 kPa CO₂ pressure for 0.5 and 3.6 M aqueous MEA solutions satisfied the criterion of pseudo-first-order reaction, equation (7.16). Thus, 3 kPa CO₂ partial pressure was used to ensure the reaction is in the range when pseudo-first-order reaction may be assumed.

The kinetics of the chemical reaction of CO₂ absorbed in aqueous MEA solution with wider concentration ranges, 0.5, 1, 2, 3.6, 5, 8, 10, and 12 M, were measured from 298.15 to

323.15 K by the stirred cell with batchwise operation with respect to both gas and liquid. The initial CO₂ partial pressures were set to 4 kPa in the measurements. The results are tabulated in Table 7.8. The k_2 values determined are in agreement with most literature values. The Arrhenius relation of the experimental data is plotted in Figure 7.9, and the equation (7.48) was obtained by regression of the experimental data.

$$k_2 = 4.14 \times 10^{11} \exp\left(\frac{-5399}{T}\right) \quad (7.48)$$

Table 7.7 Typical values of Ha and estimated infinite enhancement factor in this work

T (K)	P_{CO_2} (Pa)	C_{MEA} (mol dm ⁻³)	$D_{\text{MEA,L}}$ (10 ⁻⁹ m ² s ⁻¹)	$D_{\text{CO}_2,L}$ (10 ⁻⁹ m ² s ⁻¹)	H_{CO_2} (Pa m ³ mol ⁻¹)	k_L (10 ⁻⁵ m s ⁻¹)	k_2 (dm ³ mol ⁻¹ s ⁻¹)	Ha	E^∞
298.15	3000	0.5	1.50	1.83	2940	2.30	3371	76	445
298.15	3000	3.6	1.27	1.50	3042	1.70	6527	349	3360
298.15	5000	3.6	1.27	1.50	3042	1.70	6527	349	2016
313.15	5000	3.6	1.80	2.13	4276	2.27	17135	505	2831

This result is very close to the values derived by Versteeg et al.,² as shown in equation (7.1). It can be obtained from the equation (7.48) that the reaction activation energy (E_a) of aqueous MEA + CO₂ is 44.89 kJ mol⁻¹ and the pre-exponential factor value is high, 4.14×10^{11} , implying that the reaction of aqueous MEA solution with CO₂ is in the fast reaction regime.

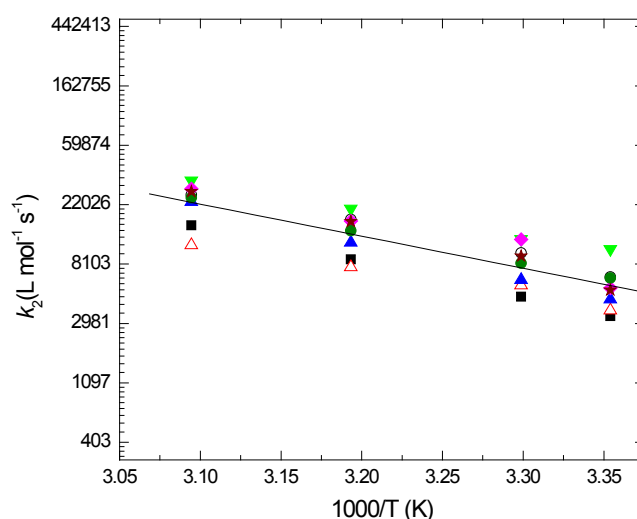


Figure 7.9 Arrhenius plot for k_2 of the aqueous MEA + CO₂:
 ■, 0.5 M; △, 1 M; ▲, 2 M; ○, 3.6 M; ▼, 5 M; ◆, 8 M; ●, 10 M; ★, 12 M;
 The solid line was calculated by equation (7.48)

Table 7.8 the k_2 of aq. MEA+CO₂ at various temperatures and concentrations

T (K)	C_{MEA} (mol L ⁻¹)	D_{CO_2} (10 ⁻⁹ m ² s ⁻¹)	H_{CO_2} (kPa m ³ kmol ⁻¹)	Slope (s ⁻¹)	$k_1 E$ (10 ⁻³ m s ⁻¹)	k_{ps} (s ⁻¹)	k_2 (L mol ⁻¹ s ⁻¹)
298.15	0.5	1.83	2940	0.01214	1.76	1686	3372
303.15	0.5	2.07	3354	0.01355	2.20	2337	4674
313.15	0.5	2.58	4123	0.01741	3.36	4383	8766
323.15	0.5	3.23	5044	0.0219	5.01	7786	15572
298.15	1	1.81	2938	0.01796	2.60	3725	3725
303.15	1	2.04	3358	0.02095	3.40	5682	5682
313.15	1	2.56	4126	0.02300	4.44	7721	7721
323.15	1	3.16	5035	0.02600	5.94	11178	11178
298.15	2	1.70	2959	0.02683	3.90	8977	4489
303.15	2	1.91	3391	0.02969	4.87	12429	6215
313.15	2	2.4	4161	0.03841	7.48	23360	11680
323.15	2	2.97	5052	0.05106	11.70	46177	23089
298.15	3.6	1.50	3042	0.03966	5.93	23496	6527
303.15	3.6	1.69	3498	0.04552	7.70	35137	9760
313.15	3.6	2.13	4276	0.05722	11.50	61688	17136
323.15	3.6	2.65	5149	0.06737	15.70	93589	25997
298.15	5	1.26	3170	0.05197	8.10	52157	10431
303.15	5	1.47	3675	0.05355	9.52	61706	12341
313.15	5	1.92	4375	0.06851	14.00	102700	20540
323.15	5	2.38	5242	0.08339	19.80	165476	33095
298.15	8	0.93	3249	0.03972	6.35	43361	5420
303.15	8	1.08	3846	0.05537	10.30	98345	12293
313.15	8	1.35	4465	0.06432	13.40	134094	16762
323.15	8	1.73	5314	0.08276	20.00	230424	28803
298.15	10	0.70	3341	0.04075	6.70	64117	6412
303.15	10	0.79	3838	0.0434	8.06	82257	8226
313.15	10	1.02	4541	0.05661	12.00	142199	14220
323.15	10	1.28	5285	0.07426	17.80	248016	24802
298.15	12	0.48	3032	0.03676	5.48	62666	5222
303.15	12	0.54	3552	0.04513	7.75	111453	9288
313.15	12	0.71	4245	0.05973	11.90	198742	16562
323.15	12	0.87	4913	0.07597	16.90	330027	27502

Figure 7.10 compares the calculated and measured k_{ps} for each experimental condition with aqueous MEA over the temperature range from 298.15 to 323.15 K. The absolute average deviation (AAD) is 30 %. This may be attributed to the uncertainties in the physical properties (solubility and diffusivity) used and the assumption of negligible gas-phase resistance beyond what has been accounted for.

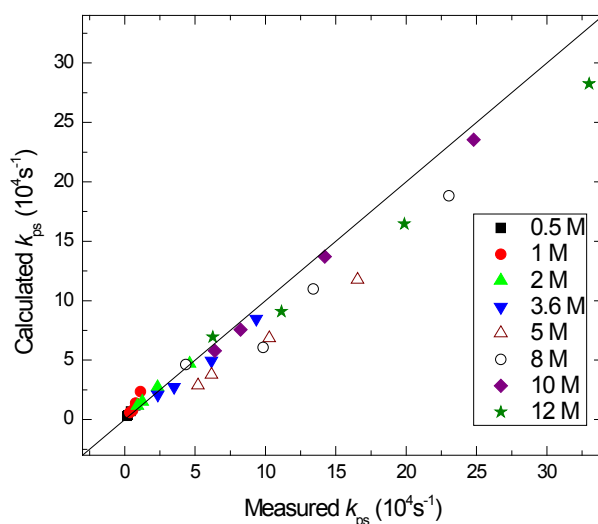


Figure 7.10 Comparisons the k_{ps} of aqueous MEA+ CO₂ between measured and predicted by equations (7.48) and (7.35): ■, 0.5 M; ●, 1 M; ▲, 2 M; ▼, 3.6 M; △, 5 M; ○, 8 M; ◆, 10 M; ★, 12 M;

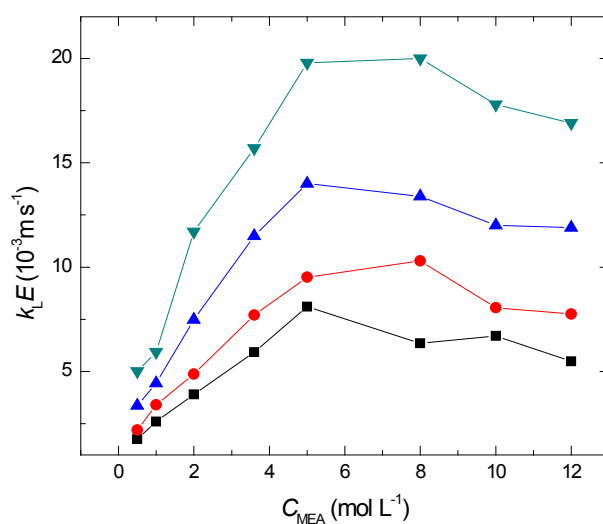


Figure 7.11 Mass transfer in liquid phase as a function of the molarity of MEA: ■, 298.15 K; ●, 303 K; ▲, 313.15 K; ▼, 323.15 K.

Figure 7.11 shows that the enhanced mass transfer coefficient in the liquid phase, $k_L E$, varies with the concentration of the MEA solution. It manifests that the CO₂ absorption rate increases with increasing MEA concentration, and reaches a maximum when the MEA molarity is in the range of 5 – 8 M, and then decreases softly with the a further increase of the MEA concentration. This is probably because the viscosity of the solution becomes higher when the concentration of the solution is higher than 8 M, and this leads to the stirring being insufficient to keep the mass transfer coefficient k_L from decreasing. Increased viscosity will correlate to decreased diffusivity of CO₂ and other liquid species in the solution. When the concentration of MEA is higher than 8 M, the negative effect of increased viscosity on the mass transfer rate outweighs the positive effect of the increased MEA concentration. This effect is more a property of the stirred cell than the gas–liquid system. The absorption process changes to a type of mass transfer control from a type of reaction control. An exploratory run at 100 rpm showed a higher mass transfer rate with no turbulence observed when the liquid was viscous. This was not pursued further even if no rippling was observed because there were smooth waves created on the liquid surface.

In the industrial absorption process, many factors affect the efficiency of the CO₂ absorption in aqueous MEA solution, the issues of reaction kinetics, degradation of chemicals, corrosion properties, liquid transportation, and the reaction heat emission should be considered comprehensively. The results of chemical kinetics in this study imply that the overall absorption rate approaches the maximum in the stirred cell when the MEA molarity is in the range of 5 – 8 M. With respect to conventional packed column, due to the transport force is gravity and the spaces in the packs are limited, when increasing the MEA molarity further, the viscosity could be too high to transport and lead to the difficulty of the reaction heat emission, then many problems become significant such as degradation, corrosion and so on. From the point of kinetics, the concentrated aqueous MEA solution concentration around 8 M is suggested to the CO₂ capture process of conventional absorption tower for reducing energy consumption and improving the efficiency of the CO₂ absorption.

7.5. Conclusions

The absorption of a gas in a liquid was determined with a stirred cell from the fall in pressure and the liquid-side mass transfer coefficient and the reaction rate constant were determined by two data treatment methods, viz. “differential” and “integral” methods. The results indicate that the differential method is better than the integral method when the absorption rate is high because the latter is very sensitive to the start pressure, but the integral

method is more stable when the absorption rate is low due to the differential method being too sensitive to lead to the dispersion of the plot.

The gas-phase resistance was investigated to avoid the effect of the gas-phase resistance on the measurement of the reaction rate constant. The result shows that the gas-phase resistance cannot be neglected if the resistance cannot be ignored. It is found that very low inert gas pressures of N₂ and solution vapor was needed. The stirrer was sped up to reduce the gas-phase resistance which is a good and simple method to reduce the gas phase resistance.

The liquid-side mass transfer coefficient without chemical reaction in the stirred cell reactor was determined via the pressure drop method based on the absorption equation (7.27). The well-known equation with respect to the Sherwood (*Sh*) number to the Reynolds (*Re*) and Schmidt (*Sc*) numbers was obtained by experiment and the exponents on *Re* and *Sc* are 0.84 and 0.5, respectively.

The kinetics of the reaction of carbon dioxide with aqueous MEA solutions over a wide concentration range from 0.5 to 12 M at a temperature range from 298.15 to 323.15 K were studied using a stirred cell absorber with a plane gas–liquid interface. Low CO₂ partial pressure was employed to satisfy the criterion for pseudo-first-order reaction. The results showed that the investigated reactions belong to the pseudo-first-order fast reaction regime systems, and the reaction rate constant of MEA with CO₂ at 298.15 K agrees with literature. The reaction activation energy (*E_a*) of aqueous MEA + CO₂ is 44.89 kJ mol⁻¹, and the pre-exponential factor value is 4.14×10¹¹. The enhanced mass transfer coefficient in the liquid phase, *k_LE*, increases with the concentration of MEA solutions but decreases when the molarity of MEA becomes higher than 8 M. The molarity of the concentrated aqueous MEA solution, approximately 8 M, is suggested to the CO₂ capture process of conventional absorption tower for reducing energy consumption and improving the efficiency of the CO₂ absorption.

Nomenclature

Abbreviations

B = base assisting in zwitterion deprotonation

RNH₂ = monoethanolamine (MEA) in this chapter

Parameters and Variables

A = the area of the interface of the gas and the liquid, (m²)

AAD = absolute average deviation between calculated values and experimental data, (%)

AMD = absolute maximum deviation between calculated values and experimental data, (%)

- b = slope defined in equations (7.33) and (7.34), (s^{-1})
 c, C = molar concentration of a substance in a solution, ($kmol\ m^{-3}$, $mol\ L^{-1}$)
 C_A^* = equilibrium molarity of gas A in the solution, ($kmol\ m^{-3}$, $mol\ L^{-1}$)
 d = diameter of the stirrer, (m)
 D = diffusivity ($m^2\ s^{-1}$)
 D_A = diffusivity of gas A in a liquid, ($m^2\ s^{-1}$)
 E_a = activation energy ($kJ\ kmol^{-1}$)
 E = enhancement factor due to the existence of chemical reaction
 E^∞ = infinite enhancement factor
 H = Henry's constant, ($kPa\ m^3\ kmol^{-1}$)
 H_A = Henry's constant of gas A in a liquid, ($kPa\ m^3\ kmol^{-1}$)
 Ha = Hatta number
 k = chemical reaction rate constant, mass transfer coefficient
 k_{-1} = reverse reaction rate constant, (s^{-1})
 k_1 = forward reaction rate constant with respect to C_{CO_2} , (s^{-1})
 k_2 = forward reaction rate constant with respect to C_{MEA} and C_{CO_2} , ($m^3\ kmol^{-1}\ s^{-1}$)
 k_b = reaction rate constant combined all the bases ($m^3\ kmol^{-1}\ s^{-1}$)
 k_G = gas-side mass transfer coefficient ($m\ s^{-1}$)
 k_{H_2O} = reaction rate constant contributed by water ($m^3\ kmol^{-1}\ s^{-1}$)
 k_L = liquid-side mass transfer coefficient ($m\ s^{-1}$)
 k_{obs} = overall chemical reaction rate constant with respect to all bases in the solution, (s^{-1})
 K_G = overall mass transfer coefficient including gas-side and liquid-side, gas phase units, ($m\ s^{-1}$)
 k_{OH^-} = reaction rate constant contributed by hydroxyl ion, ($m^3\ kmol^{-1}\ s^{-1}$)
 k_{ps} = reaction rate constant of the pseudo-first-order reaction, (s^{-1})
 k' = reaction rate constant combined water, ($m^3\ kmol^{-1}\ s^{-1}$)
 m = chemical reaction order
 n = chemical reaction order
 n_A = mole amount of gas A, (mol)
 N_A = overall mass transfer flux of gas A, ($mol\ s^{-1}$)
 P = gas pressure, (kPa)
 P_A = partial pressure of gas A, (kPa)
 $P_{H_2O}^v$ = vapor pressure of pure water, (kPa)
 P_{MEA}^v = vapor pressure of pure MEA, (kPa)
 P_{total} = total pressure (kPa)
 r = reaction rate ($m^3\ kmol^{-1}\ s^{-1}$)

R = universal gas constant, =8.314, (Pa m³ K⁻¹ mol⁻¹)

RD = relative deviation, (%)

Re =Reynolds number

t = contact time, (s)

T = temperature, (K)

Sc =Schmidt number

Sh =Sherwood number

V_G = volume of gas phase, (m³)

V_L = volume of liquid phase, (m³)

x_{H_2O} = mole fraction of water

x_{MEA} = mole fraction of MEA

Subscript

0 = initial

A = gas A

am = amine

B = base assisting in zwitterion deprotonation

z = zwitterion

N₂O = nitrous oxide

CO₂ = carbon dioxide

G = gas phase

i = the i -th species of the reactants

j = the j -th species of the reactants

L = liquid phase

MEA = monoethanolamine

N₂ = nitrogen

total = total gas in the cell

H₂O= water

Superscript

cal = calculation

i = interface of the gas-liquid

v = vapor

e = equilibrium

exp = experiment

Greek Symbols

δ_L = liquid–film thickness (m)

μ = viscosity of the solution, (mPa s)

References

1. Kohl, A. L.; Nielsen; R. B. Gas Purification. Gulf Publishing Company, Houston, 5th edition, **1997**.
2. Versteeg, G. F.; van Dijck, L. A. J.; van Swaaij, W. P. M. on the Kinetics between CO₂ and Alkanolamines Both in Aqueous and Non–Aqueous Solutions. An Overview. *Chem. Eng. Commun.* **1996**, *144*, 113–158.
3. Vaidya, P. D.; Kenig, E. Y. CO₂–Alkanolamine Reaction Kinetics: A Review of Recent Studies. *Chem. Eng. Technol.* **2007**, *30*, 1467–1474.
4. Clarke, J. K. A. Kinetics of Absorption of Carbon Dioxide in Monoethanolamine Solutions at Short Contact Times. *Ind. Eng. Chem. Fundam.* **1964**, *3*, 239–245.
5. Little, R. J.; Versteeg, G. F.; and Van Swaaij, W. P. M. Kinetics of CO₂ with Primary and Secondary Amines in Aqueous Solutions–II. Influence of Temperature on Zwitterion Formation and Deprotonation Rates. *Chem. Eng. Sci.* **1992**, *47*, 2037–2045.
6. Aboudheir, A.; Tontiwachwuthikula, P.; Chakrab, A. Kinetics of the Reactive Absorption of Carbon Dioxide in High CO₂–Loaded Concentrated Aqueous Monoethanolamine Solutions. *Chem. Eng. Sci.* **2003**, *58*, 5195 – 5210.
7. Laddha SS, Danckwerts PV. Reaction of CO₂ with Ethanolamines: Kinetics from Gas-Absorption. *Chem Eng Sci* **1981**, *36*, 479–482.
8. Versteeg GF, van Swaaij WPM. On the Kinetics between CO₂ and Alkanolamines Both in Aqueous and Non-Aqueous Solutions — I. Primary and Secondary Amines. *Chem Eng Sci* **1988**, *43*, 573–585.
9. Blauwhoff, P. M., Versteeg, G. F., van Swaaij, W. P. M. A Study on the Reaction between CO₂ and Alkanolamines in Aqueous Solutions. *Chem. Eng. Sci.* **1984**, *39*, 207–225.
10. Rinker EB, Ashour SS, Sandall OC. Absorption of Carbon Dioxide into Aqueous Blends of Diethanolamine and Methyl-diethanolamine. *Ind Eng Chem Res* **2000**, *39*, 4346–4356.
11. Vaidya, P. D.; Konduru, P.; Vaidyanathan, M.; Kenig, E. Y. Kinetics of Carbon Dioxide Removal by Aqueous Alkaline Amino Acid Salts. *Ind. Eng. Chem. Res.* **2010**, *49*, 11067–11072.
12. Kucka, L.; Richter, J.; Kenig, E.Y.; Górak, A. Determination of Gas/Liquid Reaction Kinetics with a Stirred Cell Reactor. *Sepa Purif Tech*, **2003**, *31*, 163–175.
13. Thomas, W. J. The absorption of Carbon Dioxide in Aqueous Monoethanolamine in a Laminar Jet. *AIChE J.* **1996**, *12*, 1051–1057.
14. Caplow, M. Kinetics of Carbamate Formation and Breakdown. *J. Am. Chem. Soc.* **1968**, *90*, 6795–6803.
15. Danckwerts, P. V. The Reaction of CO₂ with Ethanolamines. *Chem. Eng. Sci.* **1979**, *34*, 443–446.
16. Crooks, J. E.; Donnellan, J. P. Kinetics and Mechanism of the Reaction between Carbon Dioxide and Amines in Aqueous Solution. *J. Chem. Soc., Perkin Trans.* **1989**, *4*, 331–333.

17. Da Silva, E. F.; Svendsen, H. F. Ab Initio Study of the Reaction of Carbamate Formation from CO₂ and Alkanolamines. *Ind. Eng. Chem. Res.* **2004**, *43*, 3413–3418.
18. Danckwerts, P. V. Gas–Liquid Reactions; McGraw–Hill: New York, **1970**.
19. Hikita, H.; Asai S., Gas Absorption with (m, n) th Order Irreversible Chemical Reaction, *Int. Chem. Eng.* **1964**, *4*, 332–340.
20. Westerterp, K. R.; van Swaaij, W. P. M.; Beenackers, A. A. C. M. Chemical Reactor Design and Operation. John Wiley & Sons, Chichester, New York, Brisbane, Toronto, Singapore, 2nd edition, **1987**.
21. Higbie, R. The Rate of Absorption of a Pure Gas into a Still Liquid during Short Periods of Exposure. *Trans. Am. Inst. Chem. Eng.* **1935**, *35*, 36–60.
22. Cornelisse, R.; Beenackers, A. A. C. M.; van Beckum, F. P. H.; van Swaaij W. P. M. Numerical Calculation of Simultaneous Mass Transfer of Two Gases Accompanied by Complex Reversible Reactions. *Chem. Eng. Sci.* **1980**, *35*, 1245–1260.
23. Jou, F. Y.; Mather, A. E.; Otto, F. D. The Solubility of CO₂ in a 30 Mass Percent Monoethanolamine Solution. *Can. J. Chem. Eng.* **1995**, *73*, 140–147.
24. Ying, J.R.; Eimer, A. D.; Yi, W.J. Measurements and Correlation of Physical Solubility of Carbon Dioxide in (Monoethanolamine + Water) by a Modified Technique. *Ind. Eng. Chem. Res.* **2012**, *51*, 6958–6966.
25. Ying, J.R.; Eimer, A. D. Measurements and Correlations of Diffusivities of Nitrous Oxide and Carbon Dioxide in Monoethanolamine + Water by Laminar Liquid Jet. *Ind. Eng. Chem. Res.* **2012**, Accepted
26. Littel, R. J.; Versteeg, G. F.; van Swaaij, W. P. M. Physical Absorption into Non–Aqueous Solutions in A Stirred Cell Reactor. *Chem. Eng. Sci.* **1991**, *46*, 3308–3313.
27. Versteeg, G. F.; Blauwhoff, P. M. M.; van Swaaij, W. P. M. The Effect of Diffusivity on Gas–Liquid Mass Transfer in Stirred Vessels. Experiments at Atmospheric and Elevated Pressures. *Chem. Eng. Sci.* **1987**, *42*, 1103–1119.
28. Critchfield J. PhD Dissertation, the University of Texas, Austin, USA, **1988**.
29. Hikita, H.; Asai, S.; Ishikawa, H.; Saito, Y. Kinetics of Absorption of Chlorine in Aqueous Acidic Solutions of Ferrous Chloride. *Chem. Eng. Sci.* **1975**, *30*, 607–616.
30. Haimour, N.; Bidarian, A.; Sandall, O. C. Kinetics of the Reaction Between Carbon Dioxide and Methyl-diethanolamine, *Chem. Eng. Sci.* **1987**, *42*, 1393–1398.
31. Hamborg, E. S.; Kersten, S. A. R.; Versteeg, G. F. Absorption and Desorption Mass Transfer Rates in Non-Reactive Systems. *Chem. Eng. J.*, **2010**, *161*, 191–195.
32. Gilliland, E. R.; Sherwood, T. K. Diffusion of Vapors into Air Streams. *Ind. and Eng. Chem.* **1934**, *26*, 516–523.
33. Han, J. Y.; Jin, J.; Eimer, D. A.; Melaaen, C. C. Density of Water (1) + Monoethanolamine (2) + CO₂ (3) from (298.15 to 413.15) K and Surface Tension of Water (1) + Monoethanolamine (2) from (303.15 to 333.15) K. *J. Chem. Eng. Data* **2012**, *57*, 1095–1103
34. Cussler, E. L. Diffusion Mass Transfer in Fluid Systems, 3rd Edition, Cambridge University Press, **2009**.
35. Versteeg, G. F.; van Swaaij, W. P. M. Solubility and Diffusivity of Acid Gases (CO₂, N₂O) in Aqueous Alkanolamine Solutions. *J. Chem. Eng. Data* **1988**, *33*, 29–34.

Chapter 8

8. Summary and Suggestion for Future Work

1. This thesis proposes the concentrated aqueous MEA solution as absorbent to decrease the mass of the transport liquid to reduce the energy consumption and improve the CO₂ absorption efficiency in the CO₂ capture process. The physical properties of the aqueous MEA solution were measured and correlated. The chemical reaction kinetics of CO₂ with the aqueous MEA solution over a wide concentration range was explored. All the data and the correlated equations of the properties measured in this work can be used to perform engineering calculations and are important for dimensioning of pipes, pumps and heat exchangers. The use of such data and mass transfer kinetics research are typically for dimensioning column diameters and packing heights.
2. A novel physical solubility apparatus was designed to measure the solubility of gas in to liquid, and a mathematical model was developed to treat the experimental data. The results of the solubility measurements of N₂O and CO₂ in water indicate that the novel technique is feasible and reliable. The advantages of the new method include easy operation, lower mercury inventory, higher sensitivity and greater accuracy.
3. A new procedure and calculation model was proposed make the new physical solubility apparatus work. This procedure and model take almost all factors into account, and found that the fluctuation of the room pressure is one of the main uncertainty sources. This uncertainty source has always been neglected by other researchers.
4. The physical solubilities of CO₂ in aqueous MEA solutions over the full range of concentrations were measured using this novel technique over the temperature range from 298.15 to 323.15 K. A semiempirical model of the excess Henry's constant proposed by Wang et al. was used to correlate the solubilities of N₂O and CO₂ in MEA solutions, and the simulated results were in agreement with experimental data over the full MEA concentration range and a wide temperature range. The solubilities of N₂O in aqueous NaCl solutions and (NaCl or CuCl₂ +aq. 5 M MEA) solutions were measured

at 313.15 K as well. The results show that the solubilities of N_2O in the solution decrease with the increasing of salt concentration, namely “salting-out”. The Sechenov constant K was used to describe the “salting-out” effect. K values relative to NaCl in water and aqueous 5 M MEA solution are very close, but The K value relative to $CuCl_2$ in aqueous 5 M MEA solution is much higher than that of NaCl.

5. Viscosities of the aqueous MEA solutions over full concentration range were measured from 298.15 to 353.15 K. The results are in good agreement with literature and extend the values to a larger concentration and temperature range. The diffusivities of the aqueous MEA solutions were also measured over a wide concentration range by a laminar liquid jet absorber.
6. A linear additive principle was employed to explain the relationship of the physical properties as functions of concentration of the aqueous MEA solutions. The solubility capacity for N_2O and CO_2 in MEA+ H_2O showed negative deviation behavior, and the viscosity versus mole fraction of MEA shows both positive and negative deviation behavior, and the critical mole fraction of MEA is 0.2.
7. The liquid-side mass transfer coefficient without chemical reaction in the stirred cell reactor was determined via the pressure drop method. The well-known equation with respect to the Sherwood (Sh) number to the Reynolds (Re) and Schmidt (Sc) numbers was obtained by experiment and the exponents on Re and Sc is 0.84 and 0.5, respectively.
8. The chemical reaction kinetics of CO_2 in aqueous MEA solutions was measured over the ranges from 0.5 to 12 M by a stirred cell absorber with batchwise operation for both gas and liquid. As same as for the dilute solution, the reaction of concentrated aqueous MEA solution with CO_2 is also 1st order with respect to MEA and the reaction is in the fast reaction regime. The differential method and integral method were compared using the same experimental data to determine the reaction kinetics, and it was found that the differential method is better than the integral method for treating the data of fast chemical reaction because the latter is very sensitive to the initial pressure in the cell. The reaction activation energy (E_a) of aqueous MEA + CO_2 is $44.89 \text{ kJ mol}^{-1}$ is not high and the pre-exponential factor value is 4.14×10^{11} . The enhanced mass transfer coefficient in the liquid phase, $k_L E$, increases with the concentration of MEA solutions but decreases when the molarity of MEA is higher than 8 M. The molarity of the concentrated aqueous MEA solution, 5 – 8 M, is

suggested as best for the CO₂ capture process for reducing energy consumption and improving the efficiency of the CO₂ absorption.

In order to realize the concentrated aqueous MEA solution as absorbent in industry, the research of equilibrium solubility of CO₂ into concentrated aqueous MEA solution and the study of degradation of the concentrated aqueous MEA solution are progressing simultaneously in our research group. The suggestions for this future work are as follows:

1. The present work focus on unloaded MEA solutions is the basic science research. Since the CO₂-loaded MEA solutions are what really matters for practical applications, the physical and chemical properties of the CO₂-loaded concentrated aqueous MEA solutions are more important for industrial research. A given suggestion is that the future work should focus on the CO₂-loaded MEA solutions, the properties and gas absorption of the system can be measured and discussed by the same way mentioned in this thesis.
2. Like the gas absorption process, desorption is also an important process in CO₂ capture. The gas absorption and desorption from the CO₂-loaded aqueous MEA solutions should be performed in the future work as well. The study of gas desorption should include desorption with/without chemical reaction. The stirred cell or laminar liquid jet can be employed in these studies under a suitable pressure.
3. If we say the idea is the “brain” for the scientific research, then the equipment and apparatus are the “hands”. The solubility cell is developed in this work and can be employed for the next-step work. But the stirred cell and liquid laminar jet in next work should be modified, especially the construction of the temperature control parts.

For example, the absorption cell of the liquid laminar jet can be smaller, due to the smaller the gas volume, the more sensitive and accurate the measurement; the nozzle or receiver should be adjustable and then the operation will be easier, because it is vitally important of the liquid jet can be straight down into the receiver from the nozzle. With respect to the modified method of temperature control, the main idea is to immerse all the gas and liquid pipes in to the same water bath as absorption cell. To achieve the target, all the gas and liquid pipes are immersed the same water bath and pass through the water transport hose to the absorption cell. The modified constructions suggested here are exhibited in the appendix A6 (laminar liquid jet absorber) and appendix A9 (stirred cell absorber) of this thesis.

4. The issue of heat transfer should be taken into account and be investigated when the concentrated aqueous MEA solution is used as an absorbent in the process of CO₂ capture. The absorption process will produce more heat because of the higher viscosity of the absorbent and the faster reaction rate between CO₂ and concentrated aqueous MEA solution.

Appendix

A1. Raw Experimental Data of Solubility Measurement

Table A.1 The raw experimental data of physical solubility measurements of N₂O in aq. MEA solutions

C_{MEA} mol L ⁻¹	T K	time hr	$P_{\text{room}}^{\text{ini}}$ mbar	$P_{\text{room}}^{\text{end}}$ mbar	P_{MEA} mbar	$P_{\text{H}_2\text{O}}$ mbar	P_{A} mbar	V_{L} mL	$V_{\text{A}}^{\text{exp}}$ mL	$V_{\text{G}}^{\text{ini}}$ mL	V_{A} mL	$H_{\text{A},i}$ Pa m ³ mol ⁻¹	H_{A}
0	298.15	14.0	1019	1025.3	0.0	31.7	994	15.01	9.763	116.99	9.04	3987	4022
0	298.15	3.0	1016	1017	0.0	31.7	985	15.17	9.080	116.83	8.97	4064	
0	298.15	5.0	1009	1010	0.0	31.7	978	15.11	9.150	116.89	9.03	4016	
3	298.15	3.0	1022.2	1019.7	0.0	29.8	990	15.08	8.240	116.92	8.53	4256	4221
3	298.15	4.0	1020.2	1016.4	0.0	29.8	987	15.01	8.170	116.99	8.61	4196	
3	298.15	19.0	1024.5	1022	0.0	29.8	992	14.97	8.270	117.03	8.56	4211	
5	298.15	20.0	1019.4	1011	0.1	28.1	983	14.70	7.210	117.30	8.18	4328	4321
5	298.15	6.0	1011.7	1016.9	0.1	28.1	989	15.27	9.130	116.73	8.53	4313	
8	298.15	7.0	1007	1007	0.1	24.9	982	14.59	7.960	117.41	7.96	4430	4428
8	298.15	8.0	1001.1	998.2	0.1	24.9	973	15.19	7.954	116.81	8.29	4426	
12	298.15	15.0	1006.1	1009.6	0.2	18.2	991	14.68	9.061	117.32	8.65	4128	4132
12	298.15	10.0	987.2	987.2	0.2	18.2	969	14.93	8.780	117.07	8.78	4136	
15	298.15	16.0	1010.6	998.3	0.4	8.8	989	14.57	8.789	117.43	10.24	3496	3515
15	298.15	20.0	1010.8	1008	0.4	8.8	999	14.57	9.799	117.43	10.13	3534	
16.4	298.15	20.0	1038.5	1041.7	0.5	0.0	1041	14.96	14.457	117.04	14.10	2629	2655
16.4	298.15	18.0	999.7	999.7	0.5	0.0	999	15.07	14.060	116.93	14.06	2655	
16.4	298.15	15.0	1000.1	998.1	0.5	0.0	998	14.76	13.402	117.24	13.64	2682	
0	303.15	10.0	1019	1025.3	0.0	42.5	983	15.01	8.926	116.99	8.21	4418	4422
0	303.15	5.0	1002.1	1004.3	0.0	42.5	962	15.12	8.450	116.88	8.19	4454	
0	303.15	4.0	1005.4	1004.3	0.0	42.5	962	14.98	8.101	117.02	8.23	4394	
3	303.15	17.0	1003.6	1019.6	0.1	39.9	980	14.93	9.514	117.07	7.68	4710	4692
3	303.15	20.0	999.7	1000.4	0.1	39.9	960	14.90	7.760	117.10	7.68	4696	
3	303.15	15.0	1001.6	1009.1	0.1	39.9	969	14.99	8.641	117.01	7.77	4669	
5	303.15	22.0	1020.4	1005.8	0.1	37.7	968	15.03	5.860	116.97	7.56	4824	4835
5	303.15	16.0	1010.1	1003.9	0.1	37.7	966	15.11	6.841	116.89	7.56	4846	
8	303.15	22.0	1000.7	998.9	0.2	33.4	965	15.10	7.100	116.90	7.31	5031	5060
8	303.15	16.0	1007.1	999.9	0.2	33.4	966	15.12	6.395	116.88	7.24	5089	
12	303.15	26.0	1015.9	1023.7	0.3	24.4	999	15.06	8.760	116.94	7.87	4707	4674
12	303.15	21.0	1015.9	1025.8	0.3	24.4	1001	15.16	9.162	116.84	8.03	4641	

Table continue...

C_{MEA} mol L ⁻¹	T K	time hr	$P_{\text{room}}^{\text{ini}}$ mbar	$P_{\text{room}}^{\text{end}}$ mbar	P_{MEA} mbar	$P_{\text{H}_2\text{O}}$ mbar	P_{A} mbar	V_{L} mL	$V_{\text{A}}^{\text{exp}}$ mL	$V_{\text{G}}^{\text{ini}}$ mL	V_{A} mL	$H_{\text{A},i}$ Pa m ³ mol ⁻¹	H_{A}
15	303.15	18.0	1022.8	1021.5	0.6	11.8	1009	14.98	9.595	117.02	9.74	3828	3797
15	303.15	22.0	1021.1	1001.5	0.6	11.8	989	15.08	7.679	116.92	9.97	3766	
16.4	303.15	21.0	1033.6	1024.4	0.8	0.0	1024	14.89	11.936	117.11	12.99	2887	2867
16.4	303.15	20.0	1023.1	1025.6	0.8	0.0	1025	15.02	13.574	116.98	13.29	2847	
0	313.15	5.0	1019	1025.3	0.0	73.8	952	15.01	7.120	116.99	6.40	5666	5660
0	313.15	8.0	1011.1	1012.1	0.0	73.8	938	14.98	6.545	117.02	6.43	5624	
0	313.15	16.0	1012.9	1015.4	0.0	73.8	942	15.11	6.697	116.89	6.41	5692	
3	313.15	15.0	1023.1	1018.6	0.1	69.3	949	14.87	5.710	117.13	6.23	5793	5831
3	313.15	5.0	1025.6	1023.5	0.1	69.3	954	15.16	6.080	116.84	6.32	5822	
3	313.15	20.0	1019.2	1015.4	0.2	65.5	950	14.98	5.768	117.02	6.21	5878	
5	313.15	3.0	1017.8	1016.5	0.2	65.5	951	15.07	6.001	116.93	6.15	5967	5991
5	313.15	8.0	1024.4	1023.1	0.2	65.5	957	15.11	5.972	116.89	6.12	6015	
8	313.15	4.0	1013.2	1013.1	0.3	58.1	955	15.15	6.042	116.85	6.05	6140	6115
8	313.15	8.0	1011.2	1011.6	0.3	58.1	953	15.12	6.137	116.88	6.09	6090	
12	313.15	23.0	1019	1028.7	0.7	42.5	986	15.00	7.550	117.00	6.45	5804	5814
12	313.15	8.0	1013.7	1018.2	0.7	42.5	975	15.23	7.013	116.77	6.50	5844	
12	313.15	20.0	1019	1028.7	0.7	42.5	986	14.99	7.556	117.01	6.45	5794	
15	313.15	16.0	1015.1	1013	1.2	20.5	991	15.09	8.461	116.91	8.70	4418	4413
15	313.15	8.0	1017.8	1017.1	1.2	20.5	995	15.03	8.607	116.97	8.69	4408	
16.4	313.15	20.0	1025.2	1014.9	1.6	0.0	1013	15.06	10.538	116.94	11.72	3339	3308
16.4	313.15	16.0	1022.2	1015.4	1.6	0.0	1014	15.01	11.122	116.99	11.91	3277	
0	323.15	3.0	1011.2	1012.1	0.0	123.4	889	14.99	5.136	117.01	5.03	7028	7070
0	323.15	5.0	1012.3	1014.3	0.0	123.4	891	15.01	5.232	116.99	5.00	7082	
0	323.15	6.0	1023	1025.3	0.0	123.4	902	15.11	5.291	116.89	5.03	7101	
3	323.15	3.0	1028.4	1028	0.2	115.9	912	15.32	5.032	116.68	5.08	7191	7155
3	323.15	5.0	1023.4	1024.3	0.2	115.9	908	15.12	5.162	116.88	5.06	7119	
5	323.15	5.0	1031.2	1029.2	0.4	109.5	919	15.17	4.761	116.83	4.99	7299	7311
5	323.15	4.0	1023.4	1026.1	0.4	109.5	916	14.98	5.215	117.02	4.91	7324	
8	323.15	15.0	1028.9	1029.6	0.7	97.2	932	15.14	5.063	116.86	4.98	7386	7412
8	323.15	10.0	1025.4	1028.3	0.7	97.2	930	15.02	5.239	116.98	4.91	7438	
12	323.15	16.0	1029.8	1031.7	1.4	71.1	959	15.28	5.798	116.72	5.58	6836	6853
12	323.15	10.0	1028.2	1027.6	1.4	71.1	955	14.78	5.304	117.22	5.37	6870	
15	323.15	22.0	1028.5	1029.7	2.5	34.3	993	15.42	8.110	116.58	7.97	5010	5034
15	323.15	15.0	1022.1	1024.5	2.5	34.3	988	15.12	8.016	116.88	7.74	5059	
16.4	323.15	24.0	1002.4	1015.8	3.4	0.0	1012	15.26	12.483	116.74	10.94	3734	3768
16.4	323.15	20.0	1003.5	1009.2	3.4	0.0	1006	15.22	11.379	116.78	10.72	3802	

A2. Raw Experimental Data of Diffusivity Measurement

Liquid: 0.5 M aq. MEA, Gas: N₂O, Temp.: 25 °C

No.	T-room	P-room	T	R _A	flow rate (<i>q</i>)	length (<i>l</i>)	C*	D _{A-exp.}
	°C	mbar	K	mol/s	m ³ /s	m	mol/m ³	m ² /s
0.5M-25-01	23.4	1024	298.15	3.742E-07	4.456E-07	1.871E-02	2.56E+01	1.61E-09
0.5M-25-02	23.4	1024	298.15	3.846E-07	4.456E-07	1.871E-02	2.56E+01	1.70E-09
0.5M-25-03	23.4	1024	298.15	3.882E-07	4.456E-07	1.871E-02	2.56E+01	1.73E-09
0.5M-25-04	23.4	1024	298.15	3.349E-07	3.383E-07	1.871E-02	2.56E+01	1.70E-09
0.5M-25-05	23.4	1024	298.15	3.349E-07	3.383E-07	1.871E-02	2.56E+01	1.70E-09
0.5M-25-06	23.4	1024	298.15	3.296E-07	3.383E-07	1.871E-02	2.56E+01	1.64E-09
Statistic					STD	4.463E-11	D _{N₂O}	1.68E-09

Liquid: 0.5 M aq. MEA, Gas: N₂O, Temp.: 30 °C

No.	T-room	P-room	T	R _A	flow rate (<i>q</i>)	length (<i>l</i>)	C*	D _{A-exp.}
	°C	mbar	K	mol/s	m ³ /s	m	mol/m ³	m ² /s
0.5M-30-01	22.8	1021	303.15	3.415E-07	4.197E-07	1.680E-02	2.31E+01	1.93E-09
0.5M-30-02	22.8	1021	303.15	3.401E-07	4.197E-07	1.680E-02	2.31E+01	1.91E-09
0.5M-30-03	22.8	1021	303.15	3.608E-07	3.823E-07	2.130E-02	2.31E+01	1.87E-09
0.5M-30-04	22.8	1021	303.15	3.640E-07	3.823E-07	2.130E-02	2.31E+01	1.90E-09
0.5M-30-05	22.8	1021	303.15	4.278E-07	5.118E-07	2.130E-02	2.31E+01	1.96E-09
0.5M-30-06	22.8	1021	303.15	4.322E-07	5.118E-07	2.130E-02	2.31E+01	2.00E-09
0.5M-30-07	22.8	1021	303.15	3.842E-07	4.082E-07	2.130E-02	2.31E+01	1.98E-09
Statistic					STD	4.731E-11	D _{N₂O}	1.94E-09

Liquid: 0.5 M aq. MEA, Gas: N₂O, Temp.: 40 °C

No.	T-room	P-room	T	R _A	flow rate (<i>q</i>)	length (<i>l</i>)	C*	D _{A-exp.}
	°C	mbar	K	mol/s	m ³ /s	m	mol/m ³	m ² /s
0.5M-40-01	23.1	1031	313.15	2.649E-07	3.181E-07	1.753E-02	1.83E+01	2.36E-09
0.5M-40-02	23.1	1031	313.15	2.666E-07	3.181E-07	1.753E-02	1.83E+01	2.39E-09
0.5M-40-03	23.1	1031	313.15	2.633E-07	3.181E-07	1.753E-02	1.83E+01	2.33E-09
0.5M-40-04	23.1	1031	313.15	2.948E-07	3.836E-07	1.753E-02	1.83E+01	2.42E-09
0.5M-40-05	23.1	1031	313.15	2.969E-07	3.836E-07	1.753E-02	1.83E+01	2.46E-09
0.5M-40-06	23.1	1031	313.15	2.990E-07	3.836E-07	1.753E-02	1.83E+01	2.49E-09
Statistics					STD	6.058E-11	D _{N₂O}	2.41E-09

Liquid: 0.5 M aq. MEA, Gas: N₂O, Temp.: 50 °C

No.	T-room	P-room	T	R _A	flow rate (<i>q</i>)	length (<i>l</i>)	C*	D _{A-exp.}
	°C	mbar	K	mol/s	m ³ /s	m	mol/m ³	m ² /s
0.5M-50-01	22.8	1022	323.15	2.680E-07	4.092E-07	1.753E-02	1.45E+01	2.96E-09
0.5M-50-02	22.8	1022	323.15	2.769E-07	4.092E-07	1.753E-02	1.45E+01	3.16E-09
0.5M-50-03	22.8	1022	323.15	2.751E-07	4.092E-07	1.753E-02	1.45E+01	3.12E-09
0.5M-50-04	22.8	1022	323.15	3.010E-07	5.040E-07	1.753E-02	1.45E+01	3.03E-09
0.5M-50-05	22.8	1022	323.15	2.925E-07	4.686E-07	1.753E-02	1.45E+01	3.08E-09
0.5M-50-06	22.8	1022	323.15	2.946E-07	4.686E-07	1.753E-02	1.45E+01	3.13E-09
Statistics					STD	7.303E-11	D _{N₂O}	3.08E-09

Liquid: 0.5 M aq. MEA, Gas: N₂O, Temp.: 60 °C

No.	T-room	P-room	T	R _A	flow rate (<i>q</i>)	length (<i>l</i>)	C*	D _{A-exp.}
	°C	mbar	K	mol/s	m ³ /s	m	mol/m ³	m ² /s
0.5M-60-01	23.2	1021	333.15	2.511E-07	4.478E-07	1.753E-02	1.16E+01	3.73E-09
0.5M-60-02	23.2	1021	333.15	2.527E-07	4.478E-07	1.753E-02	1.16E+01	3.78E-09
0.5M-60-03	23.2	1021	333.15	2.496E-07	4.478E-07	1.753E-02	1.16E+01	3.69E-09
0.5M-60-04	23.2	1021	333.15	2.277E-07	3.511E-07	1.753E-02	1.16E+01	3.91E-09
0.5M-60-05	23.2	1021	333.15	2.252E-07	3.511E-07	1.753E-02	1.16E+01	3.83E-09
0.5M-60-06	23.2	1021	333.15	2.204E-07	3.511E-07	1.753E-02	1.16E+01	3.67E-09
0.5M-60-07	23.2	1021	333.15	2.252E-07	3.511E-07	1.753E-02	1.16E+01	3.83E-09
Statistics					STD	8.741E-11	D _{N₂O}	3.78E-09

Liquid: 3 M aq. MEA, Gas: N₂O, Temp.: 25 °C

No.	T-room	P-room	T	R _A	flow rate (<i>q</i>)	length (<i>l</i>)	C*	D _{A-exp.}
	°C	mbar	K	mol/s	m ³ /s	m	mol/m ³	m ² /s
3M-25-01	22.5	1025	298.15	3.595E-07	5.495E-07	1.753E-02	2.43E+01	1.42E-09
3M-25-02	22.5	1025	298.15	3.534E-07	5.495E-07	1.753E-02	2.43E+01	1.37E-09
3M-25-03	22.5	1025	298.15	3.626E-07	5.495E-07	1.753E-02	2.43E+01	1.45E-09
3M-25-04	22.5	1025	298.15	3.022E-07	3.735E-07	1.753E-02	2.43E+01	1.48E-09
3M-25-05	22.5	1025	298.15	2.896E-07	3.735E-07	1.753E-02	2.43E+01	1.36E-09
3M-25-06	22.5	1025	298.15	2.937E-07	3.735E-07	1.753E-02	2.43E+01	1.40E-09
Statistics					STD	4.547E-11	D _{N₂O}	1.41E-09

Liquid: 3 M aq. MEA, Gas: N₂O, Temp.: 30 °C

No.	T-room	P-room	T	R _A	flow rate (<i>q</i>)	length (<i>l</i>)	C*	D _{A-exp.}
	°C	mbar	K	mol/s	m ³ /s	m	mol/m ³	m ² /s
3M-30-01	22.8	1024.9	303.15	3.442E-07	5.110E-07	1.753E-02	2.18E+01	1.73E-09
3M-30-02	22.8	1024.9	303.15	3.386E-07	5.110E-07	1.753E-02	2.18E+01	1.68E-09
3M-30-03	22.8	1024.9	303.15	3.359E-07	5.110E-07	1.753E-02	2.18E+01	1.65E-09
3M-30-04	22.8	1024.9	303.15	2.873E-07	3.987E-07	1.753E-02	2.18E+01	1.55E-09
3M-30-05	22.8	1024.9	303.15	2.893E-07	3.987E-07	1.753E-02	2.18E+01	1.57E-09
3M-30-06	22.8	1026	303.15	2.780E-07	3.870E-07	1.753E-02	2.19E+01	1.49E-09
3M-30-07	22.8	1026	303.15	2.856E-07	3.870E-07	1.753E-02	2.19E+01	1.57E-09
Statistics					STD	8.465E-11	D _{N2O}	1.61E-09

Liquid: 3 M aq. MEA, Gas: N₂O, Temp.: 40 °C

No.	T-room	P-room	T	R _A	flow rate (<i>q</i>)	length (<i>l</i>)	C*	D _{A-exp.}
	°C	mbar	K	mol/s	m ³ /s	m	mol/m ³	m ² /s
3M-40-01	23	1028	313.15	3.212E-07	5.528E-07	1.753E-02	1.76E+01	2.14E-09
3M-40-02	23	1028	313.15	3.139E-07	5.528E-07	1.753E-02	1.76E+01	2.05E-09
3M-40-03	23	1028	313.15	3.237E-07	5.528E-07	1.753E-02	1.76E+01	2.17E-09
3M-40-04	22.5	1026.5	313.15	2.686E-07	3.757E-07	1.753E-02	1.76E+01	2.21E-09
3M-40-05	22.5	1026.5	313.15	2.677E-07	3.757E-07	1.753E-02	1.76E+01	2.19E-09
3M-40-06	22.5	1026.5	313.15	2.729E-07	3.757E-07	1.753E-02	1.76E+01	2.28E-09
Statistic					STD	7.859E-11	D _{N2O}	2.17E-09

Liquid: 3 M aq. MEA, Gas: N₂O, Temp.: 50 °C

No.	T-room	P-room	T	R _A	flow rate (<i>q</i>)	length (<i>l</i>)	C*	D _{A-exp.}
	°C	mbar	K	mol/s	m ³ /s	m	mol/m ³	m ² /s
3M-50-01	22.8	1024.9	323.15	2.740E-07	4.811E-07	1.753E-02	1.43E+01	2.71E-09
3M-50-02	22.8	1024.9	323.15	2.653E-07	4.811E-07	1.753E-02	1.43E+01	2.54E-09
3M-50-03	22.8	1024.9	323.15	2.264E-07	3.410E-07	1.753E-02	1.43E+01	2.61E-09
3M-50-04	23.4	1022.8	323.15	2.279E-07	3.388E-07	1.753E-02	1.43E+01	2.68E-09
3M-50-05	23.4	1022.8	323.15	2.212E-07	3.388E-07	1.753E-02	1.43E+01	2.52E-09
Statistic					STD	8.257E-11	D _{N2O}	2.61E-09

Liquid: 3 M aq. MEA, Gas: N₂O, Temp.: 60 °C

No.	T-room	P-room	T	R _A	flow rate (<i>q</i>)	length (<i>l</i>)	C*	D _{A-exp.}
	°C	mbar	K	mol/s	m ³ /s	m	mol/m ³	m ² /s
3M-60-01	23.2	1022.6	333.15	2.546E-07	4.977E-07	1.753E-02	1.18E+01	3.34E-09
3M-60-02	23.2	1022.6	333.15	2.531E-07	4.977E-07	1.753E-02	1.18E+01	3.30E-09
3M-60-03	23.2	1022.6	333.15	2.485E-07	4.977E-07	1.753E-02	1.18E+01	3.18E-09
3M-60-04	22.8	1022	333.15	2.282E-07	3.984E-07	1.753E-02	1.18E+01	3.36E-09
3M-60-05	22.8	1022	333.15	2.239E-07	3.984E-07	1.753E-02	1.18E+01	3.23E-09
3M-60-06	22.8	1022	333.15	2.308E-07	3.984E-07	1.753E-02	1.18E+01	3.43E-09
3M-60-07	22.8	1022	333.15	2.282E-07	3.984E-07	1.753E-02	1.18E+01	3.36E-09
Statistic					STD	8.435E-11	D _{N2O}	3.32E-09

Liquid: 5 M aq. MEA, Gas: N₂O, Temp.: 25 °C

No.	T-room	P-room	T	R _A	flow rate (<i>q</i>)	length (<i>l</i>)	C*	D _{A-exp.}
	°C	mbar	K	mol/s	m ³ /s	m	mol/m ³	m ² /s
5M-25-01	22.9	1045.6	298.15	3.426E-07	5.244E-07	1.970E-02	2.42E+01	1.21E-09
5M-25-02	22.9	1045.6	298.15	3.243E-07	5.244E-07	1.970E-02	2.42E+01	1.09E-09
5M-25-03	22.9	1045.6	298.15	3.398E-07	5.244E-07	1.970E-02	2.42E+01	1.19E-09
5M-25-04	23.1	1044	298.15	2.683E-07	3.401E-07	1.970E-02	2.42E+01	1.15E-09
5M-25-05	23.1	1044	298.15	2.752E-07	3.401E-07	1.970E-02	2.42E+01	1.21E-09
5M-25-06	23.1	1044	298.15	2.649E-07	3.401E-07	1.970E-02	2.42E+01	1.12E-09
Statistic					STD	5.174E-11	D _{N2O}	1.16E-09

Liquid: 5 M aq. MEA, Gas: N₂O, Temp.: 30 °C

No.	T-room	P-room	T	R _A	flow rate (<i>q</i>)	length (<i>l</i>)	C*	D _{A-exp.}
	°C	mbar	K	mol/s	m ³ /s	m	mol/m ³	m ² /s
5M-30-01	23.1	1044.9	303.15	3.506E-07	5.660E-07	1.970E-02	2.16E+01	1.48E-09
5M-30-02	23.1	1044.9	303.15	3.449E-07	5.660E-07	1.970E-02	2.16E+01	1.43E-09
5M-30-03	23.1	1044.9	303.15	3.421E-07	5.660E-07	1.970E-02	2.16E+01	1.40E-09
5M-30-04	23.1	1044.9	303.15	3.367E-07	5.660E-07	1.970E-02	2.16E+01	1.36E-09
5M-30-05	23.1	1044.9	303.15	2.318E-07	3.905E-07	1.431E-02	2.16E+01	1.29E-09
5M-30-06	23.1	1044.9	303.15	2.383E-07	3.905E-07	1.431E-02	2.16E+01	1.36E-09
5M-30-07	23.1	1044.9	303.15	2.344E-07	3.905E-07	1.431E-02	2.16E+01	1.32E-09
Statistic					STD	6.514E-11	D _{N2O}	1.38E-09

Liquid: 5 M aq. MEA, Gas: N₂O, Temp.: 40 °C

No.	T-room	P-room	T	R _A	flow rate (<i>q</i>)	length (<i>l</i>)	C*	D _{A-exp.}
	°C	mbar	K	mol/s	m ³ /s	m	mol/m ³	m ² /s
5M-40-01	22.8	1045.5	313.15	2.470E-07	4.870E-07	1.431E-02	1.75E+01	1.80E-09
5M-40-02	22.8	1045.5	313.15	2.401E-07	4.870E-07	1.431E-02	1.75E+01	1.70E-09
5M-40-03	22.8	1045.5	313.15	2.456E-07	4.870E-07	1.431E-02	1.75E+01	1.78E-09
5M-40-04	22.8	1045.5	313.15	2.309E-07	4.104E-07	1.431E-02	1.75E+01	1.86E-09
5M-40-05	22.8	1045.5	313.15	2.297E-07	4.104E-07	1.431E-02	1.75E+01	1.84E-09
5M-40-06	22.8	1045.5	313.15	2.248E-07	4.104E-07	1.431E-02	1.75E+01	1.77E-09
Statistic					STD	5.951E-11	D _{N2O}	1.79E-09

Liquid: 5 M aq. MEA, Gas: N₂O, Temp.: 50 °C

No.	T-room	P-room	T	R _A	flow rate (<i>q</i>)	length (<i>l</i>)	C*	D _{A-exp.}
	°C	mbar	K	mol/s	m ³ /s	m	mol/m ³	m ² /s
5M-50-01	23.4	1026.5	323.15	2.263E-07	4.808E-07	1.431E-02	1.40E+01	2.36E-09
5M-50-02	23.4	1026.5	323.15	2.191E-07	4.808E-07	1.431E-02	1.40E+01	2.21E-09
5M-50-03	23.4	1026.5	323.15	2.263E-07	4.808E-07	1.431E-02	1.40E+01	2.36E-09
5M-50-04	23.4	1026.5	323.15	2.288E-07	5.364E-07	1.431E-02	1.40E+01	2.16E-09
5M-50-05	23.4	1026.5	323.15	2.339E-07	5.364E-07	1.431E-02	1.40E+01	2.26E-09
Statistic					STD	8.822E-11	D _{N2O}	2.27E-09

Liquid: 5 M aq. MEA, Gas: N₂O, Temp.: 60 °C

No.	T-room	P-room	T	R _A	flow rate (<i>q</i>)	length (<i>l</i>)	C*	D _{A-exp.}
	°C	mbar	K	mol/s	m ³ /s	m	mol/m ³	m ² /s
5M-60-01	22.8	1025.4	333.15	2.033E-07	4.791E-07	1.431E-02	1.17E+01	2.77E-09
5M-60-02	22.8	1025.4	333.15	2.053E-07	4.791E-07	1.431E-02	1.17E+01	2.82E-09
5M-60-03	22.8	1025.4	333.15	1.966E-07	4.791E-07	1.431E-02	1.17E+01	2.59E-09
5M-60-04	22.8	1025.4	333.15	1.975E-07	4.791E-07	1.431E-02	1.17E+01	2.61E-09
5M-60-05	22.8	1025.4	333.15	2.159E-07	3.987E-07	1.920E-02	1.17E+01	2.80E-09
5M-60-06	22.8	1025.4	333.15	2.148E-07	3.987E-07	1.920E-02	1.17E+01	2.77E-09
5M-60-07	22.8	1025.4	333.15	2.105E-07	3.987E-07	1.920E-02	1.17E+01	2.66E-09
Statistic					STD	9.465E-11	D _{N2O}	2.72E-09

Liquid: 8 M aq. MEA, Gas: N₂O, Temp.: 25 °C

No.	T-room	P-room	T	R _A	flow rate (<i>q</i>)	length (<i>l</i>)	C*	D _{A-exp.}
	°C	mbar	K	mol/s	m ³ /s	m	mol/m ³	m ² /s
8M-25-01	22.5	1047.5	298.15	2.354E-07	4.642E-07	1.650E-02	2.37E+01	8.08E-10
8M-25-02	22.5	1047.5	298.15	2.449E-07	4.642E-07	1.650E-02	2.37E+01	8.75E-10
8M-25-03	22.5	1047.5	298.15	2.020E-07	4.215E-07	1.260E-02	2.37E+01	8.58E-10
8M-25-04	22.5	1047.5	298.15	1.982E-07	4.215E-07	1.260E-02	2.37E+01	8.26E-10
8M-25-05	22.5	1047.5	298.15	1.991E-07	4.215E-07	1.260E-02	2.37E+01	8.34E-10
8M-25-06	22.5	1047.5	298.15	2.069E-07	4.215E-07	1.260E-02	2.37E+01	9.00E-10
Statistic					STD	3.385E-11	D _{N2O}	8.50E-10

Liquid: 8 M aq. MEA, Gas: N₂O, Temp.: 30 °C

No.	T-room	P-room	T	R _A	flow rate (<i>q</i>)	length (<i>l</i>)	C*	D _{A-exp.}
	°C	mbar	K	mol/s	m ³ /s	m	mol/m ³	m ² /s
8M-30-01	22.8	1046	303.15	2.074E-07	4.677E-07	1.260E-02	2.07E+01	1.07E-09
8M-30-02	22.8	1046	303.15	2.084E-07	4.677E-07	1.260E-02	2.07E+01	1.08E-09
8M-30-03	22.8	1046	303.15	2.286E-07	4.066E-07	1.970E-02	2.07E+01	9.54E-10
8M-30-04	22.8	1046	303.15	2.298E-07	4.066E-07	1.970E-02	2.07E+01	9.64E-10
8M-30-05	22.8	1046	303.15	2.779E-07	4.661E-07	2.370E-02	2.07E+01	1.02E-09
8M-30-06	22.8	1046	303.15	2.725E-07	4.661E-07	2.370E-02	2.07E+01	9.83E-10
8M-30-07	22.8	1046	303.15	2.760E-07	4.661E-07	2.370E-02	2.07E+01	1.01E-09
Statistic					STD	4.836E-11	D _{N2O}	1.01E-09

Liquid: 8 M aq. MEA, Gas: N₂O, Temp.: 40 °C

No.	T-room	P-room	T	R _A	flow rate (<i>q</i>)	length (<i>l</i>)	C*	D _{A-exp.}
	°C	mbar	K	mol/s	m ³ /s	m	mol/m ³	m ² /s
8M-40-01	22.6	1041.5	313.15	2.380E-07	4.275E-07	2.370E-02	1.70E+01	1.20E-09
8M-40-02	22.6	1041.5	313.15	2.380E-07	4.275E-07	2.370E-02	1.70E+01	1.20E-09
8M-40-03	22.6	1041.5	313.15	2.448E-07	4.275E-07	2.370E-02	1.70E+01	1.27E-09
8M-40-04	22.6	1041.5	313.15	2.327E-07	5.358E-07	1.634E-02	1.70E+01	1.33E-09
8M-40-05	22.6	1041.5	313.15	2.340E-07	5.358E-07	1.634E-02	1.70E+01	1.35E-09
8M-40-06	22.6	1041.5	313.15	2.206E-07	5.358E-07	1.634E-02	1.70E+01	1.20E-09
Statistic					STD	6.840E-11	D _{N2O}	1.26E-09

Liquid: 8 M aq. MEA, Gas: N₂O, Temp.: 50 °C

No.	T-room	P-room	T	R _A	flow rate (<i>q</i>)	length (<i>l</i>)	C*	D _{A-exp.}
	°C	mbar	K	mol/s	m ³ /s	m	mol/m ³	m ² /s
8M-50-01	24	1040.3	323.15	2.339E-07	6.123E-07	1.634E-02	1.40E+01	1.74E-09
8M-50-02	24	1040.3	323.15	2.240E-07	6.123E-07	1.634E-02	1.40E+01	1.59E-09
8M-50-03	24	1040.3	323.15	2.301E-07	6.123E-07	1.634E-02	1.40E+01	1.68E-09
8M-50-04	24	1040.3	323.15	1.855E-07	3.521E-07	1.943E-02	1.40E+01	1.60E-09
8M-50-05	23.4	1038.5	323.15	1.915E-07	3.521E-07	1.943E-02	1.40E+01	1.71E-09
8M-50-06	23.4	1038.5	323.15	1.906E-07	3.521E-07	1.943E-02	1.40E+01	1.69E-09
8M-50-07	23.4	1038.5	323.15	1.827E-07	3.521E-07	1.943E-02	1.40E+01	1.55E-09
Statistic					STD	6.899E-11	D _{N₂O}	1.65E-09

Liquid: 8 M aq. MEA, Gas: N₂O, Temp.: 60 °C

No.	T-room	P-room	T	R _A	flow rate (<i>q</i>)	length (<i>l</i>)	C*	D _{A-exp.}
	°C	mbar	K	mol/s	m ³ /s	m	mol/m ³	m ² /s
8M-60-01	23.5	1038.9	333.15	1.923E-07	4.132E-07	1.943E-02	1.17E+01	2.09E-09
8M-60-02	23.5	1038.9	333.15	1.839E-07	4.132E-07	1.943E-02	1.17E+01	1.91E-09
8M-60-03	23.5	1038.9	333.15	1.856E-07	4.132E-07	1.943E-02	1.17E+01	1.94E-09
8M-60-04	23.5	1038.9	333.15	1.800E-07	4.514E-07	1.630E-02	1.17E+01	2.00E-09
8M-60-05	23.5	1038.9	333.15	1.808E-07	4.514E-07	1.630E-02	1.17E+01	2.01E-09
8M-60-06	23.5	1038.9	333.15	1.848E-07	4.514E-07	1.630E-02	1.17E+01	2.10E-09
8M-60-07	23.5	1038.9	333.15	1.770E-07	4.514E-07	1.630E-02	1.17E+01	1.93E-09
Statistic					STD	7.600E-11	D _{N₂O}	2.00E-09

Liquid: 10 M aq. MEA, Gas: N₂O, Temp.: 30 °C

No.	T-room	P-room	T	R _A	flow rate (<i>q</i>)	length (<i>l</i>)	C*	D _{A-exp.}
	°C	mbar	K	mol/s	m ³ /s	m	mol/m ³	m ² /s
10M-30-01	23	1034	303.15	1.900E-07	3.926E-07	1.960E-02	2.05E+01	6.98E-10
10M-30-02	23	1034	303.15	1.883E-07	3.926E-07	1.960E-02	2.05E+01	6.85E-10
10M-30-03	23	1034	303.15	2.187E-07	4.846E-07	1.960E-02	2.05E+01	7.49E-10
10M-30-04	23	1034	303.15	2.234E-07	4.846E-07	1.960E-02	2.05E+01	7.81E-10
10M-30-05	23	1034	303.15	1.615E-07	4.137E-07	1.280E-02	2.05E+01	7.33E-10
10M-30-06	23	1034	303.15	1.666E-07	4.137E-07	1.280E-02	2.05E+01	7.80E-10
10M-30-07	23	1034	303.15	1.640E-07	4.137E-07	1.280E-02	2.05E+01	7.56E-10
Statistic					STD	3.754E-11	D _{N₂O}	7.40E-10

Liquid: 10 M aq. MEA, Gas: N₂O, Temp.: 40 °C

No.	T-room	P-room	T	R _A	flow rate (<i>q</i>)	length (<i>l</i>)	C*	D _{A-exp.}
	°C	mbar	K	mol/s	m ³ /s	m	mol/m ³	m ² /s
10M-40-01	22.9	1033.4	313.15	1.52E-07	4.11E-07	1.28E-02	1.66E+01	9.95E-10
10M-40-02	22.9	1033.4	313.15	1.49E-07	4.11E-07	1.28E-02	1.66E+01	9.58E-10
10M-40-03	23.4	1034.3	313.15	1.56E-07	4.11E-07	1.28E-02	1.66E+01	1.05E-09
10M-40-04	23.4	1034.3	313.15	1.91E-07	4.88E-07	1.88E-02	1.66E+01	9.03E-10
10M-40-05	23.4	1034.3	313.15	1.93E-07	4.88E-07	1.88E-02	1.66E+01	9.20E-10
10M-40-06	23.4	1034.3	313.15	1.88E-07	4.88E-07	1.88E-02	1.66E+01	8.73E-10
Statistic					STD	6.433E-11	D _{N2O}	9.50E-10

Liquid: 10 M aq. MEA, Gas: N₂O, Temp.: 50 °C

No.	T-room	P-room	T	R _A	flow rate (<i>q</i>)	length (<i>l</i>)	C*	D _{A-exp.}
	°C	mbar	K	mol/s	m ³ /s	m	mol/m ³	m ² /s
10M-50-01	23.5	1023.6	323.15	1.77E-07	4.09E-07	1.88E-02	1.39E+01	1.32E-09
10M-50-02	23.5	1023.6	323.15	1.74E-07	4.09E-07	1.88E-02	1.39E+01	1.27E-09
10M-50-03	23.5	1023.6	323.15	1.65E-07	4.09E-07	1.88E-02	1.39E+01	1.15E-09
10M-50-04	23.5	1023.6	323.15	1.53E-07	4.72E-07	1.31E-02	1.39E+01	1.22E-09
10M-50-05	23.5	1023.6	323.15	1.48E-07	4.72E-07	1.31E-02	1.39E+01	1.14E-09
10M-50-06	23.5	1023.6	323.15	1.53E-07	4.72E-07	1.31E-02	1.39E+01	1.22E-09
10M-50-07	23.5	1023.6	323.15	1.55E-07	4.72E-07	1.31E-02	1.39E+01	1.26E-09
Statistic					STD	6.357E-11	D _{N2O}	1.22E-09

Liquid: 10 M aq. MEA, Gas: N₂O, Temp.: 60 °C

No.	T-room	P-room	T	R _A	flow rate (<i>q</i>)	length (<i>l</i>)	C*	D _{A-exp.}
	°C	mbar	K	mol/s	m ³ /s	m	mol/m ³	m ² /s
10M-60-01	22.9	1022.8	333.15	1.484E-07	4.696E-07	1.310E-02	1.20E+01	1.56E-09
10M-60-02	22.9	1022.8	333.15	1.517E-07	4.696E-07	1.310E-02	1.20E+01	1.63E-09
10M-60-03	22.9	1022.8	333.15	1.448E-07	4.696E-07	1.310E-02	1.20E+01	1.48E-09
10M-60-04	22.9	1022.8	333.15	1.724E-07	4.274E-07	2.010E-02	1.20E+01	1.51E-09
10M-60-05	22.9	1022.8	333.15	1.710E-07	4.274E-07	2.010E-02	1.20E+01	1.48E-09
10M-60-06	22.9	1022.8	333.15	1.717E-07	4.173E-07	2.010E-02	1.20E+01	1.53E-09
10M-60-07	22.9	1022.8	333.15	1.791E-07	4.173E-07	2.010E-02	1.20E+01	1.67E-09
Statistic					STD	7.153E-11	D _{N2O}	1.55E-09

Liquid: 12 M aq. MEA, Gas: N₂O, Temp.: 40 °C

No.	T-room	P-room	T	R _A	flow rate (<i>q</i>)	length (<i>l</i>)	C*	D _{A-exp.}
	°C	mbar	K	mol/s	m ³ /s	m	mol/m ³	m ² /s
12M-40-01	23	1021.1	313.15	1.73E-07	5.08E-07	2.01E-02	1.76E+01	5.88E-10
12M-40-02	23	1021.1	313.15	1.83E-07	5.08E-07	2.01E-02	1.76E+01	6.58E-10
12M-40-03	23.6	1022.1	313.15	1.40E-07	4.39E-07	1.22E-02	1.76E+01	7.36E-10
12M-40-04	23.6	1022.1	313.15	1.37E-07	4.39E-07	1.22E-02	1.76E+01	7.10E-10
12M-40-05	23.6	1022.1	313.15	1.31E-07	4.39E-07	1.22E-02	1.76E+01	6.43E-10
Statistic					STD	5.828E-11	D _{N₂O}	6.67E-10

Liquid: 12 M aq. MEA, Gas: N₂O, Temp.: 50 °C

No.	T-room	P-room	T	R _A	flow rate (<i>q</i>)	length (<i>l</i>)	C*	D _{A-exp.}
	°C	mbar	K	mol/s	m ³ /s	m	mol/m ³	m ² /s
12M-50-01	23.3	1022.3	323.15	1.25E-07	4.00E-07	1.22E-02	1.49E+01	9.01E-10
12M-50-02	23.3	1022.3	323.15	1.15E-07	4.00E-07	1.22E-02	1.49E+01	7.60E-10
12M-50-03	23.3	1022.3	323.15	1.71E-07	4.93E-07	1.98E-02	1.49E+01	8.41E-10
12M-50-04	23.3	1022.3	323.15	1.70E-07	4.93E-07	1.98E-02	1.49E+01	8.35E-10
12M-50-05	23.3	1022.3	323.15	1.68E-07	4.93E-07	1.98E-02	1.49E+01	8.10E-10
Statistic					STD	5.125E-11	D _{N₂O}	8.30E-10

Liquid: 12 M aq. MEA, Gas: N₂O, Temp.: 60 °C

No.	T-room	P-room	T	R _A	flow rate (<i>q</i>)	length (<i>l</i>)	C*	D _{A-exp.}
	°C	mbar	K	mol/s	m ³ /s	m	mol/m ³	m ² /s
12M-60-01	23.1	1022.9	333.15	1.75E-07	4.83E-07	1.98E-02	1.32E+01	1.14E-09
12M-60-02	23.1	1022.9	333.15	1.63E-07	4.83E-07	1.98E-02	1.32E+01	9.99E-10
12M-60-03	23.1	1022.9	333.15	1.18E-07	4.08E-07	1.23E-02	1.32E+01	1.00E-09
12M-60-04	23.1	1022.9	333.15	1.21E-07	4.08E-07	1.23E-02	1.32E+01	1.05E-09
12M-60-05	23.1	1022.9	333.15	1.16E-07	4.08E-07	1.23E-02	1.32E+01	9.63E-10
Statistic					STD	9.881E-11	D _{N₂O}	1.03E-09

A3. Raw Experimental Data of Chemical Reaction Kinetics Measurement

The raw experimental data were recorded by data logger including the total gas pressure in the cell, the temperature gas storage pipe (the top metal flange), and the temperature of gas and liquid in the cell. The total gas pressure, gas and liquid temperature of the experiments are listed here with figures. The common experimental conditions: stirrer speed: 60 rpm; sample frequency: 1 s; liquid volume: 500 mL.

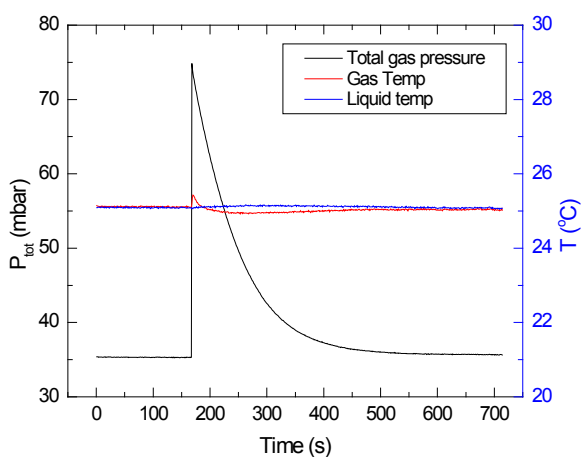


Figure A3.1. 25°C, 0.5 M aq. MEA +CO₂

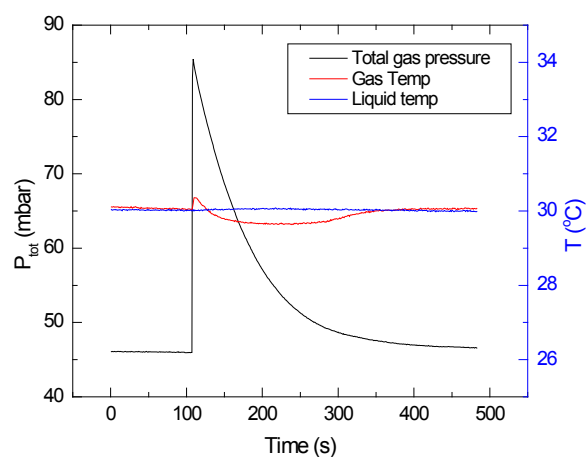


Figure A3.2. 30°C, 0.5 M aq. MEA +CO₂

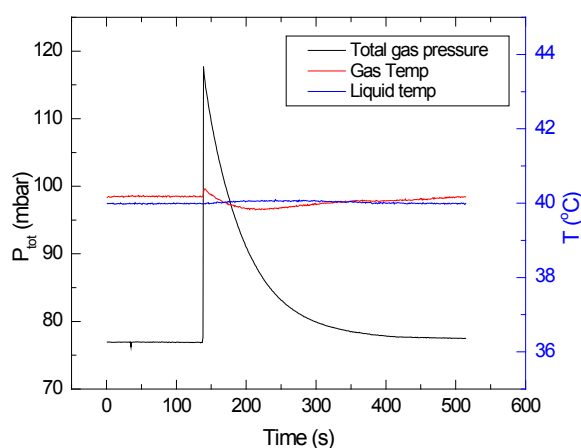


Figure A3.3. 40°C, 0.5 M aq. MEA +CO₂

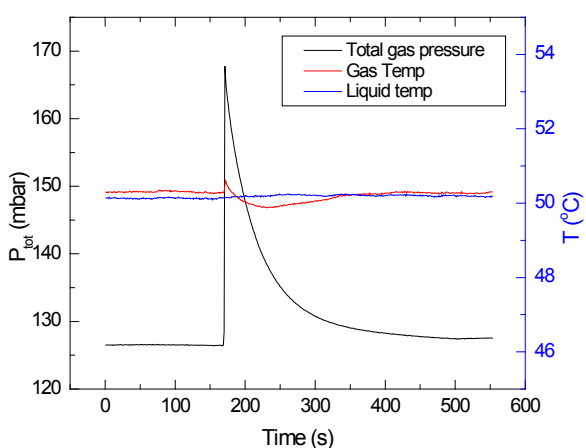


Figure A3.4. 50°C, 0.5 M aq. MEA +CO₂

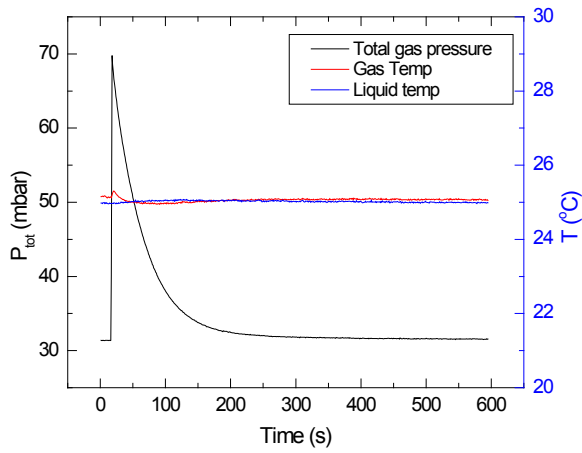


Figure A3.5. 25°C, 1 M aq. MEA +CO₂

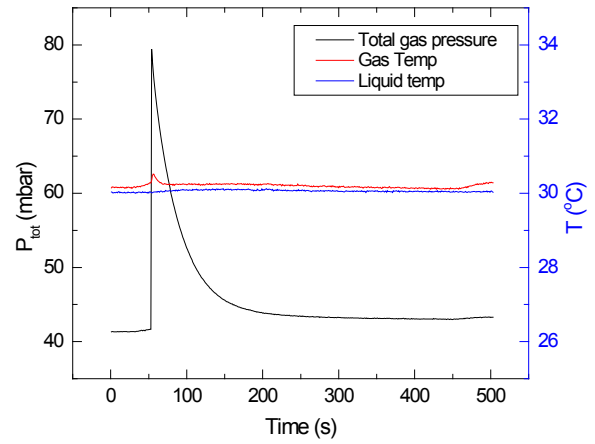


Figure A3.6. 30°C, 1 M aq. MEA +CO₂

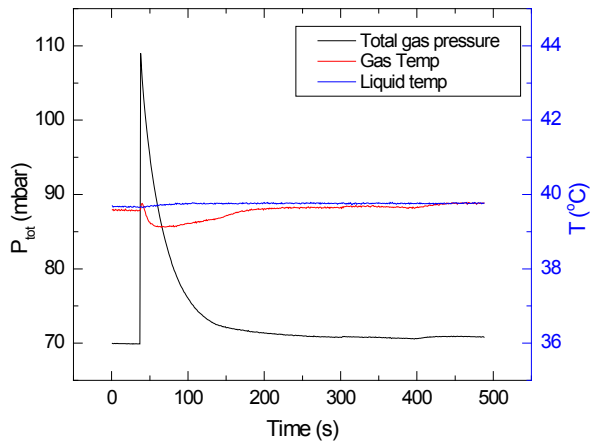


Figure A3.7. 40°C, 1 M aq. MEA +CO₂

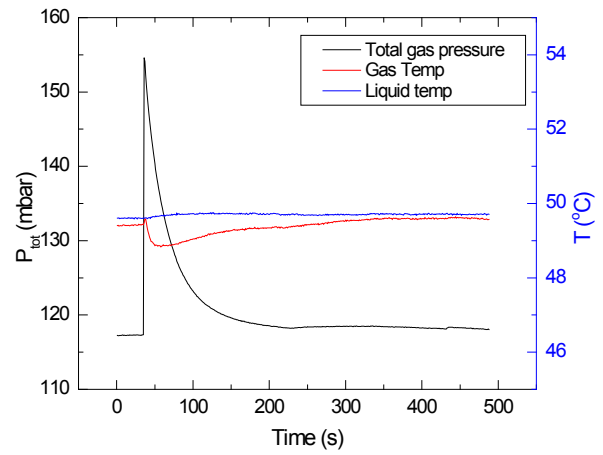


Figure A3.8. 50°C, 1 M aq. MEA +CO₂

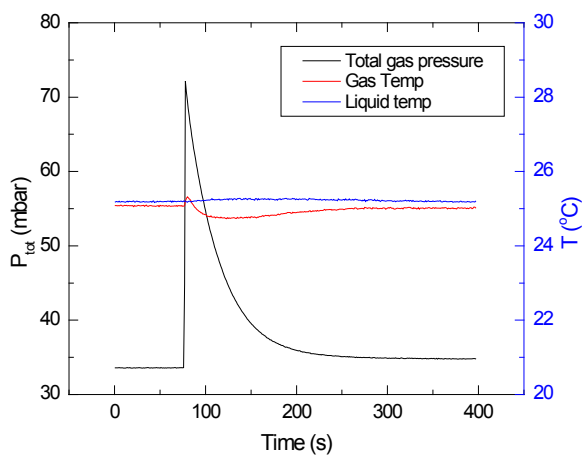


Figure A3.9. 25°C, 2 M aq. MEA +CO₂

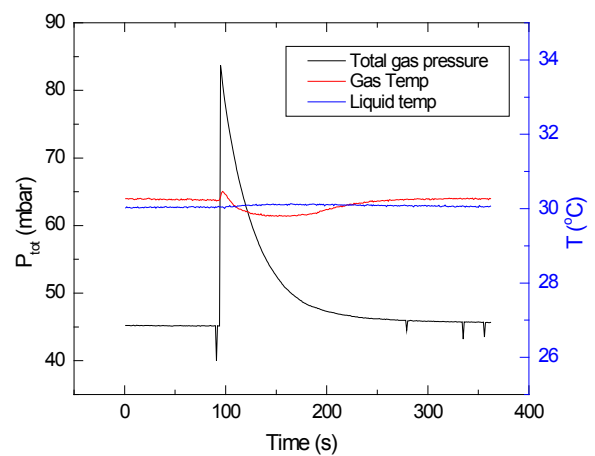


Figure A3.10. 30°C, 2 M aq. MEA +CO₂

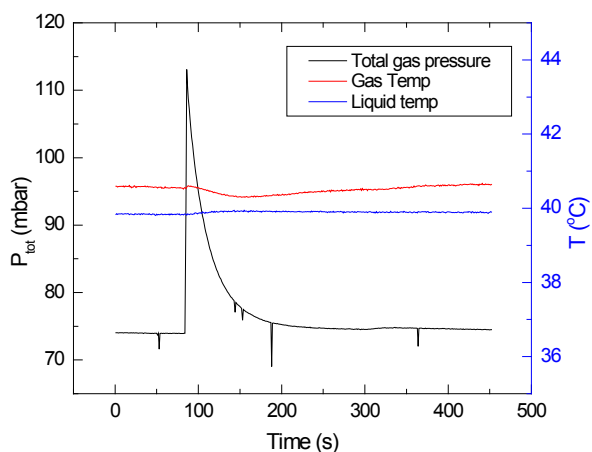


Figure A3.11. 40°C, 2 M aq. MEA +CO₂

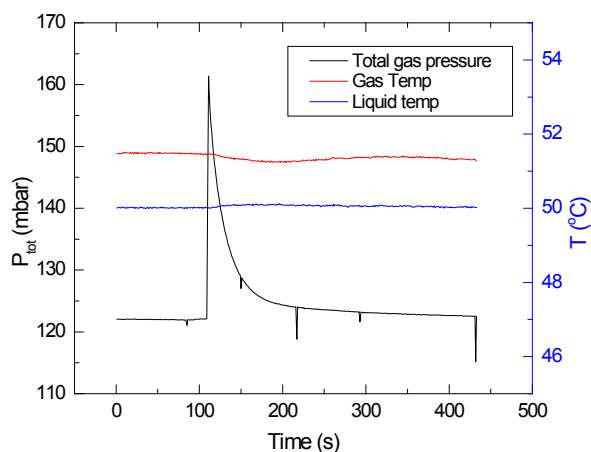


Figure A3.12. 50°C, 2 M aq. MEA +CO₂

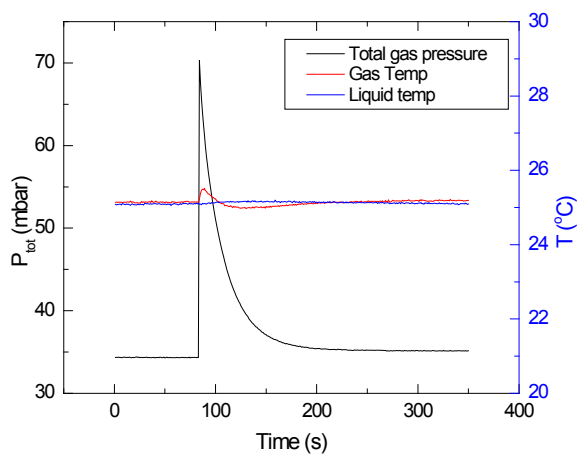


Figure A3.13. 25°C, 3.6 M aq. MEA +CO₂

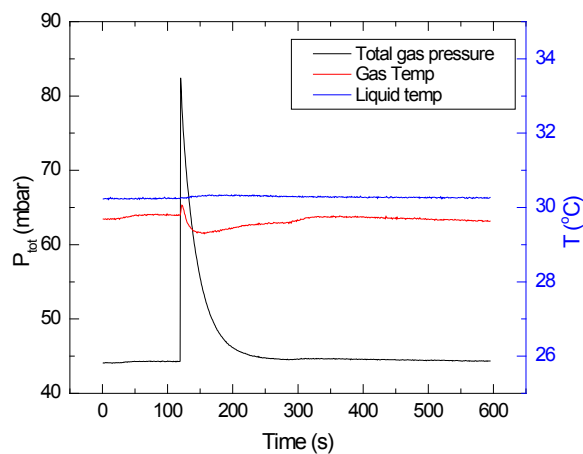


Figure A3.14. 30°C, 3.6 M aq. MEA +CO₂

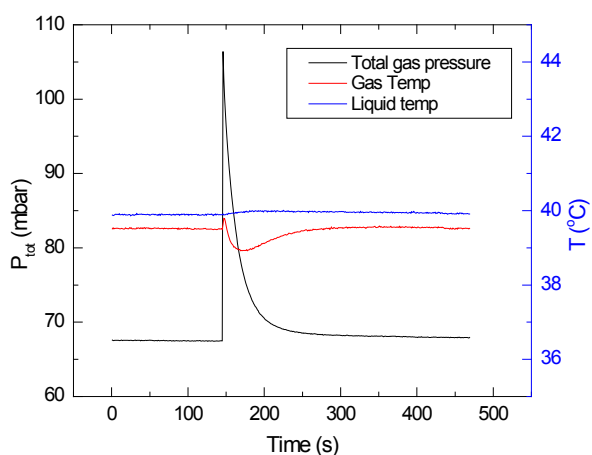


Figure A3.15. 40°C, 3.6 M aq. MEA +CO₂

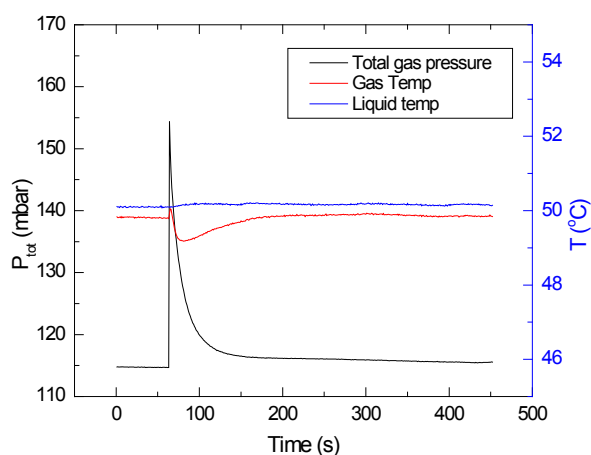
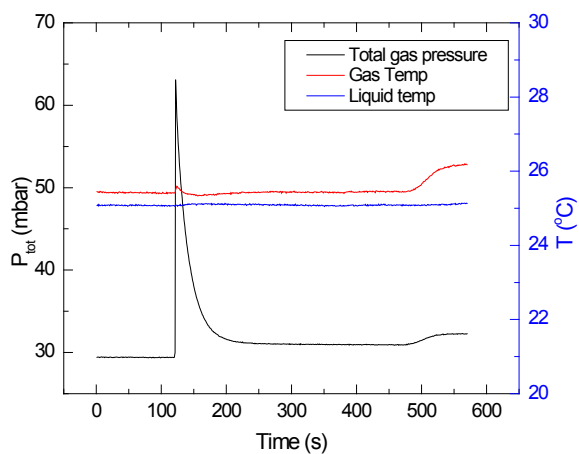
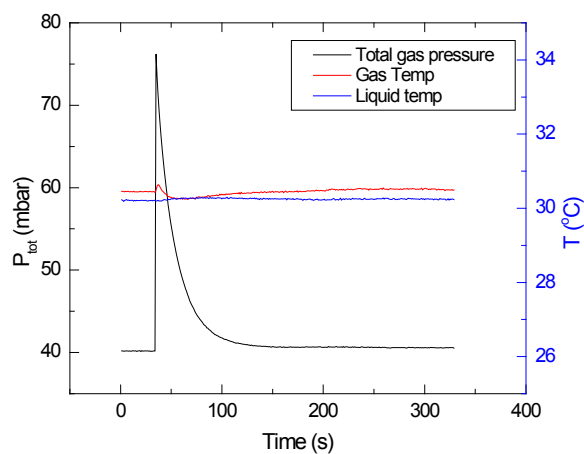
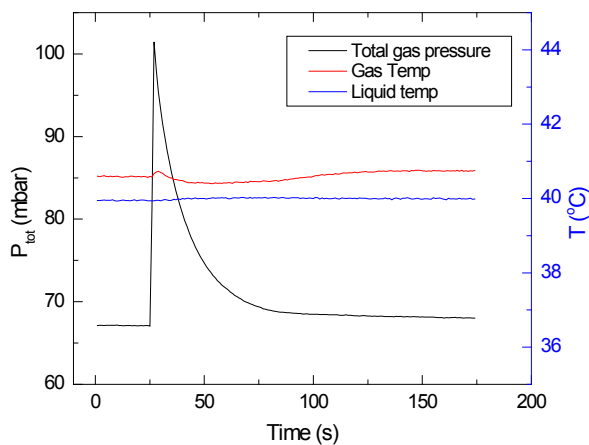
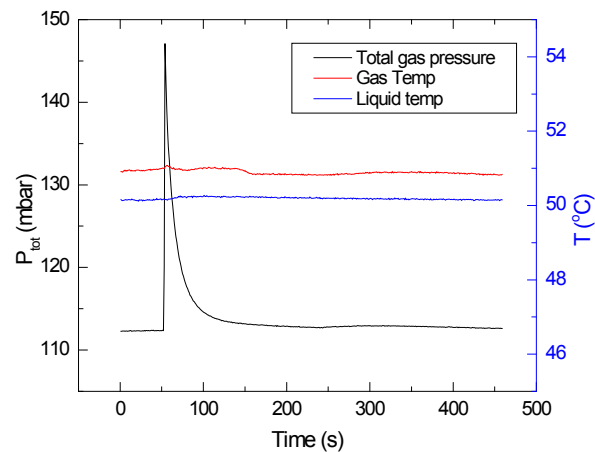
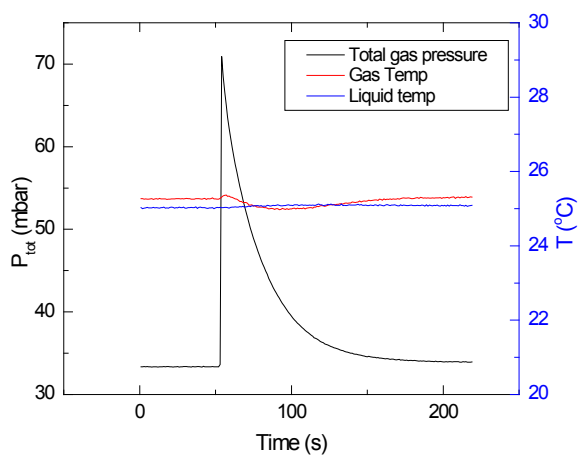
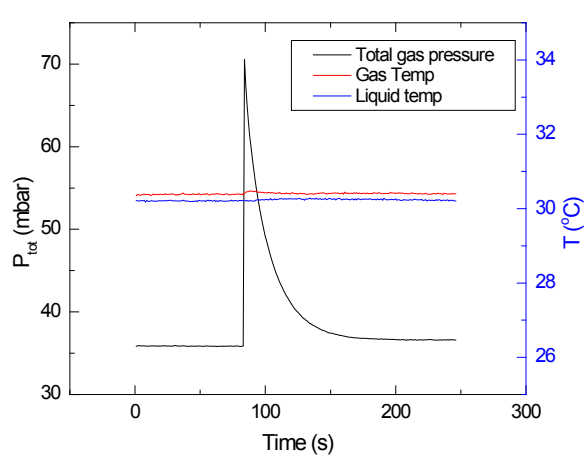


Figure A3.16. 50°C, 3.6 M aq. MEA +CO₂

Figure A3.17. 25°C, 5 M aq. MEA +CO₂Figure A3.18. 30°C, 5 M aq. MEA +CO₂Figure A3.19. 40°C, 5 M aq. MEA +CO₂Figure A3.20. 50°C, 5 M aq. MEA +CO₂Figure A3.21. 25°C, 8 M aq. MEA +CO₂Figure A3.22. 30°C, 8 M aq. MEA +CO₂

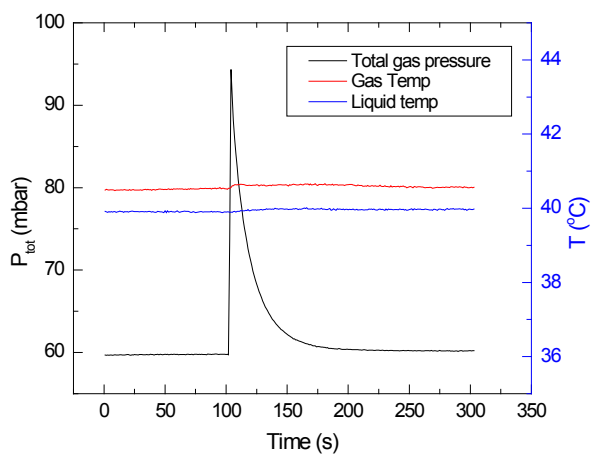


Figure A3.23. 40°C, 8 M aq. MEA +CO₂

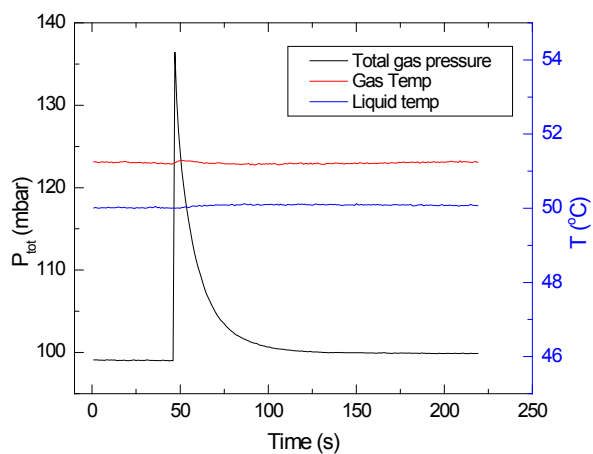


Figure A3.24. 50°C, 8 M aq. MEA +CO₂

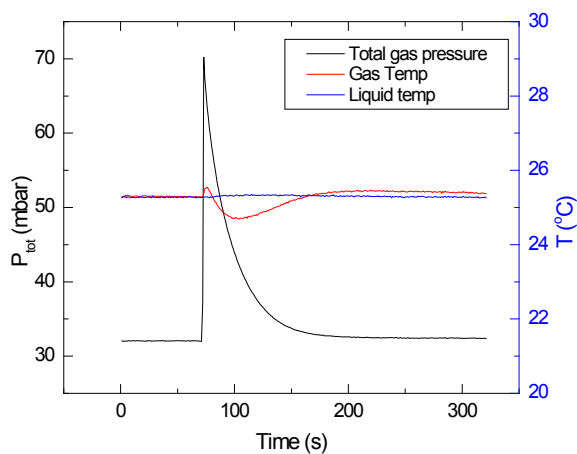


Figure A3.25. 25°C, 10 M aq. MEA +CO₂

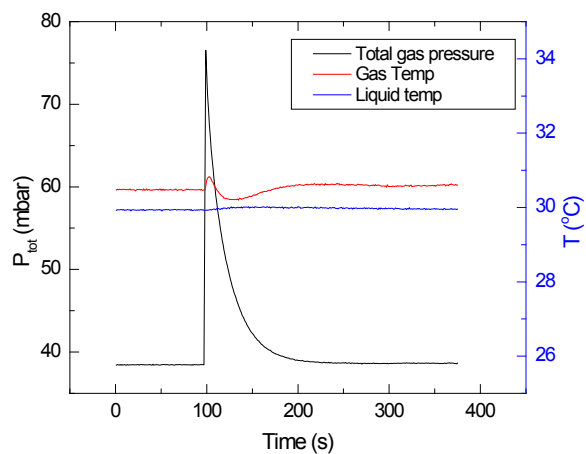


Figure A3.26. 30°C, 10 M aq. MEA +CO₂

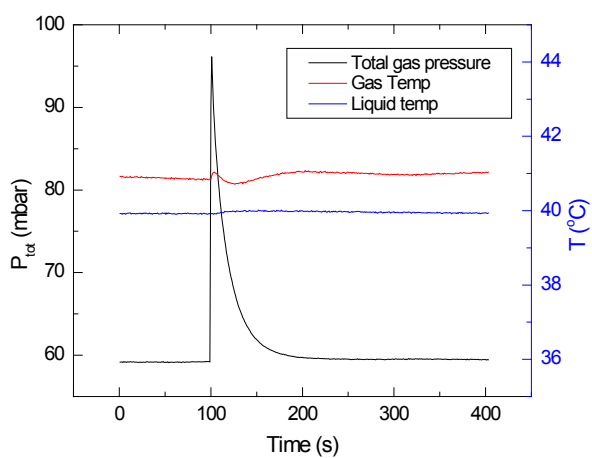


Figure A3.27. 40°C, 10 M aq. MEA +CO₂

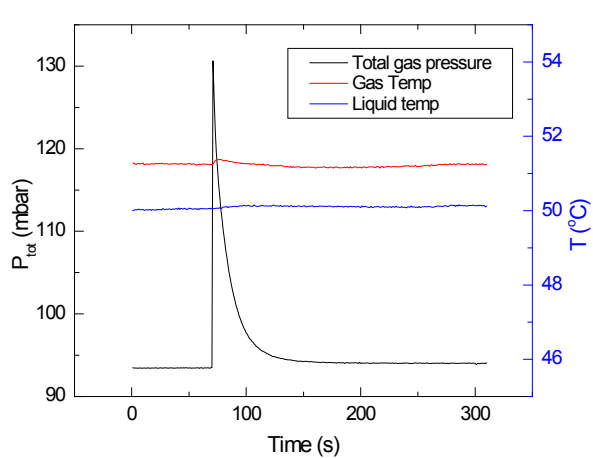


Figure A3.28. 50°C, 10 M aq. MEA +CO₂

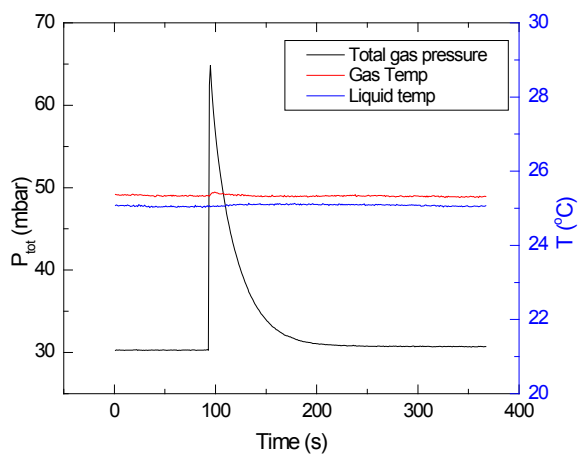


Figure A3.29. 25°C, 12 M aq. MEA +CO₂

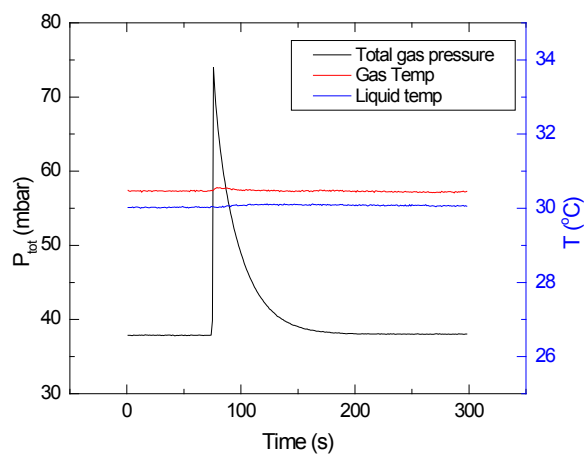


Figure A3.30. 30°C, 12 M aq. MEA +CO₂

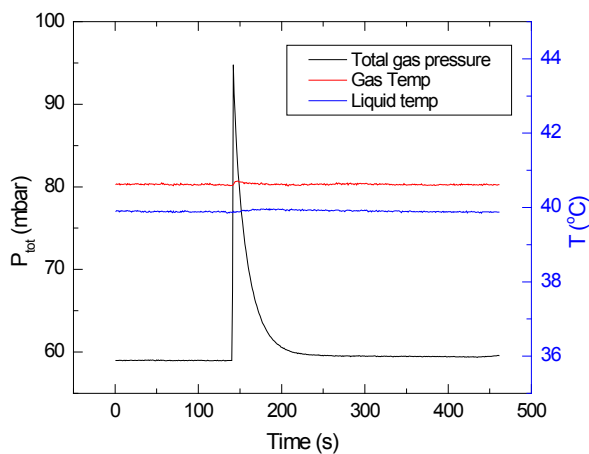


Figure A3.31. 40°C, 12 M aq. MEA +CO₂

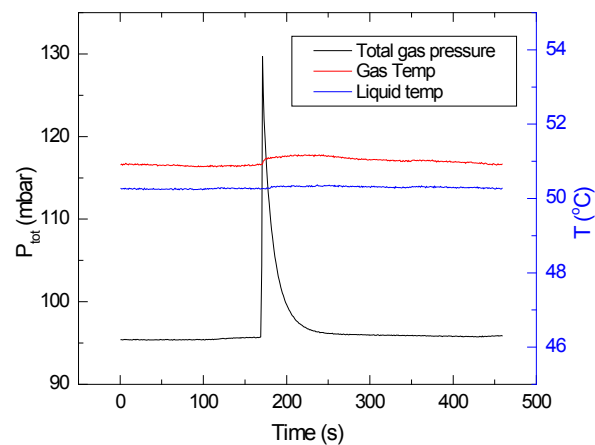


Figure A3.32. 50°C, 12 M aq. MEA +CO₂

A4. Overshoot of Pressure and Temperature of Stirred Cell

When introducing gas into the cell, the gas pressure and the temperatures in the cell could fluctuate. The following tests are the CO₂ from the gas storage tank with 3 bar pressure were introduced in the cell (no liquid inside) with a initial CO₂ pressure 1027.4 mbar and 724 mbar, respectively. The relationship of pressure vs. time and temperature vs. time were recorded and shown in the following figures:

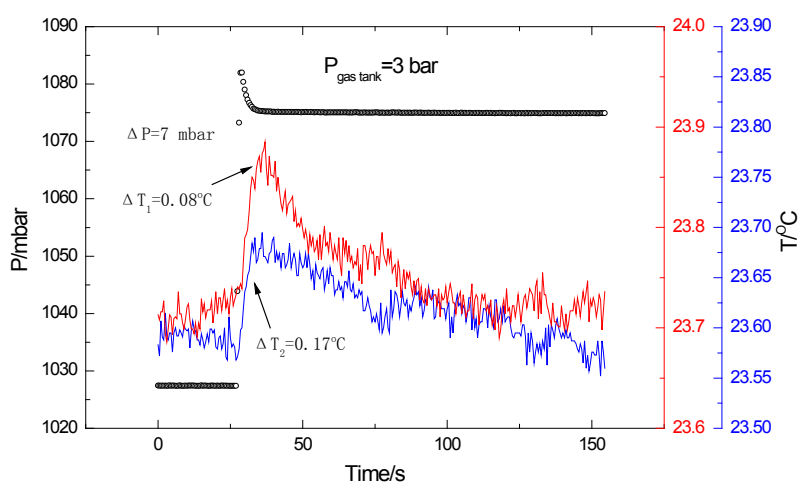


Figure A4.1. Overshoot of pressure and temperature at room T (23.6°C), only CO₂ in the cell. (red line, thermocouple for gas; blue line, thermocouple for liquid)

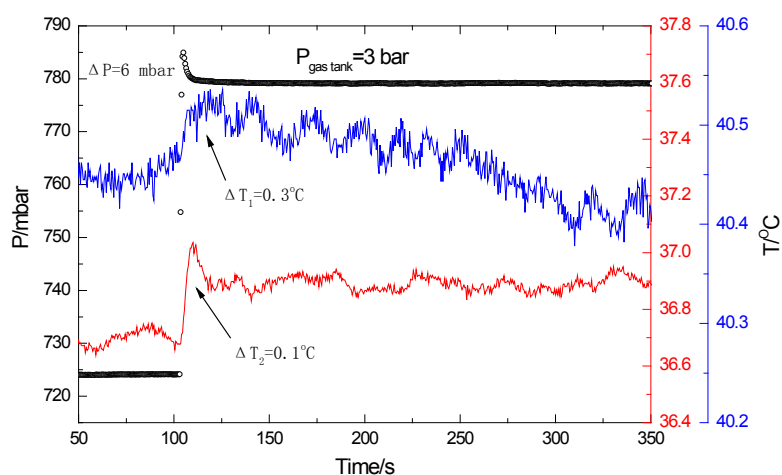


Figure A4.2. Overshoot of pressure and temperature at 40°C, only CO₂ in the cell. (red line, thermocouple for gas; blue line, thermocouple for liquid)

The pressure overshoot is about 6 – 7 mbar when the initial pressure is 1027.4 or 724 mbar. This may be caused by the rearrangement of the instant compressed gas molecules after the gas is introduced in the cell. When the gas is introduced in the cell, the gas in the cell was compressed by the freshly introduced gas, then the pressure in the cell increases. But at this time, the gas molecules are more chaos, the entropy is much bigger. After few seconds, the gas molecules rearrange and the entropy decrease. Thus, the pressure decreases to the normal level.

The overshoot phenomena of temperature may be caused by the gas in the cell is compressed in a short time when the gas is introduced in the cell; this is a compress process at constant volume. According to the physical–chemistry principle, the temperature could increase.

It takes about 10 s to reach the equilibrium due to the pressure overshoot after introducing the gas into the cell. Therefore, regarding the measurement by the stirred cell, the pressure drop in 0 – 10 s at beginning should be avoided to use in the calculation.

A5. Deduction and Applications of Models and Equations

A5.1. Calculation of Dimensionless Solubility (m)

This is the deduction of dimensionless solubility (m):

ideal gas law:

$$PV_g = nRT$$

For T constant, before absorption, the mole mass of gas is:

$$n_{ini} = \frac{P_{ini}V_g}{RT}$$

When reach equilibrium the mole mass of gas is:

$$n_{eq} = \frac{P_{eq}V_g}{RT}$$

The absorption into liquid of gas is:

$$n = n_{ini} - n_{eq} = \frac{(P_{ini} - P_{eq})V_g}{RT}$$

According to Henry's law, the solubility is:

$$H = \frac{P_{eq}}{C^*} = \frac{V_l P_{eq}}{n} = \frac{P_{eq}RT}{(P_{ini} - P_{eq})} \cdot \frac{V_l}{V_g} \quad (\text{Pa} \cdot \text{m}^3 \cdot \text{mol}^{-1})$$

Correction for aqueous solution due to water vapor:

$$m = \frac{RT}{H} = \frac{P_{ini} - P_{eq}}{P_{eq} - P_{vapor}} \cdot \frac{V_g}{V_l} = \frac{n_2}{n} \cdot \frac{V_g}{V_l} = \frac{C_l}{C_g} \quad (\text{mol} \cdot \text{mol}^{-1})$$

A5.2. Calculation of Mass Transfer Coefficient k_L (without Chemical Reaction)

In a stirred cell, solution is fed first, after temperature and gas-liquid reached equilibrium, then gas quickly introduce into the cell in 5s. Then measure the absorbed gas by pressure drop method. The liquid side mass transfer coefficient can be obtained:

$$N = -k_L A (C_L^i - C_L^b)$$

$$V_g \frac{dC_g^b}{dt} = -k_L A (mC_g^b - C_L^b)$$

where

$$m = \frac{C_L^i}{C_g^i} = \frac{P_g^0 - P_g^\infty}{P_g^\infty} \cdot \frac{V_g}{V_L} = \frac{(P_g^0 - P_g^\infty) / RT}{P_g^\infty / RT} \cdot \frac{V_g}{V_L} = \frac{C_g^0 - C_g^\infty}{C_g^\infty} \cdot \frac{V_g}{V_L}$$

boundary condition is :

$$C_g^b = C_g^0 \quad \text{at } t = 0$$

$$V_g C_g^0 = V_g C_g^b + V_L C_L^b$$

$$C_g^\infty = \frac{V_g C_g^0}{mV_L + V_g}$$

Integration

$$\ln \frac{C_g^b - C_g^\infty}{C_g^0 - C_g^\infty} = - \frac{(mV_L + V_g)k_L At}{V_L V_g}$$

or

$$\ln \frac{P_g^b - P_g^\infty}{P_g^0 - P_g^\infty} = - \frac{(mV_L + V_g)k_L At}{V_L V_g}$$

$$k_L \text{ can be obtained from the slope } - \frac{(mV_L + V_g)k_L A}{V_L V_g}$$

A5.3. Calculation for Mass Transfer Coefficient k_L by Volume-drop Method

If the procedure of operating stirred cell or solubility cell is: solution is fed first, after temperature and gas-liquid reached equilibrium, then gas quickly introduce into the cell in 5s. Then measure the absorbed gas by volumetric method. The liquid side mass transfer coefficient can be obtained:

$$-\frac{dn}{dt} = k_L A (C_i^i - C_i^b)$$

$$n = \frac{PV}{RT}$$

when P is constant, $C_i^b \approx 0$, $C_i^i = P/H$

$$-\frac{dn}{dt} = -\frac{P}{RT} \frac{dV}{dt} = k_L A (P/H - 0)$$

$$dV = \frac{RATk_L}{H} dt$$

Integration

$$V = \frac{RATk_L}{H} t + V_0$$

or

$$(V_2 - V_1) = \frac{RATk_L}{H} (t_1 - t_2)$$

k_L can be obtained from the slope $\frac{RATk_L}{H}$

A5.4. Calculation of Pseudo first order Chemical Reaction Rate by Pressure-drop Method (Stirred Cell) (1)

This is the deduction of k_{ps} and pseudo first order chemical reaction rate coefficient k_2 measured by stirred cell with pressure-drop method:

$$\frac{dn}{dt} = -k_L^0 AE(C_L^i - C_L^b)$$

$$PV = nRT$$

$$V_G \text{ is constant, } C_L^i = P / H$$

when chemical reaction is fast,

$$k_L = \sqrt{k_{ps} D} = k_L^0 E$$

then,

$$\frac{V_G}{RT} \frac{dP_G}{dt} = -\sqrt{k_{ps} D} A \left(\frac{P_G}{H} - C_L^b \right)$$

when CO_2 loading less than 0.1 mol / mol

or

$C_L^i \gg C_L^b$ when stirrer speed is low, then

$$C_L^b \approx 0$$

$$\int_{P_1}^{P_2} \frac{dP_G}{P_G} = \int_{t_1}^{t_2} \left(-\frac{RAT}{V_G H} \sqrt{k_{ps} D} \right) dt$$

Integration

$$\ln \frac{P_2}{P_1} = \frac{RAT}{V_G H} \sqrt{k_{ps} D} (t_1 - t_2)$$

Or

$$\ln P = \left(\frac{RAT}{V_G H} \sqrt{k_{ps} D} \right) t + \ln P_0$$

A5.5. Calculation of Pseudo first order Chemical Reaction Rate by Volume-drop Method (2)

This is the deduction of k_{ps} and pseudo first order chemical reaction rate coefficient k_2 measured by stirred cell or solubility cell with volumetric method:

$$\frac{dn}{dt} = -k_L^0 AE(C_L^i - C_L^b)$$

$$PV = nRT$$

$$P \text{ is constant, } C_i^i = P / H$$

$$\frac{P_G}{RT} \frac{dV_G}{dt} = -\sqrt{k_{ps} D} A \left(\frac{P_G}{H} - C_L^b \right)$$

when CO_2 loading less than 0.1 mol / mol

or

$C_L^i \gg C_L^b$ when stirrer speed is low, then

$$C_L^b \approx 0$$

$$\int_{V_1}^{V_2} dV_G = \int_{t_1}^{t_2} \left(-\frac{RAT}{H} \sqrt{k_{ps} D} \right) dt$$

Integration

$$V_{G,2} - V_{G,1} = \frac{RAT}{H} \sqrt{k_{ps} D} (t_1 - t_2)$$

or

$$V_G = \frac{RAT}{H} \sqrt{k_{ps} D} t + V_0$$

A5.6. Calculation of Pseudo-first-order Chemical Reaction Rate (3)

$$r_{CO_2} a = \frac{P_{CO_2}}{\frac{1}{k_G a} + \frac{H_{CO_2}}{k_L a E}}$$

Can be written as

$$\frac{P_{CO_2}}{r_{CO_2}} = \frac{1}{k_G} + \frac{H_{CO_2}}{k_L^0 E}$$

The gas-side mass transfer resistance was absent, then

$$\frac{P_{CO_2}}{r_{CO_2}} = \frac{H_{CO_2}}{k_L^0 E}$$

Defining Hatta number (Ha) as follows:

$$Ha = \frac{\sqrt{\frac{2}{m+1} k_{m,n} C_i^{m-1} C_j^n D_i}}{k_L^0}$$

Where $k_{m,n}$ is the reaction rate constant of (m,n) th order, for MEA+CO₂ chemical reaction, $m=1$ and $n=1$,

$$Ha = \frac{\sqrt{k_2 C_{MEA} D_{CO_2}}}{k_L^0}$$

For the film model of mass transfer:

$$E = \frac{Ha}{\tanh Ha}$$

$$E^\infty = \sqrt{\frac{D_{CO_2,L}}{D_{MEA,L}}} + \sqrt{\frac{D_{MEA,L}}{D_{CO_2,L}}} \frac{C_{MEA} H_{CO_2}}{\nu_{MEA} P_{CO_2}}$$

where ν_{MEA} is the stoichiometric coefficient of MEA, H_{CO_2} is the Henry's constant, $D_{CO_2,L}$ and $D_{MEA,L}$ are the diffusivities of CO₂ and MEA in the liquid, respectively. When $E^\infty \gg Ha > 3$, $\tanh Ha \approx 1$, the reaction is fast reaction regime, then

$$E = Ha = \frac{\sqrt{k_2 C_{MEA} D_{CO_2}}}{k_L^0}$$

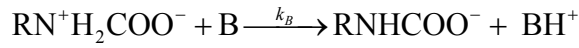
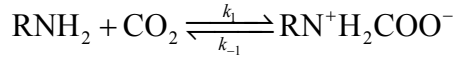
Then

$$\frac{P_{CO_2}}{r_{CO_2}} = \frac{H_{CO_2}}{k_L^0 E} = \frac{H_{CO_2}}{\sqrt{k_2 C_{MEA} D_{CO_2}}}$$

$$r_{CO_2} = \frac{P_{CO_2}}{H_{CO_2}} \sqrt{k_2 C_{MEA} D_{CO_2}} = C_{CO_2}^i \sqrt{k_2 C_{MEA} D_{CO_2}} \quad (\text{mol} \cdot \text{m}^{-2} \cdot \text{s}^{-1})$$

A5.7. Deduction of the Reaction Kinetics for Amine+CO₂

This is the deduction of reaction rate equation for MEA+CO₂ chemical reaction with zwitterion mechanism:



$$r_{\text{CO}_2} = k_1 C_{\text{CO}_2} C_{\text{Am}} - k_{-1} C_Z = C_Z \sum k_B C_B$$

thereby,

$$C_Z = \frac{k_1 C_{\text{CO}_2} C_{\text{Am}}}{k_{-1} + \sum k_B C_B}$$

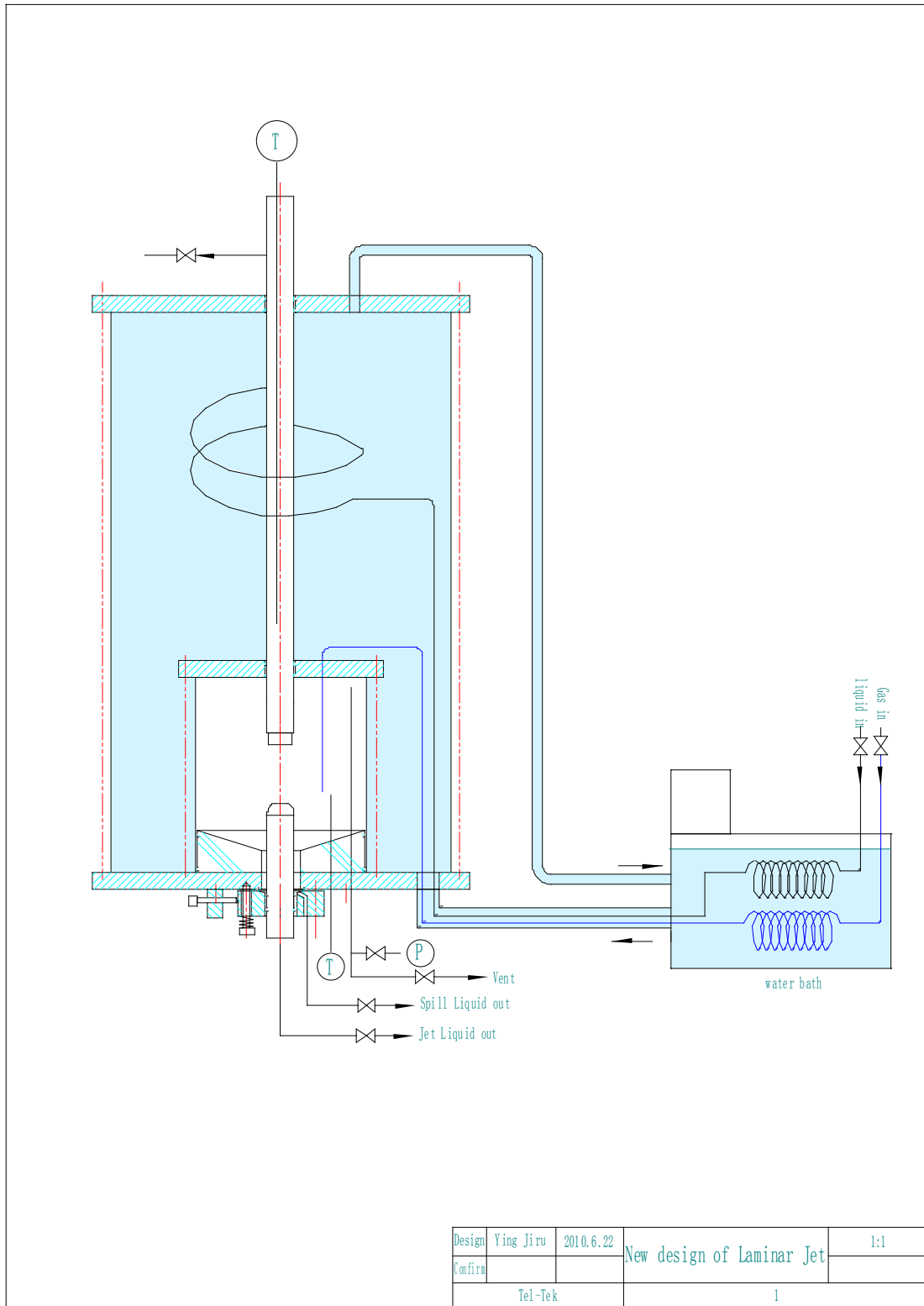
then

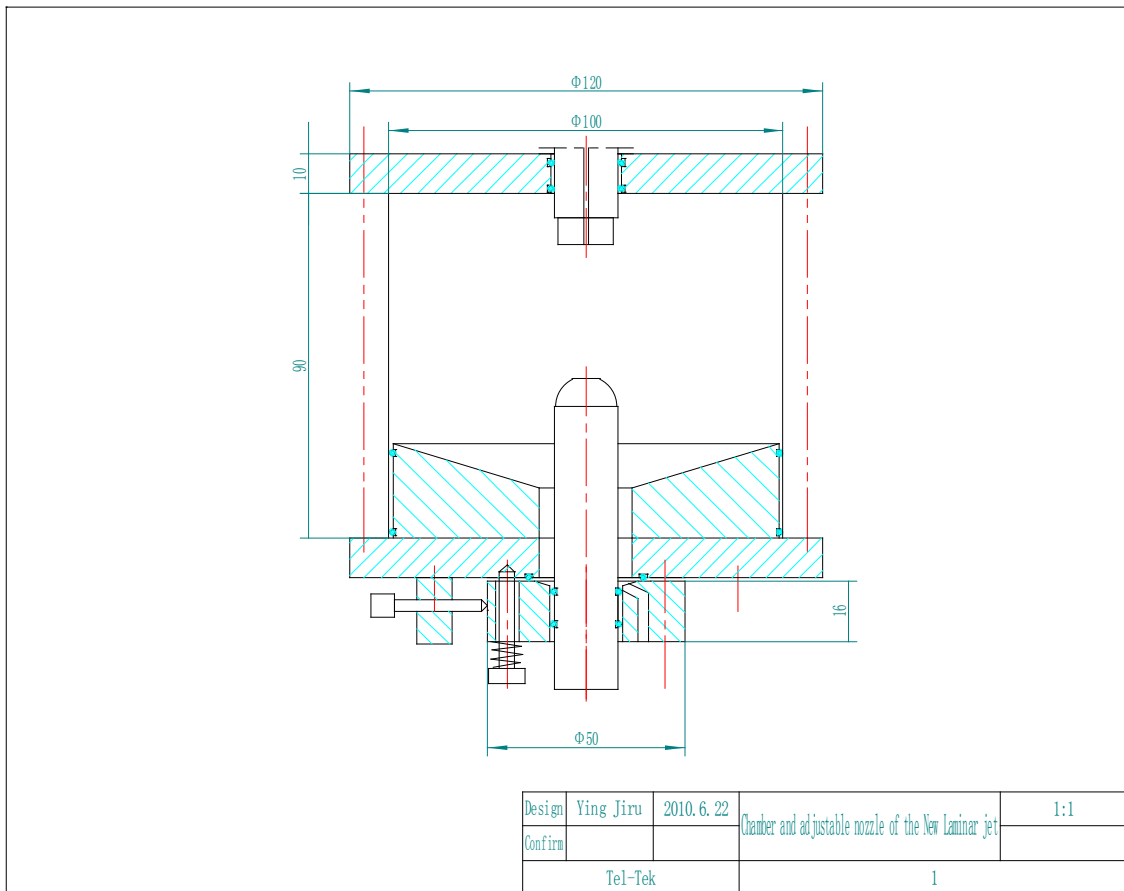
$$r_{\text{CO}_2} = C_Z \sum k_B C_B = \frac{k_1 C_{\text{CO}_2} C_{\text{Am}}}{1 + k_{-1} / \sum k_B C_B} \quad (\text{mol.m}^{-3}\text{s}^{-1})$$

when $k_{-1} / \sum k_B C_B \ll 1$

$$r_{\text{CO}_2} = k_1 C_{\text{CO}_2} C_{\text{Am}} \quad (\text{mol.m}^{-3}\text{s}^{-1})$$

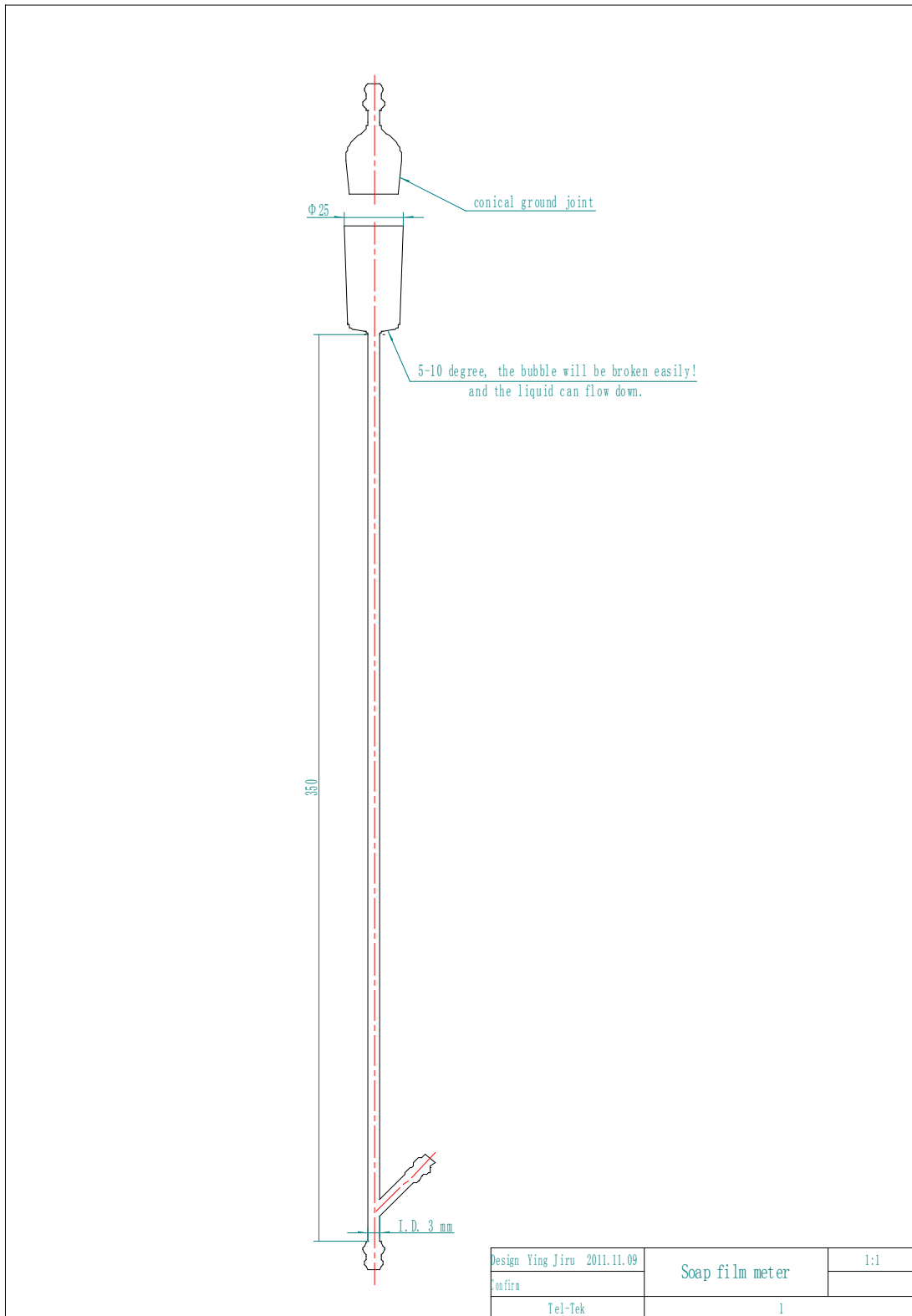
A6. The Modified Construction of Laminar Jet Absorber



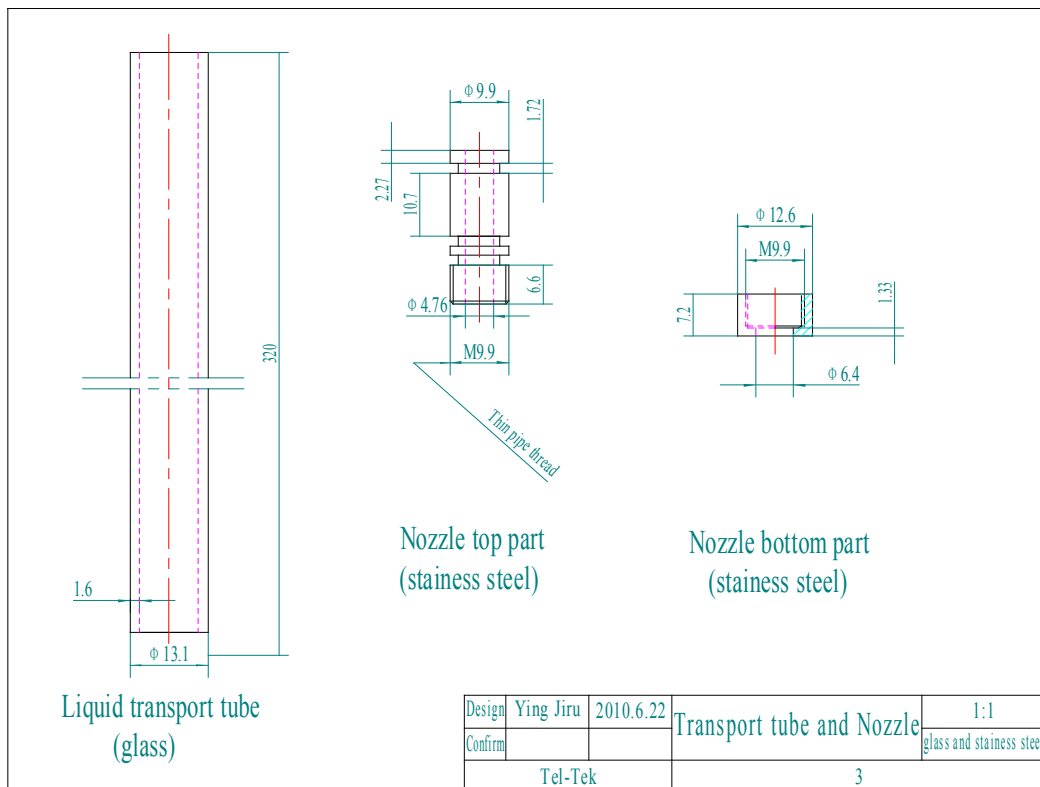
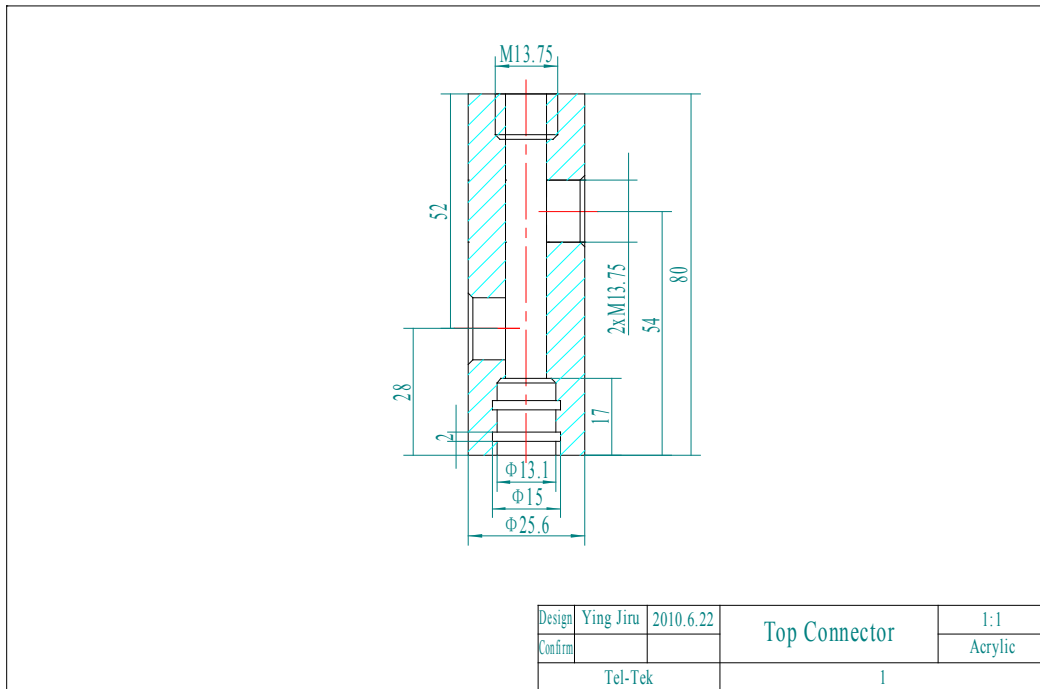


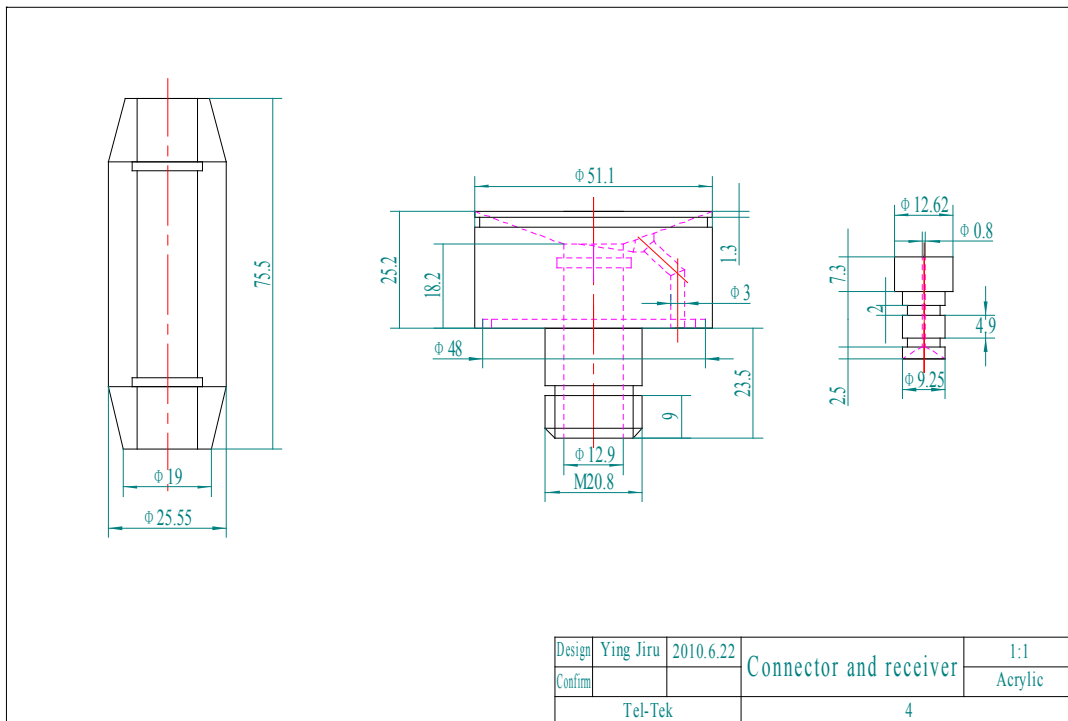
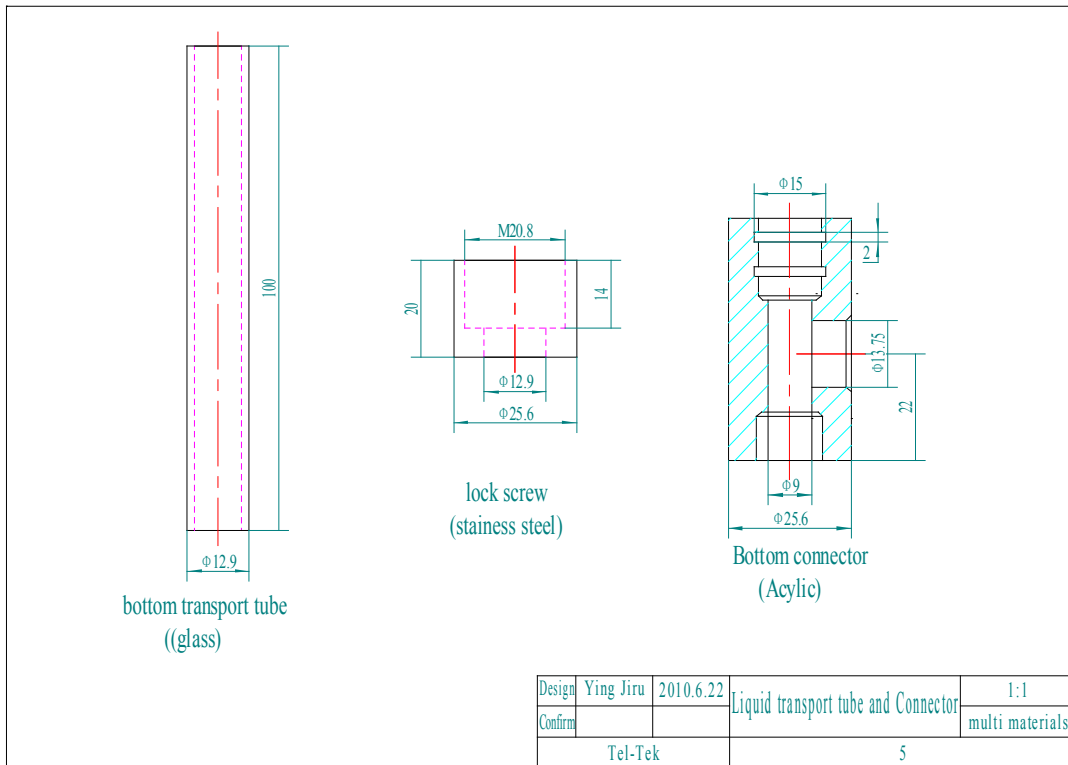
Advantage of the modified laminar jet:

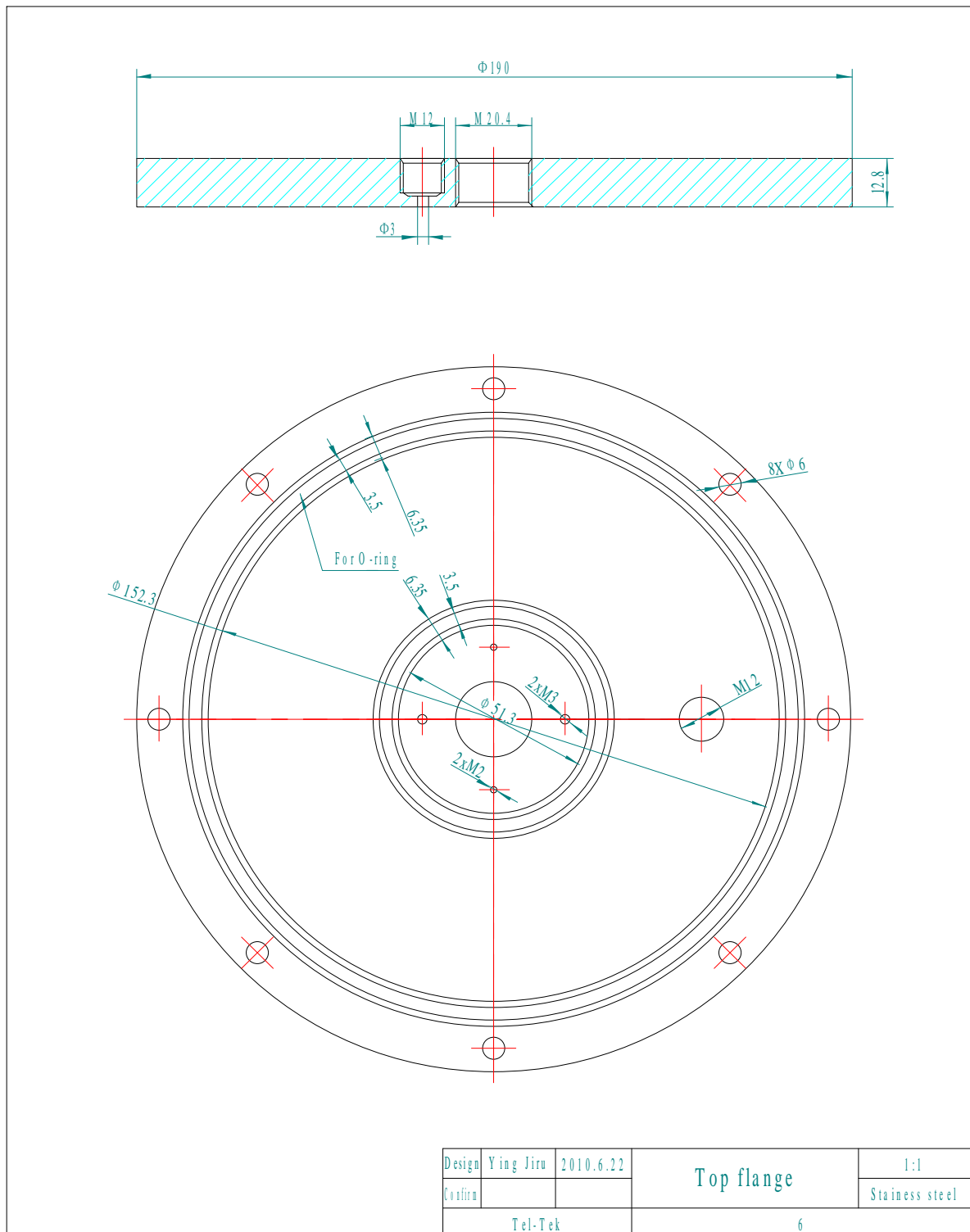
- 1) All the key parts are in the water bath, there are almost not different of the temperatures. This is very important!
- 2) The chamber is small, the effect of gas temperature in the chamber will be reduced and more sensitive to variation of pressure ;
- 3) There is no a long liquid tube in the chamber as the old design, then there is no effect of liquid temperature on the gas temperature in the chamber, and the gas pressure will be more stable;
- 4) It's easy to assemble. The small chamber is mounted first, then mount outside of the jacket, Many in-outlet are mounted on the bottom plate;
- 5) There is a adjust part can adjust the position of the receiver to align the holes.
- 6) The position of both receiver and nozzle can be adjusted to change the length of the jet.

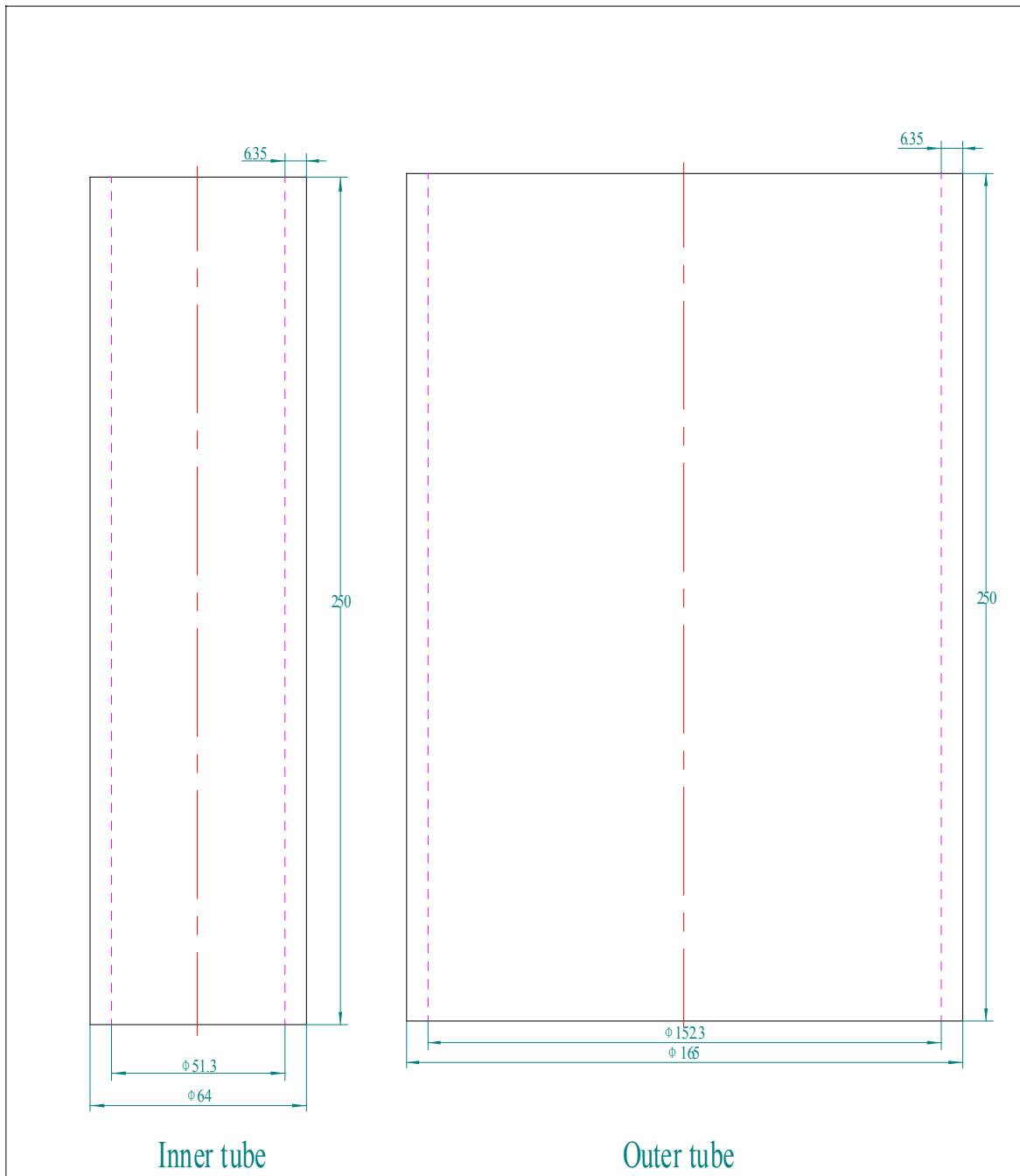


A7. The Present Construction of Laminar Jet Absorber

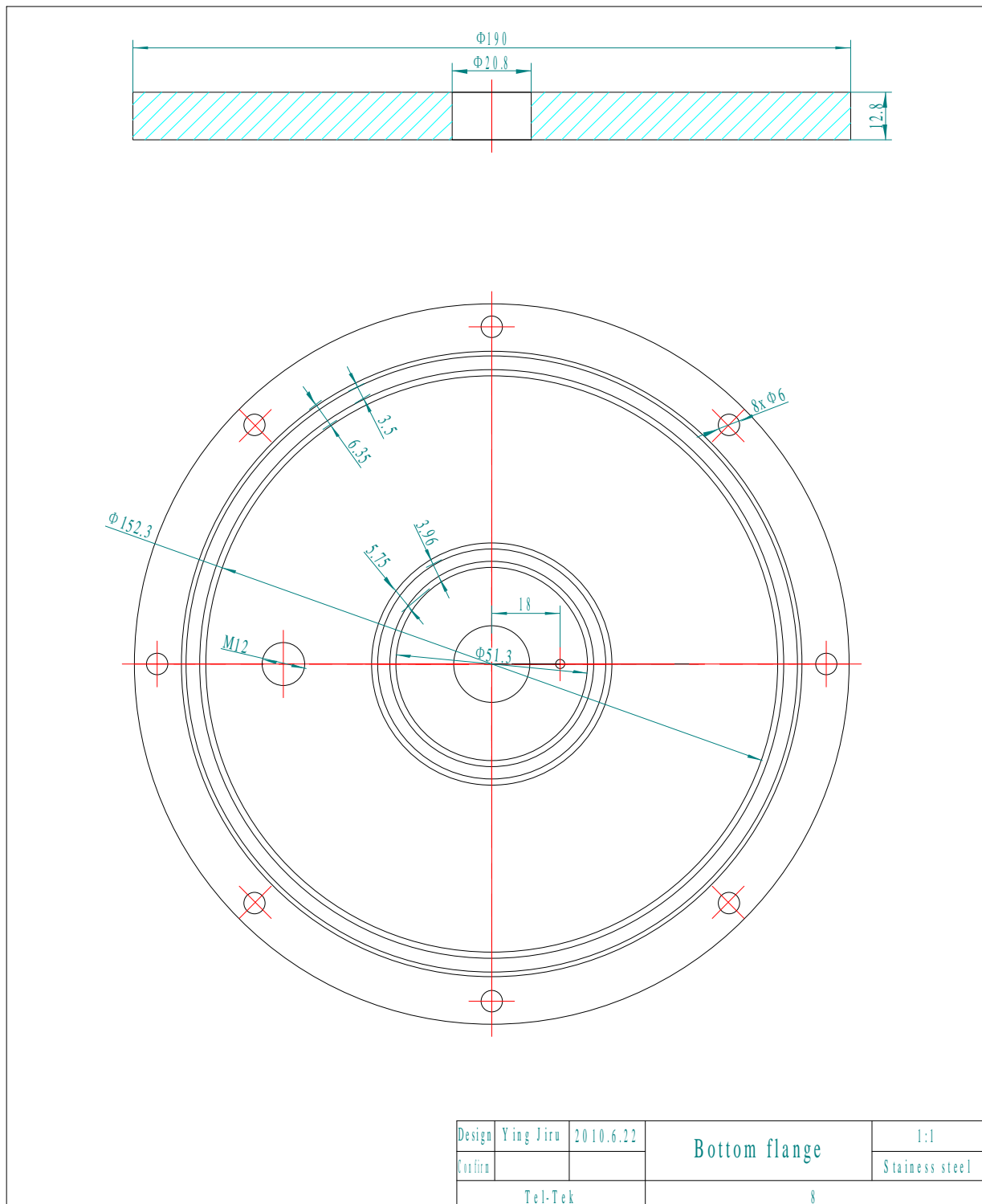




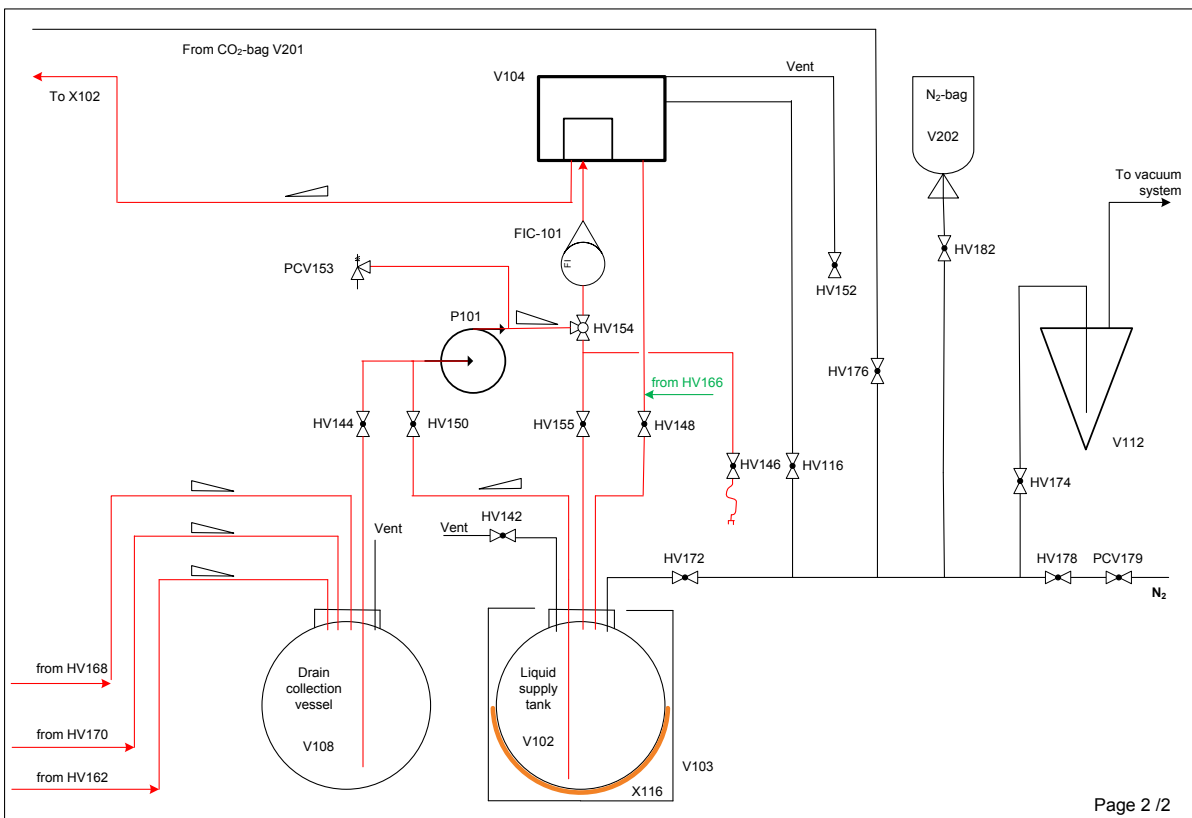
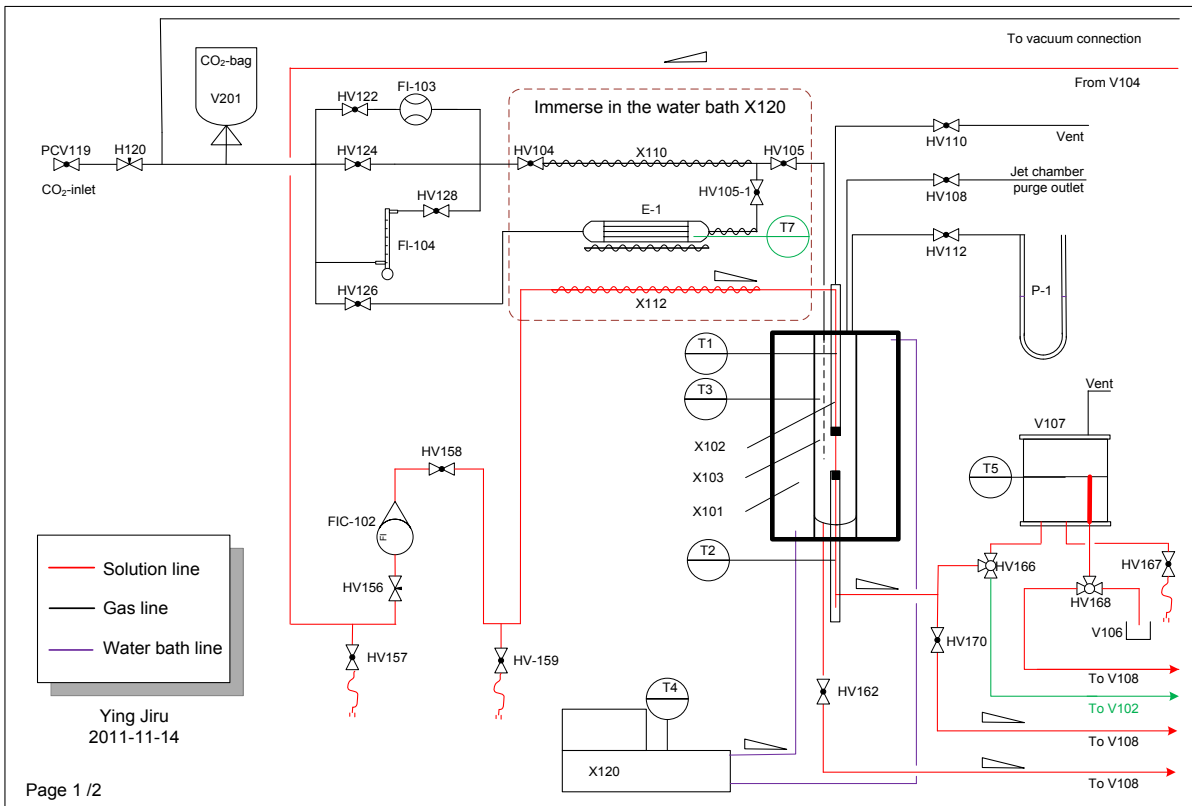




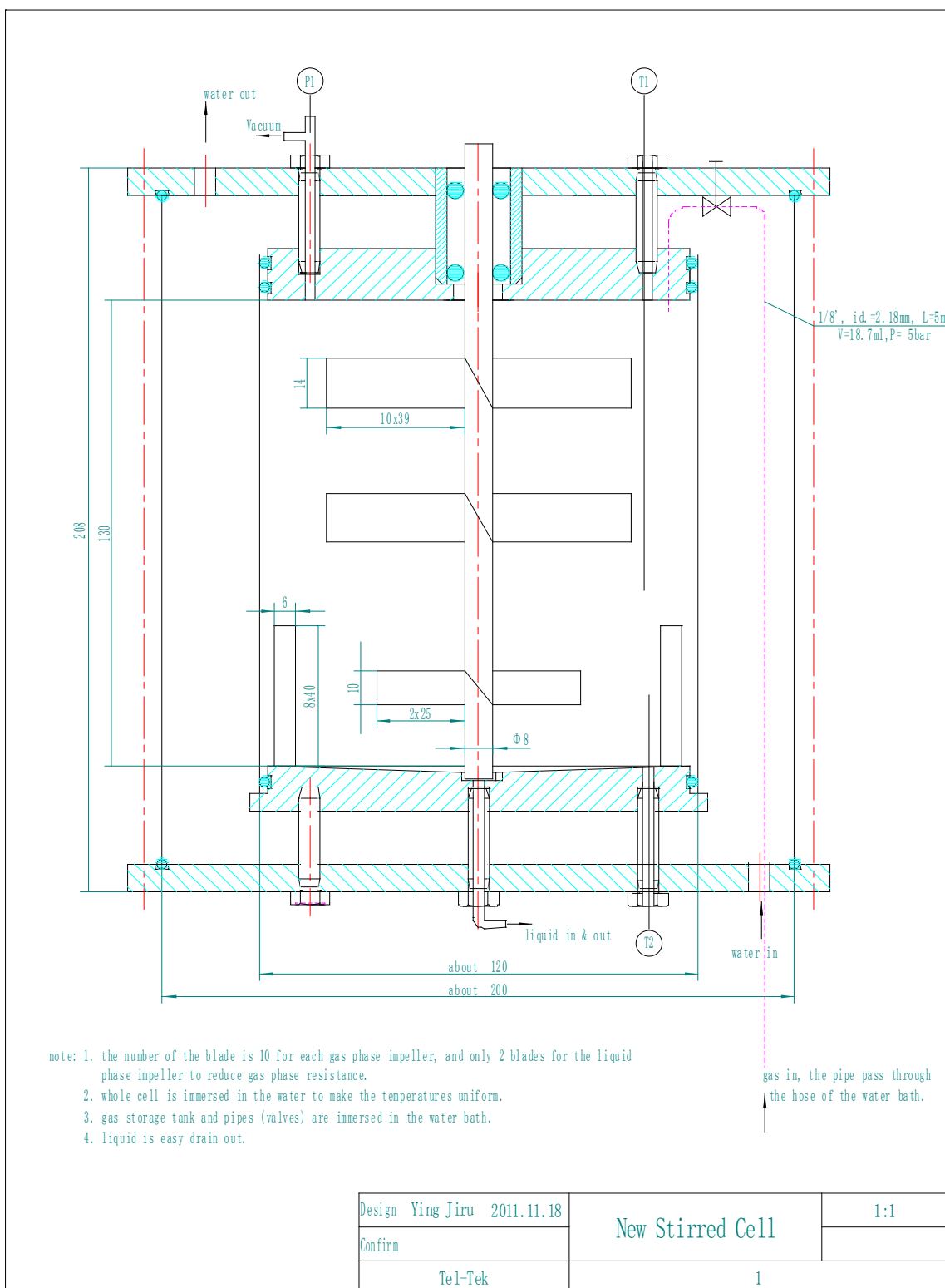
Design	Ying Jiru	2010.6.22	Inner and outer tube	1:1
Confirm				Acrylic
Tel-Tek			7	



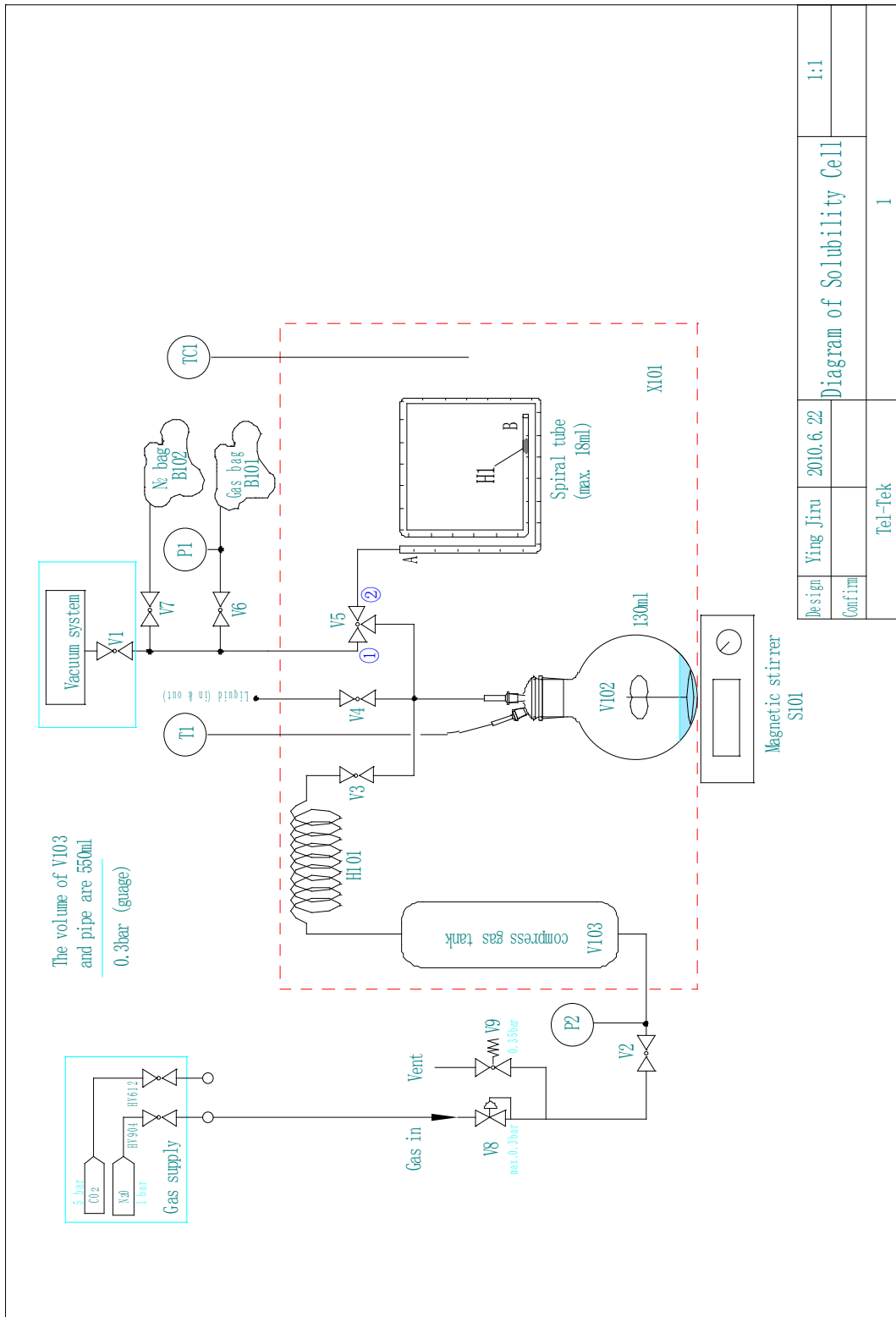
A8. Flowsheet of Laminar Liquid Jet



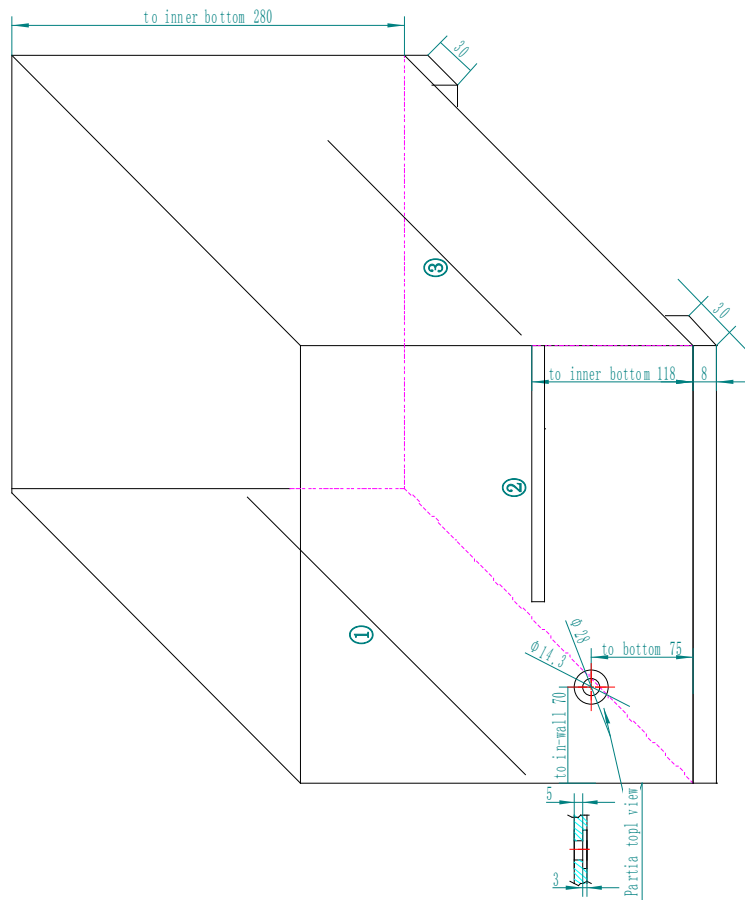
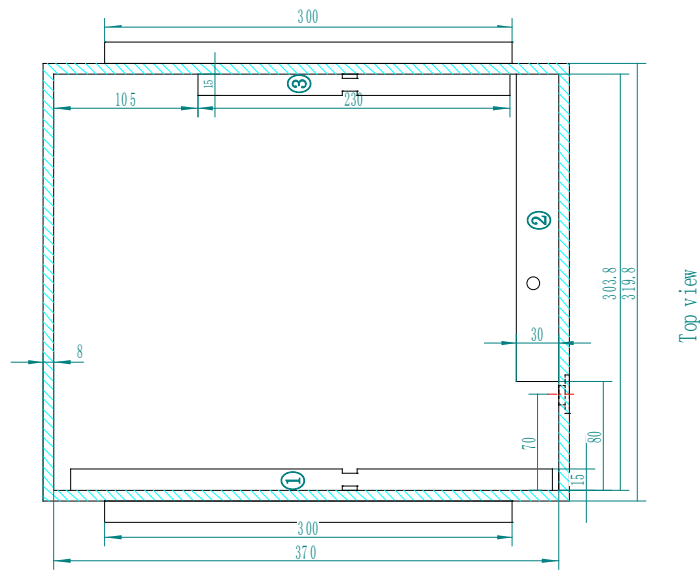
A9. The Modified Construction of Stirred Cell Reactor



A10. Flow Sheet and Construction of Solubility Cell



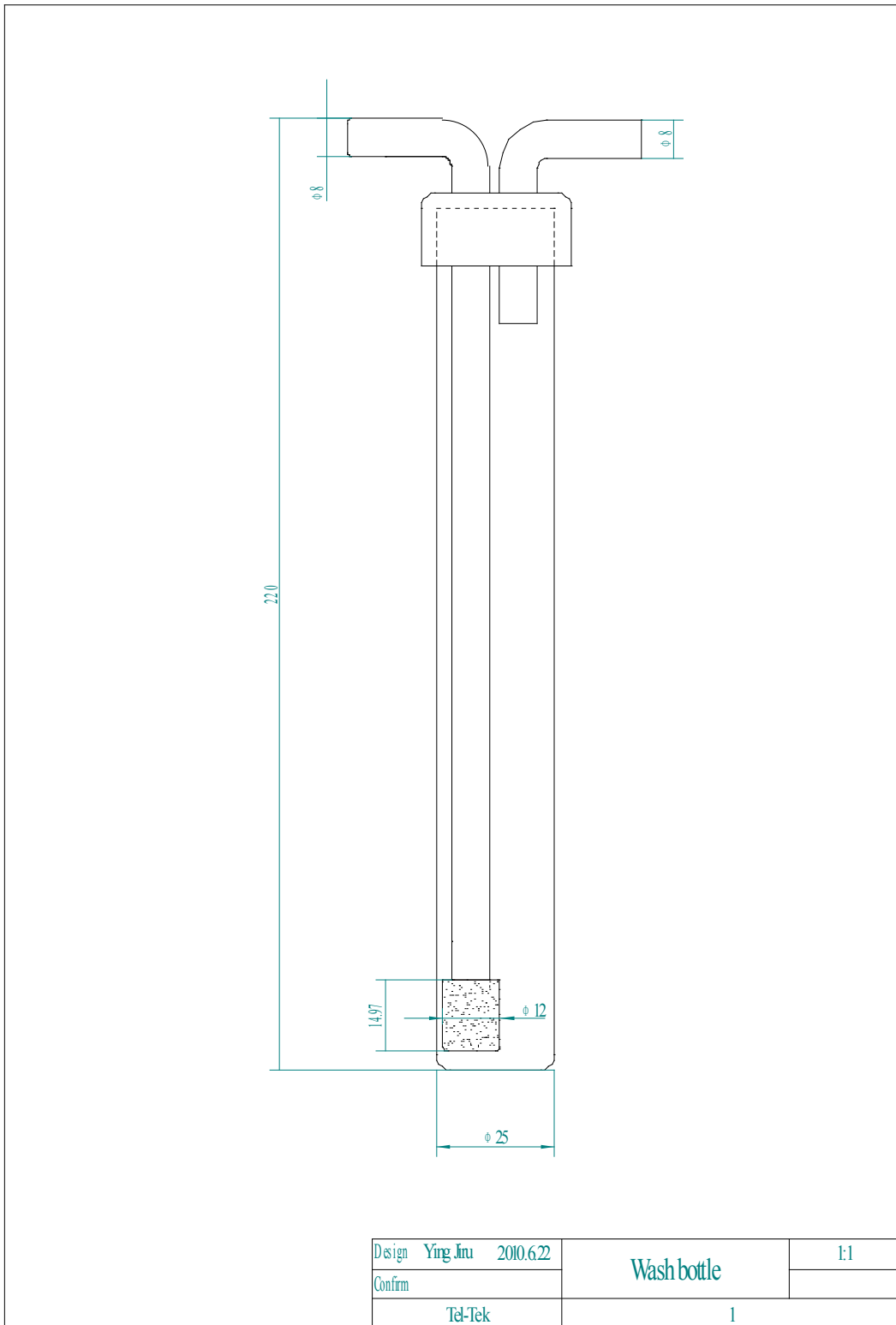
Design	Ying Jiru	2010.6.22	Diagram of Solubility Cell	1:1
Confirm				
Tel-Tek			1	



Note:

1. Plat ①, ②, ③ for lying spiral tube should be the same horizontal. (Important!)
2. The materials is Acrylic sheet material (PMMA).

Design	Ving Jiru	2000.6.22	Water bath tank for Solubility Cell	1:1
Constr				
Tel-Fek			1	



A11. The Possible Method to Reduce the Influence of Pressure on Solubility Measurement

The measurements run in atmosphere (room pressure) which often fluctuates in different time. The pressure fluctuation will cause fluctuation of the gas volume, and then will affect the result of solubility in the volume–drop method measurement.

$$PV = nRT$$

The temperature is constant during the measurement, and the absorbed CO₂ amount is presumed neglect due to it is smaller than the amount of gas volume. Then the equation can be modified as follows:

$$P_1V_1 = P_2V_2$$

In our experiment, the gas volume is about 120 mL while the liquid volume is 15 mL. For example, when $P_1=1010\text{mbar}$, $P_2=1011\text{mbar}$, according to equation $PV=nRT$, the gas volume will vary from 120 mL to 119.881 mL and the decrease amount is 0.119 mL; when $P_1=980\text{bar}$, $P_2=981\text{mbar}$, the decrease amount is 0.122 mL. Therefore, the average variation is about **0.118 mL**, and this causes $35.0 \text{ kPa} \cdot \text{m}^3 \cdot \text{kmol}^{-1}$ uncertainty in H_A measurement. This uncertainty is the biggest one of the sources of uncertainty (see the uncertainty analysis).

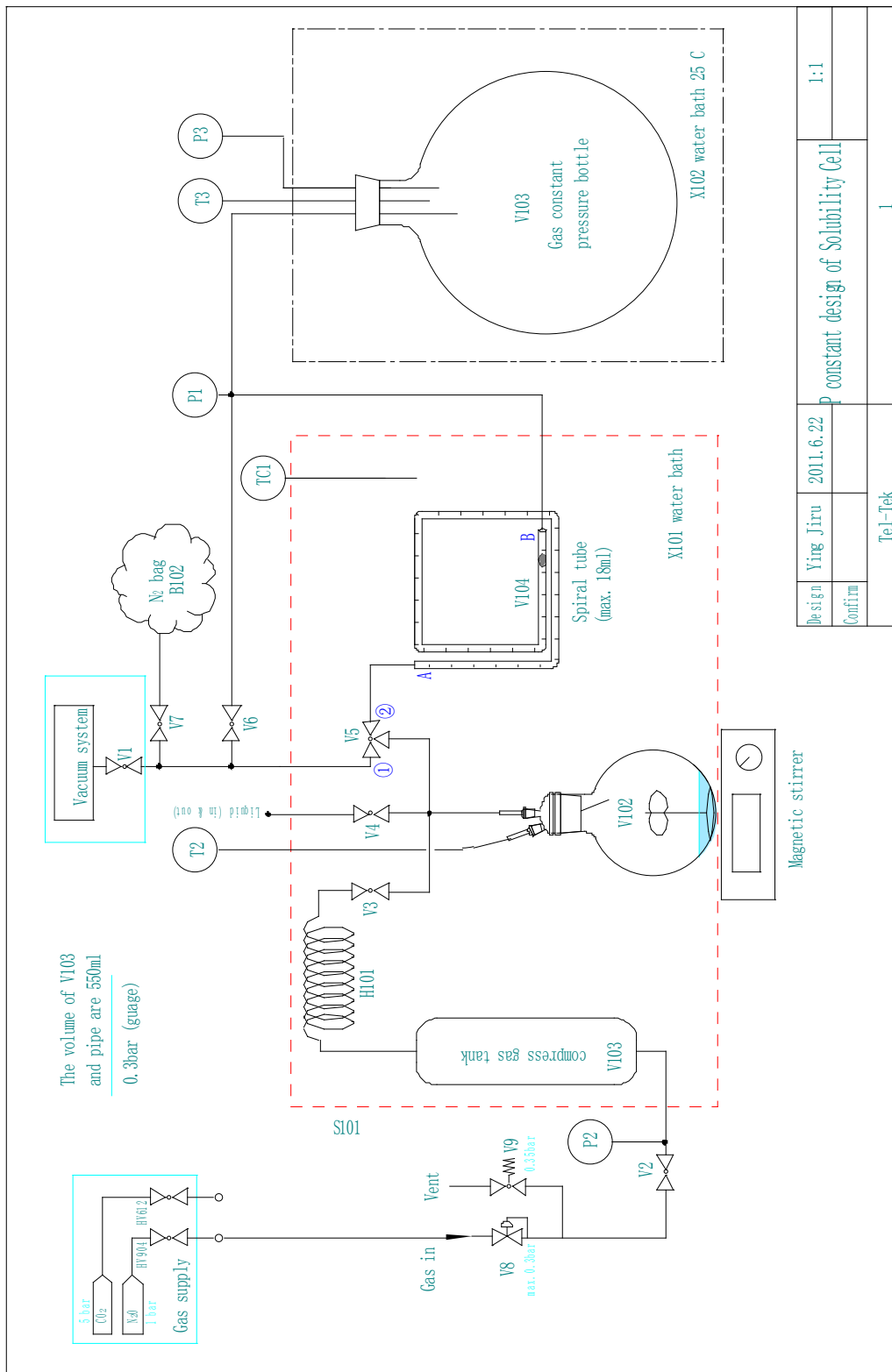
On the other hand, the volume decrease amount will be less if the gas volume is smaller according to the above equation.

So, in order to reduce the error caused by room pressure fluctuation, we can make effort as follows:

- Use smaller volume of gas as possible; (The volume caused by pressure fluctuation will be small.)
- Use large amount of liquid; (due to the absolute absorption volume will be higher than that volume caused by pressure fluctuation.)
- Avoid to measure at large fluctuation of room pressure;
- Stir fast in the measurement to increase the absorption rate and reduce absorption time of equilibrium.
- To avoid room pressure fluctuation, we can use put the gas bag into a sealed little big bottle to isolate from room pressure. The bottle should be avoiding temperature fluctuation and put into the water bath (or is isolated to room gas).

As follows figure shown.

According to present situation, the last method is the feasible solution to avoid room pressure fluctuation.



Design	Ying Jiru	2011.6.22	P	constant design of Solubility Cell	1:1
Confirm					
Tel-Tek			1		

A12. The Issues of Viscosity Measurement

The viscosity of aqueous MEA solution was measured using an Anton Paar rheometer (MCR 101) with a double-gap measuring system. The viscometer was calibrated against the petroleum distillate and mineral oil calibration fluid from Paragon Scientific Ltd. Some key points were not mentioned in the instruction, but they are very important. For this aqueous amines system, some points summarized as follows according to this study:

- 1) For high viscosity liquid, shear will cause heat and a little higher liquid temperature. The viscosity will drop as function of time, for example, for pure MEA at 40°C:

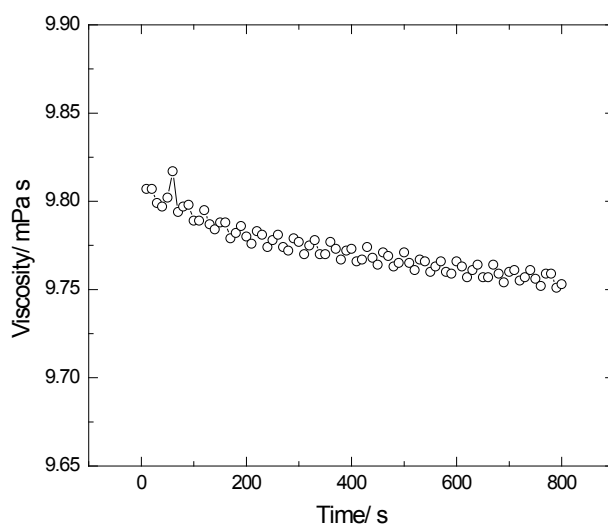


Figure A12.1 viscosity as a function of time of pure MEA at 40°C

- 2) For the mixed liquid system like MEA+H₂O, at high temperature, more water vaporization will cause the change of the solution concentration and the measured viscosity is not the true concentration you desire. For example, Figure A12.2 shows the measurements were used the same solution to measure the viscosities at the temperatures from 25 °C rising to 80 °C.

The viscosities of 3 M MEA solution in Figure A12.2 are apparently higher than the true values when temperature is higher than 50°C. This implies that one sample should be only measured at one temperature, and should be completed in a short time (maybe 5 – 10 minutes) to reduce the change of concentration due to vaporizing, especially at high temperature

- 3) The volume of the injected liquid should be a little higher than 7 mL, because the density will be decreased (and the volume will be increased) with the increasing of the

temperature. If the volume is less than 7 mL, the amount of the liquid in the gap will be different when temperature changes. When the liquid volume is a little higher than 7 mL (maybe caused by the increase of temperature), the redundant liquid will overflow in the concave of the middle cylinder, then the measured volume of the liquid will be constant.

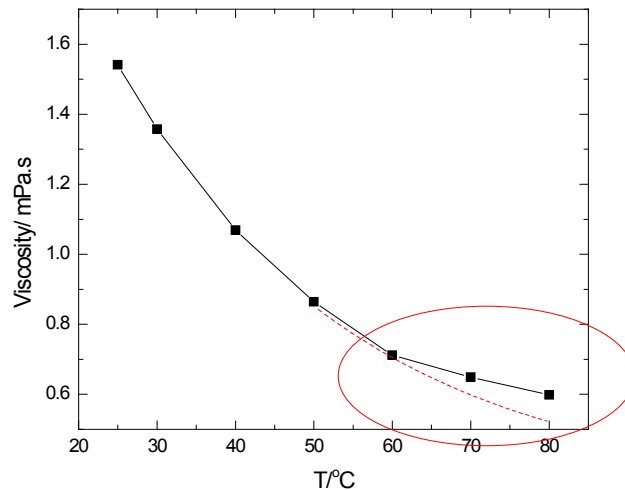


Figure A12.2 Viscosity as a function of temperature of 3M MEA

- 4) Regarding calibration, if the calibration factor is fixed, that will be happy; but unfortunately, the factors are different at different temperatures (maybe viscosities). So we can measure the standard sample (oil) to obtain the factors at different temperatures (or viscosities), then calibrate the measured valves by different factors of different temperatures or viscosities.
- 5) According to my experience, the calibration factor depends on temperature, due to the thermal expansion coefficient of material, lead to the size and shape of the measuring tools change with the variation of temperature.
- 6) The calibration factor is perhaps changed after changing the bearings of the measuring tools. Then it must be calibrated it again.
- 7) The cell needs to be dry and clean. The holes to place the pressure sensor and safety valve always hold some liquid; this should be cleaned before measurement.
- 8) Mount and dismount the cell need to be done carefully because the air bearing is very accurate and damageable.
- 9) The measurement profile can be set like Figure A12.3, this setup can reduce the run time of the bearings and extend its life.

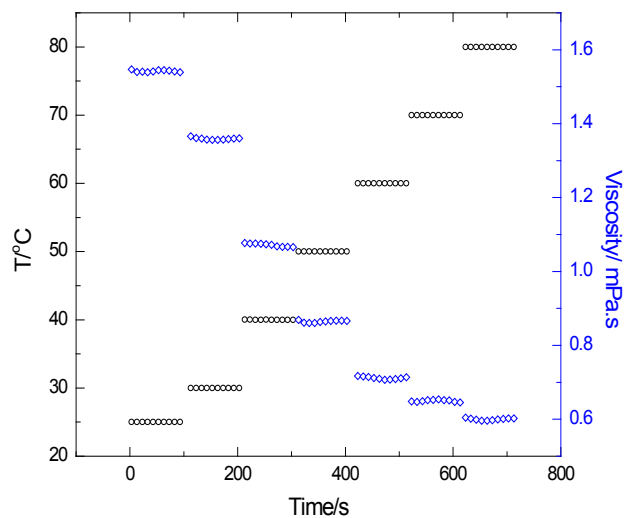


Figure A12.3 The measurement profile of temperature and the responding viscosities

At the temperature increase stage, the shear rate is set to 100 s^{-1} to reduce the wear down of the bearing, but still stirring the liquid to improve the heat transfer. At the measurement stage, the shear rate is set to 1000 s^{-1} .

A13. Key Codes of Program for Solubility Measurement

The computer program was written using Visual FoxPro language by myself. The main function of this computer program is to control the solubility experimental procedure, record the experimental data (absorbed gas volume versus time) and calculate the Henry's constant automatically. The main codes of the program are listed as follows.

List of the key codes of the computer program of "V-T Rec":

PROCEDURE Activate

```

Select v_t
Go Top
gas1=Alltrim(gas)
solution=Alltrim(sol)
Thisform.combo1.Value=gas1
Thisform.combo2.Value=solution
Select v_t
If Thisform.Tag='0'
    Thisform.Tag='11'
    If Recc()>0
        Go Top
        Thisform.text9.Value=dt
        Thisform.text13.Value=msec
        ta=dt
        isec=msec
        Incr=ls2
        Thisform.text8.Value=v
        Thisform.text11.Value=Substr(bz,At('T',bz)+2,At('C',bz)-At('T',bz)-2)
        Thisform.text12.Value=Substr(bz,3,At('mb',bz)-At('P',bz)-2)
        Thisform.text10.Value=Val(Substr(bz,At('Sol',bz)+4,At('ml',bz)-At('Sol',bz)-4))
        If !Empty(Thisform.combo2.Value)
            Thisform.text11.LostFocus
        Endi
        Thisform.spinner3.Value=Round(Thisform.text10.Value * Thisform.spinner4.Value/1000,3)
        If MessageBox('There is an ongoing Experiment , Will you Continue recording?',32+4,'Warning')=6
            Thisform.command1.Enabled=.F.
            Thisform.command2.Enabled=.T.
            Thisform.command6.Enabled=.f.
            Thisform.text9.Enabled=.F.
        Else
            Thisform.timer1.Interval=0
            Thisform.command6.Enabled=.t.
        Endif
        Thisform.text4.SetFocus
    Else
        Incr=0.25
    Endif
    Thisform.spinner1.Value=Incr
    Thisform.label22.Visible=.T.
Endif

```

ENDPROC

PROCEDURE command1.Click

```
Select 10
USE v-t
thisform.timer1.Interval=200
IF recc()=0
APPEND BLANK
ENDIF
GO top
aa=DTOC(thisform.txtt.Value)+'T'+ALLTRIM(thisform.text1.Value)+':'+ALLTRIM(thisform.text2.Value)+':'+
ALLTRIM(thisform.text3.Value)
REPLACE dt with CTOT("&aa"),msec with VAL(thisform.text13.Value)
REPLACE t with 0,ls2 with incr
REPLACE bz with ; 'P='+ALLTRIM(thisform.text12.Value)+'mbar,T='+ALLTRIM(thisform.text11.Value)+'C,V_Sol='+
ALLTRIM(STR(thisform.text10.Value,6,3))+ 'ml'
REPLACE v with thisform.text8.value
ta=dt
isec=msec
thisform.text9.value=ta
thisform.text13.value=isec
thisform.shape2.Click
thisform.spinner5.Value=2
thisform.spinner5.InteractiveChange
Select 10
USE
ENDPROC
```

PROCEDURE command2.Click

```
Select 10
USE v-t
If !Empty(Thisform.text4.Value)
If Thisform.check3.Value=1
Go Bott
Thisform.spinner5.Value=Iif((Datetime()-dt)/60<0.5,0.5,(Datetime()-dt)/60)
Endif
Append Blank
aa=Dtoc(Thisform.txtt.Value)+'T'+Alltrim(Thisform.text1.Value)+':'+Alltrim(Thisform.text2.Value);
+':'+Alltrim(Thisform.text3.Value)
Replace dt with Ctot("&aa"),msec with Val(Thisform.text13.Value), T with dt-ta+(msec-isec)/100
If Thisform.text7.Value='- '
bb=Val(Thisform.text4.Value)-Val(Thisform.text5.Value)/80
Else
bb=Val(Thisform.text4.Value)+Val(Thisform.text5.Value)/80
Endif
If Thisform.check2.Value=0
Incr=Thisform.spinner1.Value
Thisform.text4.Value=Alltrim(Str(Val(Thisform.text4.Value)+Incr,5,2))
Thisform.text5.Value='0'
Else
Incr=10
Thisform.text5.Value=Alltrim(Str(Val(Thisform.text5.Value)+Incr,2,0))
If Val(Thisform.text5.Value)>=20
Thisform.text5.Value='0'
Thisform.text4.Value=Alltrim(Str(Val(Thisform.text4.Value)+0.25,5,2))
```

```

        Endif
    Endif
    Replace v with bb,bz with Str((v-Thisform.text8.Value)/Thisform.text10.Value,6,3)
    Set Bell To '.\ch.WAV'
    ?? Chr(7)
    Set Bell To
    Thisform.spinner5.InteractiveChange
Else
    MessageBox('Position must be filled!',64+0,'Warning')
    Thisform.text4.SetFocus
Endif
Thisform.Refresh
SELECT 10
use
ENDPROC

PROCEDURE command3.Click
    nvalue=0
    Create Table ls (NUM1 N(2),DT T(8), T N(10,2), V N(10,3),Datetime T(8), TIME_s N(10,2),;
    TIME_hr N(11,5), Volume_ml N(10,3), BZ C(36), Gas C(10),sol C(10))
    Select 10
    USE v-t
    Go Top
    nam='D:\Sol_data\' + Alltrim(Alltrim(gas) + '-' + Alltrim(sol) + '-' + Alltrim(Thisform.text11.Value) + 'C-' +
    Substr(Dtoc(dt),1,2) - Substr(Dtoc(dt),4,2) - Substr(Dtoc(dt),7,2) + '-' + Alltrim(Str(Hour(dt))) - Alltrim(Str(Minute(dt))) + '.xls')
    Sele ls
    Append From v-T
    Go Top
    iniv=v
    Replace All Datetime with dt,time_s with T,time_hr with T/3600,Volume_ml with V-iniv
    Alter Table ls Drop DT Drop T Drop V
    Go Top
    Scan
        Replace num1 with Recno()
    Endscan
    Count To num2
    If num2 < 7
        For i=1 To 7-num2
            Appe Blan
            Replace num1 with Recno()
        Endfor
    Endif
    Select ls.*,remark.* From ls Full Join remark On num1=Step Into Tabl ls2
    Select ls2
    Append Blank
    zzbz1=Alltrim(Thisform.text12.Value) + 'mbar,' + Alltrim(Thisform.text11.Value) + 'C,' +
    Alltrim(Str(Thisform.spinner4.Value,9,3)) + 'g/l, Ini POS. ='
    zzbz2=Alltrim(Str(Thisform.spinner2.Value,9,3)) + 'ml, True POS. =' + Alltrim(Str(Thisform.text8.Value,9,3)) +
    'ml,Solution weight =' + Alltrim(Str(Thisform.spinner3.Value,9,3)) + 'g, Solutuion Volume =' +
    ALLTRIM(Str(Thisform.text10.Value,9,3)) + 'ml'
    Replace Note with zzbz1 + zzbz2, Procedure with 'Operation Condition:'
    Copy To &nam Type Xls
    Use
    Select 10
    Thisform.command2.SetFocus

```

```

If nvalue=0
  If MessageBox('Data have been copied to a Excel file: '+nam+Chr(13)+;
  'Do you want open it now?',4+64+256,'Hello')=6
    oExcel=Createobject("Excel.application")
    oExcel.Visible=.T.
    oExcel.Caption="V-T call Excel"
    oExcel.DisplayAlerts = .F.
    oExcel.Workbooks.Open("&nam")
  Endif
Endif
Select 10
USE
ENDPROC

PROCEDURE timer1.Timer
tt=TIME(1)
thisform.text13.Value=SUBSTR(tt,10,2)
thisform.text3.Value=SUBSTR(tt,7,2)
thisform.text1.Value=SUBSTR(tt,1,2)
thisform.text2.Value=SUBSTR(tt,4,2)
ENDPROC

PROCEDURE timer2.Timer
thisform.AlwaysOnTop=.t.
MESSAGEBOX(SPACE(10)+'Record data please!!'+SPACE(10),0+64,'Reminder!')
thisform.label36.Caption=""
dtime=DATETIME()
thisform.AlwaysOnTop=.f.
ENDPROC

PROCEDURE time3.Timer
N=N-1
Thisform.label9.Caption=Chr(13)+Str(N,2)
If N<3
  Thisform.timer4.Interval=0
  Thisform.label9.FontSize=18
  Thisform.label9.Caption=Chr(13)+'Open V5 to (1), Please!'+CHR(13)+CHR(13)+'then,Press "record" immediately. '
  Thisform.label9.ForeColor=Rgb(255,0,0)
  Set Bell To '\ready.WAV'
  ?? Chr(7)
  Set Bell To
  Wait " Window At 0,0 Timeout 2
  Thisform.label9.Visible=.F.
  Thisform.command2.SetFocus
  Thisform.Refresh
Endif
ENDPROC

```

List of the key codes of the sub-program of “Auto Photo”:

Main form

PROCEDURE main.Init

```

Set Path To Data,frm,inc,lib,Menus,photo,pic,prg,rpt,ocx
Public cx,cy,tx,ty,ex,ey,ydx,ydy
tx=0
ty=0
cx=640
cy=680
thisform.optiongroup1.InteractiveChange
IF !DIRECTORY('photo')
MD photo
ENDIF
If !File('dater.dbf')
Create Table dater Free (dt T (8),hr N (7,2),X1 N (4),Y1 N (4),X2 N (4),Y2 N (4))
Append Blank
Replace x1 WITH 0,y1 WITH 0,x2 with cx,y2 with cy
ENDIF
use
ENDPROC

```

PROCEDURE optiongroup1.InteractiveChange

```

Do Case
Case This.Value=1
cx=640
cy=480
Case This.Value=2
cx=800
cy=600
Case This.Value=3
cx=1024
cy=768
Case This.Value=4
cx=400
cy=300
ENDCASE
ENDPROC

```

PROCEDURE command1.Click

```

If !Used('DATER')
Use dater
Endif
Delete All For y2=0 and x2=0
Pack
Use
ENDPROC

```

Snap form

PROCEDURE appl

```

#Define rgn_and 1
#Define rgn_or 2
#Define rgn_xor 3
#Define rgn_diff 4
#Define rgn_copy 5
#Define radius 84
#Define interspace 12

```



```

Local hrgnbase, hrgn, HWnd, x0,y0,x1,y1
* create a rectangle region
* and set it by the rectangle of the form
hrgn = createrectrgn (0,0,1,1)
HWnd = getfocus() && get window handle for the form
thisformset.getrect (HWnd, @x0,@y0,@x1,@y1)
hrgnbase = createrectrgn (0,0,x1-x0,y1-y0)
WITH thisformset.form2
hrgnexcludett = CreateRectRgn(3,35, .width+4,.height+35) &&(120, 200, 400, 300)&&create ellipticrgn
ENDWITH
= combinergn (hrgn, hrgn, hrgnexcludett, rgn_or)
= combinergn (hrgn, hrgnbase, hrgn, rgn_xor)
= setwindowrgn (HWnd, hrgn, 1)
= deleteobject (hrgn)
= deleteobject (hrgnbase)
ENDPROC

```

PROCEDURE buf

```

LPARAMETERS lcbuffer
Return;
asc(substr(lcbuffer, 1,1)) + ;
asc(substr(lcbuffer, 2,1)) * 256 +;
asc(substr(lcbuffer, 3,1)) * 65536 +;
asc(substr(lcbuffer, 4,1)) * 16777216
ENDPROC

```

PROCEDURE getrect

```

LPARAMETERS hwnd, x0,y0,x1,y1
Local lprect
lprect = space (16)
= getwindowrect (hwnd, @lprect)
x0 = this.buf(substr(lprect, 1,4))
y0 = this.buf(substr(lprect, 5,4))
x1 = this.buf(substr(lprect, 9,4))
y1 = this.buf(substr(lprect, 13,4))
ENDPROC

```

PROCEDURE photo

```

WM_USER = 1024
WM_CAP_START = WM_USER
WM_CAP_STOP = WM_CAP_START + 68
WM_CAP_DRIVER_CONNECT = WM_CAP_START + 10
WM_CAP_DRIVER_DISCONNECT = WM_CAP_START + 11
WM_CAP_SAVEDIB = WM_CAP_START + 25
WM_CAP_GRAB_FRAME = WM_CAP_START + 60
WM_CAP_SEQUENCE = WM_CAP_START + 62
WM_CAP_FILE_SET_CAPTURE_FILEA = WM_CAP_START + 20
WM_CAP_SEQUENCE_NOFILE = WM_CAP_START + 63
WM_CAP_SET_OVERLAY = WM_CAP_START + 51
WM_CAP_SET_PREVIEW = WM_CAP_START + 50
WM_CAP_SET_CALLBACK_VIDESTREAM = WM_CAP_START + 6
WM_CAP_SET_CALLBACK_ERROR = WM_CAP_START + 2
WM_CAP_SET_CALLBACK_STATUSA = WM_CAP_START + 3
WM_CAP_SET_CALLBACK_FRAME = WM_CAP_START + 5
WM_CAP_SET_SCALE = WM_CAP_START + 53
WM_CAP_SET_PREVIEWRATE = WM_CAP_START + 52
hWndC = capCreateCaptureWindowA("My Own Capture 42177280,1,4,cx,cy,this.form1.HWnd,0)
IF hWndC <> 0
SendMessage(hWndC, WM_CAP_SET_CALLBACK_VIDESTREAM, 0, 0)
SendMessage(hWndC, WM_CAP_SET_CALLBACK_ERROR, 0, 0)
SendMessage(hWndC, WM_CAP_SET_CALLBACK_STATUSA, 0, 0)
SendMessage(hWndC, WM_CAP_DRIVER_CONNECT, 0, 0)
SendMessage(hWndC, WM_CAP_SET_SCALE, 1, 0)

```

```

SendMessage(hWndC, WM_CAP_SET_PREVIEWRATE, 66, 0)
SendMessage(hWndC, WM_CAP_SET_OVERLAY, 1, 0)
SendMessage(hWndC, WM_CAP_SET_PREVIEW, 1, 0)
    this.form1.Activate
ENDIF
ENDPROC

```

PROCEDURE Init

```

Set Path To Data,frm,inc,lib,Menus,photo,pic,prg,rpt,ocx
Public WM_CAP_DRIVER_DISCONNECT
Public _CAP_SAVEDIB,WM_CAP_FILE_SET_CAPTURE_FILEA,WM_CAP_SEQUENCE,WM_CAP_STOP
Declare Integer capCreateCaptureWindowA In "AVICAP32.DLL" String lpszWindowName ;
    ,Integer dwStyle , Integer x, Integer Y, Integer nWidth ,;
    integer nHeight,Integer ParentWin,Integer nId
Declare Integer SendMessage In "user32" Integer HWnd, Integer wmsg,Integer wpar1, Integer wpar2
Declare Integer SendMessage In "user32" As SendMessageA Integer HWnd, Integer wmsg,Integer ng wpar2
Thisformset.photo
ENDPROC

```

PROCEDURE form1.Load

```

Declare Integer formtobmp IN "pctlib.dll" integer hwnd,String bmpFileName
Declare Integer formtobmpA IN "pctlib.dll" String bmpFileName,integer,integer,integer,integer
Declare Integer BMP2JPG IN "pctlib.dll" String bmpfilename, String jpgfilename
Declare Integer jpg2bmp IN "pctlib.dll" String jpgfilename, String bmpfilename
Declare Integer getbmpdimension IN "pctlib.dll" string bmpfilename, integer @ nwidth,integer @ nheight
Declare Integer getjpgdimension IN "pctlib.dll" string jpgfilename, integer @ nwidth,integer @ nheight
Declare integer CreateRectRgn in gdi32 integer nLeftRect, integer nTopRect, integer nRightRect, integer ct
Declare integer CombineRgn in gdi32 integer hrgnDest, integer hrgnSrc1, integer hrgnSrc2, integer Mode
Declare integer SetWindowRgn in user32 integer hwnd, integer hRgn, SHORT bRedraw
Declare integer GetWindowRect in user32 integer hwnd, string @ lpRect
Declare integer DeleteObject in gdi32 integer hObject
Declare integer GetFocus in user32
ENDPROC

```

PROCEDURE form1.Destroy

```

If !Used('DATER')
    Use dater
Endif
Go Top
Replace X1 with Thisform.COntainer2.SPINner1.Value,Y1 with Thisform.COntainer2.SPINner2.Value,;
    X2 with Thisform.COntainer2.SPINner3.Value,Y2 with Thisform.COntainer2.SPINner4.Value
USE
thisformset.release
ENDPROC

```

PROCEDURE form1.Init

```

Set Path To Data,frm,inc,lib,Menus,photo,pic,prg,rpt,ocx
PUBLIC ydx,ydy
Thisform.Width=cx+140
Thisform.Height=cy+6
Thisform.Resize
Thisform.AutoCenter=.T.
If !Used('DATER')
    Use dater
ENDIF
Go Top
Thisform.container2.spinner1.Value=x1
Thisform.container2.spinner2.Value=y1
Thisform.container2.spinner3.Value=x2
Thisform.container2.spinner4.Value=y2
tx=x1
ty=y1

```

```

ex=x2
ey=y2
thisform.container1.spinner1.Value=hr
thisform.timer1.Interval=hr*60000
Use
ENDPROC

```

PROCEDURE command3.Click

```

If !Used('DATER')
    Use dater
ENDIF
GO top
SKIP
IF !EOF()
    tim=dt
ELSE
    tim=DATETIME()
ENDIF
Append Blank
tt=Datetime()
Replace dt with tt,hr WITH (tt-tim)/3600
p1=Strt(Strt(Ttoc(tt),':',''),':','')
tp = '\photo\'-p1-.jpg'
pd= formtobmpA("c:\temp.bmp",Thisform.Left+tx+4,Thisform.Top+ty+66,Thisform.Left+ex+4,Thisform.Top+ey+66)
pd=BMP2JPG("c:\temp.bmp",tp)
Use
ENDPROC

```

PROCEDURE spinner1.InteractiveChange

```

thisform.timer1.Interval=this.Value*60000
If !Used('DATER')
    Use dater
ENDIF
GO top
REPLACE hr WITH this.Value
USE
ENDPROC

```

PROCEDURE form2.Moved

```

If This.Left<Thisformset.form1.Left
    This.Left=Thisformset.form1.Left
Endif
If This.Top<Thisformset.form1.Top
    This.Top=Thisformset.form1.Top
Endif
If This.Left+This.Width>Thisformset.form1.Left+cx
    This.Left=Thisformset.form1.Left+cx-This.Width
Endif
If This.Top+This.Height>Thisformset.form1.Top+cy
    This.Top=Thisformset.form1.Top+cy-This.Height
ENDIF
Thisformset.form1.container2.spinner1.Value=This.Left-Thisformset.form1.Left
Thisformset.form1.container2.spinner2.Value=This.Top-Thisformset.form1.Top
tx=This.Left-Thisformset.form1.Left
ty=This.Top-Thisformset.form1.Top
Thisformset.form1.container2.spinner3.Value=tx+This.Width
Thisformset.form1.container2.spinner4.Value=ty+This.Height
ex=This.Width+tx
ey=This.Height+ty
ENDPROC

```

A14. Lists of Publications

Articles

1. Ying, J. R.; Eimer, D. A.; Yi, W. J. Measurements and Correlation of Physical Solubility of Carbon Dioxide in (Monoethanolamine + Water) by a Modified Technique. *Ind. Eng. Chem. Res.* 2012, 51, 6958–6966.
2. Ying, J. R.; Eimer, D. A. Measurements and Correlations of Diffusivities of Nitrous Oxide and Carbon Dioxide in Monoethanolamine + Water by Laminar Liquid Jet. *Ind. Eng. Chem. Res.* 2012, 51, 16517–16524.
3. Ying, J. R.; Eimer, D. A. Determination and Measurements of Mass Transfer Kinetics of CO₂ in Concentrated Aqueous Monoethanolamine Solutions with a Stirred Cell. Accepted, <http://dx.doi.org/10.1021/ie303450u>, *Ind. Eng. Chem. Res.* 2013.
4. Ying, J. R.; Eimer, D. A. A Study of Mass transfer Kinetics of Carbon Dioxide in (Monoethanolamine + Water) by Stirred Cell. Accepted, *Energy procedia*, 2013.
5. Jayarathna, C. K; Elverhøy, A. B., Ying, J. R.; Eimer, D. A. Experimentally Based Evaluation of Accuracy of Absorption Equilibrium Measurements. Accepted, *Energy procedia*, 2013.
6. Ying, J. R.; Yi, W. J.; Eimer, D. A. Physical Solubility Measurement and Mass Transfer Estimation of N₂O in Aqueous (Salt) MEA Solutions. (In preparation).
7. Ying, J. R.; Eimer D. A. A Study of Viscosity Measurement by a Rotational Rheometer. (In preparation).

Presentations

8. Ying, J. R.; Eimer, D. A. Physical Solubility Measurement of CO₂ (N₂O) + MEA Solution. *Climit PhD seminar*, Oslo, Norway. 1st – 2nd November 2010 (Keynote lecture).
9. Ying, J. R.; Eimer, D. A. Mass transfer Kinetics of Carbon Dioxide in Aqueous MEA Solutions. *PhD workshop – Energy*, UiA, Grimstad, Norway. 7th – 8th December 2011 (Keynote lecture).
10. Ying, J. R.; Eimer, D. A. A Study of Mass transfer Kinetics of Carbon Dioxide in (Monoethanolamine + Water) by Stirred Cell. *GHGT-11*, Kyoto, Japan, 2012.11. (Poster).
11. Jayarathna, C. K; Elverhøy, A. B., Ying, J. R.; Eimer, D. A. Experimentally Based Evaluation of Accuracy of Absorption Equilibrium Measurements. *GHGT-11*, Kyoto, Japan, 2012.11. (Poster).